# RADIO EMISSIONS FROM JUPITER AND THE SUN

by

Peter Maxwell McCulloch, B. Sc. (Hons.)

A thesis submitted in fulfilment of the

requirements for the Degree of

Doctor of Philosophy

in the

UNIVERSITY OF TASMANIA

HOBART

November, 1968

ACKNOWLEDGEMENTS

I am indebted to my supervisor Professor G.R.A. Ellis for his encouragement, criticism and advice throughout the duration of my project. I also thank Mr. P.A. Hamilton for many stimulating discussions on various aspects of the work. I am grateful for assistance received from members of the technical staff of the Physics Department of the University of Tasmania.

I would like to thank Dr. E.G. Bowen, Chief of the C.S.I.R.O. Division of Radiophysics and many of his officers for making available to me the facilities of the Australian National Radio Astronomy Observatory at Parkes. In particular I thank Mr. M.M. Komesaroff and Mr. O.B. Slee with whom I co-operated on several phases of the work.

Apart from the acknowledgements made above and in the body of the text the material presented in this thesis is my own work.

During the course of this project I have held at different times scholarships from the C.S.I.R.O. and University of Tasmania.

P. McCulloch

P.M. McCulloch

November, 1968.

CONTENTS

SECTION A

# SUMMARY


## SECTION A Radio Emissions From Jupiter.

The thesis begins with a detailed review of the observed properties of Jupiter's decimetric and decametric radio emissions.

It then describes observations of the mean power of Jupiter's emissions at six frequencies in the range 4.7 to 28.0 MHz which were used to prepare histograms of relative power and probability of occurrence at each frequency. The spectral variations of mean flux density and peak flux density were determined and the data at several frequencies examined for the influence of Jupiter's satellite Io.

Observations of linear polarisation at 2500 MHz were made to determine the radio rotation period of Jupiter and the configuration of Jupiter's magnetic field.

An explanation of the decametric emission was sought in terms of natural emission from energetic charged particles. All emission processes other than Cerenkov and cyclotron radiation were eliminated on general grounds and further close examination of the Cerenkov process showed that it was unable to account for the observed size of the emission region and intensity of the radiation. Analysis shows that coherent cyclotron radiation can explain in detail the observed properties of the emission. This theory has been used to derive a model of Jupiter's magnetosphere which has a maximum electron density of about $10^6$/cc near the surface of Jupiter decreasing to 1500/cc when extrapolated to the orbit of Io. The magnetic field is basically a dipole closely centered on the disc

of Jupiter with a polar field strength of about 30 gauss. The dipole axis is tilted $10^{o}$ to the rotational axis with the longitude of the north magnetic pole near $200^{o}$ system III in February, 1967.

Using this model magnetosphere and the cyclotron process a theory has been developed to explain the influence of Io on the radiation. This theory proposes that Io's motion relative to Jupiter's magnetosphere accelerates large numbers of electrons which in turn emit low frequency electromagnetic waves. These waves propagate in the whistler mode towards the lower regions of Jupiter's magnetosphere where they interact with the electron streams by means of the gyroresonant interaction causing them to emit the decametric radiation. Sufficient energy may be transferred from the incoming whistler waves to the electron streams to induce them to emit cyclotron radiation above the local gyrofrequency. When allowance is made for the ray paths and attenuation of these waves the strength of the interaction is sufficient to account for the observed properties of the Io modulation. In particular it accounts for the enhanced emission at the appropriate orientations and longitudes of Io and explains the change in character of individual dynamic spectra with Io's position.

SECTION B Fine Structure in Solar Radio Emissions.

A new type of solar radio burst showing frequency splitting has been observed regularly below 60 MHz. The bursts have a duration of 1 - 2 sec and a frequency interval between their elements of 0.1 - 1.0 MHz. Their wave frequency generally decreases with time at about 0.1 MHz/sec. The bursts may occur either in isolation, in

chains associated with type III bursts, or in large numbers during noise storms. Triple splitting is observed in about 10% of the bursts. The properties of the bursts are consistent with those expected from magnetic splitting of the radiation.

CORRIGENDA

Page 61, line 7:

Duncan (1966) has suggested that Io controls theccommencement .....

should read

Duncan (1966) has suggested that Jupiters' rotation controls the commencement .....

Page 73, caption to figure 3.3

Add the following:

Note that the longitude system used here differs from that used in the original publications of Ellis and Mc Culloch.

## SECTION A

# RADIO EMISSIONS FROM JUPITER

# CHAPTER 1.

# REVIEW OF JUPITER'S DECIMETRIC EMISSIONS

## 1.1 Introduction.

Radio emissions from Jupiter were first observed by Mayer, McCullough and Sloanaker (1958a,b) at a wavelength of 3.15 cm. They obtained an equivalent disc temperature of $145 \pm 26^{\circ}$ K, in reasonable agreement with the infra red temperature of $130^{\circ}$ measured by Menzel, Coblentz and Lampland (1926).

Two years later Sloanaker (1959) made observations at a wavelength of 10 cm and obtained an equivalent disc temperature of $600^{\circ}$ K, much higher than expected. This result prompted observations over a much wider range of wavelengths by many researchers.

There have been a number of comprehensive reviews of these microwave emissions of Jupiter, the most important being by Roberts (1963, 1965). This review follows on from Roberts and includes important new observations.

## 1.2 The Spectrum of the Microwave Emission.

The spectrum of the emission over the decimetric and centimetric ranges is shown in Fig. 1.1. In the decimetric range the flux density is approximately constant having the value $6.7 \pm 1.0 \times 10^{-26}$ $Wm^{-2}$ $Hz^{-1}$ at the standard distance of 4.04 A.U., this being made up of the sum of two orthogonal polarisations. In the shorter wavelength range the contribution of the thermal emission from the disc becomes significant. The two components, thermal and non-thermal contribute equally at about 5,000 MHz with the thermal

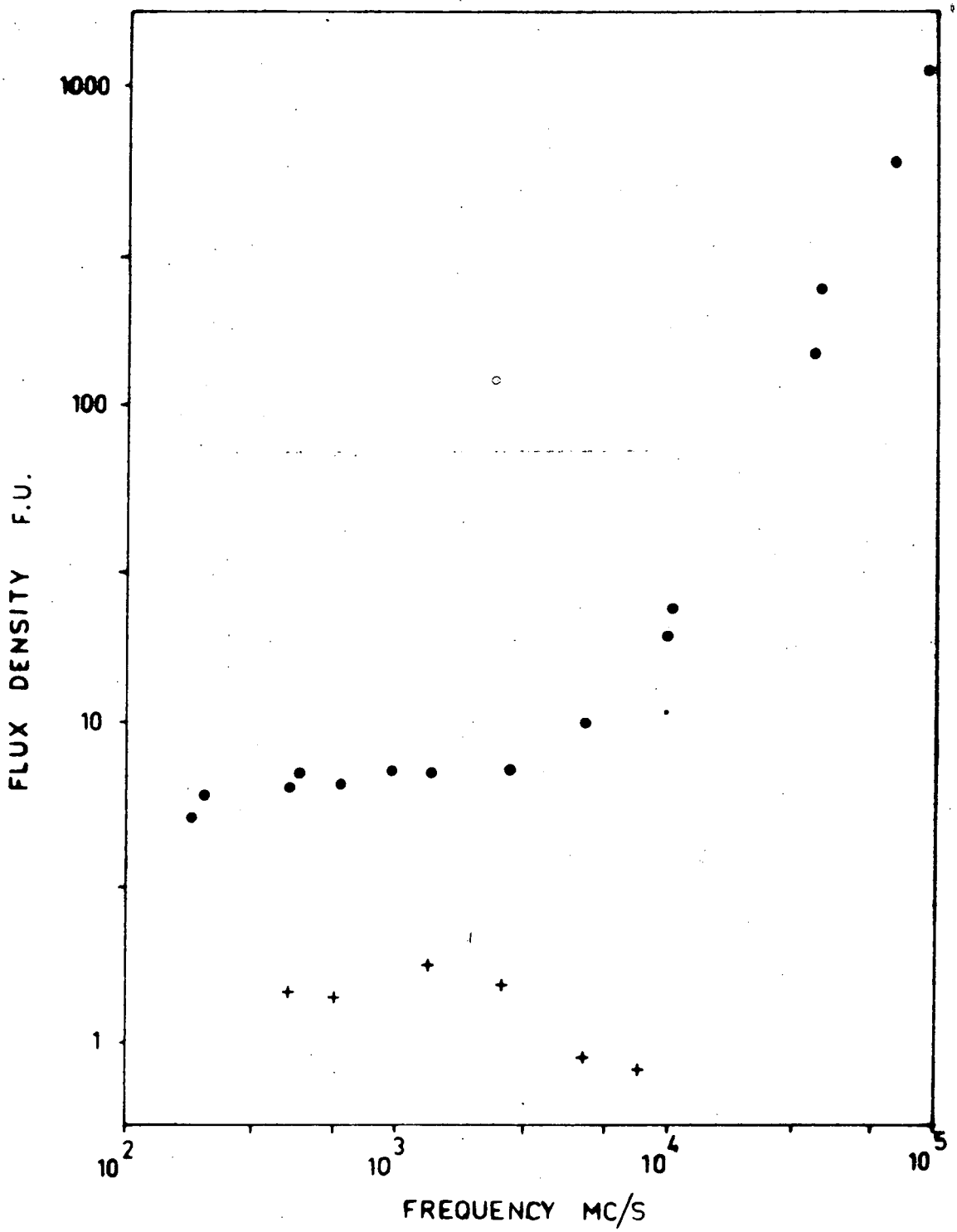


Figure 1.1 The spectrum of the microwave emissions from Jupiter at a distance of 4.04 A.U. The total flux density is shown by circles, and the polarised flux density by crosses.

component becoming increasingly important at shorter wavelengths. The actual contribution from the non-thermal source is difficult to determine at the highest frequencies because its contributions to the total emission is small and the thermal contribution cannot be estimated accurately due to absorption effects. However, the two components can be determined observationally by studying the angular distribution of the radiation. Berge (1964, 1965) working at 10.4 cm has found evidence that the disc component is about twice that expected on the basis of the infrared temperature. This has been confirmed at 21 cm by Branson (1968). However, at higher frequencies the results of Tolbert (1966) indicate a brightness temperature of about $110^{\circ}$ K. At the low frequency limit of observations of 178 MHz, Barber and Gower (1965) determined a flux density of $5.1 \pm 0.8 \times 10^{-26}$ $Wm^{-2}$ $Hz^{-1}$ which is an indication of a low frequency cut-off in the radiation.

Some of the earlier measurements of flux density indicated values which were significantly different from those given above (Drake and Hvatum 1960, Long and Elsmore 1960). However, it now appears that these results were due to observational difficulties.

## 1.3 Linear Polarisation.

Drake and Hvatum (1959) suggested that the Jupiter radiation might originate from electrons spiralling in a radiation belt surrounding Jupiter similar to the Van Allen belts surrounding the Earth. This idea was developed by several authors (Roberts and Stanley, 1959; Field, 1959, 1960, 1961; Chang and Davis, 1962) and two main theories were developed invoking synchrotron and cyclotron radiation

as the source of the emissions. Predictions of the polarisation properties of the radiation led Radhakrishnan and Roberts (1960) to search for linear polarisation. They found that at a wavelength of 31 cm the radiation was 20 to 30 per cent linearly polarised with the E-vector approximately in the equatorial plane of the planet.

More recent observations have shown that the polarised component of the extrathermal emission is essentially constant over the range from 300 MHz to 2650 MHz (Fig. 1.1). It is approximately $1.5 \times 10^{-26}$ $Wm^{-2}$ $Hz^{-1}$ and the degree of polarisation of the extrathermal emission is about 0.22. The polarised component appears to decrease at higher frequencies so that at 8000 MHz it amounts to only $0.8 \times 10^{-26}$ $Wm^{-2}$ $Hz^{-1}$. However, due to confusion between the thermal and extrathermal components at these frequencies, it is not clear whether this decrease is due to a decrease in the percentage polarisation of the extrathermal component, or an overall decrease in the contribution from this component.

## 1.4 Rocking of the Plane of Polarisation.

In 1961 Morris and Berge (1962) discovered that the direction of polarisation was not constant, but as the planet revolved the direction rocked through about $\pm 10^{\circ}$ from a mean value almost perpendicular to the axis of rotation. Theoretical predictions that the direction of polarisation of the radiation is determined by the direction of the magnetic field led Morris and Berge to suggest that the magnetic axis on Jupiter was displaced $10^{\circ}$ from the rotational axis. As the planet rotates the mean direction of the magnetic field as seen from the Earth rocks first to one side and then to the other

side of the rotational axis.

The most comprehensive observations of the rocking of the plane of polarisation were made by Roberts and Komesaroff (1964, 1965). They found that the pole in the northern hemisphere of Jupiter is located at $193^{o} \pm 8^{o}$ and is displaced $10.0 \pm 0.5^{o}$ from the axis of rotation. The rocking of the plane of polarisation as recorded by Roberts and Komesaroff at 11.3 and 21 cm is shown in Fig. 1.2. The curves show a distinct departure from a sine wave, which is due mainly to a second harmonic term, amounting to 7% in the 11.3 cm data and 15% in the 21 cm data. This departure from a sinusoidal form apparently indicates some asymmetry in the magnetic field of Jupiter, although a similar effect may be observed due to variable shadowing of the emitting regions by the planet itself. This shadowing hypothesis is however, only likely to produce the required effect if there is appreciable radiation from an asymmetrically placed belt close to the planet.

By observing the rocking of the plane of polarisation, the rotation period of the magnetic field of Jupiter can be determined. Curves such as those in Fig. 1.2 are based on about one week's observing and indicate that the rotation period is close to system III. More accuracy is obtained if curves obtained many months apart are compared. Roberts and Komesaroff using a baseline of twelve months obtained a rotation period within $0.5^{s}$ of I.A.U. system III. Davies and Williams (1966) using data obtained over a period of 3.5 years determined the rotation period as $9^{h}\ 55^{m}\ 29.50^{s} \pm 0.29^{s}$, which is $0.13^{s}$ longer than system III.

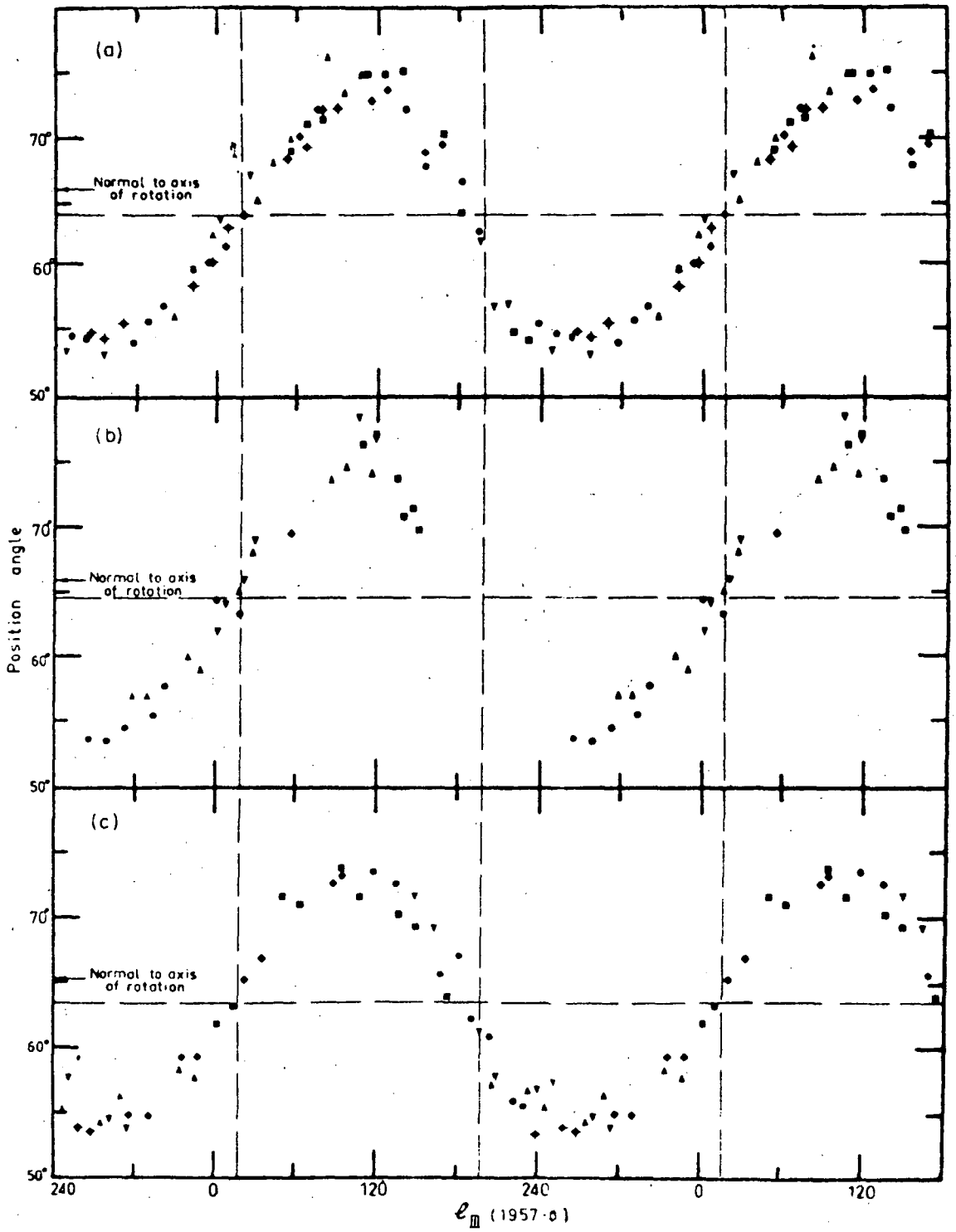


Figure 1.2 Position angle of the maximum electric vector of the received Jovian radiation as a function of system III longitude.
(a) 21 cm August 1963 (b) 21 cm August - September 1962
(c) 11.3 cm November 1963. (Roberts and Komesaroff, 1964)

## 1.5 Circular Polarisation.

Berge (1965) made a series of observations of Jupiter at 21 cm using the two element interferometer at the Owens Valley Radio Observatory. He obtained the data from which the existence of a circularly polarised component in Jupiter's decimetric radiation was first recognised. This is plotted in Fig. 1.3, and represents the difference in phase between a crossed-horn measurement with the E-vectors of the feed horns at $45^{\circ}$ on either side of Jupiter's equatorial direction and a parallel-horn measurement. Two different cases are shown, one with the parallel-horn arrangement aligned along the equatorial direction. Both give very nearly the same average variation as a function of system III longitude. The systematic deviation of the phase difference from zero is interpreted as being due to a small, variable amount of circularly polarised radiation. Similar measurements have been made at a wavelength of 10.6 cm, giving a similar result, but with the amplitude of the variation only three-fourths as great.

This observation of circular polarisation allows a direct determination of the sense of Jupiter's magnetic field. In the region near $150^{\circ}$ system III, the sense is left handed and the magnetic axis is tipped towards the Earth at the north. This means that the magnetic pole in the northern hemisphere is a north magnetic pole, and the one in the southern hemisphere is a south magnetic pole.

Morris, Komesaroff and Roberts (1967) have made direct measurements of the circularly polarised component at 20 cm; they find a cyclic variation with a maximum of about 2% circular polarisation which occurs near $180^{\circ}$ system III and is in the same sense as that

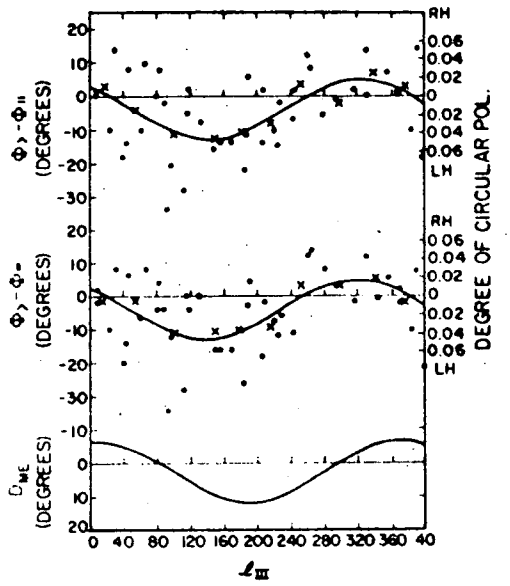


Figure 1.3 The upper graphs show the evidence for circular polarisation at 21.2 cm. The filled circles are data points, the crosses are means for 40° of longitude, and the curves are least squares fits of a sinusoid to the data. The lower curve represents the magnetic declination of the Earth. (Berge, 1965)

reported by Berge. The longitude of maximum circular polarisation as recorded by Morris, Komesaroff and Roberts, agrees very closely with the positions of the magnetic poles as recorded by Roberts and Komesaroff (1964).

## 1.6 Variation of Intensity.

A variation of the total intensity as the planet rotates has been reported by several authors, (McClain, 1959; Morris and Berge, 1962; Gary, 1963; Rose, Bologna and Sloanaker, 1963; Bash, Drake, Gunderman and Heiles, 1964; Roberts and Komesaroff, 1964, 1965; Roberts and Ekers, 1965; Davies and Williams, 1966; Kazes, 1965; Barber, 1966). In some of these observations only one plane of polarisation was recorded so that the effects of the rocking of the plane of polarisation and the variation of the total intensity cannot be uniquely separated. Figure 1.4 shows observations in which at least two orthogonal polarisations were recorded (Roberts and Komesaroff, 1965; Roberts and Ekers, 1965). The results at wavelengths of 11.3 cm, 21 cm and 48 cm are all very similar. The total intensity has two approximately equal maxima per revolution, with the minimum near longitude 198° somewhat lower than the minimum near longitude 18°. Barber (1966) working at a wavelength of 49 cm has found that the total intensity varies in a similar manner.

Several authors (Drake and Hvatum, 1960; Sloanaker and Boland, 1961; McClain, Nichols and Waak, 1962; Roberts 1962 a, b; Roberts and Huguenin, 1963) have reported long term variations in the total intensity, and have suggested correlations with solar activity. However, that constancy of the total flux as shown in Fig. 1.4 between

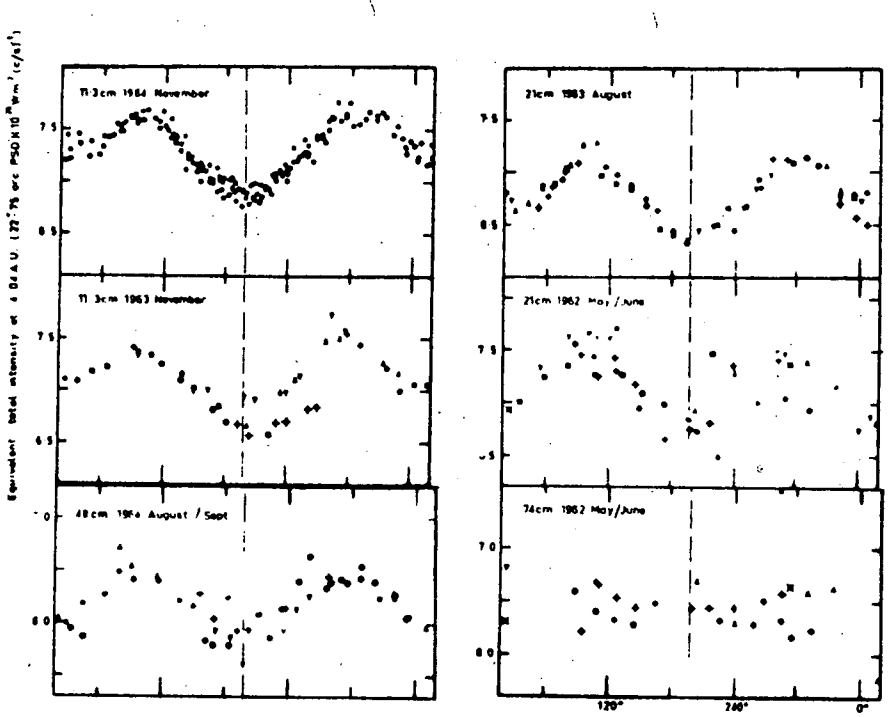


Figure 1.4 Variation of the total flux densities as Jupiter revolves. The flux densities have been normalised to a distance of 4.04 A.U. In all except the November 1964 11.3 cm data, different symbols are used for different observing days. (Roberts and Komesaroff, 1965; Roberts and Ekers, 1966)

1962 and 1963 at 21 cm, and between 1963 and 1964 at 11.3 cm, indicates that any variations that may occur are less than 4% and are within the measurement errors. Bash, et al, (1964) also set a very low limit to long term changes in intensity, and Dickel (1965) and Barber (1966) have failed to find any effect due to the Jovian satellite Io.

The features of the variation of intensity with longitude are sufficiently stable to provide a means of determining the rotation rate of the Jovian magnetic field. Roberts (1965) and Barber (1966) have both used this method and find that the rotation rate is coincident with I.A.U. system III to $\pm$ 0.8 sec.

## 1.7 Beaming of the Radiation.

In order to explain the variation in the total intensity and the degree of polarisation as the planet rotates, it has been supposed that the radiation is beamed towards the magnetic equator (Gary, 1963; Bash et al, 1964; Roberts and Komesaroff, 1965; Barber, 1966). Using this beaming effect and combining the tilt of the magnetic axis to the rotation axis with the present tilt of the north rotational pole towards the Earth, the qualitative features of the observations are reproduced.

If the emission were symmetric about the magnetic axis and the magnetic equator, the total intensity of the radiation would depend only on the Jovomagnetic latitude of the Earth $\varphi$. However, if the data of Figure 1.4 are replotted as a function of magnetic latitude as in Figure 1.5a, it is seen that this is not true. When the Earth is at northern magnetic latitudes (open circles in Figure 1.5a) the intensity decreases approximately as $\cos^{4.5}\varphi$, but at southern mag-

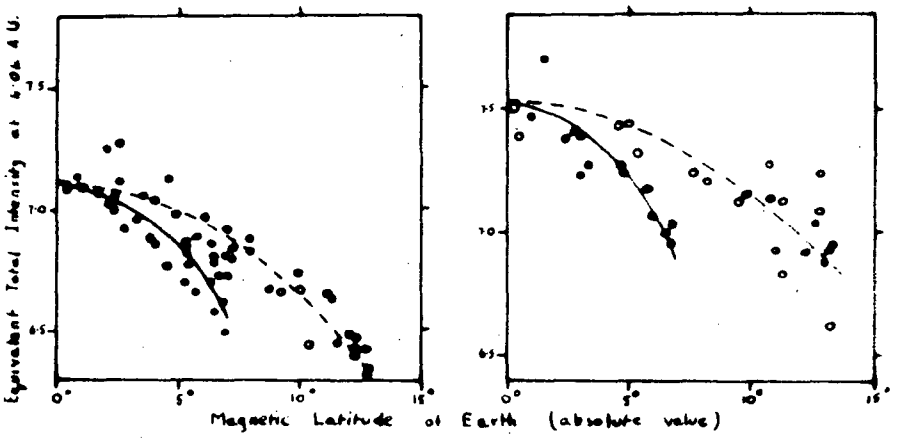


Figure 1.5a The variation of total intensity as a function of the Jovomagnetic latitude of the Earth. Points for northern latitudes are open circles, those for southern latitudes are filled circles. (Roberts, 1965)

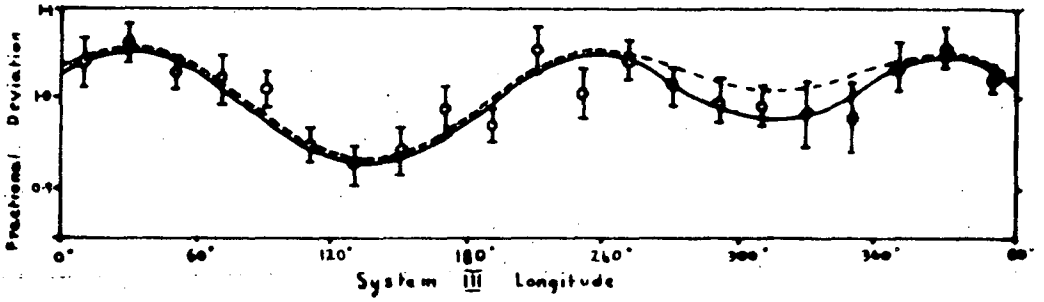


Figure 1.5b Fractional deviation of the total intensity due to the beaming effect. The points shown are means over $20^{\circ}$ of longitude. The continuous curve has been fitted to the data, while the dashed curve represents a $\cos^5$ dependence of the flux on the Jovomagnetic latitude of the Earth. (Barber, 1966)

netic latitudes (filled circles), it decreases more rapidly, approximately as $\cos^{10}\varphi$. In other words, the minimum near longitude $18^{\circ}$ is relatively deeper than would be expected. This is illustrated in Fig. 1.5b (from Barber, 1966) for 49 cm radiation, the dashed curve illustrates beaming as $\cos^{5}\varphi$ whereas the full curve is a better representation of the data and goes as $\cos^{8}\varphi$ in the region $300^{\circ} <$ longitude $< 80^{\circ}$.

This qualitative disagreement with the symmetrical model is not altered by small changes in the parameters adopted - unless one is prepared to change the tilt of the axis of rotation. Roberts and Komesaroff therefore conclude that this is additional evidence for departures of the field from that of a dipole.

## 1.8 Shape and Location of the Radiation Source.

Using the two 90' radio telescopes of the Caltech Interferometer, Radhakrishnan and Roberts (1960) showed that the E-W angular extent of the source at 31 cm was several times the diameter of the planet. The same instrument was used later by Morris and Berge (1962) to measure both the E-W and N-S angular sizes at 21 cm and 31 cm and has been used by Berge (1964, 1965) to produce a complete map of the brightness over the source at wavelengths of 10.4 cm and 21.2 cm. Figure 1.6a shows the map produced by Berge at 10.4 cm for a longitude of $20^{\circ}$. The corresponding model determined at 21.2 cm is essentially the same except that the flux from the disc is reduced due to the drop in the contribution of the thermal source at the longer wavelength.

Branson (1968) using the techniques of aparture synthesis has mapped the distribution of brightness of the source at wave-

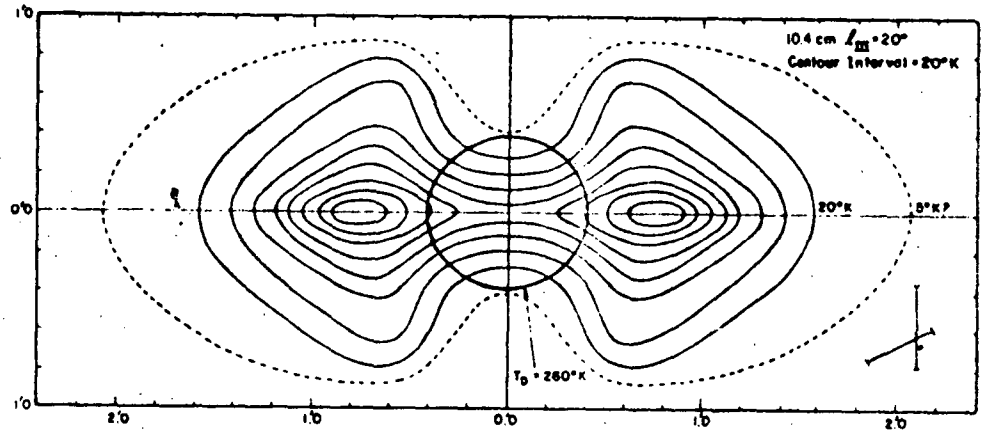


Figure 1.6a The 10.4 cm brightness distribution determined for a system III longitude of 20°. The scale, in minutes of arc, refers to a distance of 4.04 A.U. (Berge, 1965)

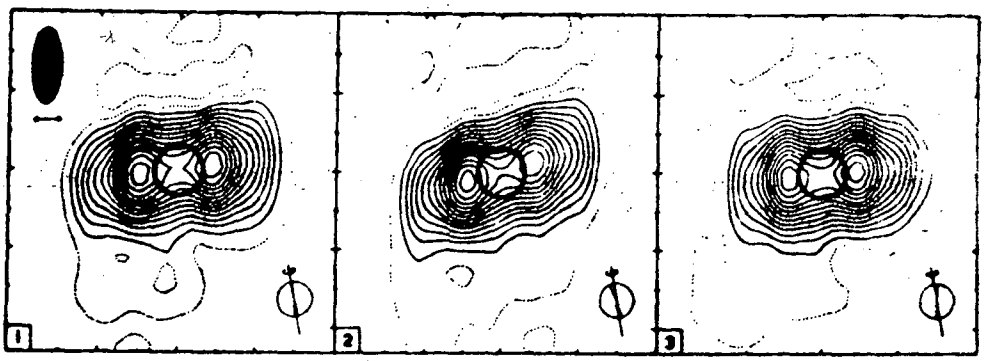


Figure 1.6b Maps of Jupiter at 21 cm for central meridian longitudes of 15°, 135° and 255° respectively. In each map north is at the top and east is at the left, and the half power beamwidth and direction of polarisation are shown in the top left hand corner of Map 1. The planet is at a distance of 4.8 A.U. and the contour intervals are 47°K. (Branson, 1968)

lengths of 21 cm and 74 cm. Figure (1.6b) shows brightness contours at 21 cm for central meridian longitudes of $15^{o}$, $135^{o}$, and $255^{o}$. The disc of the planet is shown by the dark circles.

Two lunar occultations of the Jovian radio source have been recorded Roberts and Komesaroff (1965). The occultation results confirm the broad details derived from interferometry, and suggest that the shape of the source does not change appreciably over the wavelength range from 21 cm to 74 cm.

Barber (1966) has recently measured the E-W diameter of the source at 49 cm and found it to be 3.6 planetary diameters. He also found that the apparent diameter varied with the longitude of Jupiter in such a way as to be consistent with an elliptical source elongated along Jupiter's magnetic equator which is inclined at an angle of $10.1^{o}$ to the rotation axis. This gives an independent determination of the inclination of the magnetic axis and confirmed Roberts and Komesaroff (1964) results.

The equatorial extent of Jupiter's emission region at 74 cm has been measured by McAdam (1966) using the E-W arm of the 1 mile Mills Cross which has a fan beam of 88" arc. More than 80% of the radiation was found to originate from a symmetrical double source centered 1.6 radii each side of the discs center. A second region which contributes 20% of the emission lies much further out at 6 to 7 radii.

At centimetric wavelengths Korol'jov, Pariiskii and Timofeeva (1964) and Gol'ner, Lipovka and Pariiskii (1965) have measured the angular size of the source. At 3.02 cm they find that 95% of the radiation comes from a region 1.1 times the diameter of the planet,

while at 6.5 cm the emitting region is equivalent to a gaussian source with a diameter of 1.25 planetary diameters.

## 1.9 Location of the Radio Source in Relation to the Planet.

Roberts and Ekers (1965) used a pencil beam instrument to make direct observations of the position of Jupiter relative to nearby radio sources. They found that the radio centroid agreed with the position of the center of the planet's disc to within $\pm$ 0.1 radii in right ascension and $\pm$ 0.3 radii in declination (Roberts, 1965). Observations made by McAdam (1966) suggest that if only the central part of the emission is considered it precedes the center of the optical disc by 0.14 $\pm$ 0.07 radii in right ascension; however if the extended emission is considered, the centroid coincides with the optical center.

The observations of Branson (1968) Figure (1.6b) show that the radiation belts are centered on the disc of Jupiter to better than a tenth of a radius. They also show a small asymmetry located near the north magnetic pole, which is consistent with other observations of a distortion in Jupiter's dipole field.

## 1.10 Theoretical Model.

The synchrotron and cyclotron theories of the emission involve radically different predictions about the properties of the radiation. The most obvious of these is that for cyclotron radiation the size of the emission region will be proportional to the inverse cube root of the frequency, while for synchrotron radiation the source size will be independent of frequency. Field (1960) has

shown that, for cyclotron radiation, the degree of polarisation would be strongly frequency dependent, whereas Chang and Davis (1962) have shown that for synchrotron radiation the degree of polarisation is substantially constant over a range of frequencies of more than 20:1. The results reported here are incompatable with the cyclotron process which has been abandoned in favour of a model based on synchrotron radiation.

The synchrotron radiation is produced when high energy electrons oscillate in Jovian van Allen belts. The results of Berge (1965) suggest that there are two radiation belts contributing to the emission at 10.4 and 21 cm, one having an equatorial extent of about two radii containing electrons with pitch angles $\varphi$ near $90^{\circ}$, and the other at $3\frac{1}{2}$ radii containing electrons with pitch angles distributed uniformly over the range $\sin \varphi \geq 0.4$. The two pitch angle distributions mentioned above were deduced by Roberts and Komesaroff (1964) by applying the theory of synchrotron radiation to observations from northern magnetic latitudes. The observations of McAdam (1966) at 49 cm suggests the existence of a third belt at about 8 radii with pitch angles of about $40^{\circ}$. The field intensity in this belt would be significantly lower than in the inner belts and hence the low critical frequency would ensure that it was not visible at higher frequencies.

Barber and Gower (1965) have examined the spectrum of the emission and find that it is consistent with mono-energetic electrons having a cutoff frequency of 3000 MHz, which corresponds to an energy of about 10 Mev. The number of electrons needed to produce the radiation is then about $10^{28}$. They were not aware of the presence of the third outer radiation belt which could contain a large proportion

of low energy electrons, which would allow a flat spectrum for the integrated radio flux, with a steep electron energy spectrum.

$$N(E) \propto E^{-\gamma} \quad \text{with } \gamma > 1$$

No satisfactory theory has been proposed as to the source of the large numbers of high energy electrons required. Field (1960) has shown that enhanced radiation from primary cosmic ray electrons is not sufficient, and so the primary source of electrons appears to be the Sun. Due to the intermittent nature of the solar wind and the exceptional constancy of the radiated flux over a period of years, the mean life of an electron in the Jovian van Allen belts would need to be very long.

Several authors have given estimates of the parameters relevant to the synchrotron emission from Jupiter. For example, Chang and Davis (1962) suggest that the field in the emitting region should be in the range of 0.1 - 1.0 gauss, that the electrons have energies in the 5 - 75 Mev range with densities of the order of $10^{-2}$ to $10^{-3}$ $cm^{-3}$.

Field gives the following values, field strength 0.30 gauss electron energy, assumed nonenergetic, 21 Mev and electron density of $7 \times 10^{-2}$ $cm^{-3}$.

## 1.11 Summary.

The basic information that has been obtained is:-

Jupiter's decimetric emission is synchrotron radiation from electrons in van Allen belts associated with a dipole field. The magnetic axis is inclined at $10^{o}$ to the rotation axis and the longitude of the north magnetic pole is $193^{o} \pm 8^{o}$.

The magnetic field shows deviations from that of a pure dipole, and the field intensity in the neighbourhood of the emission regions is in the range 0.1 to 1 gauss, corresponding to a polar field intensity of approximately 15 gauss. The magnetic axis is closely centered on the optical disc of the planet.

## 1.12 References.


BARBER, D. (1966) Mon. Not. R. Astr. Soc 133, 285-308

BARBER, D., J.F.R. GOWER (1965) J. Res. Nat. Bureau Standards 69D, 1563.

BASH, F.N., F.D. DRAKE, E. GUNDERMAN and C.E. HEILES (1964) Astrophys J. 139, 975-985.

BERGE, G.L. (1964) paper presented to the A.A.S. meeting, Montreal.

BERGE, G.L. (1965) J. Res. Nat. Bureau Standards 69D, 1552-1556

BRANSON, N.F.B.A. (1968) Mon. Not. R. Astr. Soc 139, 155-162

CHANG, D.B. and L. DAVIS (1962) Astrophys J. 136, 567-581

DAVIES, R.D. and D. WILLIAMS (1966) Planet Space Sci. 14, 15-32.

DICKEL, J.R. (1965) paper presented at the A.A.S. meeting, Lexington.

DRAKE, F.D. and S. HVATUM (1959) Astron. J. 64, 329-330

FIELD, G.B. (1959) J.G.R. 64, 329-330

FIELD, G.B. (1960) J.G.R. 65, 1661-1671

FIELD, G.B. (1961) J.G.R. 66, 1395-1405

GARY, B. (1963) Astron. J. 68, 568-572

GOL'NER, V. Ya, N.M. LIPOVKA, and Yu.N. PARIISKII (1965) Soviet Phys. Dokl. 9. 512-514.

GOWER, J.F.R. (1963) Nature 199, 1273

HADDOCK, F.T. and J.R. DICKEL (1963) Trans. Am. Geophys. Union 44, 886.

KAZES, I. (1965) J. Res. Nat. Bureau Standards 69D, 1561-1563

KOROL'JOV, D.V., Yu.N. PARIISKII, and G.M. TIMOFEEVA (1964) Astron. Tsirkuliar No. 283, 1.

McADAM, W.B. (1966) Planet Space Sci 14, 1041-1046

McCLAIN, E.F. (1959) Astron. J. 64, 339-340

McCLAIN, E.F., J.H. NICHOLS, and J.A. WAAK (1962) Astron. J 67, 724-727.

MAYER, C.H. (1961) The Solar System 3, Planets and Satellites ed. G.P. Kuiper and B.M. Middlehurst pp 442-472

MAYER, C.H., T.P. McCULLOUGH, and R.M. SLOANAKER (1958a) Astrophys J. 127, 11-16

MAYER, C.H., T.P. McCULLOUGH and R.M. SLOANAKER (1958b) Proc. Inst Radio Engrs. 46, 260-266

MENZEL, D.H., W.W. COBLENTZ, and C.O. LAMPLAND (1926) Astrophys J. 63, 177-187

MORRIS, D. and G.L. BERGE (1962) Astrophys J. 136, 276-282

MORRIS, D., M.M. KOMESAROFF, and J.A. ROBERTS (1967) Private Comm.

RADHAKRISHNAN, V. and J.A. ROBERTS (1960) Phys. Rev Let. 4, 493-4

ROBERTS, J.A. (1963) Planet, Space Sci 11, 221-259

ROBERTS, J.A. and G.J. STANLEY (1959) Pub. Astron Soc Pacific 71, 485-496

ROBERTS, J.A. (1965) J. Res. Nat. Bureau Standards 69D, 1543-1552

ROBERTS, J.A. and R.D. EKERS (1965) Icarus 5, 149-153

ROBERTS, J.A. and M.M. KOMESAROFF (1964) Nature 203, 827-830

ROBERTS, J.A. and M.M. KOMESAROFF (1965) Icarus 4, 127-156

ROBERTS, M.S. (1962a) Astron. J. 67, 280

ROBERTS, M.S. (1962b) I.R.E. Trans. Ant. Prop AP-10, 494-495

ROBERTS, M.S. and G.R. HUGUENIN (1963) Mem. Soc. Roy. Sci Liege 7, 569-587

ROSE, W.K., J.M. BOLOGNA, and R.M. SLOANAKER (1963) Astron J 68, 78

SLOANAKER, R.M. (1959) Astron J. 64, 346

SLOANAKER, R.M. and J.W. BOLAND (1961) Astrophys J. 133, 649-656

THORNTON, D.D. and W.J. WELCH (1963) Icarus 2, 228-232

TOLBERT, C.W. (1966) Astron. J. 71, 30-32

# CHAPTER 2.

## REVIEW OF OBSERVATION OF JUPITER'S DECAMETRIC EMISSIONS

### 2.1 Introduction.

In 1954 Burke and Franklin (1955) discovered that Jupiter emits intense bursts of radio emission in the decametric band. The intensity of these bursts often exceeds that of any other known cosmic source of radio emission with the exception of the disturbed sun.

Several reviews of observations of Jupiter's decametric emissions have been published, among the most comprehensive of which are those of Roberts (1963), Douglas (1964) and Warwick (1964).

### 2.2 Burst Structure.

The radiation was found to be quite sporadic and occurs as a series of short bursts which are grouped together to form a storm which may last from a few minutes to several hours. The duration of the individual bursts may range from a fraction of a second up to many seconds; however bursts have been observed with durations of the order of a few milliseconds, Kraus (1956), Gallet and Bowles (1956), Gallet (1961) and Baart et al (1966). The durations of the bursts appear to fall in four distinct categories, which are described in Table (2.1). A typical record of part of a storm recorded by Douglas (1964) is shown in Figure (2.1) which illustrates three of the four types of bursts. Figure (2.1a) is composed of clumps of radiation or burst groups, each lasting a minute or two and possessing unresolved fine structure. These bursts would be classified type L. Figure (2.1b) made with a high speed photographic recorder and time

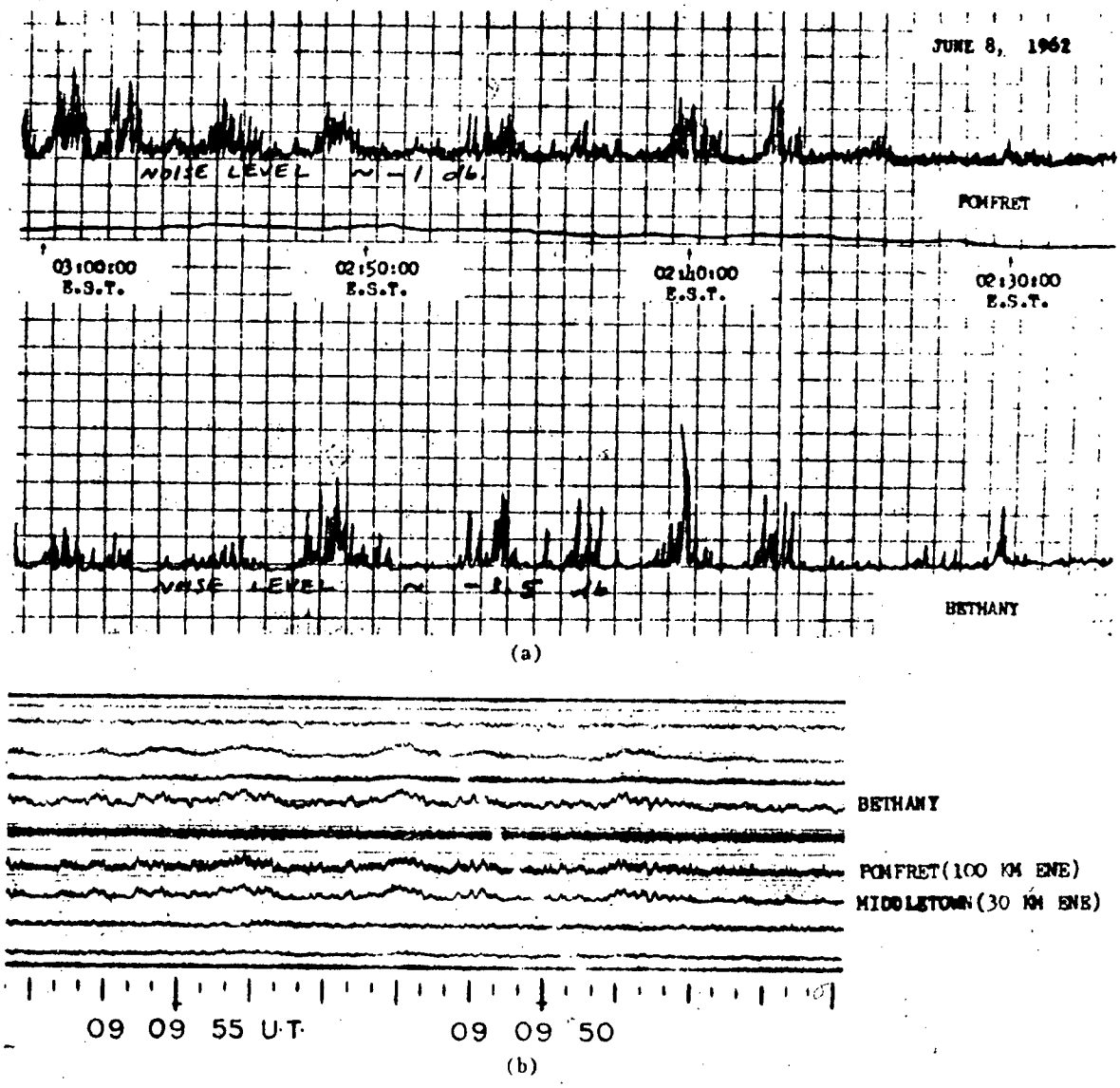


Figure 2.1 (a) Jupiter 22.2 MHz total-power tracings produced on a common recorder by a set of identical antennae and receivers located at Bethany and Pomfret, Connecticut, separated by 100 km on an ENE line.

(b) A 10 sec portion of a high speed recording of the Jupiter storm of July 18, 1961, showing close correlation of fine structure at three spaced receivers. (Douglas, 1964)

constant of 30 msec, shows ten seconds of a burst group. The spike like structure unresolved in (a) is seen in (b) as a gentle rise and fall of a second's duration, which corresponds to type N, although Gallet called these features L pulses. Superimposed on the N pulses, shorter pulses are seen, having durations of less than 0.1 sec. and hence presumably correspond to the S pulses referred to in the above classification.

Observations made by Ellis (1962) and Carr et al (1965) suggest that at lower frequencies the duration of the noise bursts lengthen, being about 10 to 100 secs at 6 MHz while at 10 MHz and higher the majority are between 1 and 10 secs in length.

Douglas and Smith (1963) have reported that Jupiter storms are usually characterised by an hierarchy of structure with elements having durations ranging from about 0.01 sec (perhaps less) up to many minutes. The strong or main phase of a Jupiter storm tends to last for about 20 to 30 minutes, and is often characterised by an active plateau (which may be distorted by scintillations) having rather abrupt beginning or ending with a rise or fall time which is usually around 5 minutes, but may be much less. Long storms usually have several such periods of enhanced activity. Under favourable conditions a weak pre-cursor or post-cursor may be found. Such noise storms are typically 5 to 10 times weaker than the main storm and suggest that very weak activity may almost always occur. This is supported by the observations of Alexander and Stone (1964) who found that at 26.3 MHz the radiation could be divided into two groups, one involving a large concentration of activity at low intensities and a smaller secondary peak at higher intensities.

| CHARACTER OF EMISSION | | SUGGESTED N.A.S.A. CLASSIFICATION | NAME |
|---|---|---|---|
| BURST TYPE | TIME SCALE IN SECS. | | |
| Very Short | Less than 0.05 | | I |
| Short | 0.05 - 0.2 | 1 | S |
| Normal | 0.2 - 2.0 | 2 | N |
| Long | Greater than 2.0 | 3 | L |

Table (2.1)

Not all noise storms possess all four elements of the structure discussed above, Douglas (1964). The I pulses are relatively rare and when present, usually continue throughout the entire storm. Burst groups may merge, giving the storm the appearance of 10 to 15 minutes of rather continuous burst like activity. L pulses are almost continuous emissions with bursts superimposed.

Gardner and Shain (1958) made the first attempt to determine to what extent the short period structure in the Jupiter decametric radiation was either produced or modified by the ionosphere. In three pairs of records made at two sites 25 km apart they found considerable differences in burst structure. Subsequent observations have been made over various baselines by Smith and Douglas (1959, 1961) and by Smith et al (1960) and Slee and Higgins (1963), which combine to show that all degrees of correlation can be obtained. At times there is very little correlation between relatively closely spaced sites; at other times there is a very good correlation at widely spaced sites. Figure (2.1a) shows fair correlation between

L bursts recorded at sites 100 km apart, while Figure (2.1b) shows very close correlation between S pulses recorded over the same baseline.

These results are consistent with the theory that the Jovian emissions impinging on the Earth's ionosphere are in the form of bursts which, in passing through the ionosphere, are often severely modulated by scintillations.

Douglas and Smith (1961, 1962) have found that the L and N pulses may display all degrees of correlation. In many cases where envelope correlation is sufficiently good to permit recognition of equivalent events at two sites, a systematic time lag is seen, which on different records may be anything from $0^s$ to $\pm 1^s$, and remains constant for many minutes during a particular storm. The observed sense of time lag seems to reverse at opposition; this led Smith to suggest an origin of the L and N pulses in a diffraction process by interplanetary electron clouds whose motion perpendicular to the Earth-Jupiter line might be expected to change at opposition. These observations have been supported by Slee and Higgins (1966), Douglas and Smith (1967) and Riihimaa (1968), and it now appears certain that the 1 - 10 sec component of the burst structure originates in interplanetary scintillations. Slee and Gent (1967) have concluded that the fine structure in the emission with periods of 0.2 and 10 msec is not due to interplanetary scintillations but comes from the planet itself.

## 2.3 Rotational Period.

Following Burke and Franklin's discovery, Shain (1955, 1956) examined 18.3 MHz records of cosmic noise made in 1951 and

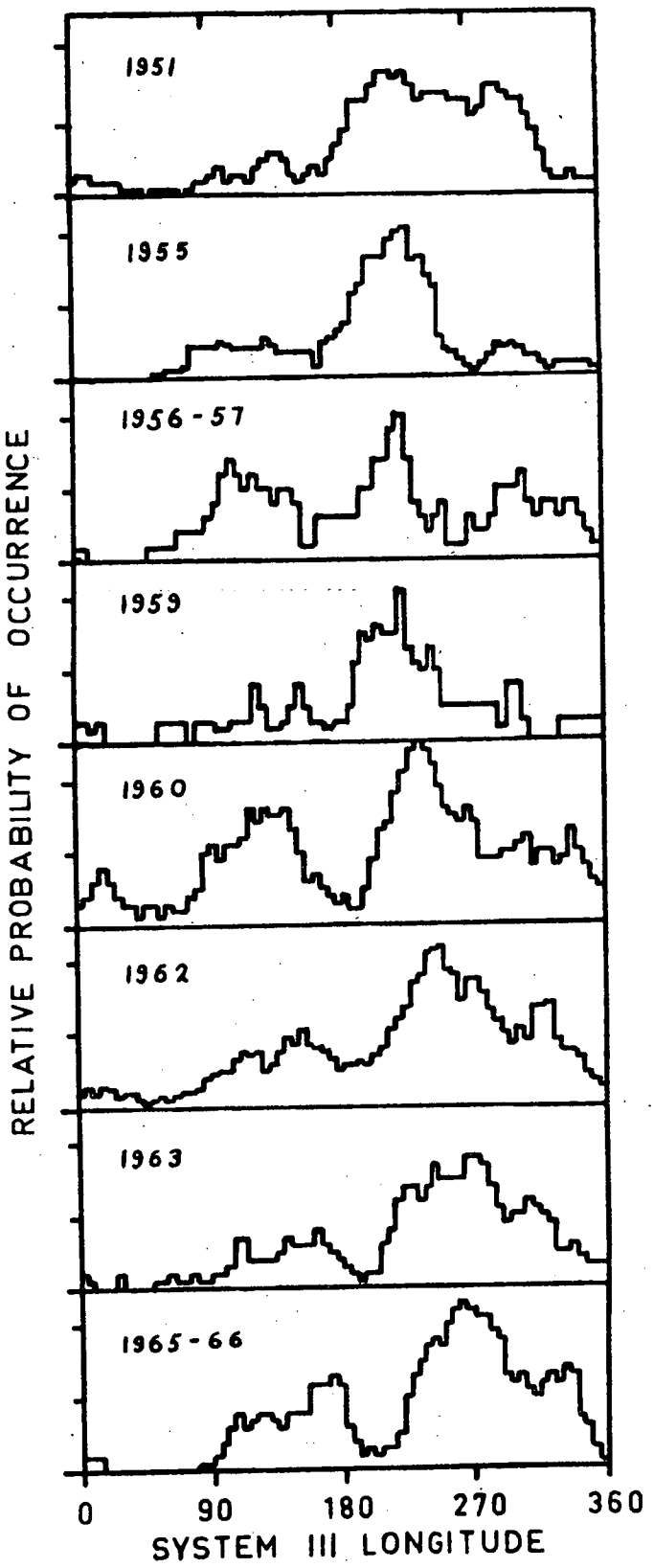


Figure 2.2 Longitude profiles of probability of occurrence at frequencies near 18 MHz for different apparitions between 1951 and 1965-66.

found that Jupiter radiation had frequently been recorded in that period but had been disregarded as interference. He had one set of observations which were made with equipment which was capable of observing Jupiter for 8 hours a day. The records covered 120 rotations of the planet and analysis showed a definite recurrence tendency with this period.

When the times of burst activity were plotted against the system I longitude of the central meridian on Jupiter, they showed a definite drifting tendency, but when system II longitudes were employed, there was very little drift. These two systems of longitude describe the mean rate of rotation of the clouds seen in the equatorial and temperate zones of the planet. Shain concluded that the source of radiation rotated with the planet, at a rate approximately equal to the system II rate, but somewhat faster.

Shain superimposed all the occurrences of emission that had been recorded, allowing for the slight difference in period from system II, and produced a histogram of the number of occurrences of radiation from Jupiter against the longitude of the central meridian of the planet. This is shown in Figure (2.2). The Figure suggests that there are one or more sources of emission around the planet with individual polar diagrams less than $180^{o}$ in width.

This finding of Shain has been confirmed by many authors. Gallet and Bowles (1956), Gallet (1957, 1961), Burke (1957), Franklin and Burke (1958), Gardner and Shain (1958), Carr et al (1958, 1961), Smith and Carr (1959), Douglas (1960) and Burke (1961) have all concluded that the emission from Jupiter at frequencies between 15 and 30 MHz recurs statistically with a period which is somewhat shorter

than the period of system II. It is now generally accepted that this period is the rotation period of the solid body of the planet beneath the clouds. Douglas (1960) and Carr et al (1961) have made detailed statistical analysis of data obtained prior to 1961 in order to determine the period. Douglas determined the value $9^h\ 55^m\ 29.27^s \pm 0.13^s$ while Carr et al gave the period as $9^h\ 55^m\ 29.35^s$. Many observers have realised the need to adopt a suitable system of longitude for use with the radio data and in 1962 a Working Group of Commission 40 of the International Astronautical Union (1962) recommended that a period of $9^h\ 55^m\ 29.37^s$ be adopted, the system to coincide with system II longitudes at $0^h$ U.T. on January 1, 1957. This system has been designated System III and is used throughout this thesis except where otherwise specified.

The system III period defined above represents an average period over the interval 1950-60, in which small yearly fluctuations can have gone unnoticed. Douglas and Smith (1963) have found clear-cut evidence for a change in Jupiter's apparent rotation period sometime between 1961 and 1962. Figure (2.2) shows histograms of the probability of occurrence of Jupiter radiation at frequencies near 20 MHz against system III longitude for various years over the period 1951-66. The shift in position of the major peak in the diagram since 1960 is easily recognisable.

Smith et al (1965) have confirmed the observation that Jupiter's rotation period has changed, and give an increase in period of $1.17^s$. They point out the interesting feature that the Great Red Spot underwent a similar change in period at nearly the same time, after a long period of relatively stable motion.

Dulk (1965) has found evidence for a change in rotation period over the interval 1961-65. He determined the rotation period by three methods; by comparing longitude profiles, by cross correlating longitude profiles, and by comparing so called "permanent" feature on dynamic spectra of Jupiter's emissions. These spectra will be discussed in a later section. All of these methods indicated a period longer than system III; however different periods were obtained using different methods. These are summarised in Table (2.2). The differences in the results are beyond the probable errors in the methods and hence an explanation must be sought. The longitude at which a certain spectral feature occurs would depend only on the emission pattern of the source, while the position of a peak in a longitude profile will depend on the probability of emission from each region of the planet as well. The different periods determined by them may well provide information about the factors influencing emission from Jupiter.

| APPARITION | CHANGE IN PERIOD FROM SYSTEM III | | |
|---|---|---|---|
| | COMPARISON OF LONG. PROFILES | CROSS-CORRELATION OF LONG. PROFILES | COMPARISON OF SPECTRAL FEATURES |
| 1961-62 | + 0.8 s | + 1.0 s | + 0.1 s |
| 1962-63 | + 0.4 s | + 0.3 s | + 0.8 s |
| 1963-64 | + 0.4 s | + 0.1 s | 0 |
| 1964-65 | | | - 0.2 s |

Table (2.2)

Gulkis and Carr (1966) have suggested that the apparent rotation period of Jupiter drifts cyclically about a constant mean value, the most probable drift period being 11.9 years, Jupiter's orbital period. The mean rotation period during one orbital period is about 0.3 s longer than the system III period. The cyclic drift in the rotation periods of the decametric source is explained on the basis of beaming of the escaping radiation such that the apparent rotation period depends on the rate of change of the Jovicentric declination of the Earth.

Duncan (1967) has put forward the alternative hypothesis that the rotation period is defined by the commencement time of noise storms. When this is considered he finds that the rotation period has remained constant at $9^h\ 55^m\ 29.7^s$ from 1961 to 1967.

## 2.4 Longitude Profiles - Occurrence.

Longitude profiles showing the probability of occurrence or number of occurrences as a function of the longitude of the central meridian of the planet have been given by many investigators. Diagrams showing longitude profiles obtained at frequencies near 20 MHz over a period of years are shown in Figure (2.2). Longitude profiles obtained at different frequencies in 1962 are shown in Figure (2.3).

If we examine the profiles at frequencies near 20 MHz the most obvious feature is a prominent peak between $220^\circ$ and $270^\circ$. There is a secondary peak between $270^\circ$ and $340^\circ$ and another between $90^\circ$ and $180^\circ$. The third peak mentioned is broader and flatter than the other two and on some longitude profiles there is clear evidence of bifurcation, as for example in the 18.0 MHz profile for 1961 in

Figure (2.2). In order to facilitate a discussion of the longitude profiles the peaks in the histograms will be labelled A for the main peak, B1 for that part of the secondary peak which is between $90^{\circ}$ and $130^{\circ}$ and B2 for the peak in the range of $130^{\circ}$ to $180^{\circ}$, and C for the peak between $270^{\circ}$ and $340^{\circ}$. These peaks in the longitude profiles are often called sources, although this does not necessarily imply the existence of actual physical sources at the longitudes involved.

Franklin and Burke (1958) and Gardner and Shain (1958) noticed that peak A was narrower at higher frequencies, which can be seen in Figure (2.3) for frequencies of 15 MHz and greater. The sources are found to occur at higher longitudes as the frequency decreases (Gardner and Shain 1958; Carr et al 1961), this effect being most noticeable for peak C in Figure (2.3).

At low frequencies the picture is not so clear. Ellis (1962) found that at 4.7 MHz the probability of occurrence was essentially independent of longitude, and the emission was almost continuous. At 8.9 and 10.0 MHz Clark and Dulk (1966) have found very high emission probabilities of 0.95 at 8.9 MHz and 0.75 at 10.0 MHz for fluxes greater than $2 \times 10^{-22}$ $Wm^{-2}$ $Hz^{-1}$. Other observations with greater sensitivity at 10 MHz indicate that there is continuous emission at a minimum level of about $5 \times 10^{-23}$ $Wm^{-2}$ $Hz^{-1}$, which gives rise to essentially featureless profiles of occurrence probability against longitude.

The almost continuous emission at the low frequencies below 10 MHz implies that very little information about the nature of the radiation can be obtained by just measuring the probability of occurrence at these frequencies. The observations of Alexander and

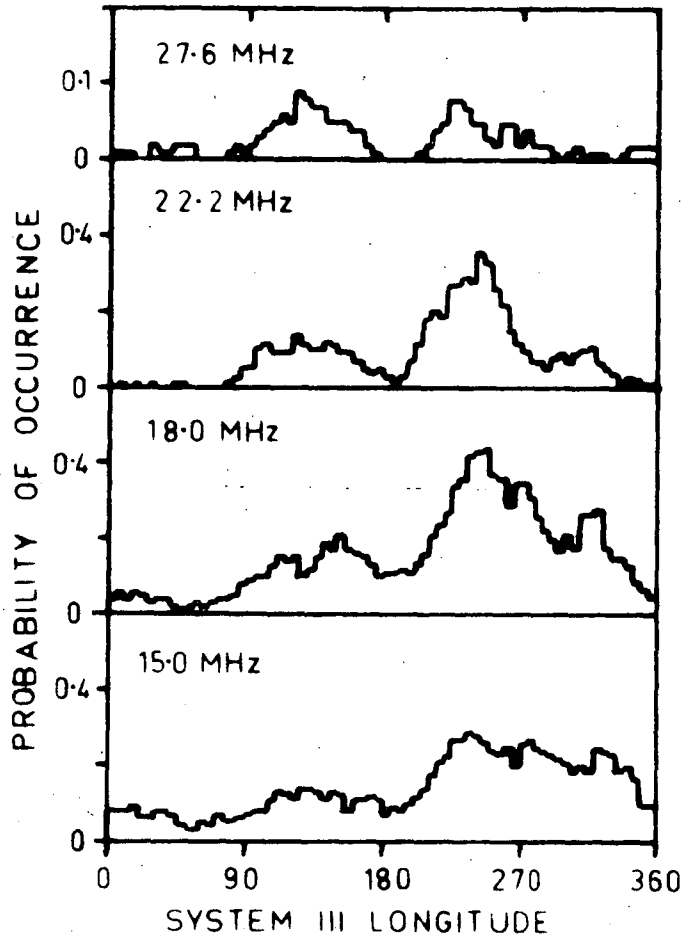


Figure 2.3 Longitude profiles of probability of occurrence at frequencies of 15.0, 18.0, 22.2 and 27.6 MHz in 1962.

Stone (1964) showed that at 26.3 MHz there was a high probability of receiving weak radiation, less than $10^{-22}$ $Wm^{-2}$ $Hz^{-1}$. The longitude profiles obtained by an observer at 26.3 MHz could then be very different depending on whether or not he could detect radiation weaker than $10^{-22}$ $Wm^{-2}$ $Hz^{-1}$. Indeed the longitude profile obtained by Alexander and Stone is significantly different from those obtained by other observers at similar frequencies. This serves to illustrate that longitude profiles showing probability of occurrence may be misleading if used to indicate the location and extent of emission regions on Jupiter. Information about the intensity of the events should be included, possibly in the form of a series of longitude profiles showing the probability of occurrence of events in various intensity ranges. This however may also be difficult due to the high degree of modulation produced by scintillations.

## 2.5 Longitude Profiles: Power.

Smith et al (1965) found that the peak burst intensity during a short interval was related to the time average of the received flux over that period. This enabled them to determine the mean flux received, from which the average flux over all listening periods was calculated. This is plotted in Figure (2.4) for frequencies between 15.0 and 27.6 MHz. The most striking feature of these profiles is the peak near $135^{\circ}$ which appears relatively much stronger than in the probability of occurrence profiles.

Clark and Dulk (1966) working at 8.9 and 10 MHz found that the intensity of the emissions was enhanced for longitudes near $0^{\circ}$ and $200^{\circ}$, while Ellis (1962) found that the intensity of the emiss-

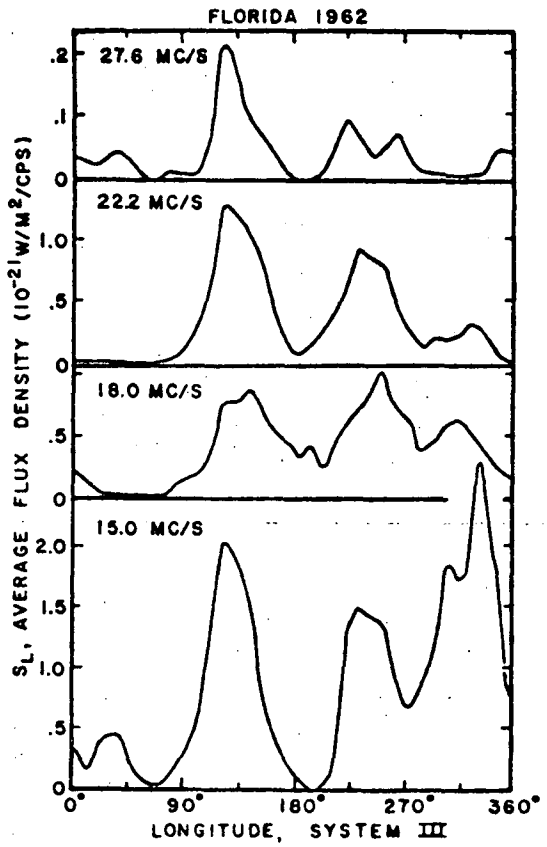


Figure 2.4 Profiles of the average received flux density $S_L$ versus system III longitude for the 1962 Florida observations. The average in this figure is taken over all effective listening time. (Smith et al, 1965)

ions at 4.7 MHz shows a longitude dependence having peaks near 180° and 340° system III longitude.

Longitude profiles showing the intensity of the received radiation at each longitude may provide much useful information; however, the use of averages in the profiles suffers from the disadvantage that the mean power is dependent on the sensitivity of the receiving equipment. If more sensitive equipment is used the number of weak events recorded will probably increase and hence the mean power will decrease.

## 2.6 Power Spectrum.

Carr et al (1964) using data obtained at Florida, Sydney and Chile, in the frequency range 5 MHz to 85.5 MHz in 1961, have calculated the mean flux density of the radiation from Jupiter as a function of frequency. The mean obtained by averaging over quiescent as well as active periods is shown in Figure (2.5a), it decreases monotonically with increasing frequency above 10 MHz. The value for the flux density obtained at 5 MHz was considered uncertain due to calibration difficulties. The rapid decrease in the flux density with increasing frequency was found to result partly from the fact that noise bursts are generally weaker at the higher frequencies, and partly from the fact that occurrence probability is lower at the higher frequencies.

Carr et al also determined the spectrum of the peak radio flux from Jupiter. They found that it has essentially the same form as the mean power spectrum, but is several orders of magnitude lower. This is plotted in Figure (2.5b).

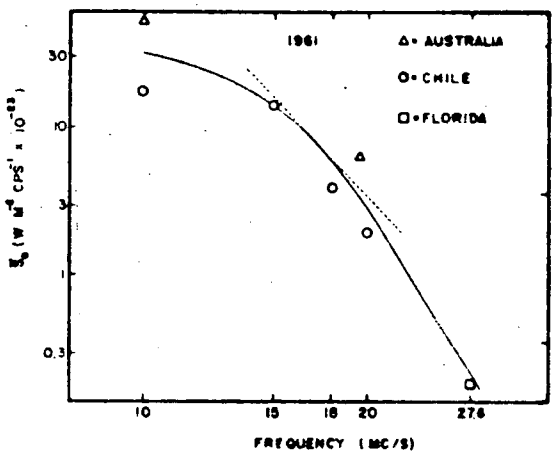


Figure 2.5a Mean flux density of the radiation from Jupiter in 1961 as a function of frequency (averaged over quiescent as well as over active periods). (Carr et al, 1964)

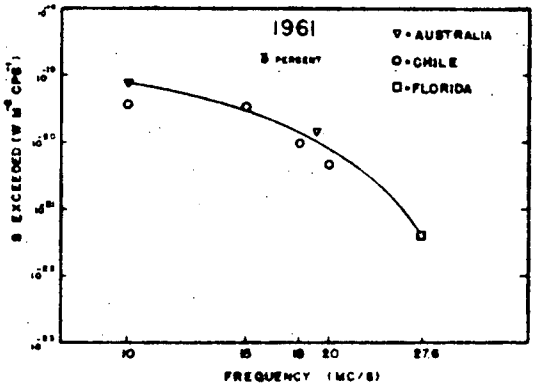


Figure 2.5b Flux densities which were exceeded in 3% of the 10 min intervals, as a function of frequency. (Carr et al, 1964)

## 2.7 Occurrence Spectrum.

Carr et al (1964) also calculated the probability of occurrence as a function of frequency. They found that it decreased monotonically with increasing frequency from 0.2 at 10 MHz to less than 0.01 at 30 MHz.

The measurements of probability of occurrence at each frequency is subject to errors for the reasons mentioned earlier. Carr et al do not appear to have made any attempt to normalise the sensitivity of their equipment at each frequency, and in fact comment that some of the observed probabilities were vastly different from the main series of observations. The published curve probably gives some indication of the variation of the probability of occurrence with frequency but it would have been better had a constant threshold been specified for the series of observations.

The results of Ellis (1962) and Clark and Dulk (1966) suggest that at lower frequencies the probability of occurrence continues to increase.

## 2.8 Polarisation of the Radiation.

The first observations of the polarisation of the Jupiter bursts were made by Franklin and Burke (1958) at 22.2 MHz and by Gardner and Shain (1958) at 19.6 MHz. Both groups found the bursts to have a strong component of right hand circular polarisation, and as these observations were made at stations in different hemispheres, it was concluded that the polarisation was not produced by the Earth's ionosphere.

Since that time, many studies have been made of the polarisation of the emission mostly at frequencies near 20 MHz. Carr et al (1961) found that at 22.2 MHz about 90% of all bursts measured had a right hand sense of rotation, this included bursts from each of the emission regions on the planet. They found the average axial ratio for each source to be very similar and close to 0.3 while the axial ratios of successive bursts varies greatly within the range 0.2 to 0.8. These observations by Carr et al were made by measuring only the intensity of left and right hand circular components, which is insufficient to completely determine the polarisation. They assumed the radiation was completely polarised and interpreted their results as determining the ellipticity of the radiation. The results could just as easily be interpreted in terms of random plus circular polarisation, the measurement then giving the degree of polarisation.

Sherrill (1965) has measured the degree of polarisation of the radiation for a range of frequencies between 15.5 MHz and 24.2 MHz. He concluded that for frequencies above 15 MHz the radiation can be regarded as fully polarised but notes a tendency towards an increasing component of random polarisation at the lower frequencies. We are then probably justified in regarding Carr et al's observations as giving a true indication of the mean axial ratio.

Barrow (1964) and Sherrill and Castles (1963) have made polarisation measurements during 1962 over the frequency range 15 MHz to 26 MHz. These observers found that right hand polarisation predominates at all frequencies, but the proportion of left hand bursts was greater at the lower frequencies. Left hand polarised bursts were observed from each region of the planet but greater

proportions were recorded in the longitude interval 300° to 360°. Barrow reports observing a few left hand bursts at 22 MHz and 26 MHz while Sherrill and Castles did not observe any above 20 MHz. Barrow found 41% and 30% left hand polarisation from the third source at 16 MHz and 18 MHz respectively. Sherrill and Castles reported events which showed mixed polarisation. They recorded two distinct types, one of which showed systematic changes from left to right hand sense at a given frequency over periods of an hour, while the other showed a maximum rate of change of polarisation sense of the order of four times per minute. This observation has been confirmed by Sherrill (1965), who also found that R.H. polarisation predominates at all frequencies between 16 MHz and 24 MHz with axial ratios generally greater than 0.7.

The first observations of polarisation below 15 MHz were made by Dowden (1963) who made an extensive study of polarisation at 10.1 MHz during 1962. Dowden analysed his data using a longitude system defined by Carr et al (1958) and to convert his results to system III it is necessary to subtract 30° from the longitudes quoted in his text and on the scales of his figures. I have made these corrections for the purposes of the following review. Dowden plotted the occurrence rate of L.H. and R.H. bursts as a function of longitude Figure (2.6). The occurrence rate of R.H. bursts shows a pronounced variation with longitude with peak occurrence near 210°; nearly half of all R.H. bursts occurred within 40° of this peak. The occurrence rate of L.H. bursts shows less variation and a number of subsidiary peaks, the largest occurring at about 10°. Dowden found that the sum of the peak powers of all bursts occurring within a given longitude

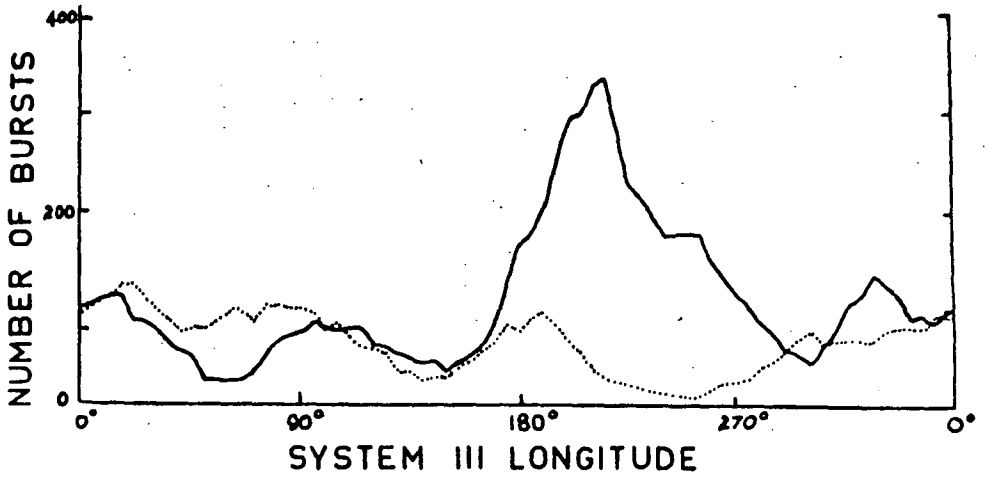


Figure 2.6 Smoothed occurrence rate of right-handed bursts (continuous line) and left-handed bursts (dotted line) at 10.1 MHz in September-October 1962. (Dowden, 1963)

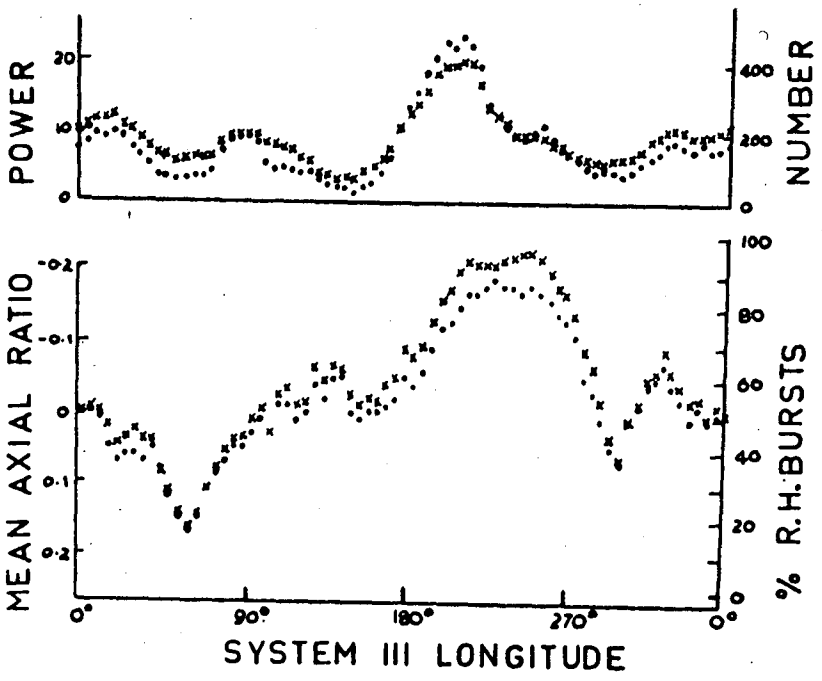


Figure 2.7 Smoothed longitude variation of total power and mean axial ratio (dots) and of burst occurrence rate and the proportion of bursts which were polarised in the right-handed sense (crosses). Observing frequency 10.1 MHz. (Dowden, 1963)

interval was closely correlated with the number of bursts occurring within that interval, although the total power seems to be more sensitive to longitude than burst occurrence rate and has a greater maximum to minimum ratio. He also found that the mean axial ratio of bursts occurring within a given longitude interval is closely correlated to the percentage of R.H. bursts in that interval, both showing a pronounced and very similar variation with longitude. Both these distributions are shown in Figure (2.7).

Dowden (1963) and Barrow (1965) have plotted the distribution of axial ratios at 10.1, 16 and 18 MHz while Sherrill (1965) has plotted the distribution at frequencies of 16, 18, 22 and 24 MHz. A selection of these histograms is shown in Figure (2.8). Sherrill and Barrow found mean axial ratios greater than 0.5. More recently Barrow and Morrow (1968) measured both the axial ratio and degree of polarisation at 18 MHz and found about 45% of the bursts were circularly polarised. The distribution of axial ratios for the remaining 55% is similar to that shown in Figure (2.8). Some of the circularly polarised bursts contained a random component and thus appear to be elliptical if only left and right components are measured. About 10% of the bursts were circularly polarised with no random component. Observations made by Warwick and Dulk (1964) suggest that the mean axial ratio of the bursts is about 0.6 over the frequency range 20 to 35 MHz. They deduced from observations of Faraday rotation that the major axis of the polarisation ellipse at Jupiter is approximately parallel to the magnetic equator of Jupiter.

Carr et al (1965) report observations of polarisation at 10, 15.8 and 22 MHz made over a period of several years. Figure

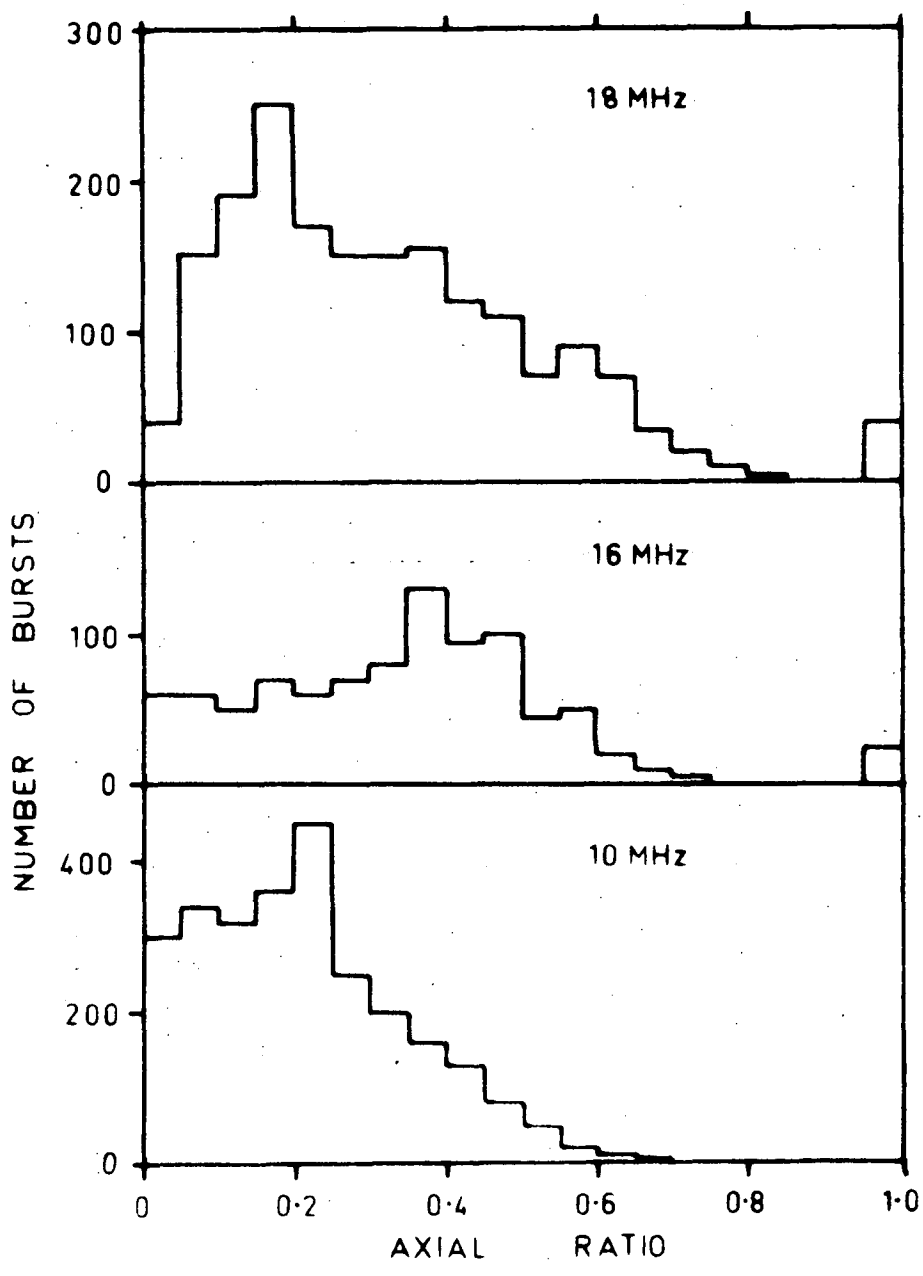


Figure 2.8 Number of bursts as a function of polarisation axial ratio. The 10 MHz data is from Dowden, 1963; the 16 and 18 MHz data is from Barrow, 1965.

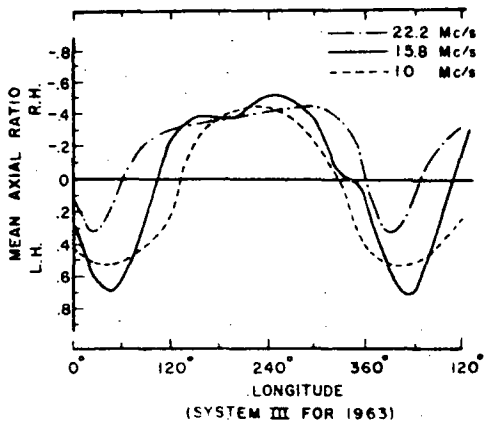


Figure 2.9a Smoothed curves showing longitude variation of polarisation at three frequencies. (Carr et al, 1965)

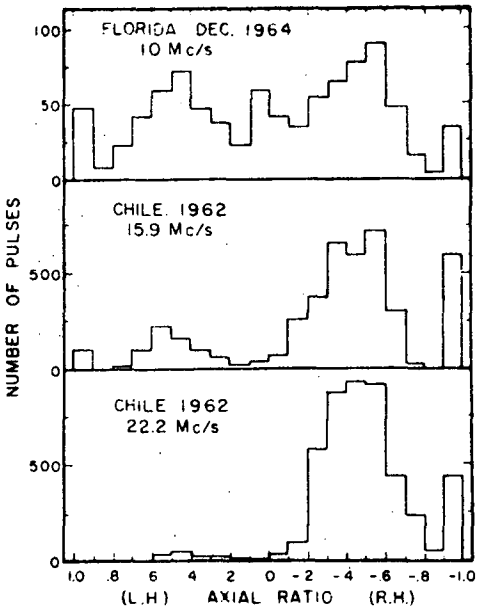


Figure 2.9b Distribution of axial ratio values at three frequencies. (Carr et al, 1965)

(2.9a), shows plots of the mean axial ratios of the bursts against longitude for each frequency, corrections having been made for the yearly longitude drift. The longitude zone in which the polarisation sense is left handed widens as the frequency is reduced, until at 10 MHz it is almost $180^{\circ}$ wide. The distribution of apparent axial ratios of individual bursts is shown in Figure (2.9b). The percentage of left handed bursts increases with decreasing frequency until at 10 MHz almost 50% of the bursts are left handed. The mean axial ratio obtained by Carr et al appears to be essentially the same at each frequency with a value near 0.5.

Warwick and Gordon (1965) and Gordon (1966) have recorded polarisation of Jupiter bursts over the continuous frequency range 24 to 36 MHz with a time resolution of 0.04 sec using a dynamic spectrum analyser. The receiving equipment operated on a time shared basis between three modes, left circular, right circular and rotating linear. A typical record is shown in Figure (2.10a). The linear record is at the top and shows pronounced Faraday rotation effects. The left circular is in the middle and right circular on the bottom. The two circular traces show striking and variable structure, Figure (2.10b), which is independent of the Faraday effect shown on the linear record. The emission is identical on the two channels, and hence must be elliptical with essentially constant axial ratio as a function of frequency above 24 MHz. Warwick has suggested that the striking periodicity in frequency may be due to a combination of direct and reflected waves from Jupiter or perhaps elliptical Faraday effect.

On one occasion extremely fast variations were recorded which are illustrated in Figure (2.11a) and (2.11b). The first

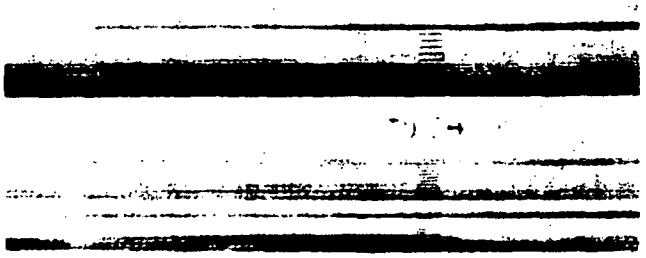

Figure 2.10a Arecibo swept frequency polarimeter record. The top record is linear polarisation, the centre is left circular and the bottom right circular. Each of the three strips covers the range 24 to 37 MHz. The total length of the record is about 15 secs. (Warwick and Gordon, 1965)

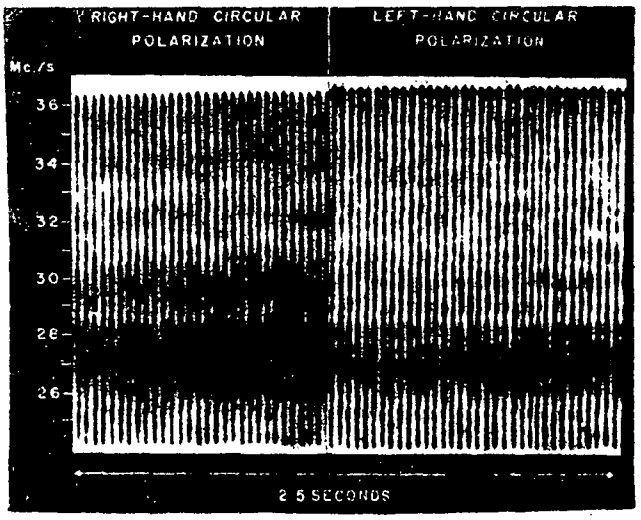


Figure 2.10b Side by side comparison of right and left hand circularly polarised spectral records. (Warwick and Gordon, 1965)

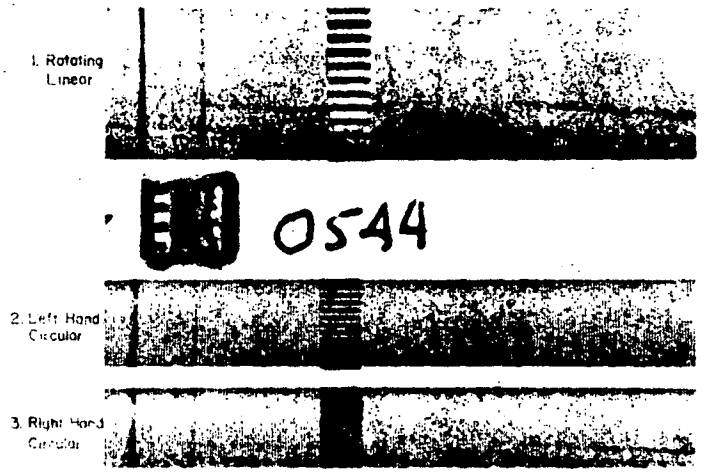


Figure 2.11a Arecibo spectrum record. Note the narrow band, but smooth emission in the form of lanes or paths. These are right-elliptically polarised. (Warwick and Gordon, 1965)

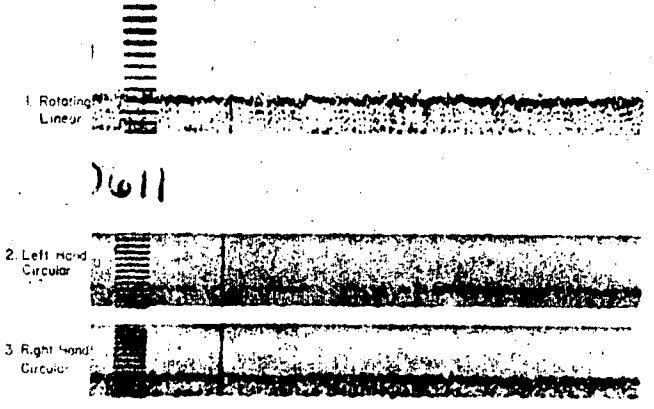


Figure 2.11b Arecibo spectrum record showing fast bursts with similar drift rates on the rotating linear trace. (Warwick and Gordon, 1965)

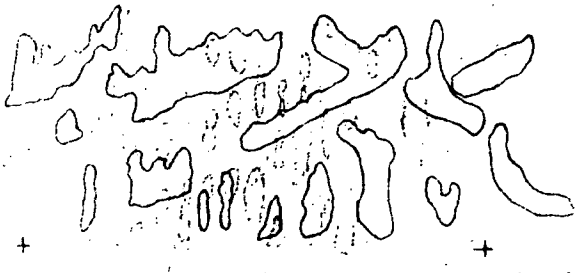

Figure 2.11c An enlarged portion of the left and right traces, which have been superimposed. The right trace is the heavy lines; the left the lighter ones. (Warwick and Gordon, 1965)

shows the initial phase of the event when a steady source appeared together with very rapid variations and the second shows the same event when only high speed fluctuations are present. On close comparison of the pips between L and R channels one finds that they are anti-correlated Figure (2.11c). The peaks of the structure are strongest on the right hand record; at the time of a burst on the left hand record, however, the burst is stronger there than the emission simultaneously appearing on the right hand record. Warwick remarks that it seems possible that the anti-correlation of frequency periodic left and right hand bursts indicates a different species of the Faraday effect than the one that occurs in the Earth's ionosphere. The Jupiter effect distorts a wave with an initial polarisation sense so that axial ratio and orientation vary periodically with frequency. Gordon (1966) has demonstrated that the Faraday effect produced by two characteristic elliptical modes could account for the variation of polarisation sense with frequency.

## 2.9 Spectra - Low Time Resolution.

Warwick (1961, 1962) has recorded dynamic spectra of the radio emissions from Jupiter initially over the frequency range 15 MHz to 34 MHz but more recently over the range of 7.6 MHz to 41 MHz. During long enduring noise storms Warwick finds that emission occurs over a range of frequencies throughout the life of the storm. He noticed a tendency for positive frequency drifts to occur at earlier longitudes and negative drifts at later longitudes. The characteristic features of the spectra tend to repeat when the same longitude is on the central meridian. The features which repeat have durat-

ions of several minutes to an hour, the finer details do not repeat. Warwick (1963) reported that the features noticed earlier in the dynamic spectra remained stable over a period of years. Radiation which originates from the early source, B1, seems to begin over the narrow ranges of longitudes from $107^{\circ}$ to $130^{\circ}$ and then drift from low to high frequencies. ( This is followed by a very narrow band feature which drifted back to lower frequencies Figure (2.12). Warwick concluded that Jupiter's dynamic spectrum represents a kind of permanent map of the surface of the planet, where radio frequency and time act as latitude and longitude respectively.

Dulk (1965) has examined Warwick's spectra in great detail. The spectral data indicate that noise storms occur more frequently when certain longitudes face the Earth, the histograms of emission versus system III longitude having one dominant peak and two subsidiary peaks. A fourth source is recognisable on spectral data but does not show on histograms. It occupies the longitude range $20^{\circ}$ to $80^{\circ}$. The 'permanent dynamic spectrum' is different for each of the four sources, and has been stable since the observations started in 1960. It exhibits a characteristic gross structure lasting up to three hours, and a finer structure lasting about 10 to 20 minutes. The spectrum characteristics of each of the four sources are detailed below.

Early Source : $(80^{\circ} < \text{LCM} < 190^{\circ})$

Six early source spectra are shown in Figure (2.12). The spectra are lined up vertically according to the LCM at the time of emission. Some notable features of these spectra are the high cut-off frequency of each of the spectra and a drift of the maximum fre-

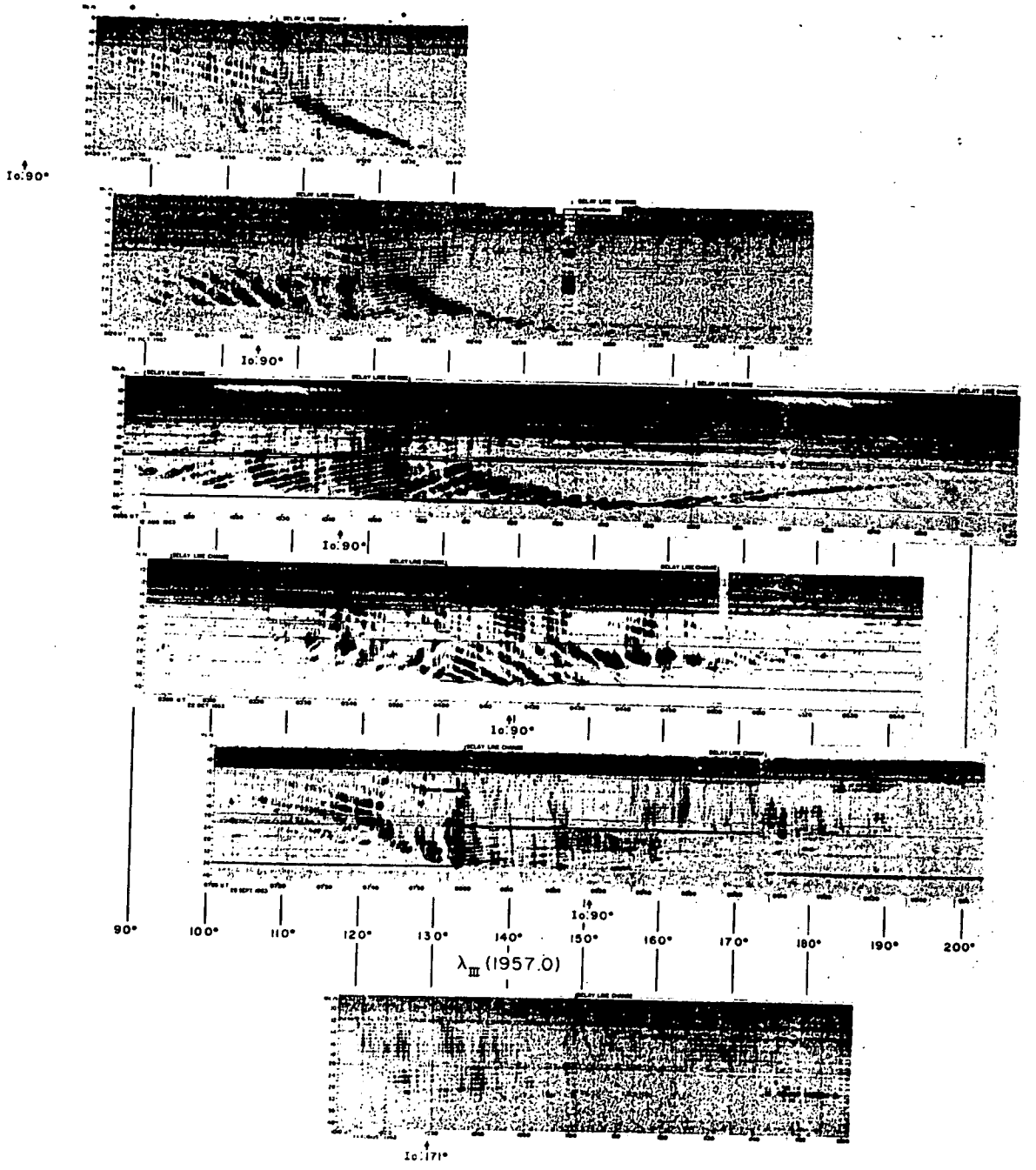


Figure 2.12 Composite of 6 early source spectra, showing the relative position of Io at the time of emission. (Dulk, 1965)

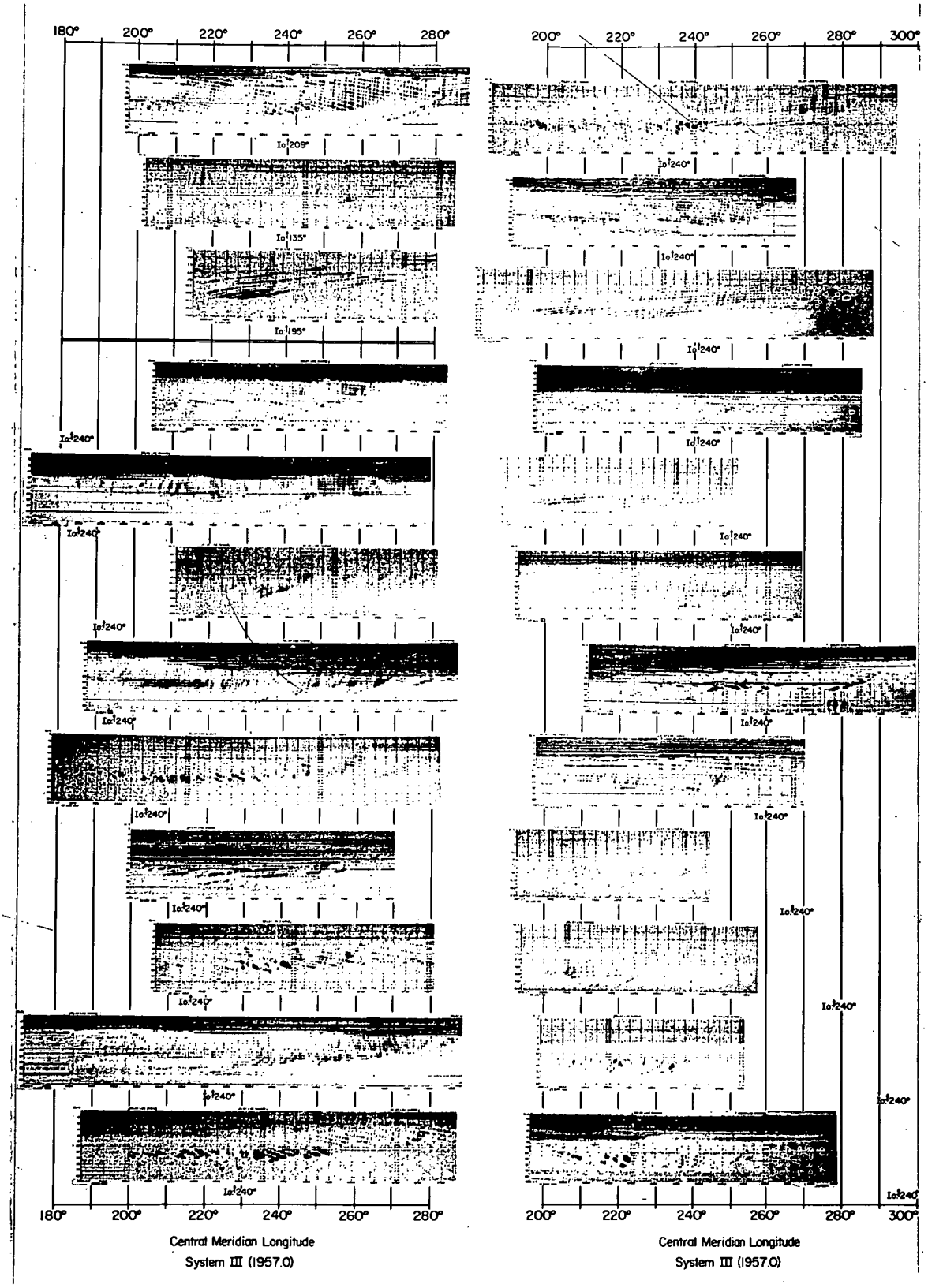


Figure 2.13 Composite of 24 main source spectra recorded from 1961 to 1964. The relative position of Io is shown. (Dulk, 1965)

quency of each of the spectra and a drift of the maximum frequency of emission from low to high frequency during the early phase of the events. There is a prominent stub of high intensity emission occurring on the top three spectra when LCM $\simeq 130^{\circ}$ to $140^{\circ}$, and there is a very long narrow band tail on the second and third spectra.

Main Source : $(190^{\circ} < \text{LCM} < 290^{\circ})$

Representative spectra of the main source are shown in Figure (2.13). Each spectrum shows that there is a drift from low to high frequency as the LCM approaches $240^{\circ}$ and a reverse drift thereafter. There are cusps of emission sweeping from high to low frequency at late longitudes (about $290^{\circ}$) on several of the long lasting spectra. Main source spectra are generally composed of separate patches of bursts, with few showing the nearly continuous emission seen in many early source spectra.

Third Source : $(290^{\circ} < \text{LCM} < 20^{\circ})$

Several spectra of third source emission are shown in Figure (2.14). The outstanding feature of these spectra is the abundance of emission cusps starting at medium frequencies (up to 32 MHz) and sweeping to the low frequency limit imposed by the equipment or the ionosphere. The emission in the cusps has a short duration and narrow bandwidth when it starts and a longer duration and wide bandwidth in the later phases. During many events it appears that the entire emission consists of these drifting cusps. Emissions of the third source rarely, if ever, attain a frequency greater than 32 MHz. Ordinarily the maximum frequency of emission decreases with time, so that at longitudes greater than about $320^{\circ}$ the emission does not exceed 20 MHz.

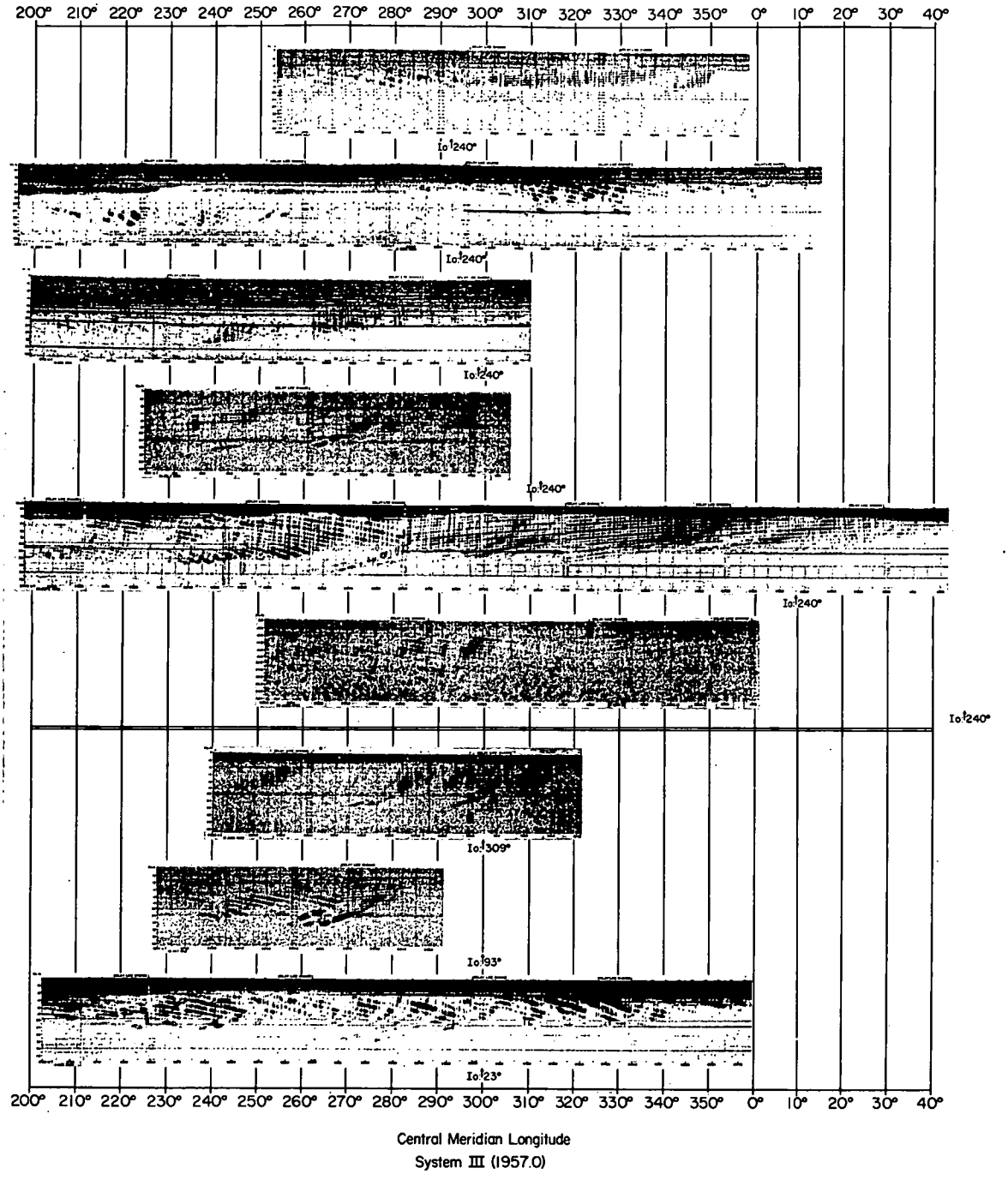


Figure 2.14 Composite of 9 third source spectra. The relative position of Io is shown. (Dulk, 1965)

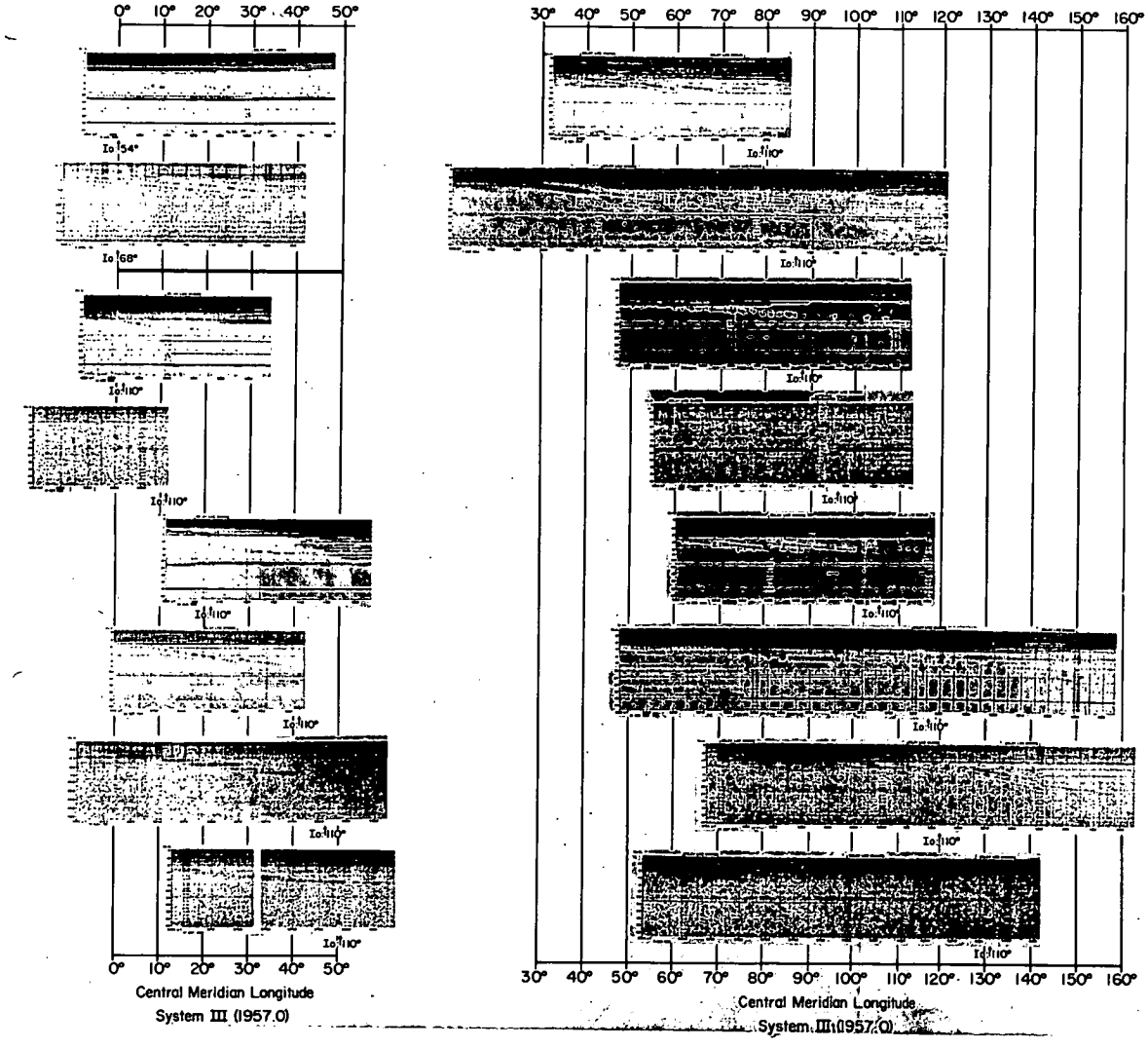


Figure 2.15 Composite of 16 fourth source spectra showing the relative positions of Io. (Dulk, 1965)

Fourth Source : ($20^{\circ} < LCM < 80^{\circ}$)

It can be seen from Figure (2.15) that fourth source emission occurs at low frequencies, and is usually obscured by interference. The major characteristics of fourth source emission are its narrow band width (less than 3 MHz) and its drift from low to higher frequencies. It seldom drifts higher than 18 MHz.

## 2.10 Spectra - High Time Resolutions.

Riihimaa (1964) has made high time resolution studies of the spectrum of the Jovian noise storms in the frequency range 18.2 to 19.2 MHz. He found that most of the spectra had the appearance of diffused blobs, often being patchy and irregular, their durations ranging from a few seconds to a minute. In a few cases blobs resolve into pips of durations down to less than 5 milliseconds, superimposed on a weaker background signal. Band structures have also been observed, which have the same appearance as ridge patterns, described by Wild and Roberts (1956) in connection with observations of the scintillation spectra of Cygnus A. The band structures and blob structures originate from the same type of bursts, ionospheric scintillations producing the different observed spectra. Typical band and blob structures are shown in Figure (2.16).

Riihimaa (1966 a,b) has repeated this work with much higher frequency resolution, and finds three types of bursts. The most common type is a structure with practically no details. It may appear as a smooth, vertical or slightly tilted bar in spectra where time runs horizontally. Typical bandwidths are 0.5 MHz or more with durations from a few seconds up to one minute. These broad

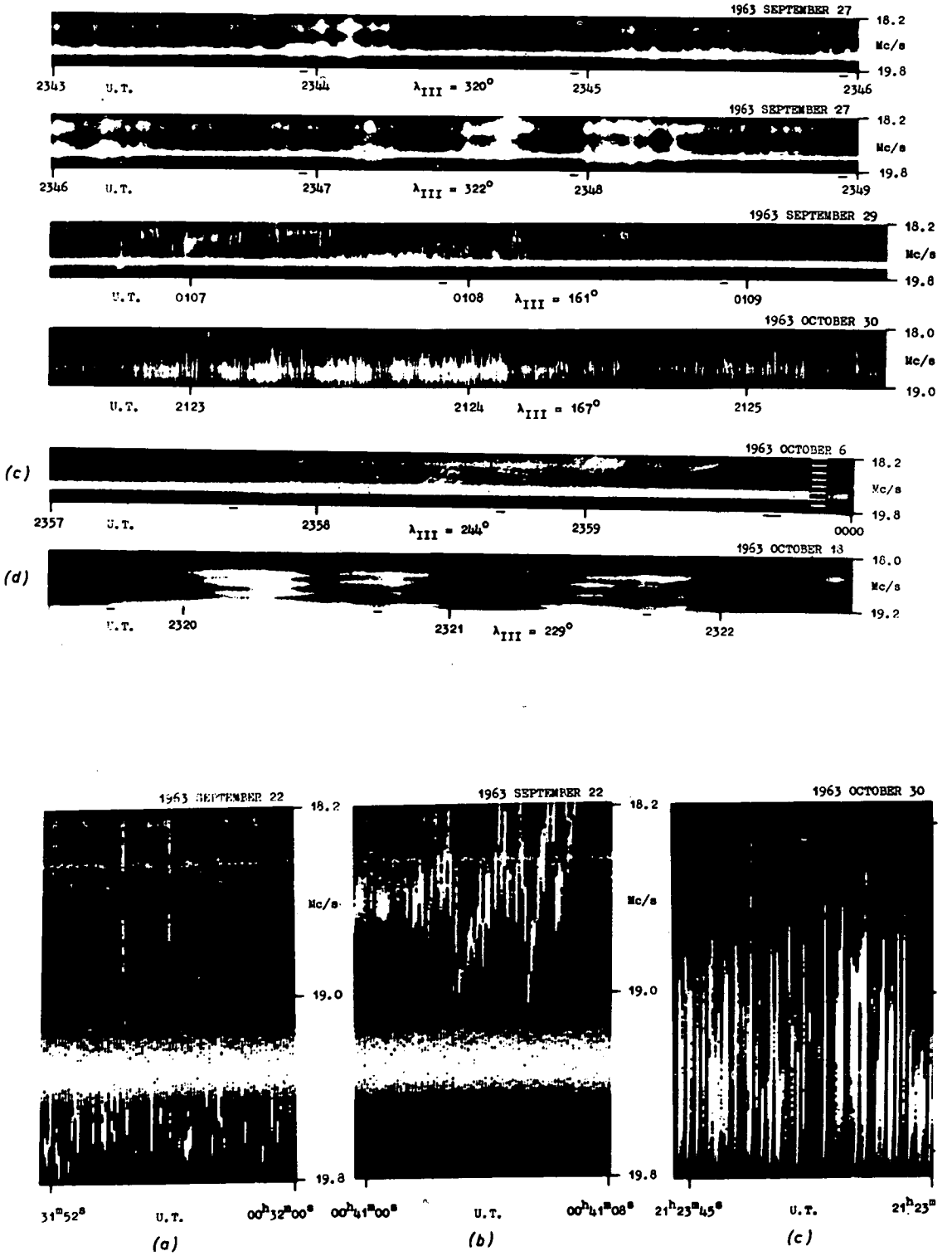


Figure 2.16 High resolution spectra showing blob, band and pip structures. (Riihimaa, 1964)

band emissions correspond to those previously classified as blobs and appear to originate primarily from the main source on Jupiter.

The second spectral type has more details; it is composed of bursts which often have bandwidths of the order of 50 KHz. The duration of individual bursts is of the order of one second. Such a spectrum has the appearance of an irregular group of flecks and patches. These bursts originate mainly from source B.

The third type is very complex; it is composed of pulses which have bandwidths down to 50 KHz, while their durations often go down to the time resolution limit of the equipment. The pulses may recur at intervals ranging from a fraction of a second to several seconds. Riihimaa (1968) has recently concluded that these bursts drift very rapidly in frequency at rates from 40 MHz/s to several hundred MHz/s. The polarisation and intensity of these bursts are similar to other types of Jupiter bursts. Similar spectra have been reported by Warwick and Gordon (1965) and Gordon (1966) in the frequency range 24 MHz to 36 MHz. They observed very short bursts which drifted in frequency at rates between 5 and 35 MHz/s from high to low frequency. These pulses are probably the same as the I type bursts reported earlier in connection with single frequency observations. The short pulse type spectra originate from the same source regions on Jupiter as do the I bursts, that is, from two sources separated by approximately $180^{\circ}$ of longitude at $150^{\circ}$ and $330^{\circ}$ system III.

## 2.11 The Io Correlation.

### (a) Effect of Io on the Occurrence of Emission

Bigg (1964) using data obtained by Warwick during 1960-63

found that the orientation of Jupiter's Gallilean satellite Io modulates both the probability of occurrence and intensity of Jovian decametric emission. He found that the effect is most pronounced when only events showing emission at frequencies above 30 MHz were considered. Bigg showed, Figure (2.17), that emission is most likely when Io is between $80^{\circ}$ and $100^{\circ}$ from superior geocentric conjunction and Jupiter's longitude is between $100^{\circ}$ and $160^{\circ}$, and also when Io is between $230^{\circ}$ and $250^{\circ}$ from superior geocentric conjunction with Jupiter's longitude between $200^{\circ}$ and $260^{\circ}$.

The initial announcement by Bigg was immediately confirmed by Alexander and Stone (1965) working at 26.3 MHz, and Lebo et al (1965) using data obtained at Florida from 1957-63 over a range of frequencies. The data obtained by Lebo et al in 1962 which serves to illustrate the stability of the Io effect with frequency, is plotted in Figure (2.18).

Dulk (1965) reports that Io affects both the probability of emission and the character of the emission spectrum, which will be discussed in the next section. He found that the emission probability approaches 1.0 when Io's position and Jupiter's longitude were simultaneously favourable. Duncan (1965) has re-analysed the data used by Bigg for frequencies over 30 MHz, and confirms Bigg's discovery. He also finds that the Jovian longitude of Io controls the emission, Figure (2.19), which is most favourable when Io is close to the $200^{\circ}$ meridian plane; i.e. when Io is near the plane containing Jupiter's magnetic axis. Duncan (1966) concludes that the Io modulation is only noticeable on events whose maximum frequency exceeds 30 MHz, and explains the modulation observed at lower frequen-

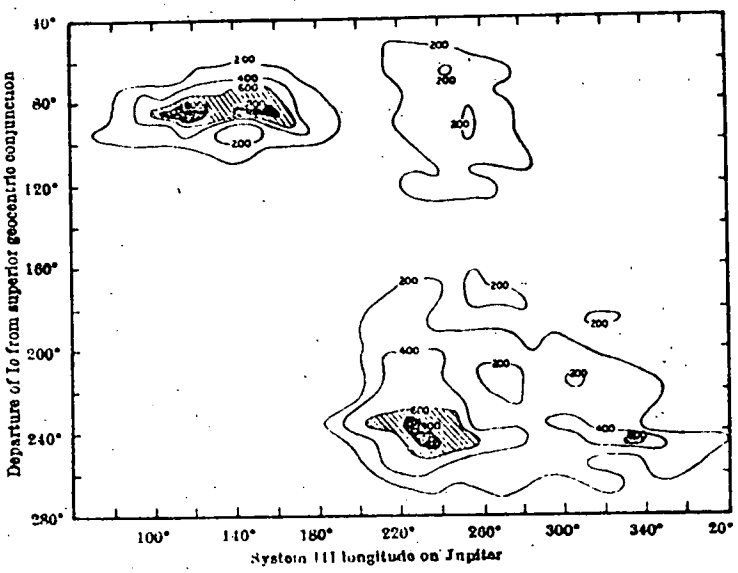


Figure 2.17 Contour diagram showing the relationship between the position of Io and the orientation of Jupiter for the reception of decametric emission at the Earth. (Bigg, 1964)

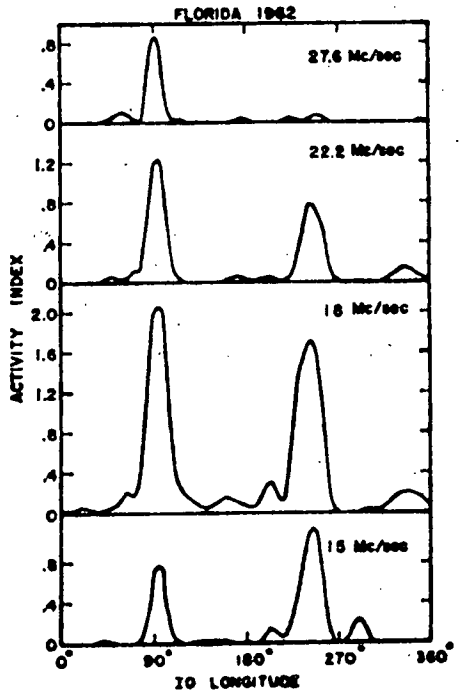


Figure 2.18 Influence of Io on Jovian radiation of various frequencies during the apparition of 1962. (Lebo et al, 1965)

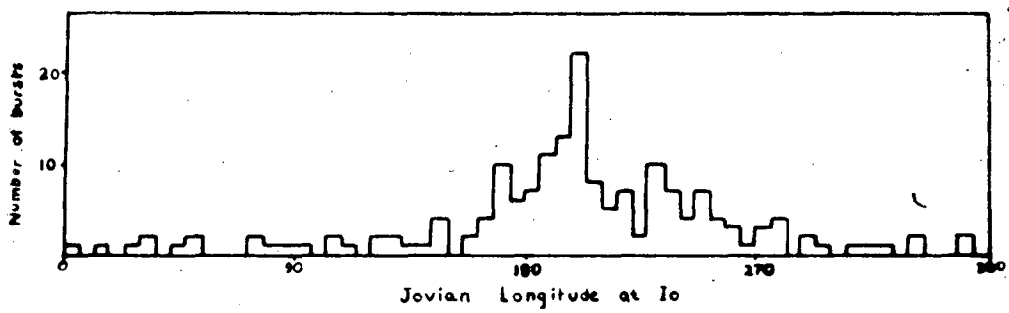


Figure 2.19 Number of bursts at frequencies greater than 30 MHz as a function of the Jovian longitude of Io. (Duncan, 1966)

cies as arising from the characteristic broad band nature of the decametric emissions. The effect has been confirmed by Gruber (1967) who studied the Io effect in relation to the maximum frequency of a noise burst. Duncan also finds that other satellites do not cause any perceptible modulation of the emission, essentially in agreement with the observations of Bigg (1966).

Duncan (1966) has suggested that Io controls the commencement time of the storm, most main-source storms being first seen when Jupiter's northern hemisphere magnetic pole crosses the central meridian.

(b) Effect of Io on the Dynamic Spectra

Dulk has found that the position of Io usually effects the dynamic spectrum of the emissions during a storm, this effect being different for each of the four sources reported to give rise to characteristic dynamic spectra. Dulk has divided the spectra into two classes depending on whether they appear to be effected by the position of Io or not. He classifies these as Io dependent and Io independent events. The characteristics of the Io dependent spectra for each of the four sources are described below.

Early Source

Figure (2.12) shows a series of early source spectra, in which the position of the arrow indicates the position of Io. Referring to this we see that the details of the spectral character appear to depend on the exact position of Io. Emission started at early Jupiter longitudes if Io reached $90^{\circ}$ early. Looking down the spectra we see that the longitudes of the stub are later in each spectrum corresponding to Io reaching $90^{\circ}$ later, and the high fre-

quency limit of the tails on the spectra decrease with a change in Io's position. The factor which seems to determine the highest frequency and the longitude ranges of the stub is the position of Io at the time of emission. Io-independent early source spectra are completely different from the Io-dependent spectra.

Main Source

A number of main source spectra are arranged in Figure (2.13) according to the relative position of Io at the time of emission. There are three spectra at the top left which are not Io related.

As in the case of the early source, the main source spectra form a slowly varying pattern according to the relative position of Io. One feature, a narrow band streak of emission, is seen to occur only in the middle of the series of spectra, where $\phi$ Io = $240^{\circ}$ and LCM $\simeq 240^{\circ}$ simultaneously. Similarly, the cusps of negative drift emission show most prominently on spectra near the ends of the sequence. Io-independent main source events more closely resemble Io-related main source events than was the case with the early source. However, they have shorter durations and do not have the narrow band streak of 35 MHz emission.

Third Source

Figure (2.14) shows the relative position of Io during several major third source events. The top six spectra were recorded with Io near $240^{\circ}$, and the bottom three were recorded with Io in other regions. The Io-independent events are similar to the Io-dependent events and so the features of the third source spectra are Io-independent.

Fourth Source

The longitude range and emission frequency of fourth source emission seems to be determined by the position of Io and the Jupiter longitude. However, Io does not appear to influence the character of the individual spectra, Figure (2.15).

## 2.12 Correlation with Solar Activity and Other Phenomena.

The activity of Jupiter has been found to show large variations over periods of many years. From the discovery in 1954 the activity decreased markedly as solar activity increased. Carr et al (1961) and Smith et al (1965) have used data extending back to 1955 to study this effect. The data suggests an inverse correlation of activity with sunspot numbers with the activity index minimum occurring about two years after sunspot maximum. Many years data will be needed to establish this correlation since the orbital period of Jupiter and the length of the solar cycle are each about 11 years.

There have been many reports of short term positive correlations between Jupiter and solar activity, Kraus (1958), Warwick (1960, 1961, 1962) and Carr et al (1960, 1961). However the majority of the data appears statistically insignificant but when Warwick uses only the days when Jupiter's activity is observed above 30 MHz, there appears to be a significant correlation with activity occurring one or two days after solar continuum events.

Several investigators, Carr et al (1961), Jelly and Petford (1961) and Dulk and Eddy (1966) have searched for visual effects on Jupiter correlated with decametric emissions. In no cases were any light pulses detected.

## 2.13 Size of the Emission Region.

Slee and Higgins (1963, 1966, 1968) using a long baseline interferometer at 19.7 MHz have measured the angular extent of the emitting regions. They found that on occasions when ionospheric effects were absent the source size was less than 6" of arc in both the equatorial and polar directions. More regularly however, source sizes in the range 10-15" arc were found. They suggest that the measured source sizes may be the extent of interplanetary irregularities responsible for the scintillations mentioned earlier. If this is so they concluded that the real angular size of the emission source would probably be less than 0.6" of arc. Estimates of the maximum size of the emitting region have been obtained by other workers; Douglas and Smith (1967) give a maximum size of 5" arc while Dulk et al (1967) find the maximum size to be 3" arc.

## 2.14 Summary.

The decametric radio emissions from Jupiter are in the form of bursts which may last from a few milliseconds to tens of seconds. The form of these bursts is often severely modulated by scintillations. The probability of occurrence of bursts is dependent upon the longitude of the central meridian of Jupiter. At frequencies above 15 MHz four peaks in the probability of occurrence are found to recur as the planet rotates. These peaks occur near longitudes $120^{\circ}$, $160^{\circ}$, $240^{\circ}$ and $330^{\circ}$; their amplitude and position change with the frequency of observation.

The probability of occurrence of the radiation and its intensity is modulated by the orientation of the Jovian satellite Io.

Radiation is enhanced when Io is situated approximately at right angles to the Earth-Jupiter line. The regions on Jupiter from which the radiation is enhanced depend on which side of the Earth-Jupiter line Io lies.

The bursts are elliptically polarised mainly in the right hand sense, although below 20 MHz left hand bursts are observed, their percentage increasing with decreasing frequency. Right and left hand bursts can originate from each of the four sources on Jupiter, corresponding to the peaks in the probability of occurrence profile, but the source near $330^{\circ}$ produces a much higher percentage of left hand bursts than the others.

Dynamic spectra of the emissions show structure which repeats when certain longitudes face the Earth, and change systematically with the orientation of Jupiter's satellite Io.

## 2.15 References.

ALEXANDER, J.K. and R.G. STONE (1964), 116th Meeting A.A.S.

ALEXANDER, J.K. and R.G. STONE (1965), Astrophys. J. 141

BAART, E.E., C.G. BARROW and R.T. LEE (1966), Nature 211, 808-810

BARROW, C.H. (1964) Icarus, 3, 66.

BARROW, C.H. (1965) Publication of Radio Astronomy Observatory Florida State University

BARROW, C.H. and D.P. MORROW (1968) Astrophys. J. 152, 593

BIGG, E.K. (1964) Nature 203, 1008-1010

BIGG, E.K. (1966) Planet Space Sci. 14, 741-758

BURKE, B.F. and K.L. FRANKLIN (1955) Nature 175, 1074

BURKE, B.F. (1957) Carnegie Institution of Washington, Yearbook, 56, 90

BURKE, B.F. (1961) The Solar System, Vol III, Planets and Satellites, G.P. Kuiper and B.M. Middlehurst P. 473

CARR, T.D., A.G. SMITH, R. PEPPLE and C.H. BARROW (1958) Astrophys. J. 127, 274

CARR, T.D., A.G. SMITH and H. BOLLHAGEN (1960) Phys Rev. Letters 5, 418

CARR, T.D., A.G. SMITH, H. BOLLHAGEN, N.F. SIX, Jr., and N.E. CHATTERTON (1961) Astrophys. J. 134, 105

CARR, T.D., G.W. BROWN, A.G. SMITH, C.S. HIGGINS, H. BOLLHAGEN, J. MAY and J. LEVY (1964) Astrophys. J. 14, 778-795

CARR, T.D., S. GULKIS, A.G. SMITH, J. MAY, G.R. LEBO, D.J. KENNEDY and H. BOLLHAGEN (1965) J. Res. Nat. Bur. Stand 69D, 1530-36

CLARK, T.A. and G.A. DULK (1966) Astron. J. 71, 1338

DOUGLAS, J.N. (1960) Ph. D. Dissertation, Yale University.

DOUGLAS, J.N. and H.J. SMITH (1961) Nature 192, 741

DOUGLAS, J.N. and H.J. SMITH (1963) Astron. J. 68, 163

DOUGLAS, J.N. and H.J. SMITH (1963b) Nature 199, 1080

DOUGLAS, J.N. (1964) I.E.E. Trans Mil. Electronics MIL8, 173

DOUGLAS, J.N. and H.J. SMITH (1967) Astrophys. J. 148, 885

DOWDEN, R.L. (1963) Aust. J. Phys. 16, 398

DULK, G.A. (1965) Ph. D. Dissertation, University of Colorado.

DULK, G.A. (1965) Science 148, 1585-1589

DULK, G.A., B. RAYHRER and R. LAWRENCE (1967) Astrophys. J. 150, L117

DULK, G.A. and J.A. EDDY (1966) Astron. J. 71, 1338

DUNCAN, R.A. (1965) Planet Space Sci. 13, 997-1002

DUNCAN, R.A. (1966a) Planet Space Sci. 14, 173

DUNCAN, R.A. (1966b) Planet Space Sci. 14, 1291-1301

DUNCAN, R.A. (1967) Planet Space Sci. 15, 1687

ELLIS, G.R.A. (1962) Nature 194, 667

FRANKLIN, K.L. and B.F. BURKE (1958) J. Geophys. Res. 63, 807

GALLET, R.M. and K.H. BOWLES (1956) Astron. J. 61, 194

GALLET, R.M. (1957) Trans. Inst. Rad. Eng. AP-5, 327

GALLET, R.M. (1961) The Solar System, Vol III Planets and Satellites
G.P. Kuiper and B.M. Middlehurst P. 500

GARDNER, F.F. and C.A. SHAIN (1958) Aust. J. Phys. 11, 55

GORDON, M.A. (1966) Ph. D. Dissertation, University of Colorado.

GRUBER, G.M. (1967) Astrophys. J. 148, 541

GULKIS, S. and T.D. CARR (1966) Science 154, 257-259

Int. Ast. Un. Inf. Bull (1962) 8

JELLEY, J.V. and A.D. PETFORD (1961) Observatory 81, 104

KRAUS, J.P. (1956) Astron. J. 61, 182

LEBO, G.R.. A.G. SMITH and T.D. CARR (1965) Science 148, 1724

N.A.S.A. Jupiter's Observers Conference, Goddard Space Flight
Center (1965)

RIIHIMAA, J.J. (1964) Ann. Acad. Sci. Fennicae Ser A VI Phys 156

RIIHIMAA, J.J. (1966a) Nature 209, 387

RIIHIMAA, J.J. (1966b) Ann. Acad. Sci. Fennicae Ser A VI Phys 206

RIIHIMAA, J.J. (1968) Astron. J. 73, 265

ROBERTS, J.A. (1963) Plan. Space Sci. II, 221-259

SHAIN, C.A. (1955) Nature 176, 836

SHAIN, C.A. (1956) Aust. J. Phys. 9, 61

SHERRILL, W.M. and M.P. CASTLES (1963) Astrophys. J. 138, 587

SHERRILL, W.M. (1965) Astrophys. J. 142, 1171-1185

SLEE, O.B. and C.S. HIGGINS (1963) Nature 197, 781

SLEE, O.B. and C.S. HIGGINS (1966) Aust. J. Phys. 19, 167

SLEE, O.B. and C.S. HIGGINS (1968) Aust. J. Phys. 21, 341

SLEE, O.B. and H. GENT (1967) Nature 216, 235

SMITH, A.G. and T.D. CARR (1959) Astrophys. J. 130, 641

SMITH, A.G., T.D. CARR, H. BOLLHAGEN, N. CHATTERTON and F. SIX (1960) Nature 187, 568

SMITH, A.G., G.R. LEBO, N.F. SIX, T.D. CARR, H. BOLLHAGEN, J. MAY and J. LEVY (1965) Astrophys. J. 141, 457-477

SMITH, H.J. and J.N. DOUGLAS (1959) Paris Symposium on Radio Astronomy P. 53 (ed. R.N. Bracewell)

SMITH. H.J. and J.N. DOUGLAS (1962) Astron. J. 67, 120

WARWICK, J.W. (1960) Science 132, 1250

WARWICK, J.W. (1961) Annals New York Acad. Sci. 95, 39

WARWICK, J.W. (1963a) Astrophys. J. 137, 41

WARWICK, J.W. (1963b) Astrophys. J. 137, 1317

WARWICK, J.W. and G.A. DULK (1964) Science 145, 380

WARWICK, J.W. and M.A. GORDON (1965) J. Res. Nat. Bur. Stand. 69D, 1537-1542

WILD, J.P. and J.A. ROBERTS (1956) J. Atmos Terr. Phys 8, 55

# CHAPTER 3.

# OBSERVATIONS OF JUPITER'S DECAMETRIC EMISSIONS

## 3.1 Introduction.

The discovery by Ellis (1961) that Jupiter emitted strong radio waves at 4.7 MHz led to the introduction of a program for the observation of Jupiter at spot frequencies in the decameter range at the University of Tasmania. Observations were made at 4.7, 15.7, 21.5, 24.5 and 28.0 MHz, McCulloch and Ellis (1966), over the period June 1961 to October 1964. Dowden (1963) made observations of polarisation at 10.1 MHz.

Some of the data, namely the longitude profiles at 18.7 MHz and part of the results at 15.7, 21.5 and 24.5 MHz obtained in 1962, have been discussed in a previous thesis (McCulloch, 1963). The 18.7 MHz profiles are included because they are needed to illustrate trends in the emission with frequency. The other data recorded in 1962 has been integrated with data recorded in 1963 and 1964 to produce final longitude profiles. The 4.7 MHz data results from a complete reanalysis of Ellis' original records obtained in 1961.

The polarisation data at 10.1 MHz has been analysed for the effect of Io.

## 3.2 Equipment.

The electronic equipment used at each frequency consisted of a phase switching interferometer (Ryle 1952). The bandwidths of the receiving systems were 8 KHz, except at 15.7 MHz where it was 2.2 KHz. The interferometers had a post-detection time constant of

three minutes, and the outputs were recorded using pen recorders with a chart speed of one inch per hour. The time resolution of the recording system corresponded to about one degree of Jupiter longitude which was considered adequate for this type of observation.

The equipment used at several of the frequencies had an output prior to the phase sensitive detector with a time constant of 0.02 s. Occasional recordings of burst profiles were made from this using chart speeds of two inches a minute and thirty inches a minute.

The aerials used at 15.7, 17.8, 21.5 and 24.5 MHz were made up of two arrays of four full-wave dipoles separated by twenty wavelengths in an east-west direction. Each array was phased to the declination of Jupiter. The primary beam widths of the antennae were $30^{\circ}$ N-S by $60^{\circ}$ E-W, allowing Jupiter to be observed for a period of four hours a day within the half power point of the antenna. The aerial used at 28.0 MHz had eight full-wave dipoles at each end of the array, which reduced the E-W beamwidth to $30^{\circ}$, and hence limited observations to two hours a day.

The aerials used at 4.7 MHz consisted of two arrays of ten full-wave dipoles separated by twenty wavelengths E-W. The dipoles in each array were orientated N-S and were separated by a half wavelength E-W giving a beamwidth of about $45^{\circ}$ N-S by $15^{\circ}$ E-W allowing Jupiter to be observed for about an hour each night.

Phase switching interferometers were used at all frequencies because of their characteristic response to a discrete radio source which provides a means of identification. In order that the identification should be certain emission had to be present for at least one full fringe width (approximately six minutes). Events

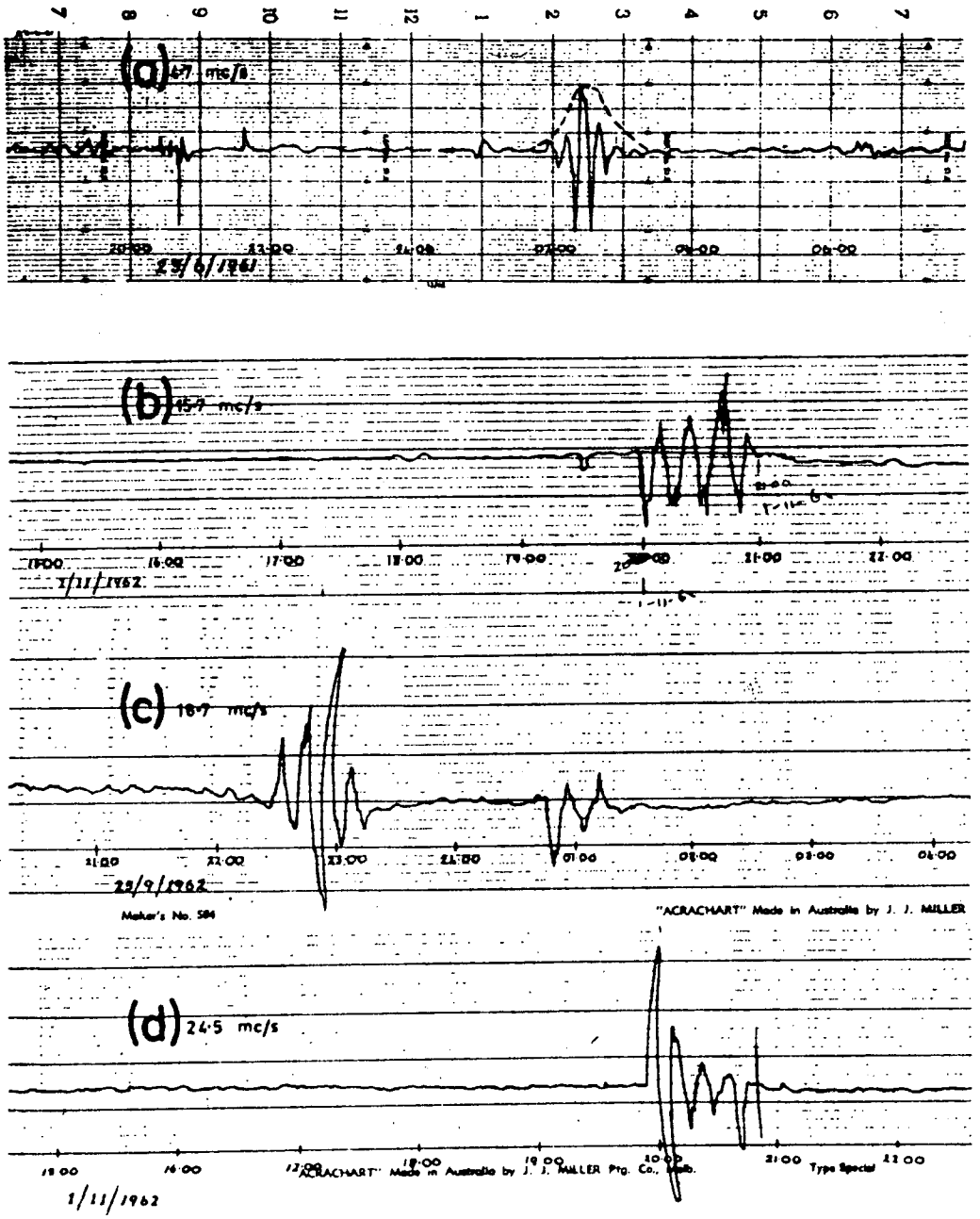


Figure 3.1 Typical interferometer records of Jupiter events at frequencies of (a) 4.7 MHz (b) 15.7 MHz (c) 18.7 MHz (d) 24.5 MHz. The dotted line in (a) indicates the envelope of the interferometer pattern.

lasting less than six minutes could not be identified and so short bursts of emission may have been missed.

## 3.3 Observations.

The observations were made at a site near Hobart, latitude 42.9°S, longitude 147°E, during the period 1961-1964. The observing conditions are summarised in Table 3.1.

| Frequency MHz | Observing Period | Number of Observing Days | Total time for which bursts were observed within antennae half power pts. | Probability of occurrence |
|---|---|---|---|---|
| 4.7 | 8. 6.61 - 30. 8.61 | 40 | 20 Hrs 30 Min | 0.51 |
| 15.7 | 4.10.62 - 30.11.63 | 106 | 99 " 20 " | 0.23 |
| 18.7 | 20. 4.62 - 16. 8.62 | 97 | 117 " 15 " | 0.30 |
| 21.5 | 28.10.62 - 30.11.63 | 197 | 54 " 40 " | 0.062 |
| 24.5 | 28.10.62 - 30.11.63 | 264 | 43 " 45 " | 0.035 |
| 28.0 | 20.10.63 - 30. 9.64 | 305 | 3 " 50 " | 0.006 |

Table 3.1

The identification of the radio emissions from Jupiter were made by examination of the interferometer records for time of occurrence and declination of the source. Typical interferometer records are shown in Figure 3.1.

The gain of the receiving equipment was calibrated using a temperature limited noise diode. At 4.7 MHz, attenuation in the ionosphere was estimated from the measured value of the ionospheric critical frequency $f_0F_2$ (Ellis, 1965) and from the level of the discrete

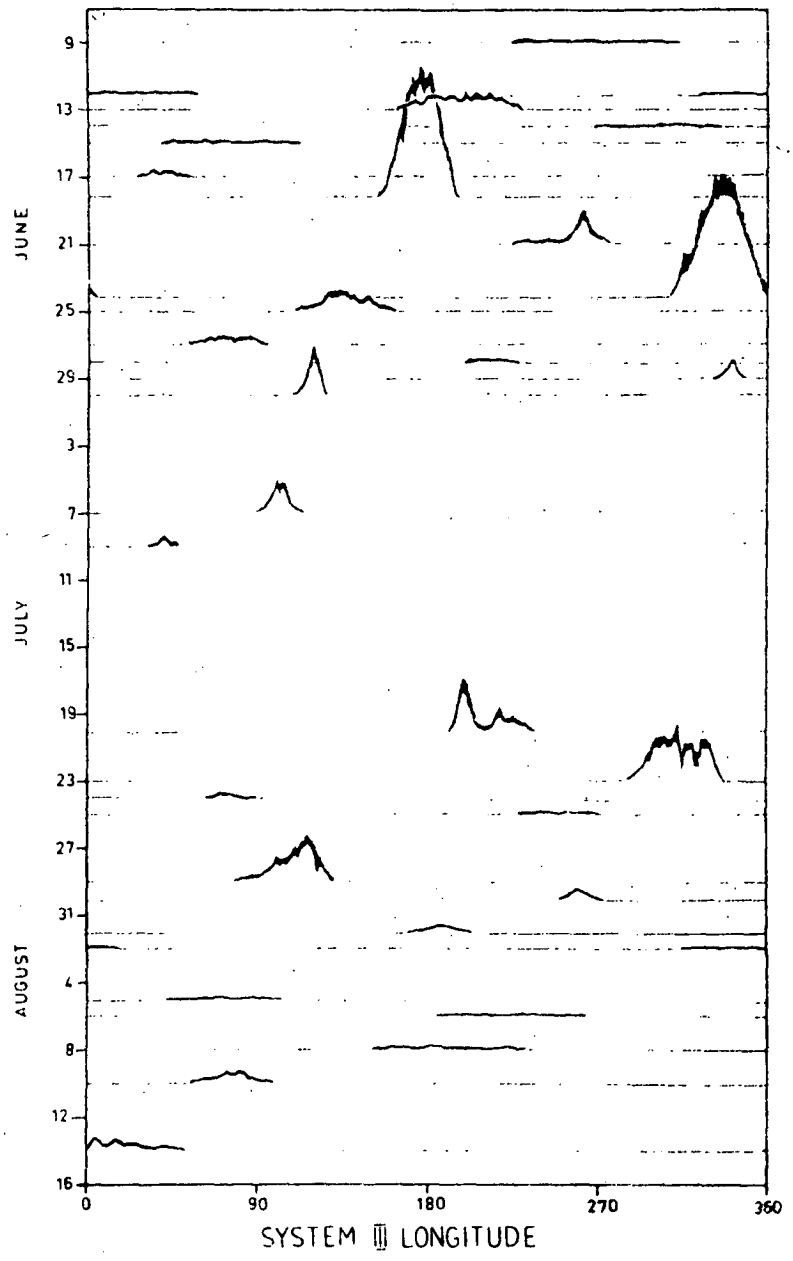


Figure 3.2 Variation of the power of each of the Jupiter events received at 4.7 MHz with system III longitude.

source Centaurus A.

The variation of the intensity of an event with Jupiter longitude was obtained by plotting the envelope of the interferometer record, e.g. the dotted line in Figure (3.1a), against I.A.U. system III longitude (rotation period $9^h\ 55^m\ 29.37^s$). This was repeated for each observation to give a diagram of the type shown in Figure (3.2) for 4.7 MHz. Profiles of total power against longitude were then obtained by summing the intensities of each of the individual events in each $9^o$ longitude interval. The variation of the number of occurrences with longitude could also be obtained by adding the number of events in each longitude interval. Total power and occurrence profiles obtained in this way are shown in Figures (3.3) and (3.4) respectively.

Observations of burst structure were made at 24.5 MHz with a time resolution of 0.2 sec. Bursts were recorded from both aerials of the interferometer, spacing 150 meters, giving a comparison of burst profiles at this baseline. Some observations of burst profiles were made at 19.7 MHz to compare with records made simultaneously by O.B. Slee of the C.S.I.R.O. division of Radiophysics at Sydney, the baseline here being about 1000 Km. A short series of runs were also made at 24.5 MHz with a time resolution of 0.02 secs.

## 3.4 Comparison of Probability and Power Longitude Profiles.

The variation of the power of the decametric emissions of Jupiter with system III longitude at each frequency is plotted in Figure (3.3), and the corresponding variations of the probability of

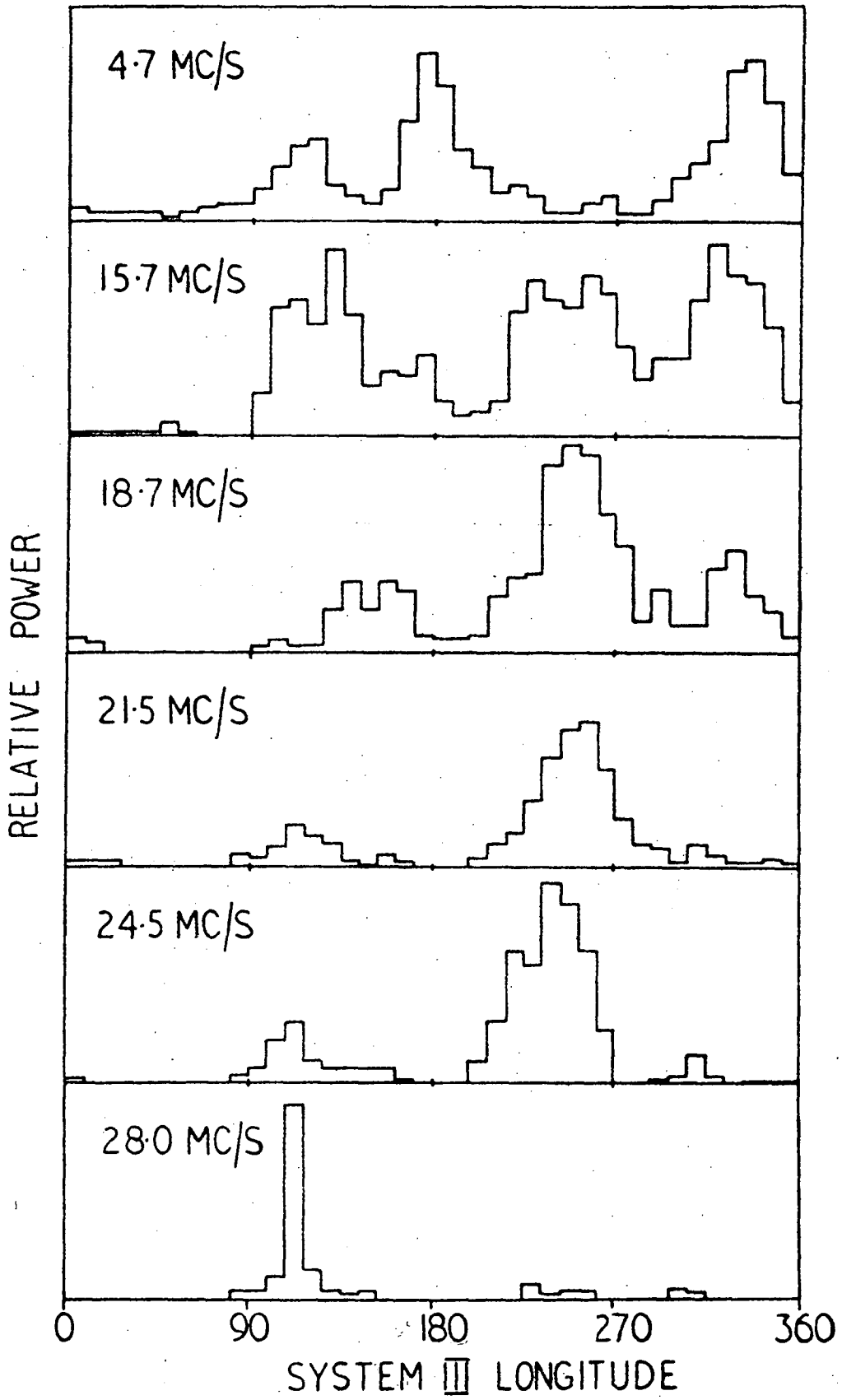


Figure 3.3 Variation of the relative power of Jupiter's emissions with longitude at each observing frequency.

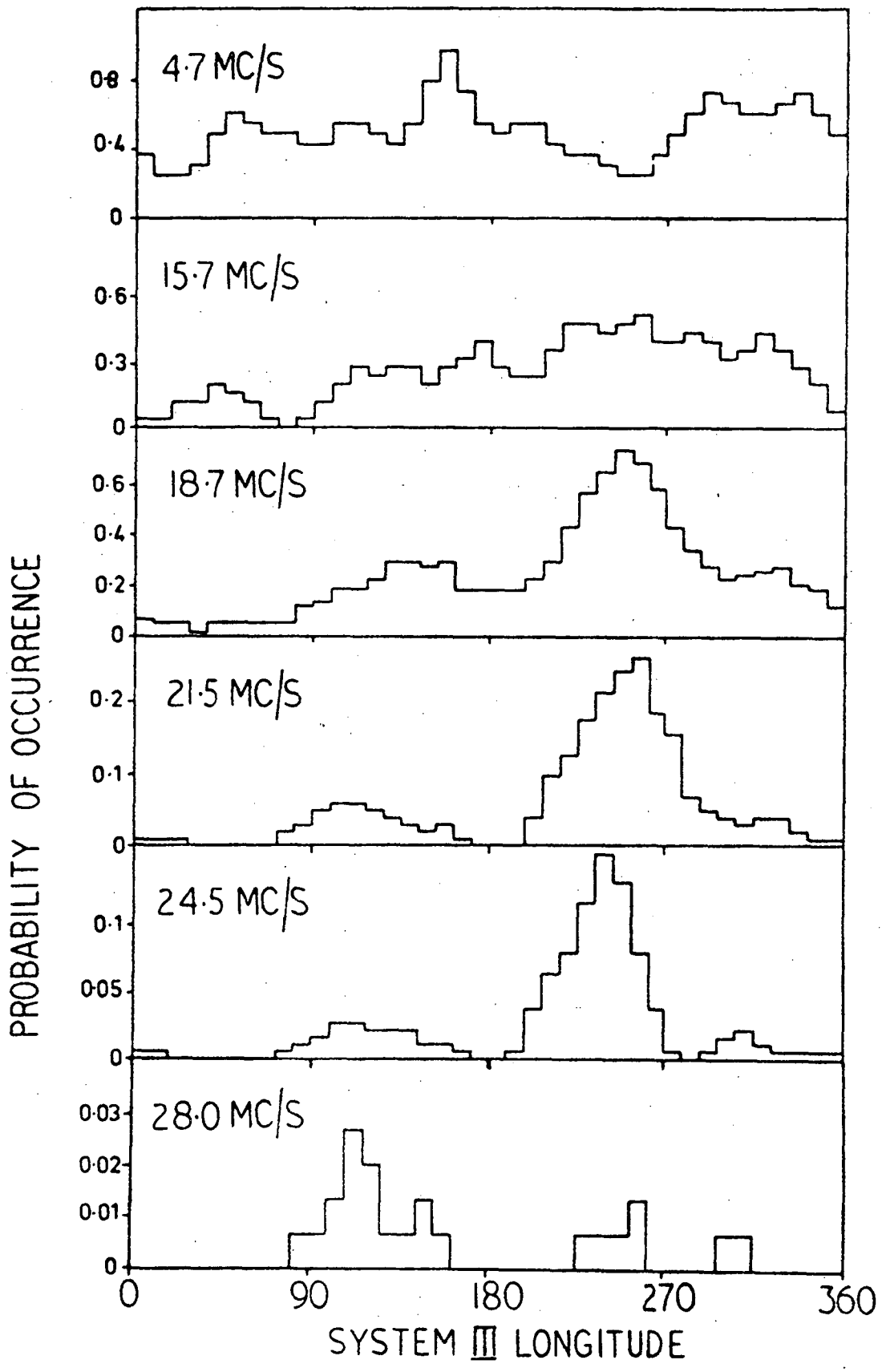


Figure 3.4 Variation of the probability of occurrence of Jupiter's emissions with longitude at each observing frequency.

occurrence with longitude is shown in Figure (3.4). Comparison of these two diagrams shows that at 18.7 MHz and higher frequencies, the general characteristics of the profiles agree quite well. However, it is apparent that there is very little similarity between the profiles at 4.7 MHz and 15.7 MHz. The power profiles show a variety of peaks and troughs while the occurrence profiles are relatively featureless. This relatively smooth variation of probability of occurrence with longitude at the low frequencies appears to be the result of the inclusion in the data of a large number of weak occurrences, which can be tested by excluding weak bursts by successive reductions in gain. The resultant longitude profile of probability of occurrence at 15.7 MHz is illustrated in Figure (3.5), which gives profiles for a reduction of gain by factors of 3 and 10. This reduction in gain only excludes the very weak occurrences which make little contribution to the relative power, so the profile of the variation of power with longitude at 15.7 MHz will not be affected. The occurrence profiles at reduced gain compare well with the power profile in their general characteristics.

This result indicates that weak events can occur over a wide range of longitudes while the stronger events are confined to narrow longitude intervals corresponding to the peaks in the power longitude profiles. The longitude profiles obtained for the probability of occurrence by including only strong events can be very different from that obtained by including all events strong and weak. This result is in agreement with the observations of Stone et al (1964), that if very sensitive equipment is used the widths of the peaks of the longitude profiles of probability of occurrences at 26.3 MHz are signifi-

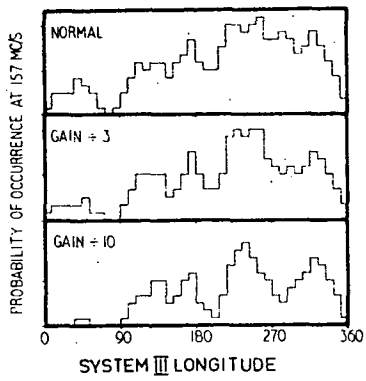


Figure 3.5 The effect of reducing the receiver gain on the variation of probability of occurrence with longitude at 15.7 MHz.

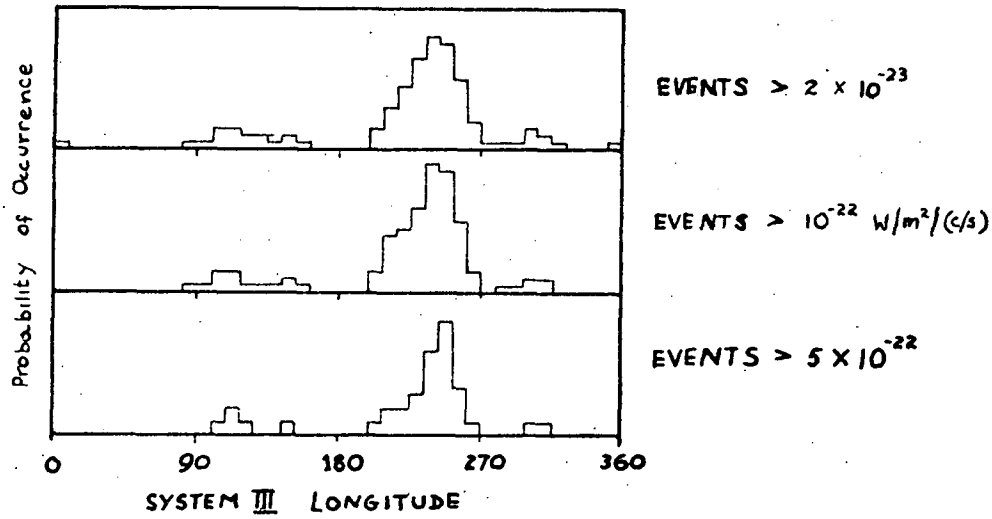


Figure 3.6 Longitude profiles of probability of occurrence at 18.7 MHz showing the effect of changes in the minimum detectable signal.

cantly broader than those obtained by observers using less sensitive equipment.

It might be expected that the longitude profiles obtained at 18.7 MHz and higher frequencies would exhibit a similar effect. However, no pronounced broadening of the maxima was obtained, Figure (3.6), due either to a decrease in the intensity of the bursts at these frequencies, or a lack of sensitivity in the receiving equipment used at the higher frequencies.

The comparison of the two methods of displaying information about Jupiter's decametric emissions indicates that at frequencies above 20 MHz very little difference is obtained by recording the probability of occurrence or total power of the bursts, unless very sensitive equipment is used such as that described by Stone (1964). The probability of occurrence profiles do not show any consistent features throughout the frequency range, and are very dependent on the receiver sensitivity. The power longitude profiles on the other hand show features such as the peaks between $100^{\circ}$ and $180^{\circ}$ and the peak near $330^{\circ}$ which are present at all frequencies and whose shape are not influenced greatly by receiver gain. This relative stability of the power longitude profiles makes them much more suitable for analysis in detail than the occurrence profiles, and for this reason they are the only ones discussed in detail in the following sections.

## 3.5 Power Longitude Profiles.

At 4.7 MHz there are three quite distinct maxima in the longitude power profile, being centered on longitude $120^{\circ}$, $175^{\circ}$ and $335^{\circ}$. At higher frequencies a fourth maxima appears near longitude

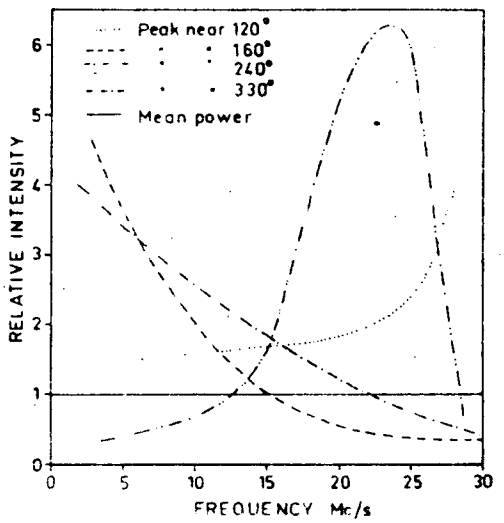


Figure 3.7 Variation of the relative intensity of each of the four maxima in the longitude profiles of Figure 3.3 with frequency. The intensities of each maxima at any frequency have been plotted relative to the mean intensity at that frequency.

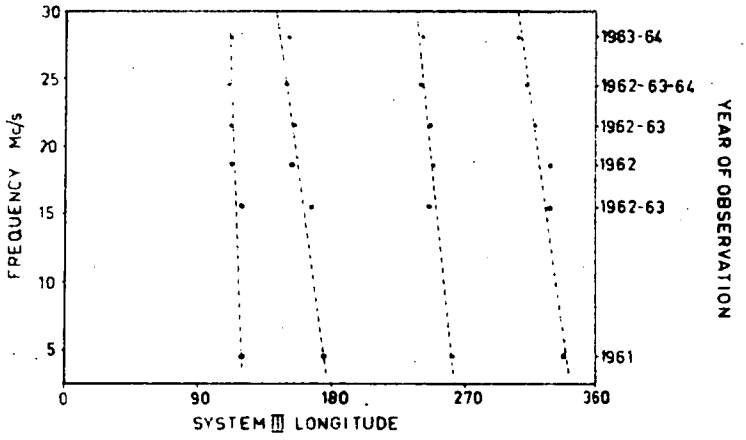


Figure 3.8 Variation in the longitude of the maxima of the longitude profiles from Figure 3.3 with frequency and year of observation.

$255^{\circ}$. This gives four peaks near longitudes $120^{\circ}$, $175^{\circ}$, $255^{\circ}$ and $335^{\circ}$ which will be designated $B_1$, $B_2$, A and C respectively. If we take C as a standard for comparison, we find that $B_1$ appears to show a general increase in amplitude with frequency. Peak $B_2$ on the other hand drops off slightly up to 18.7 MHz but thereafter remains essentially constant with frequency. Peak A shows an even more complex behaviour; at 4.7 MHz it is practically non-existent and then as the frequency increases it increases rapidly in amplitude up to 24.5 MHz, from whence it diminishes even more rapidly until at 28.0 MHz it is of similar magnitude to the standard peak C. Peaks $B_2$ and C exhibit similar characteristics with frequency which are different from the behaviour of both $B_1$ and A. This effect is illustrated in Figure (3.7).

The longitudes of the maxima show a consistent decrease at higher frequencies Figure (3.8). Peaks $B_2$ and C both decrease in longitude at approximately $1.3^{\circ}$ per megacycle, while the other peaks both show smaller changes, $0.3^{\circ}$ per megacycle for $B_1$ and $0.9^{\circ}$ per megacycle for A. This may be a genuine change in the position of the radio sources with frequency, or it may be a spurious effect introduced by an error in the rotation period of the radio sources over the period of the observations 1961-1964. The change in the rotation period required to produce a shift of the source positions by $-30^{\circ}$ in three years is a decrease of 1.1s. Douglas and Smith (1963) and Smith et al (1965), have shown that there was an apparent increase in the system III rotation period of about 1s during the period in question. This implies that the change of the radio source positions to lower longitudes at higher frequencies is a

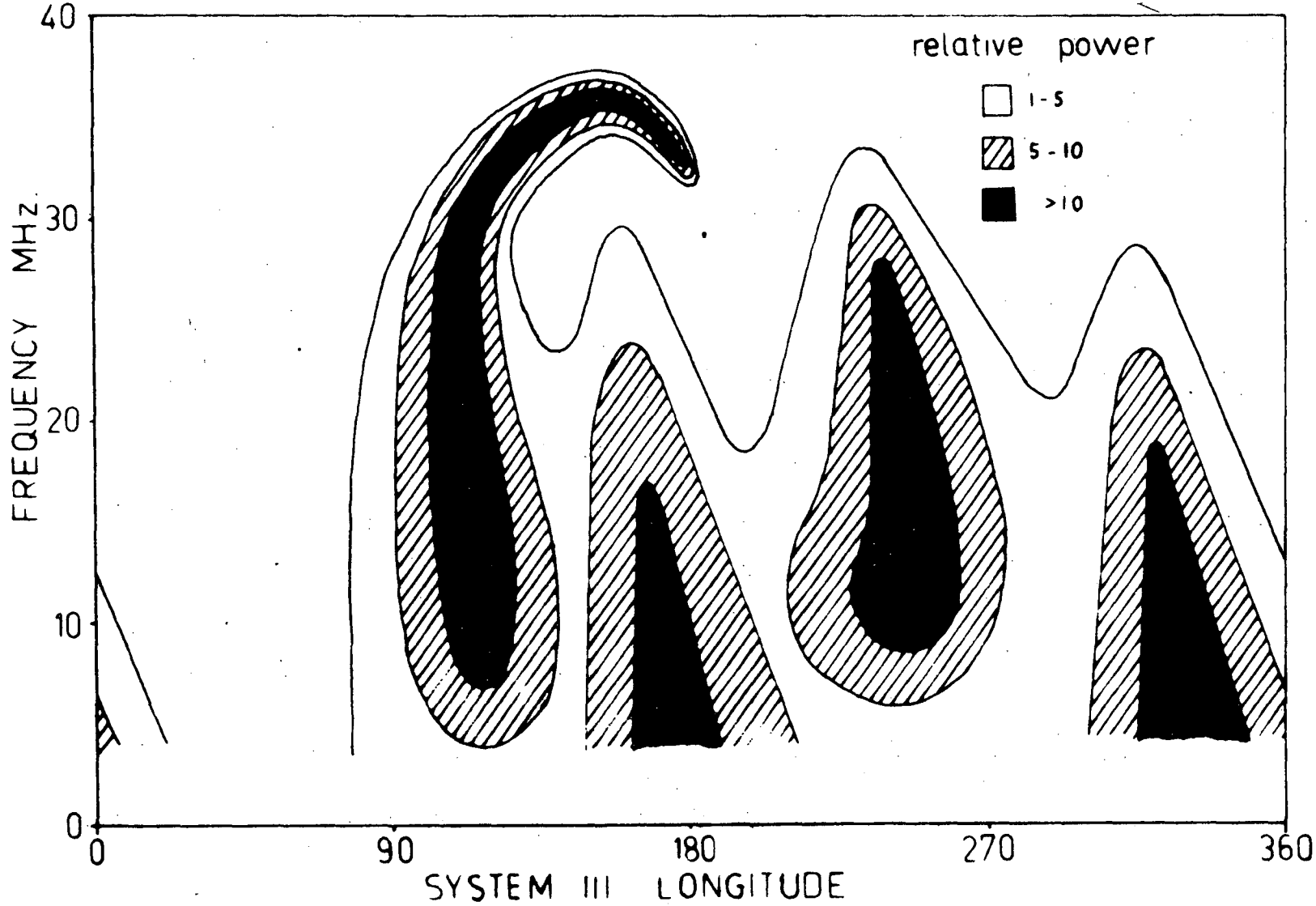


Figure 3.9 Composite diagram showing the longitudes of strong radiation at each frequency, obtained by combining the longitude profiles of Figure 3.3 with Warwick's permanent spectral features. The contours indicate the variation of relative intensity with longitude for each frequency; no attempt has been made to show how the intensity changes with frequency.

genuine phenomenon whose effect has been reduced by the change of rotation period. A similar decrease in the longitude of the source near $255^{o}$ has been reported by Carr et al (1961) for the frequency range 10 - 27.6 MHz. They also reported a decrease in the individual source widths with increasing frequency, this effect is apparent in the data of Figure (3.3).

The data contained in the longitude profiles can be displayed in a different way by means of a contour diagram in the frequency longitude plane. The diagram shown in Figure (3.9) has been prepared from longitude profiles for the frequency range 5 - 28 MHz and from published dynamic spectra (Warwick 1963, Dulk 1965) for the frequency range 28 - 40 MHz. The shaded regions indicate where strong emission occurs regularly, whereas the unshaded region indicates strong emission occasionally or weak emission more frequently. Weak emission may occur occasionally outside the contoured area. The diagram attempts to join up the dynamic spectral data and longitude profile data in a way which can be used to demonstrate the long term average behaviour of Jupiter as a low frequency radio source. The contouring of a particular region in the frequency-longitude plane is not meant to imply that a particular dynamic spectrum would have that form. However the integrated effect of a large number of dynamic spectra should have that form. The contours indicate how the relative intensity varies with longitude at a given frequency; no attempt has been made to show how the intensity changes with frequency.

## 3.6 Mean Power Spectrum.

At each frequency the mean flux of Jupiter's emissions was calculated by adding the areas enclosed by the envelope of the interferometer pattern for each individual occurrence and dividing by the total observing time. An absolute calibration of the flux density was then obtained by comparing this with the calibrations from a standard noise source. Corrections were made for the effect of ground conductivity in the manner described by Ellis (1965).

At 4.7 MHz absorption in the Earth's ionosphere may at times strongly modulate the intensity of the received signals. The amount of absorption can be calculated from a knowledge of the ionospheric critical frequency $f_oF_2$ and the electron density in the D region. A detailed discussion of the ionospheric absorption has been given by Ellis (1965).

The critical frequency $f_oF_2$ usually drops to about 2 MHz for periods of several hours during winter nights in Hobart for years near the solar minimum. The attenuation was then less than 0.5 db which was the case when most of the emission was observed.

A second method was used to check the flux density values obtained from the noise calibrations. This involved comparing the intensity of the signals received from Jupiter with those received from other discrete sources. At 4.7 MHz Centaurus A (N.G.C.5128) was used for comparison. The levels of the recorded signals from both Jupiter and Centaurus A were corrected for ionospheric absorption before comparison. At the other frequencies, Jupiter was compared with the radio source Hydra A. The flux density of Centaurus

at 4.7 MHz has been given by Ellis and Hamilton (1965) as $3.6 \times 10^{-22}$ $Wm^{-2}$ $Hz^{-1}$. The flux density of Hydra A at the higher frequencies was obtained from a spectrum produced by combining the data of Conway, Kellerman and Long (1963), Mills and Slee (1951), and Shain and Higgins (1954), which is illustrated in Figure (3.11).

The ratios of mean flux density of Jupiter's emissions over the entire observing period to the flux density of the standard sources at each frequency is given in Table (3.2).

The mean power spectrum obtained is plotted in Figure (3.10a); it can be divided into two parts, one having a spectral index of -2.5 between 4.7 MHz and 20 MHz and the other a spectral index of -13.7 between 24 MHz and 30 MHz.

| Frequency MHz | 4.7 | 15.7 | 18.7 | 21.5 | 24.5 | 28.0 |
|---|---|---|---|---|---|---|
| ratio $\frac{\text{Jupiter}}{\text{Centaurus A}}$ | 3.2 | - | - | - | - | - |
| ratio $\frac{\text{Jupiter}}{\text{Hydra A}}$ | - | 0.60 | 0.85 | 0.76 | 0.56 | 0.06 |

Table 3.2

The spectrum produced here is similar to that obtained by Carr et al (1964) for the frequency range 10 - 27.6 MHz. The spectrum is observed to increase monotonically with decreasing frequency down as far as 4.7 MHz, there being no indication of a turnover in the spectrum at low frequencies.

The mean power spectrum has been produced by averaging the total power received over all observing periods, whether activity occurred or not. We could also construct a mean power spectrum

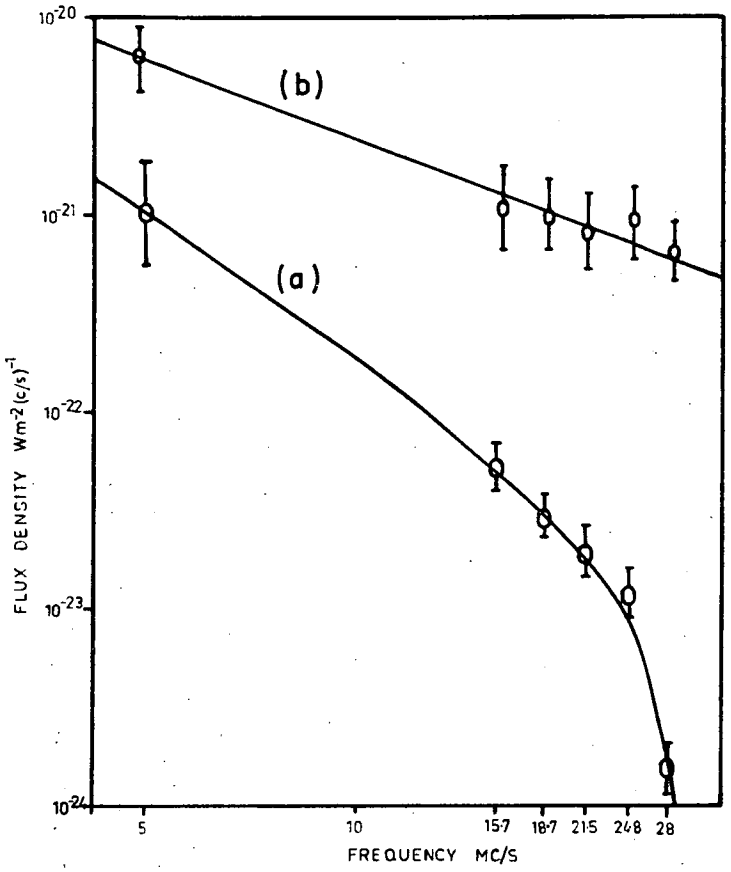


Figure 3.10 (a) The mean power spectrum of Jupiter's decametric emissions averaged over inactive as well as active periods. (b) The peak power spectrum of Jupiter's decametric emissions.

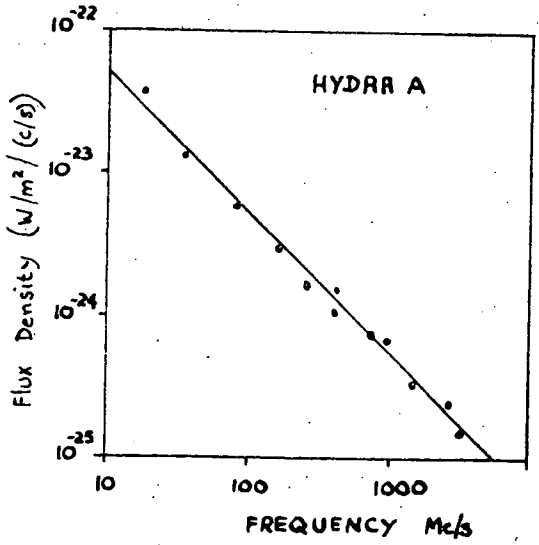


Figure 3.11 The spectrum of Hydra A.

only over active periods; however, the number of active periods is strongly dependent on receiver sensitivity and the spectrum obtained would be meaningless unless a threshold was prescribed. An estimate of the way in which the received intensity varies with frequency has been obtained by averaging the five strongest events recorded at each frequency. This is illustrated in Figure (3.10b). The peak flux spectrum approximates a straight line with a spectral index of -1.2 and hence over the high frequency region from 15 - 30 MHz the peak flux only decreases by a factor of two.

As a general trend Jupiter emitted less often at the higher frequencies than at the lower frequencies, although no accurate estimate of the variation of probability of occurrence with frequency was made due to its dependence on receiver gain.

## 3.7 Correlation with Io.

It has been shown by Bigg (1964) that Jupiter's emission is modulated by the position of the Jovian satellite Io. Jupiter's emission shows two maxima corresponding to system III longitude $100^{\circ}$ - $160^{\circ}$ and $200^{\circ}$ - $250^{\circ}$, with Io being $80^{\circ}$ - $100^{\circ}$ and $230^{\circ}$ - $250^{\circ}$ from superior geocentric conjunction respectively. The data obtained at four frequencies, 4.7, 15.7, 24.5 and 28.0 MHz, has been analysed in a similar manner to that used by Bigg. The resulting diagrams are shown in Figure (3.12). The figures for 15.7 MHz and 24.5 MHz are similar to the result of Bigg showing maxima having coordinates ($120^{\circ}$, $100^{\circ}$), ($250^{\circ}$, $240^{\circ}$) at 15.7 MHz and ($120^{\circ}$, $90^{\circ}$) and ($230^{\circ}$, $220^{\circ}$) at 24.5 MHz. At 28.0 MHz only one peak is prominent at ($110^{\circ}$, $95^{\circ}$), corresponding approximately to the position of the

first mentioned of the two sources. The pattern at 4.7 MHz is quite different, the most prominent feature being a large area in the center of the diagram from which no radiation was received. There are several intense regions, the most prominent of which corresponds to source B and has coordinates ($180^{\circ}$, $130^{\circ}$). However, there is insufficient data to allow any but the most general deductions to be made. Both of the maxima in the diagrams obtained at 15.7 MHz and 24.5 MHz correspond to radiation when Io's longitude is near $200^{\circ}$, whereas the results of Bigg put Io at $225^{\circ}$ and $165^{\circ}$ respectively for the two maxima.

The actual correspondence found between the emission and the system III longitude of Io appears to depend largely on the method of analysis. Bigg (1964) finds no pronounced dependence of emission on the longitude of Io while Duncan (1965) maintains that there is. The present analysis seems to indicate that emission is most pronounced when Io is near system III longitude $200^{\circ}$. However, whether the analysis of Duncan or Bigg is correct we can say that strong emission at frequencies greater than 25 MHz, say, only occurs when Io's system III longitude is in the range $150^{\circ}$ - $240^{\circ}$. The microwave observations of Roberts and Komesaroff (1965) place Jupiter's north magnetic pole near $190^{\circ}$, so emission is most favourable when Io is in its vicinity.

The polarisation data obtained by Dowden at 10.1 MHz has been examined for the influence by Io. The data was obtained over a short period of about three months and hence does not cover very much of the Io-Jupiter plane. For this reason that data was subdivided into four parts, right and left hand polarisation, and radiation occurring in the longitude ranges 0 - $180^{\circ}$ and $180^{\circ}$ - $360^{\circ}$ system III. The power received in each of these four subdivisions has been plotted as a

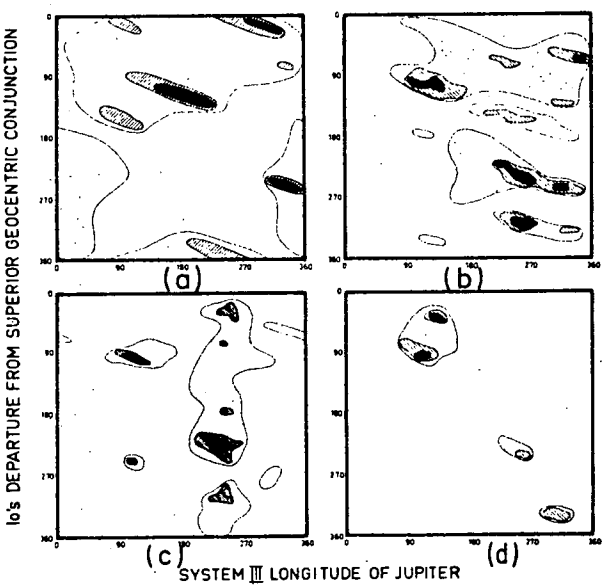


Figure 3.12 Contours of Jupiter's emission (arbitrary units) as a function of Io's departure from superior geocentric conjunction and Jupiter's longitude for (a) 4.7 MHz, (b) 15.7 MHz (c) 24.5 MHz and (d) 28.0 MHz.

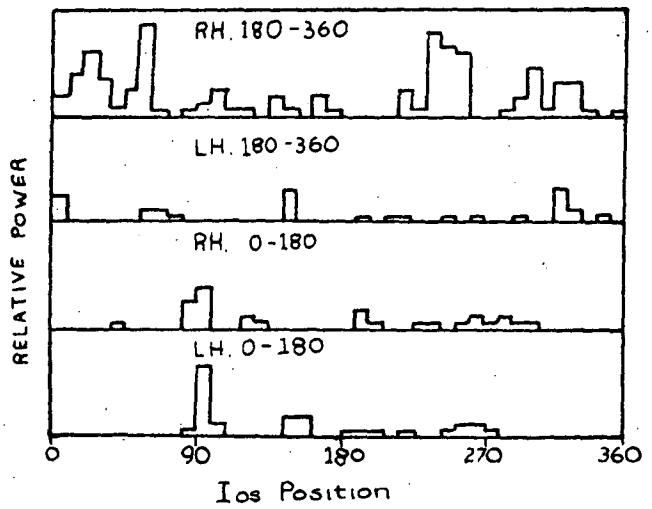


Figure 3.13 Variation of the power of Jupiter's emissions at 10.1 MHz with Io's position.

function of Io's departure from superior geocentric conjunction in Figure (3.13). The emission that originated in the range 0 - 180° shows similar trends for both polarisations, there being enhanced emission when Io was near 90°. For the emission that originated in the range 180° - 360° the most notable features are that there is a lack of right hand polarisation emission when Io was between 70° and 210° and that the left hand emission appears to be independent of Io.

The statistical significance of this data is poor and it does not warrant any definite conclusions.

## 3.8 Spaced Site Observations of Burst Structure.

Many observers have found considerable difference in the structure of bursts recorded at sites a few km apart (Section 2.2). Observations have been made at 24.5 MHz with a baseline of 150 m and at 19.7 MHz with a baseline of 1000 km. These observations show that at 150 m the correlation is usually very good, however, on occasions poor correlation can be obtained. Figure (3.14) shows an event with poor correlation at 150 m, note that the event marked "X" on (a) is not visible on (b) even allowing for the difference in gain between the two channels. This strong modulation of the received signal can be explained in terms of refraction and diffraction at irregularities in the Earth's ionosphere (Matsumoto, 1965).

The observations made with the 1000 km baseline showed very little, if any, detailed correlation. Radiation was received at both sites over the same general time interval, but no burst for burst correlation was found.

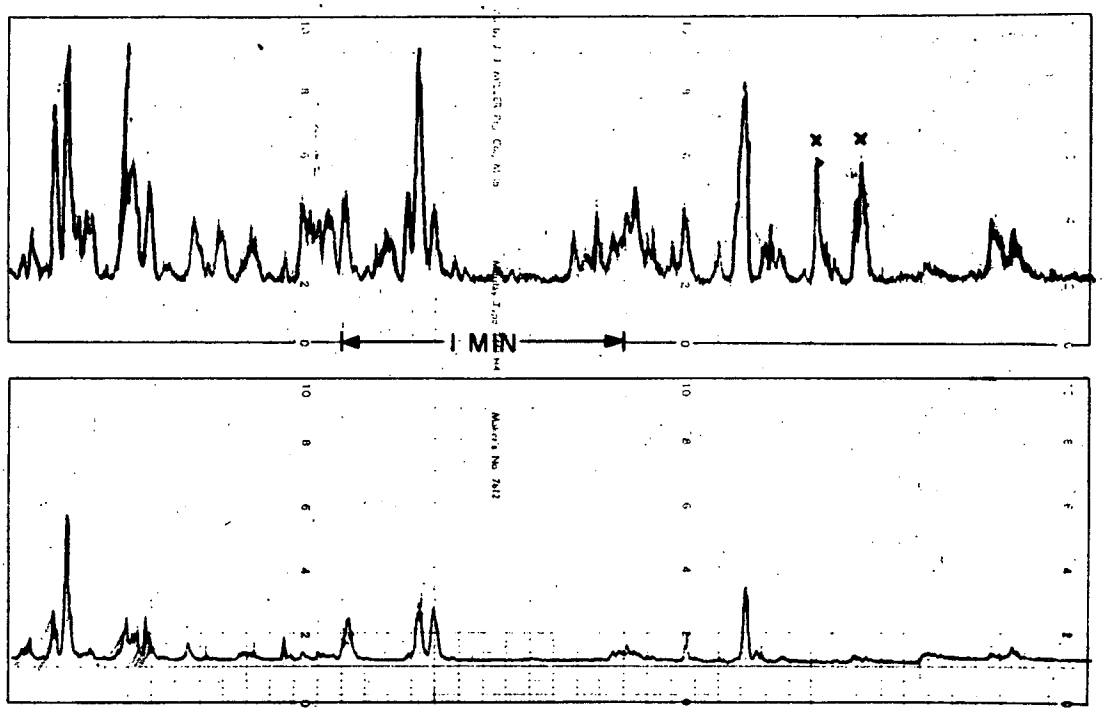


Figure 3.14 Spaced observations at 24.5 MHz showing poor correlation over a baseline of 150 m. Note the bursts marked "x" in the top figure are completely absent in the bottom figure.

These results confirm the observation that the Earth's ionosphere at times seriously modulates the incoming signals. The work of Slee and Higgins (1964) indicates that the radiation emitted by Jupiter is in the form of bursts, and these are further modified by the interplanetary medium and the Earth's ionosphere.

## 3.9 Summary.

The main features of the decametric emissions from Jupiter that would have to be explained in any theoretical model are summarised below.

(1) The high intensity of the radiation, peak powers of $10^{-18}$ $Wm^{-2}$ $Hz^{-1}$ being recorded, together with the mean power and average peak power spectrum, Figure (3.11).

(2) The average characteristics of the radiation contained in the occurrence and total power longitude profiles and in composite dynamic spectra. The long term behaviour must be as illustrated in Figure (3.9).

(3) Any theory of the decametric emissions must contain as an integral part the influence of Io on the high ($>$ 20 MHz) emission, Figures (2.17), (2.18) and (3.12).

(4) The theory must also provide an explanation of the characteristics of single events, shown in low and high time resolution dynamic spectra, Figures (2.12) and (2.16).

(5) The emitted radiation must be elliptically polarised

mainly in the R.H. sense with axial ratios around 0.5. The proportion of right and left polarised emission must show the appropriate variation with longitude, Figures (2.6) to (2.9).

(6) The emission must be in the form of bursts which show structure on several time scales, Figure (2.1).

## 3.10 References.


BIGG, E.K. (1964) Nature 203, 1008

CARR, T.D., A.G. SMITH, H. BOLLHAGEN, N.F. SIX, Jr., and N.E. CHATTERTON (1961) Astrophys. J. 134, 105

CONWAY, R.G., K.I. KELLERMAN and R.J. LONG (1963) Mon. Not. R.A.S. 125, 261

DOUGLAS, J.N. and A.G. SMITH (1963) Nature 199, 1080

DOWDEN, R.L. (1963) Aust. J. Physics 16, 398

DULK, G.A. (1965) Ph. D. Dissertation, University of Colorado.

DUNCAN, R.A. (1965) Planet Space Sci. 13, 997

ELLIS, G.R.A. (1961) Nature 194, 667

ELLIS, G.R.A. (1965) Mon. Not. R.A.S. 130, 429

ELLIS, G.R.A. and P.A. HAMILTON (1965) Astrophys. J. 143, 227

McCULLOCH, P.M. (1963) Honours Thesis, University of Tasmania.

McCULLOCH, P.M. and G.R.A. ELLIS (1966) Planet Space Sci. 14, 347

MATSUMOTO, H. (1965) Rep. Ionospheric and Space Res. Japan 19, 4

MILLS, B.Y. and O.B. SLEE (1957) Aust. J. Phys. 10, 162

ROBERTS, J.A. and M.M. KOMESAROFF (1965) Icarus 4, 127

SHAIN, C.A. and C.S. HIGGINS (1954) Aust. J. Phys. 7, 130

SMITH, A.G., G.R. LEBO, N.F. SIX, T.D. CARR, H. BOLLHAGEN, J. MAY and J. LEVY (1965) Astrophys. J. 141, 457

STONE, R.G., J.K. ALEXANDER and W.C. ERICKSON (1964) Astrophys. J. 140, 374

WARWICK, J.W. (1963) Astrophys. J. 137, 41

# CHAPTER 4.

# THE MAGNETOSPHERE OF JUPITER

## 4.1 Introduction.

There have been many theories proposed to explain the decametric emission from Jupiter. The most plausible of these invoke emission by fast electrons in a magnetoactive plasma. The theories can be divided into two classes, the most popular being that the radiation is generated close to the surface of Jupiter within the ionosphere or lower magnetosphere. The second class of theories requires the radiation to be generated in the neighbourhood of Jupiter's satellite Io.

The acceptability of any of these theories depends upon the distribution of ambient plasma in Jupiter's magnetosphere. In this chapter we calculate upper limits on the electron density in Jupiter's ionosphere and radiation belts and estimate an upper limit for the neutral particle density in the radiation belts.

## 4.2 The Ionosphere of Jupiter.

A model of the Jovian atmosphere has been proposed by Kuiper (1952). It consists of a troposphere - a region in which the temperature decreases upwards - and an isothermal stratosphere. The suggested percentage composition by weight of the atmosphere is $H_2$ 63.5, He 35, and heavier gases ($CH_4$, $NH_3$, etc) 1.5 giving a mean molecular mass 2.5 times the mass of the hydrogen atom. This atmosphere will be partially ionised by ultra-violet radiation from the sun, and by high energy cosmic ray particles, giving rise to a Jovian

ionosphere.

The temperature of the cloud layer on Jupiter is about 135°K (Allen, 1962). At heights of a few hundred km above the stratosphere the temperature may increase above this value as is observed for the Earth; however, the temperature is likely to remain in the range 100°K to 5000°K. The scale height of the various components in the atmosphere depends inversely on the molecular mass, and hence the heavier molecules will be concentrated at the lower levels, so that the region where ionisation takes place will contain only hydrogen and helium. The reactions that can take place ignoring the possibility of negative ion production are:-

(1) $H_2 + h_\nu \xrightarrow{4.2\ ev} H + H$ dissociation

(2) $H + h_\nu \xrightarrow{13.5\ ev} H^+ + e^-$ ionisation

(3) $H_2 + h_\nu \xrightarrow{15.6\ ev} H_2^+ + e^-$ ionisation

(4) $He + h_\nu \xrightarrow{24.5\ ev} He^+ + e^-$ ionisation

(5) $H_2^+ + e^- \longrightarrow H^* + H^*$ dissociative recombination

(6) $H_2 + e^- \longrightarrow H_2 + h_\nu$ radiative recombination

(7) $H^+ + e^- \longrightarrow H + h_\nu$ radiative recombination

(8) $H + H \longrightarrow H_2 + h_\nu$ radiative recombination

(9) $He^+ + e^- \longrightarrow He + h_\nu$ radiative recombination

The maximum electron density in the ionosphere will be effectively controlled by the recombination rates for the various reactions. The most rapid reaction is the dissociative recombination with a rate of approximately $10^{-8}$ $cm^3/sec$, whereas the radiative recombinations have rate co-efficients which are typically $10^{-12}$ $cm^3/sec$.

The dominant reaction will depend upon the density of molecular hydrogen. If there is an appreciable amount of molecular hydrogen present, reactions (3) and (5) will dominate whereas if there is negligible molecular hydrogen reactions (2) and (7) will dominate.

A model of the Jovian ionosphere can be constructed using the theory for the formation of a Chapman layer (see for example - Ratcliffe, 1960). Consider radiation of intensity I incident on the Jovian atmosphere of absorption co-efficient A per unit mass at an inclination $\psi$ to the vertical. The change dI in I in passing through thickness dh at h is

$$dI = AI dh \sec\psi \rho_o e^{-(\frac{h}{H})}$$

where $\rho_o$ is the density at ground level and H is the scale height, $H = \frac{kT}{mg}$

Then $I = Io \exp \{ - A\rho_o H \sec \psi \exp ( - \frac{h}{H}) \}$

where Io is the intensity of radiation before it enters the atmosphere. Let B be the number of ions produced by absorption of unit quantity of radiation.

The rate of production of ions at height h

$$q = B \frac{dI}{dh} \cos \psi$$

$$\therefore \quad q = B A Io \rho_o \exp \{ - \frac{h}{H} - A \rho_o H \sec \psi \exp (- \frac{h}{H}) \}$$

At any instant the rate of ion production q and the rate of ion decay must approximately balance. If $N_e$ is the number of electrons at any instant at height H, then assuming recombination is the only process of decay, the number of electrons lost per cc per second is $\alpha N_e^2$ where $\alpha$ is the recombination coefficient.

Hence for quasi equilibrium

$$\frac{dN_e}{dt} = q - \alpha N_e^2 = 0$$

$$\therefore \quad q \simeq \alpha \, N_e^{\,2}$$

Now $N_e$ will be a maximum when q is a maximum, and q will be a maximum when

$$\exp\left(\frac{h_{max}}{H}\right) = A \, \rho_o \, H \sec \psi$$

and $$q_{max} = B \, Io \, \frac{\cos \psi}{H} \exp(1) = \alpha \, N_e^{\,2}$$

then $$N_e = \left(\frac{B \, Io \, e}{\alpha \, H} \cos \psi\right)^{\frac{1}{2}}$$

At the Earth the energy content of the far ultraviolet likely to ionise hydrogen is approximately 0.46 erg $cm^{-2}$ $sec^{-1}$.

At Jupiter the energy will be

$$Io = \frac{0.46}{27} \text{ erg cm}^{-2} \text{ sec}^{-1}$$

for hydrogen $$B = 4.65_{10}10 \text{ erg}^{-1}$$

The scale height $H \simeq 3.12_{10}4$ cm/°K

and hence $$N_e = \frac{2.62_{1}}{(\alpha T)^{\frac{1}{2}}} 100 \, (\cos \psi)^{\frac{1}{2}} \text{ cm}^{-3}$$

If all the molecular hydrogen is dissociated at this height the appropriate recombination coefficient is that for atomic hydrogen which is

$$\alpha = 4.3_{10}{-13} \left(\frac{-10^4}{T}\right)^{0.8} \text{ cm}^3/\text{sec}$$

and $$N_e = 1.0_{10}7 \, T^{-0.1} \, (\cos \psi)^{\frac{1}{2}} \text{ cm}^{-3}$$

The temperature is likely to be in the range 100°K to 5000°K and so $T^{0.1} \simeq 2.0$. In the equatorial plane the maximum electron density in the Jovian ionosphere will be

$$N_{max} \simeq 5.0_{10}6 \text{ electrons/cc.}$$

The assumption that dissociative recombinations do not control the electron density should be examined. If the density of hydrogen molecules is of the same order as the electron density then dissoc-

iative recombinations will have to be taken into account. The relative concentrations of atomic and molecular hydrogen at temperature T has been given by Fowler and Guggenheim (1939).

$$\frac{(C_H)^2}{C_{H_2}} = \frac{2(\pi mkT)^{3/2}}{h^3} \frac{\theta_r}{T} \frac{v_H^2}{v_{H_2}} \frac{\exp(\frac{-I}{kT})}{q(T)}$$

where $v_H$ and $v_{H_2}$ are the statistical weights of the particular states, q(T) is the vibrational partition function of the hydrogen molecule, I is the dissociation energy and $\theta_r$ is the temperature associated with the rotational energy of the molecule.

This may be simplified to give

$$R = \frac{(C_H)^2}{C_{H_2}} = \frac{(\pi mkT)^{3/2}}{h^3} \exp\left(\frac{-I}{kT}\right)$$

for $T = 5000^{\circ}K$ $R = 7.2_{10}21$

$T = 1000^{\circ}K$ $R = 5.24$

$T = 100^{\circ}K$ $R = 4.0_{10}-253$

We can estimate the total number density, atomic plus molecular, at the level of maximum electron density $h_{max}$ as

$N = No \exp\left(\frac{-h_{max}}{H}\right)$ where No is the density at the ground

$= \frac{No}{N\ a\ H}$ where a is atomic absorption coefficient

$\therefore N^2 = \frac{No}{a\ H}$

Kuiper estimated the total molecular hydrogen content as $7.1_{10}26\ cm^{-2}$. For the purpose of an order of magnitude calculation it does not matter whether we take this to be the number of hydrogen atoms or molecules.

$$N_{total} = \int N(h)\, dh$$

$$= \int No \exp\left(\frac{-h}{H}\right) dh$$

$$= No\, H$$

$$\therefore No = \frac{7.1_{10}26}{H}$$

$$\therefore N^2 = \frac{7.1_{10}26}{a\, H^2}$$

$$\therefore N = \frac{4.9_{10}21}{H}$$

at $T = 5000^{\circ}K$ $N = 6.1_{10}13\ cm^{-3}$

$T = 1000^{\circ}K$ $N = 3.0_{10}14\ cm^{-3}$

$T = 100^{\circ}K$ $N = 3.0_{10}15\ cm^{-3}$

The number of hydrogen molecules is given by

$$N_{H_2} = N + \tfrac{1}{2}R - (N\,R + \tfrac{1}{4}R^2)^{\frac{1}{2}}$$

for $T = 5000^{\circ}K$ $N_{H_2} = 2.1_{10}5\ cm^{-3}$

$T = 1000^{\circ}K$ $N_{H_2} = N - 4.0_{10}7 = 3.0_{10}14\ cm^{-3}$

$T = 100^{\circ}K$ $N_{H_2} = N = 3.0_{10}15\ cm^{-3}$

The hydrogen molecules will dominate all reactions up to a temperature of several thousand degrees. The maximum electron density below this temperature is obtained by substituting the dissociative recombination rates in the expression for the electron density. This gives $N_e = 2.6_{10}6\ T^{-\frac{1}{2}} (\cos \psi)^{\frac{1}{2}}$

The corresponding electron densities in the equatorial plane for temperatures up to several thousand degrees are about $10^5\ cm^{-3}$. At the higher temperatures both recombination processes have to be

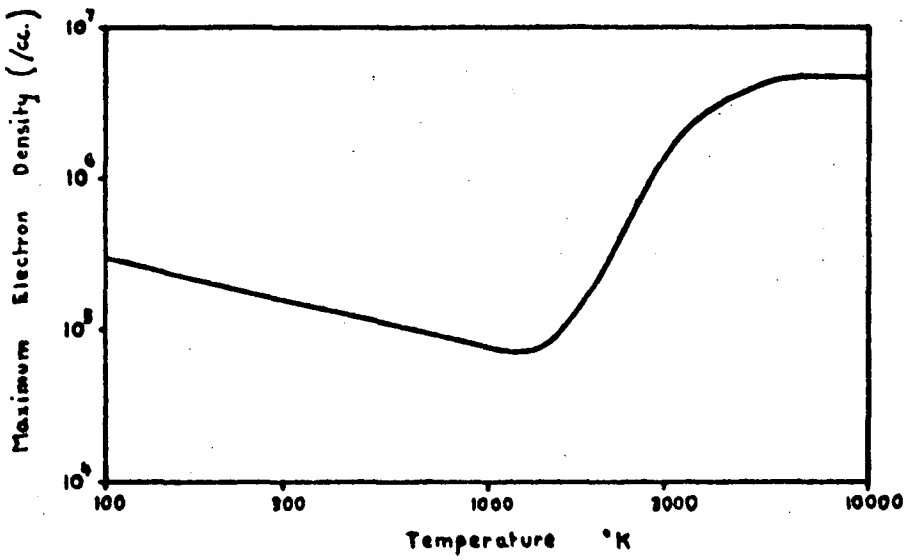


Figure 4.1 Variation of the maximum electron density in Jupiter's ionosphere as a function of the temperature of the ambient plasma.

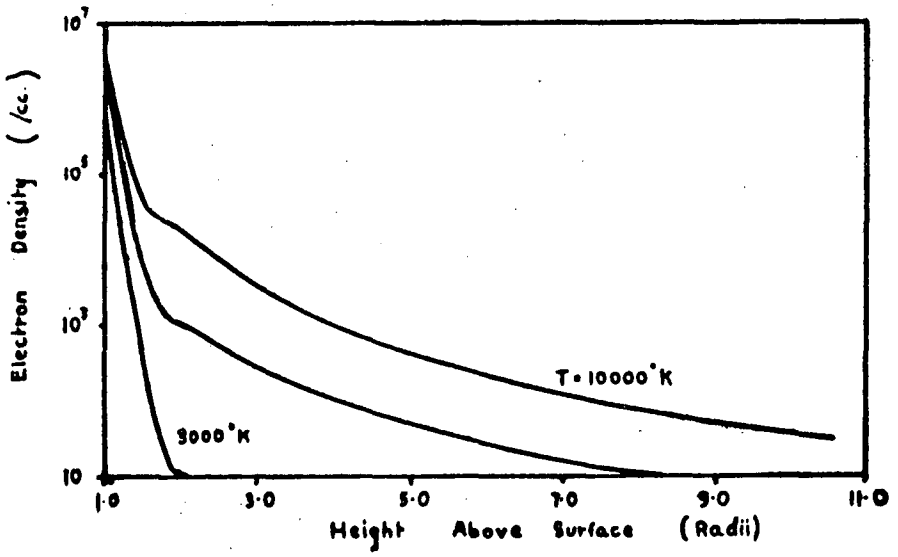


Figure 4.2 Variation of the electron density in Jupiter's equatorial plane for various values of the ionospheric temperature. The density variation is that of Melrose (1967).

considered. A graph of the maximum electron density against temperature is shown in Figure (4.1). The most likely maximum electron density in Jupiter's ionosphere appears to be about $10^5$ cm$^{-3}$, however, if the temperature is above 2000$^{o}$K densities of up to 5 x $10^6$ cm$^{-3}$ could be obtained.

## 4.3 The Magnetosphere of Jupiter.

Evidence obtained from the microwave emission from Jupiter (see Chapter 1) suggests that Jupiter has a magnetic field that is essentially dipolar with a polar field strength between 5 and 50 gauss. The region above the maximum in the ionosphere will be one in which the motion of the electrons and ions are controlled by the magnetic field. Jupiter rotates once every 10 hours and if the magnetosphere corotates with the planet, then beyond about 3 radii the net acceleration, gravitational plus centrifugal, will be directed outwards away from the planet (Ellis, 1965).

The effect of the rapid rotation of Jupiter on the distribution of thermal plasma in its magnetosphere has been discussed by Melrose (1967). The model magnetosphere proposed by Melrose can be divided into two regions - an inner and outer region, the boundary between the two regions being defined by the point at which the net acceleration along a field line is zero. The inner region is qualitatively similar to the magnetosphere of the Earth, the net acceleration is towards the planet and so particles tend to be trapped. Collisions between unlike particles tend to randomise the velocity distribution i.e. the distribution tends to be Maxwellian. The distribution of particles in this region can be written

$$N = No \exp\left[ - \tfrac{1}{2}a \left\{ \left(1 - \frac{1}{r}\right) - \tfrac{1}{2}b \sin^2 \theta \left(r^2 - \frac{1}{r}\right) \right\} \right]$$

where $a = R/H$ is the ratio of the radius of Jupiter to the scale height and $b = \Omega^2 R/g$ is a dimensionless quantity that characterises the relative importance of gravitational and centrifugal accelerations and No is the ionospheric density.

The outer region is dominated by rotational effects and is derived from the condition that the magnetosphere be stable with respect to interchange of magnetic field lines. The stability requirements lead to a model in which at some distance out from the boundary the density varies according to

$$N \propto r^{-B} \qquad \text{where} \quad 3 \leq B \leq 4$$

Beyond 7 to 8 radii the corotating magnetosphere is expected to break down due to interchange instabilities and fragmentation. The thermal plasma then extends beyond the orbit of Io but breaks down inside the orbit of the next closest satellite. The boundary between the two regions is given by $r_b = \left(\frac{3}{2} b \sin^2 \theta\right)^{-\frac{1}{3}}$

The electron distribution in the equatorial plane in the magnetosphere is plotted in Figure (4.2) for various ionospheric temperatures.

## 4.4 Limits on the Density of Jupiter's Magnetosphere from the Lifetime of the van Allen Belts.

We know from microwave observations of Jupiter that the energy radiated by the high energy electrons in Jupiter's magnetosphere has been constant over a period of years. The most likely source of high energy particles is the Sun and as solar outbursts are rare during solar minimum we require the mean life of a high energy

electron in Jupiter's magnetosphere to be long, about one year. The main contributions to the decametric radiation comes from radiation belts within $3\frac{1}{2}$ radii from the planet. The requirement that the mean life time of an electron within these belts should be about a year enables us to place an upper limit on the ambient electron density in these regions.

Electrons can be lost from a radiation belt by several processes, the most important being small angle scattering leading to lowering of the mirror point and hence eventual absorption in dense regions of the atmospheres, and energy loss due to collision. We can determine the mean lifetime of an electron due to the former process by following a similar line of reasoning to Welch and Whittaker (1959).

We assume that the electrons are on lines of force such that the dip angle near their mirror points is large, so that motion parallel to the lines of force (near the mirror points) may be approximated to motion along the radius vector. We will refer all field strengths to their value at the mirror points and consider only the $r^{-3}$ dependance in field strength, then $r_m^3 = r^3 \sin^2\alpha$ where $r_m$ is the mirror radius and $\alpha$ is the pitch angle at radius r. Suppose that the electron is scattered through a small angle $\varepsilon$

then $\sin^2(\alpha + \varepsilon) = \sin^2\alpha + \sin(2\alpha)\,\varepsilon + \cos(2\alpha)\,\varepsilon^2 + \ldots\ldots$

We are interested in the average behaviour of the electrons where $\varepsilon$ is distributed in a symmetric random distribution about $\varepsilon = 0$

Then $\langle \sin^2(\alpha + \varepsilon) \rangle = \sin^2\alpha + \cos(2\alpha)\,\langle \varepsilon^2 \rangle$

The change in $\sin^2\alpha$ averaged over $\varepsilon$ is

$$\Delta(\sin^2\alpha) = \cos(2\alpha)\,\langle \varepsilon^2 \rangle$$

Consider a beam of electrons of energy E traversing a scattering medium of thickness D and density N

Average number of collisions per traversal is

$$P = \int_{b_{min}}^{b_{max}} 2\pi\, b\, D\, N\, db$$

where b is the effective radius of the scattering particle. Then the mean square scattering angle per collision is

$$\overline{\varphi^2} = \int \{\varphi(b)\}^2 \psi(b)\, db \qquad \text{(Fermi, 1937)}$$

where $\psi(b)$ is the normalised probability density

$$\psi(b)\, db = 2\pi\, b\, D\, N\, db/P$$

and so $$\langle \varepsilon^2 \rangle = P\,\overline{\varphi^2}$$

$$= 2\pi\, D\, N \int_{b_{min}}^{b_{max}} \{\varphi(b)\}^2\, b\, db$$

but $$\varphi(b) \simeq \frac{2\,Z\,e^2}{b\,m\,V^2} \simeq \frac{4\,Z\,e^2}{E\,b} \quad \text{for small } \varphi$$

where E is the particle energy and Z is the atomic number of the scatterer.

$$\therefore \langle \varepsilon^2 \rangle = 2\pi\, D\, N\, \frac{16\,Z^2\,e^4}{E^2} \int_{b_{min}}^{b_{max}} b^{-1}\, db$$

$$= \frac{32\pi\, D\, N\, Z^2\, e^4}{E^2} \log_e \left(\frac{b_{max}}{b_{min}}\right)$$

for small angle scattering $\varphi < 1$ we can put $b_{min} = 4\,Z\,e^2/E$

We have for the maximum effective radius for coulomb scattering in an ionised medium (Kwal, 1950)

$$b_{max} = 3\left(\frac{kT}{8\pi\, Ne^2}\right)^{\frac{1}{2}}$$

where T is the kinetic temperature of the scattering nuclei

for $T \simeq 300^{\circ}$ $\quad b_{max} = (7_{10}4/N)^{\frac{1}{2}}$

$$b_{min} = (9_{10}-19/E)$$

$$\therefore \; b_{max} / b_{min} = 3_{10}20 \; E/N^{\frac{1}{2}}$$

$$\therefore \; \langle \varepsilon^2 \rangle = \text{const } D \; N \; Z^2 \; e^4/E^2$$

but the distance D travelled through the scattering medium by a relativistic electron is $D = c\,\Delta(t)$ where c is the velocity of light and $\Delta(t)$ is the time interval.

Hence $\langle \varepsilon^2 \rangle = K \; N \; \Delta(t)$ $\quad$ K constant

the change in mirror radius is given by

$$\Delta(r_m^3) = 3\, r_m^2 \, \Delta(r_m) = r^3 \, \Delta(\sin^2\alpha)$$

$$\therefore \; \Delta(r_m) = r^3 \cos(2\alpha) \; K \; N \; \Delta(t) / (3\, r_m^2)$$

then the velocity of the mirror point of the mean scattered particle is $V' = \dfrac{\Delta(r_m)}{\Delta(t)} = r^3 \cos(2\alpha) \; K \; N / (3\, r_m)$

We want the average value of $V'$ over the path of the particle

$$V = \frac{\int_o^T V' \, dt}{\int_o^T dt}$$

where the integrals are over the path from the mirror point to the equator. The quantities under the integral sign can be expanded in terms of $x = r - r_m$. We can approximate the particle density by $N(r) = N_m \exp(-x/H)$ $\quad$ H scale height.

If we consider only the case $H \leq r_m$ we can express V in the approximate form $V = -\dfrac{\pi^{\frac{1}{2}} K \; N_m \; (H \, r_m)^{\frac{1}{2}}}{12}$

The average velocity is proportional to the density at the mirror point and is directed downward into the exponentially increasing

atmosphere. The characteristic lifetime of the electron is then

$$\tau = \left| \frac{H}{V} \right|$$

For a 10 Mev electron and a temperature T = 3000°K the condition that

$$\tau \geq 1 \text{ year} \qquad \text{gives } N_m \leq 3_{10}6 \text{ cm}^{-3}$$

The half life of an electron due to energy loss through scattering can be estimated from the range of a high energy electron.

Mean range $\simeq$ 5 gm/cm$^2$ in a neutral medium

Mean velocity $\simeq$ $3_{10}10$ cm/sec

$\therefore$ Mean life $\simeq$ $\frac{10^{14}}{N}$ sec

For the mean life to be greater than 1 year this gives $N \leq 3_{10}6$ cm$^{-3}$. The densities obtained from both methods are similar and indicate that if the loss of high energy particles from the radiation belts on Jupiter is not to be too great the ionised and neutral particle densities must not exceed $3_{10}6$ cm$^{-3}$.

## 4.5 Limits on the Density of Jupiter's Magnetosphere from the Faraday Rotation of the Decimetric Emissions.

Decimetric observations of the linear polarisation of Jupiter's emissions indicate that the plane of polarisation can be determined to better than 1° (Roberts and Komesaroff, 1965). This limits any Faraday rotation that may occur when the radiation leaves Jupiter to about 1°.

For frequencies in the decimetric range the magnetoionic parameters $Y = \omega_H / \omega \ll 1$

and $X = \omega_o^2 / \omega^2 \ll 1$

at all points in the Jovian magnetosphere.

The condition for a quasi longitudinal propagation becomes

$$\tfrac{1}{4}\, Y^2 \sin^4\theta / \cos^2\theta \ll 1$$

For a frequency of 2500 MHz and a field strength in the emitting region of 1 gauss, this condition is satisfied for all wave normal angles $\theta$ less than about $89.9^\circ$. Hence we can regard the propagation of these waves as quasi longitudinal.

The Faraday rotation in this case is given by

$$d\psi = \frac{\omega}{2c} X\, Y \cos\theta\, dL$$

where dL is an element of path length.

Then $\psi = 0.93_{10}6 / \omega^2 \cdot N\, H \cos\theta\, dL$ where N is the electron density / cc, H is the field strength in gauss and dL is the path length in cm. If we take an equatorial field strength of 5 gauss as a lower limit and make the approximation $H = Ho\, R^{-3}$ and further assume that beyond the radiation belt the electron density falls off as $N = No\, R^{-3}$ we can estimate the Faraday rotation in the exosphere. We get

$$\psi = 0.93_{10}6\, R_J\, No\, Ho \cos\theta / \omega^2 \int_2^6 \frac{dL}{R^6}$$

$$= 0.93_{10}6\, No\, Ho\, R_J \cos\theta / (160\, \omega^2)$$ where $R_J$ is the radius of Jupiter. Taking a mean value of $\cos\theta = 0.1$ we get

$$\psi = 0.12_{10}{-7}\, No \quad \text{radians.}$$

We require that $\psi \leq 0.01$ and hence $No \leq 8_{10}5$ which implies a maximum electron density in the radiation belts at a height of 2 radii of $10^5$ /cc.

The assumed values of the parameters used in this analysis need to be justified. The assumed field intensity gives a value of

about 0.1 gauss in the radiation belts, which is the lower limit of the field strength suggested from observations of the decimetric emission. The inverse cube variation of field strength with height is a good approximation to a dipole field near the equatorial plane. A power law variation of electron density with height is indicated by the analysis of Melrose (1967) for distances greater than about two radii. The most likely power law is inverse cube or fourth power although the actual power taken does not affect the result appreciably.

The observations of Berge (1965) show that the bulk of the decimetric emission originates close to Jupiter's equatorial plane so that an estimate of $\cos\theta = 0.1$ is probably accurate within a factor of two.

The analysis indicates that a reasonable upper limit to the ambient electron density within Jupiter's radiation belts is about $5_{10}5$ /cc. This value is in reasonable agreement with the upper limit of $10^7$ /cc derived for the maximum electron density in Jupiter's ionosphere. However, it is significantly less than the limits obtained by considering the lifetime of radiation belt electrons.

This indicates that the limit on the lifetime of radiation belt electrons is not a significant factor in estimating an upper limit to the ambient electron density unless the actual lifetime of the electrons is much longer than was assumed.

## 4.6 References.

ALLEN, C.W. (1962) Astrophysical Quantities 2nd Ed. London

BERGE, C.L. (1965) J. Res Nat. Bureau Standards 69D, 1552

ELLIS, G.R.A. (1965) J. Res Nat. Bureau Standards 69D, 1513

FERMI, E. (1937) Nuclear Physics University of Chicago Press.

FOWLER, R.H. and E.A. GUGGENHEIM (1939) Stat. Thermodynamics, Cambridge

KUIPER, G.P. (1952) The Atmosphere of the Earth and Planets, University of Chicago Press

KWAL, B. (1950) C.R. Acad. Sci. Paris 230, 1662

MELROSE, D.B. (1967) Planet Space Sci. 15, 381

RATCLIFFE, J.A. (1960) Physics of the Upper Atmosphere, Academic Press

ROBERTS, J.A. and M.M. KOMESAROFF (1965) Icarus 4, 127

WELCH, J.A. and W.A. WHITAKER (1959) J.G.R. 64, 909

# CHAPTER 5.

# THE PROPAGATION AND GENERATION OF RADIATION IN JUPITER'S MAGNETOSPHERE

## 5.1 Introduction.

Many radiation mechanisms have been proposed to explain the decametric emission from Jupiter. The most plausible of these explain the radiation as natural generation of radio waves by particles moving in a magnetic field. All the known mechanisms for producing narrow band emissions whose frequency can change rapidly with time involve high energy particles. The object of this chapter is to examine the possible radiation and find which is most likely to account for the observed properties of the emission.

The medium immediately surrounding Jupiter in which the radiation is generated is likely to be a highly ionised plasma with a maximum electron density which may be as high as $10^7$/cc. The decametric observations of Jupiter indicate the presence of a basically dipolar magnetic field having a polar intensity in the range 10-100 gauss. The distribution of the ambient plasma near the surface of Jupiter will then be controlled by the magnetic field giving rise to an extensive magnetosphere. The decimetric observations further indicate the presence of "van Allen belts" containing large numbers of highly energetic electrons.

The observed properties of radio-waves generated in such a plasma will be controlled to a large degree by the propagation conditions within the plasma. We will first examine the propagation of radio waves in a plasma, and then discuss the radiation mechanisms.

## 5.2 Propagation of Radio Waves in Plasmas.

A plasma is a gas which is macroscopically neutral and microscopically ionised, when a static magnetic field is present the plasma is said to be magnetoactive. The microscopic qualities of a plasma are contained in its particle density N, kinetic temperature T, and external magnetic field intensity H. In considering the propagation of a wave of angular frequency $\omega = 2\pi f$ through a plasma it is convenient to use the following derived parameters.

Electron plasma frequency $f_o = \omega_o/2\pi = (Ne^2/\pi m)^{\frac{1}{2}}$

$= 9.0_{10}{}^{-3} N^{\frac{1}{2}} (cm^{-3})$ MHz

Electron gyro-frequency $f_H = \omega_H/2\pi = eH/2\pi mc$

$= 2.8$ H (gauss) MHz

where e is the electronic charge, m is its mass and c is the velocity of light in vacuum.

Electron-ion collision frequency

$$\nu = \frac{Z^2 e^4}{3}\left[\frac{8\pi}{m(kT)^3}\right]^{\frac{1}{2}} N_i \left[\log_e\left\{\frac{8(kT)^3}{m(\pi Ze^2 f)^2}\right\} - 5\gamma\right]$$

$$= 31\ N_i\ (cm^{-3})\ T^{-3/2}$$

where Z is the degree of ionisation, k is Boltzmann's constant, $\gamma$ is Euler's constant and $N_i$ is the density of ions.

Root mean square velocity of thermal electrons

$$v_{th} = (3kT/m)^{\frac{1}{2}} = 6.7\ T^{\frac{1}{2}} \text{ km/sec}$$

The maximum values of the various parameters that are likely to be encountered in Jupiter's magnetosphere are

$$f_o \leq 10 \text{ MHz}$$

$$f_H \leq 100 \text{ MHz}$$

$$\nu \leq 50 \text{ Hz}$$

$$v_{th} \leq 500 \text{ km/sec}$$

Waves of angular frequency $\omega$ propagating in the z direction in a plasma take the form of monochromatic plane waves, the electrostatic field of which is specified by

$$E = E_o \exp \{ i(kz - \omega t) \} \exp ( - qz + \delta t) \qquad 5.2.1$$

where $k = 2\pi/\lambda = \omega n/c$ is the real part of the wave number

$\lambda$ = wavelength

$n$ = real part of the refractive index

and $q$, $\delta$ are the imaginary parts of the wave number and angular frequency respectively.

The phase and group velocities of the wave described by 5.2.1 are

$$V_{ph} = \frac{\omega}{k}$$

$$V_{gp} = \frac{d\omega}{dk}$$

The propagation of a wave through a plasma is controlled by an equation, called the dispersion equation, relating $\omega$ and $k$. The general form and properties of the dispersion equation have been discussed by Denisse and Delcroix (1963). There are in general four distinct modes of electromagnetic disturbance capable of propagating in a warm magnetoactive plasma (Astron, 1950; Piddington, 1955). Two of the four modes tend to be longitudinal or pressure waves which can only exist if the plasma temperature is not absolute zero.

These waves depend in part on the elastic forces resulting from compression of the gas (either as a whole or the electron gas alone).

The lower frequency mode of the two, called the ion mode or magnetic sound mode, appears when thermal motions of the heavy gas particles, both ions and atoms, are taken into account; that is when the whole gas has a finite pressure. The motion of the plasma tends to be longitudinal and the velocity of propagation is near the velocity of sound. When propagation is along the magnetic field the wave is almost a pure sound wave, having an associated electric field only.

The second or higher frequency longitudinal mode, called the electron or p-mode, appears when electron thermal motions and the electron gas pressure are taken into account. The p-wave becomes a pure electric wave for propagation along the magnetic field and propagates independently of the two other transverse modes. For large values of refractive index the p-mode has the character of a pure longitudinal wave; however, in the region of refractive index less than one it changes its physical character to a transverse electromagnetic wave. (Wild, Smerd and Weiss, 1963).

The second pair of modes correspond to transverse electromagnetic waves and are called the ordinary or o-mode and extraordinary or x-mode. The polarisation of both these modes is in general elliptical (Ratcliffe, 1959). The principal directions of the wave are the projections in the plane of the wave front of the magnetic field direction and the normal to that projection. The polarisation ellipses of the waves are contained within rectangular boxes whose sides are parallel to the principal directions. The ratio of

the lengths of the sides of each rectangular box is the polarisation axial ratio of the corresponding wave. The polarisation ellipse for one wave is obtained from the ellipse for the other wave by reflecting about a line at $45^{\circ}$ to the principal directions and reversing the sense of rotation of the E vector. If the phase velocity of the wave is along the magnetic field the polarisation tends to be circular, the sense of rotation of the x-mode being the same as the sense of rotation of an electron in the same magnetic field. When the phase velocity is transverse to the magnetic field the polarisation of the wave tends to be linear with the o-mode along the magnetic field and the x-mode orthogonal to it.

At frequencies well below the electron plasma and gyrofrequencies the motion of the ions becomes important and the phase velocities of the ion mode and both transverse modes remain almost constant for changes in plasma density. The waves of these modes are grouped together as hydromagnetic waves.

The propagation properties of a warm collisionless magnetoactive plasma are illustrated in Figure (5.1a) in which the square of the refractive index is plotted against the parameter $X = f_o^2/f^2$. The two transverse modes, ordinary and extraordinary are labelled (1) and (2) respectively while the two longitudinal modes are labelled (3) for the ion mode and (4) for the electron mode.

For transverse waves the plasma acts as a dielectric medium, merely changing the propagation constants. In the case of longitudinal waves however, the plasma takes part in the wave motion and the waves cannot exist outside the plasma. In the absence of a transverse magnetic field the o and x modes are purely transverse

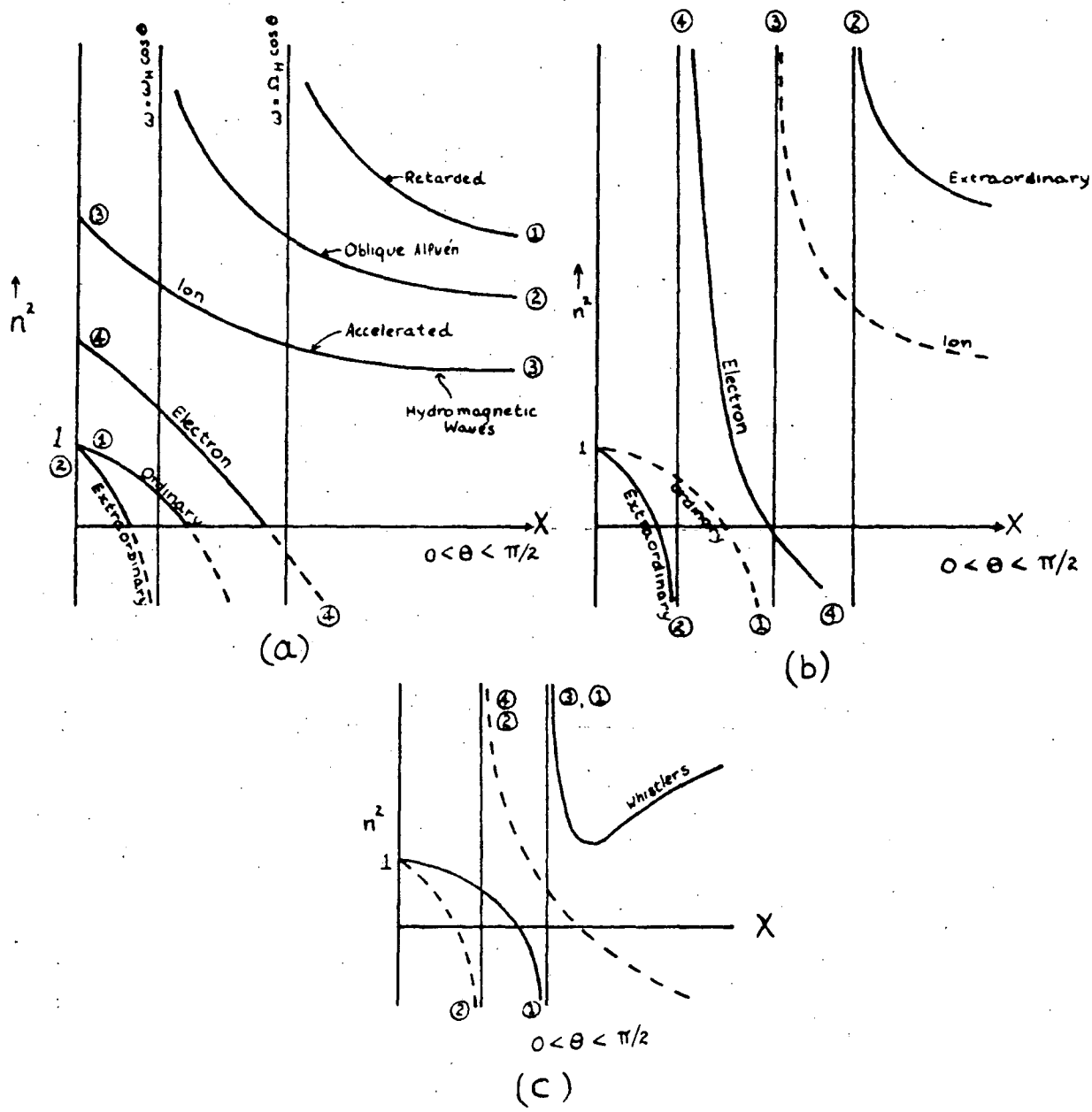


Figure 5.1 The four modes of propagation in a collisionless magnetoactive plasma (a) when the plasma is warm (b) when the plasma is cold (c) when the plasma is cold and the wave frequency is sufficiently high so that the effect of the motion of the ions can be neglected. (Denisse and Delcroix, 1963)

electromagnetic waves while the electron and ion modes are purely longitudinal waves. The presence of a transverse magnetic field provides coupling between the longitudinal and transverse electric fields.

In the special case for which the thermal motion of the electrons and ions can be neglected (T = 0), the dispersion equation takes the form illustrated in Figure (5.1b). Only the transverse modes exist. If in addition the wave frequency is considered high such that the effects of ions can be neglected, the dispersion equation takes the form of the Appleton-Hartree equation

$$n^2 = 1 - \frac{X(1 - X)}{1 - X - \frac{1}{2}Y^2 \sin^2\theta \pm (\frac{1}{4}Y^4 \sin^4\theta + \{1 - X\}^2 Y^2 \cos^2\theta)^{\frac{1}{2}}}$$

where $Y = \omega_H / \omega$ and $\theta$ is the wave normal angle. This is illustrated in Figure (5.1c). Modes (2) and (4) group together to form the transverse extraordinary mode intersecting the x-axis at X = 1 + Y. Mode (3) is transformed to the transverse whistler mode in this approximation, which can be identified as mode (1). Each mode does not represent a particular sense of polarisation, for $n > 1$ mode (3) and part of mode (4) have the same polarisation, while for $n < 1$ the polarisation of mode (4) is reversed.

The path of propagation within each region is determined from the refractive index by Snell's law. In a general medium the direction of phase propagation and the direction of energy flow (ray direction) do not coincide. If the effect of collisions can be neglected the ray direction can be determined by a method devised by Poeverlein (1949, 1950). A surface called the refractive index surface can be constructed as the locus of a vector having as its magni-

tude, the refractive index, and direction the wave normal direction. As the magnitude of the refractive index depends only on the wave normal angle and not on its azimuth, the surface will clearly be a surface of revolution about the magnetic field direction. The radius vector at a point on the surface gives the refractive index and wave normal angle at that point, the direction normal to the refractive index surface at that point is the direction of the ray. The geometry of the situation is illustrated in Figure (5.2). The ray direction is always in the plane defined by the magnetic field and wave normal vector and the angle $\alpha$ between the ray and wave normal directions is given by

$$\tan \alpha = \frac{1}{n} \frac{dn}{d\theta}$$

The velocity of the wave is called the group velocity and is given by $U = \frac{c}{n_{gp}} \sec \alpha$ where $n_{gp}$ is the group refractive index.

If the effect of collision is included the refractive index becomes complex in general so that $n' = n - i\chi$ and the wave in the medium is represented by

$$E = Eo \exp \{i\omega(t - n'z/c)\}$$

which can also be written

$$E = Eo \exp ( - \omega\chi z/c) \exp \{i\omega (t - nz/c)\} \qquad 5.2.2$$

(c.f. equation 5.2.1) This represents a wave which is attenuated by $\exp ( - \chi )$ in a distance $z = c/\omega = \lambda/2\pi$ and travels with phase velocity $c/n$. The refractive index is therefore given by n and the absorption co-efficient $\kappa$ is defined by

$$\kappa = \omega\chi/c$$

such that the integrated absorption along the path s of radiation is expressed in terms of the optical depth

$$\tau = \int_s \kappa \, ds$$

where the damping factor is just exp ( $-\tau$ )

It is possible under some circumstances to obtain coupling between the electron or ion modes of the dispersion equation and the o or x-modes. This coupling requires the passage of the wave through a region in which the refractive index is predominantly imaginary, with the result that the wave is usually severely attenuated in the process. This process is analagous to the "tunnel effect" in quantum mechanics. The attenuation of a wave passing through a region of imaginary refractive index will be discussed in more detail later in this chapter.

## 5.3 The Generation of Radio Frequency Waves in a Plasma.

The various emission processes that can generate high frequency waves in a plasma are:-

Bremsstrahlung or braking radiation

Cerenkov plasma or plasma radiation

cyclotron or gyro-radiation

synchrotron radiation.

Bremsstrahlung or "braking radiation" is the term applied to electromagnetic radiation from charged particles deflected by other charged particles; these deflecting encounters are the free-free transitions of quantum theory. The radiation is emitted in close, or binary encounters as well as in distant, or multiple encounters in which the total emission is essentially the same as in

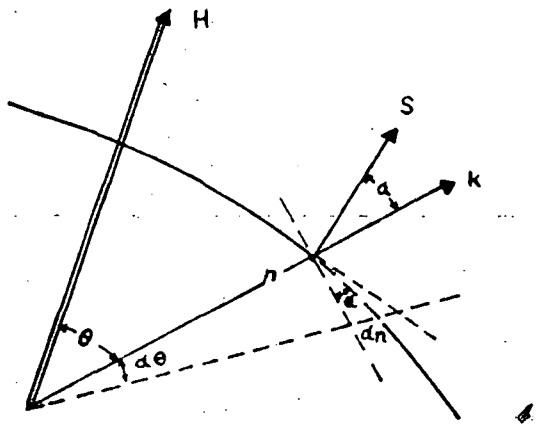


$$\tan \alpha = \frac{1}{r} \frac{dr}{d\theta}$$

Figure 5.2 Diagram illustrating the relation between the direction of the field H, the wave normal direction K and the direction of energy flow S, in a magnetoactive plasma.

binary encounters out to a distance of $v/2\pi f$, where v is the electron velocity (Scheuer, 1960). The collisions which give rise to Bremsstrahlung are random collisions of electrons and ions in thermal motion and hence the radiation is unpolarised and broadband. The observed intensity, polarisation and narrow band characteristics of the Jovian decametric emissions are inconsistent with this form of radiation. In particular it would be impossible to explain the high time resolution dynamic spectra observed by Warwick and Gordon (1965) which has bandwidths of about 1 MHz at a frequency of 25 MHz. However it has been invoked to explain the highest frequency component of Jupiter's microwave emissions.

When a charged particle travels through a neutral medium so that its velocity exceeds the phase velocity for electromagnetic waves in the medium, a Cerenkov wave is emitted on the surface of a cone. The angle of the cone $\theta$ is related to the particle velocity by $\cos\theta = c/nv$. Clearly Cerenkov emission can only be generated in a medium in which the refractive index is greater than unity. In a plasma the electron and ion modes are the only modes that possess this property. The motion of the charged particles in a magnetoactive plasma will be along the magnetic field line and the angle $\theta$ becomes the wave normal angle of the radiation. In a warm plasma the electron and ion modes tend to be longitudinal for $n > 1$ and hence the Cerenkov waves generated in a warm plasma will be longitudinal or plasma waves. If the plasma is cold ($T = 0$) the electron and ion modes correspond to transverse electromagnetic modes and the Cerenkov waves in this case will be transverse with the characteristic polarisation of their mode of generation i.e. they will be x-mode.

The motion of an electron in a magnetic field is in the form of a helix about the magnetic field lines. The electron gyrates with frequency

$$f_H = \frac{eH}{2\pi mc}(1 - \beta_T^2)$$

where $\beta_T$ is the thermal velocity, usually $\beta_T \ll 1$ and

$$f_H = \frac{eH}{2\pi mc}$$

The motion of the electron in a helix requires that it undergoes continuous acceleration in the plane normal to the external magnetic field, and hence the electron radiates electromagnetic energy as it gyrates.

Consider an electron gyrating about a magnetic field in a vacuum. If the velocity of the electron is small $\beta \ll 1$ the wave received by a stationary observer in the orbital plane of the electron will be simple harmonic. The spectrum of the received radiation is just the Fourier transform of the wave train and will consist of a single spike at frequency $f_H$. When the velocity of the electron approaches c the received wave train is no longer simple harmonic but is peaked when the electron is approaching the observer. The resultant frequency spectrum contains components at the first few harmonics of the relativistic gyro-frequency $\gamma f_H$ where $\gamma = (1 - \beta^2)^{\frac{1}{2}}$ (Figure 5.3) and the radiation is called cyclotron radiation. In the limit when the velocity of the electron is very close to c the radiation is received in a series of short sharp packets, one per cycle during the phase of the electrons velocity of light approach. The spectrum of the received radiation is just the Fourier transform of this regular pulse train, its form is that of a long series of harmonics of the frequency $\gamma f_H$. The higher the energy of the electron the greater

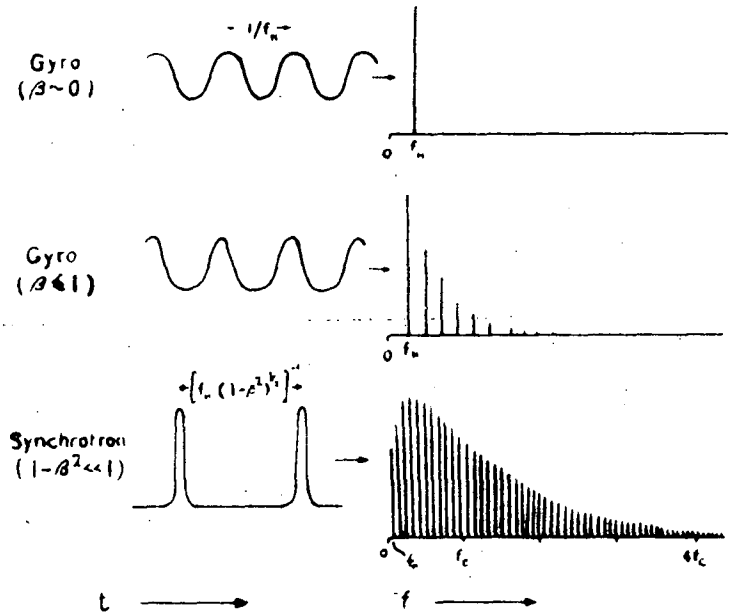


Figure 5.3 Illustrating the origin of synchrotron radiation. The variation of the electric field at a stationary observer in the orbital plane of an electron gyrating at βc is shown together with the emission spectrum which is the Fourier transform of the field variation. (Wild, Smerd and Weiss, 1963)

the number of harmonics and the closer their spacing. The individual harmonics in the radiation due to a group of electrons is smeared out with the result that the frequency spectrum becomes continuous. This type of radiation from highly relativistic electrons is called synchrotron radiation.

In the general case in which the electron moves along a helical path, a stationary observer situated on a line which passes through the electron and makes an angle $\theta$ with the magnetic field receives radiation at the harmonics s = 1, 2, 3, ..... of the Doppler shifted gyro-frequency, given by

$$f = f_H (1 - \beta^2)^{\frac{1}{2}} \mid 1 - n\beta_{\parallel} \cos \theta \mid^{-1}$$

where $\beta_{\parallel}$ c is the component of the electrons velocity along the field line.

If the condition $n\beta_{\parallel} \cos \theta < 1$ is satisfied, the Doppler effect is said to be normal, and radiation of a quanta is accompanied by a change of the electron to a state of smaller transverse momentum (Ginzburg and Frank, 1947). The observed frequency f may be higher or lower than the frequency $s\gamma f_H$ depending on whether the electron is moving towards $(0 \leqslant \theta < \pi/2)$ or away $(\pi/2 < \theta \leqslant \pi)$ from the observer.

When $n\beta_{\parallel} \cos \theta > 1$ holds the Doppler effect is said to be anomalous. The component of $v_{\parallel}$ in this case is larger than the phase velocity and the electron leaves a polarised wake which radiates electromagnetic energy into the forward hemisphere. Radiation in the anomalous Doppler mode is accompanied by a change of the radiating electron to a state of larger transverse momentum (Ginzburg, Zheleznyakov and Eidman, 1962). We must have $n > 1$ and waves can

only propagate in the whistler mode and part of the electron mode.

Synchrotron radiation occurs when $n \simeq 1$ and hence propagates as if in a vacuum. The intensity of synchrotron radiation has been given by Schwinger (1949). The polarisation of synchrotron radiation is mainly linear although the low harmonics may contribute some x-mode elliptical polarisation. The wide bandwidth and linear polarisation characteristics of synchrotron radiation do not agree with the observed characteristics of the decametric emission; however it has been used to explain the majority of the microwave emission.

Cyclotron radiation occurs when n is different from unity and hence propagation conditions may play a significant role in the observed intensities. The theory of the generation of cyclotron radiation by a single electron has been given by Eidman (1958) and Liemohn (1965) while the effect of a stream of electrons has been investigated by Fung (1966). Cyclotron radiation is normally elliptically polarised and both modes may be generated.

The only radiation processes which generate waves with the required bandwidth and polarisation characteristics are plasma Cerenkov emission and cyclotron emission. The characteristics of these mechanisms will be investigated in the following sections.

## 5.4 Cerenkov Radiation.

### (a) Power Radiated by a Single Electron

Expressions for the power radiated by a single electron moving parallel to a static magnetic field have been derived by several authors (McKenzie, 1966; Seshadri and Tuan, 1965). However,

in practice the electron never moves parallel to the field but gyrates around it in a helix. The theory of Cerenkov radiation from an electron moving in a helix in a cold magneto-plasma has been given by Liemohn (1965). The angular spectrum of the radiation is given by

$$\frac{dP}{d\Omega} = \left(\frac{e^2}{2\pi c}\right) \frac{\left[\omega^2 nK \left\{ -\beta_1 J_o'(x) + \alpha_z \beta_2 J_o(x) \right\}^2 \left\{ 1 + \frac{\omega}{n}\frac{\partial n}{\partial \omega} \right\}\right]}{\left| \left\{ 1 - \beta_2 n \cos\theta \left(1 + \frac{\omega}{n}\frac{\partial n}{\partial \omega}\right)\right\}\right|}$$

where $\beta_1$ and $\beta_2$ are the relative velocities of the electron perpendicular and parallel to the field, $\theta$ is the wave normal angle and $\omega$ is the angular frequency. The argument of the Bessell functions $J_o$ and $J_o'$ is given by $x = n\beta_1 \sin\theta / \gamma Y$

where $\gamma = (1 - \beta^2)^{\frac{1}{2}}$, $\beta^2 = \beta_1^2 + \beta_2^2$, $Y = \omega_H / \omega$

and $\alpha_z = \alpha_k \cos\theta - \alpha_\theta \sin\theta$

$\alpha_\theta = - Y \cos\theta / \{1 + X / (n^2 - 1)\}$

$\alpha_k = - Y \sin\theta \, (n^2 - 1) / (X - 1)$

and $K = (1 + \alpha_\theta^2)^{-1}$

where $X = \omega_o^2 / \omega^2$

The variables n, $\theta$, X and Y are not all independent, they must simultaneously satisfy the Appleton Hartree equation $n = n(\theta, X, Y)$ and the Cerenkov equation $n\beta_2 \cos\theta = 1$. The direction of propagation does not in general coincide with the wave normal direction. If the wave normal angle is $\theta$ then the direction of the ray is $\theta + \alpha$ where $\tan\alpha = -\frac{1}{n}\frac{dn}{d\theta}$. The conditions for Cerenkov radiation are illustrated graphically in Figure (5.4). The full curves are the refractive index surfaces for various values of the parameters X and Y, the dashed line represents the Cerenkov condition for an electron with $\beta_2 = 0.33$. The wave normal direction is from the origin to

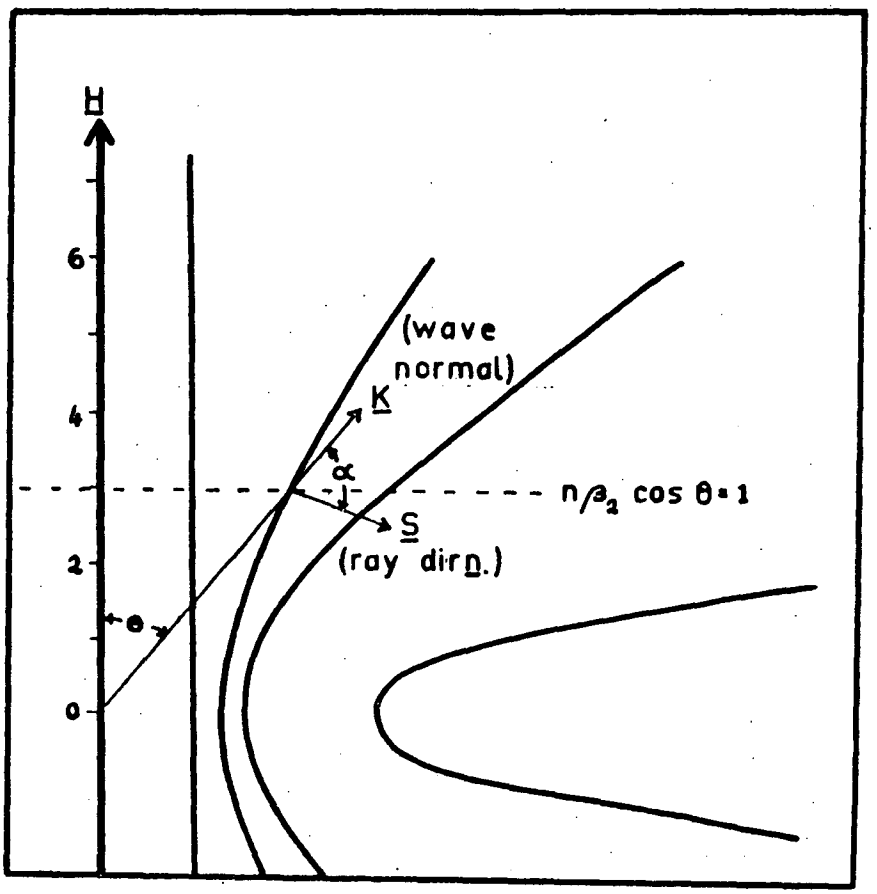


Figure 5.4 The conditions for Cerenkov emission by an electron whose longitudinal velocity is $\beta_2$. The wave normal and ray directions are shown.

the intersection of the refractive index surface with the Cerenkov line, and the ray direction is the outward normal to the refractive index surface at that point. The diagram shows that the direction of the ray is very nearly normal to the wave normal direction.

According to the above expression the power radiated by an electron is infinite, since as $\theta$ tends to $\pi/2$, the refractive index and group refractive index tend to infinity. However, in a real medium the temperature is never absolute zero and thermal effects place a limit on the magnitude of the refractive index, and hence keep the radiated energy finite. The radiated power increases monotonically with decreasing electron velocity, however, a limit is reached and the electron ceases to emit transverse electromagnetic waves when its velocity is less than the geometric mean of the velocity of light, and the thermal velocity of the ambient plasma electrons (McKenzie, 1966).

(b) Cerenkov Radiation from a Helical Stream of Electrons

The radiation from a single electron is enhanced by the effect of neighbouring electrons in a helical electron stream. The overall effect is an amplification of the radiation to give $N\eta'$ times the radiation from a single electron where $\eta' \geqslant 1$ and N is the number of electrons in the helical stream. $\eta'$ is called the growth of the wave.

Fung (1966) has investigated this problem in the case of an electron stream magnetoactive plasma system in which the ambient plasma is cold and the helical electron stream has a delta function momentum distribution. Many authors (e.g. Stepanov and Kitsenko, 1961, and Neufeld and Wright, 1964) have considered this problem but

have only solved it for some special cases.

The growth of the wave is given by $\exp(i\delta t)$ where $\delta$ is obtained by solving the equation

$$\left(\frac{\delta}{\omega}\right)^3 + b\left(\frac{\delta}{\omega}\right) + d = 0$$

where $b = -\sigma A J_o^2(x)\{1/\beta_2^2 - 1\} Y^2 \beta_2^2 \cos^2\theta$

and $$d = \frac{Y^2 \sigma A\{\beta_2^{-2} - 1\}\{J_o'(x)^2 \beta_1^2 + J_o(x)^2 \sin^2\theta\}}{\{A L Y^2 - 2\}}$$

where $\sigma = \omega_p^2/\omega_o^2$ = density of stream / density of ambient plasma

and $$L = \Big[2 A Y^2 D - (1 - A Y^2)\Big\{2 A Y^2 + Y^2 \sin^2\theta - B^{-\frac{1}{2}} .\{-Y^4 \sin^4\theta + 4 A Y^4 \cos^2\theta (1 - A Y^2) - 2 Y^2 \cos^2\theta (1 - A Y^2)^2\}\Big\}\Big] / D^2$$

where $D = 1 - A Y^2 - 2 Y^2 \sin^2\theta - B^{\frac{1}{2}}$

and $B = \frac{1}{4} Y^4 \sin^4\theta + (1 - A Y^2)^2 Y^2 \cos^2\theta$

where $A = \omega_o^2/\omega_H^2$

$Y = |\omega_H| / \omega$

$x = n\beta_1 \sin\theta/\gamma Y$

and $\gamma = (1 - \beta^2)^{\frac{1}{2}}$

The values of the parameters n, $\theta$, A, Y in these expressions must be obtained by simultaneously solving the refractive index equation and the Cerenkov condition, this allows us to obtain the wave frequency $\omega$. The growth rate can then be calculated.

$$\mathrm{Im}\left(\frac{\delta}{\omega}\right) = \tfrac{1}{2}\sqrt{3}\,(M^{\frac{1}{3}} - C^{\frac{1}{3}})$$

where $M = -\frac{1}{2} d + (\frac{1}{4} d^2 - b^3/27)^{\frac{1}{2}}$

and $C = -\frac{1}{2} d - (\frac{1}{4} d^2 - b^3/27)^{\frac{1}{2}}$

As $\omega$ changes for different wave normal angles it is more convenient to take the quantity $\left|\frac{\delta}{\omega_H}\right| = \frac{1}{Y}\left|\frac{\delta}{\omega}\right|$ as a measure of the growth rate. Near the region of cyclotron resonance the group refractive index is large so that the group velocity is small. The time interval during which the wave grows is $t = n_{gp} R \cos\alpha/c$ where $n_{gp}$ is the group refractive index, $\alpha$ is the angle between the wave normal and ray directions, c is the velocity of light, and R is the characteristic dimension of the amplifying region. The relative growth rate is then $\eta = n_{gp} \cos\alpha \left|\frac{\delta}{\omega_H}\right|$

## 5.5 Cyclotron Radiation.

### (a) Cyclotron Radiation from a Single Electron

The theory of generation of cyclotron radiation by a single electron was first given by Eidman (1958) and was later corrected and modified to include relativistic effects by Liemohn (1965). The power radiated per unit solid angle at frequency $f = \omega/2\pi$ and wave normal angle $\theta$ is

$$W_s(\theta) = \left(\frac{e^2}{2\pi c}\right) \omega^2 n K \{ -\beta_1 J_s'(x) + (\alpha_y s\beta_1/x + \alpha_z \beta_2) J_s(x)\}^2 \cdot\left(1 + \frac{\omega}{n}\frac{\partial n}{\partial \omega}\right) / \left| 1 - \beta_2 n \cos\theta \left(1 + \frac{\omega}{n}\frac{\partial n}{\partial \omega}\right)\right|$$

$$= \omega^2 W_s'(\theta)$$

where $\omega$, n, and $\theta$ are obtained by solving equations (1) and (2) and

$$x = n\beta_1 \sin\theta/\gamma Y$$

$$K = (1 + \alpha_\theta^2)^{-\frac{1}{2}}$$

$$\alpha_y = \alpha_\theta \cos\theta + \alpha_k \sin\theta$$

$$\alpha_z = \alpha_k \cos\theta - \alpha_\theta \sin\theta$$

$$\alpha_\theta = - Y (n^2 - 1) \cos\theta / (n^2 - 1 + X)$$

$$\alpha_k = - Y (n^2 - 1) \sin\theta / (X - 1)$$

$$\beta_1 = v_1/c = \beta \sin\varphi$$

$$\beta_2 = v_2/c = \beta \cos\varphi$$

and $v_1$ and $v_2$ are the electron velocity components perpendicular and parallel to the field respectively. $J_s$ and $J_s'$ are the Bessell functions of order s and its derivative. The term $n\left(1 + \frac{\omega}{n}\frac{\partial n}{\partial \omega}\right)$ is the group refractive index $n_{gp}$ of the medium. The power per steradian tends to infinity as the denominator of the expression for W tends to zero. This occurs when $n_{gp} = (\beta \cos\theta \cos\varphi)^{-1}$ which is just the group analogue of the conventional Cerenkov condition.

(b) Radiation from a Helical Electron Stream

The emission from a single electron is amplified by the helical stream. The amplification is given by

Amplification = $\exp | \mathrm{Im}(\delta)\, t |$ (Fung, 1966)

where $\delta$ is obtained by solving the equation

$$\left(\frac{\delta}{\omega}\right)^3 + b\left(\frac{\delta}{\omega}\right) + d = 0$$

$$b = - \frac{\sigma A J_s(x)^2 \{ (1 - s\gamma Y)^2/\beta_\parallel{}^2 - 1 \} Y^2 \beta_\parallel{}^2 \cos\theta}{(s\gamma Y - 1)^2}$$

$$d = \sigma A Y^2 \{ (1 - s\gamma Y)^2/\beta_\parallel{}^2 - 1 \} \{ J_s'(x)^2 \beta_\perp{}^2 + J_s(x)^2 \beta_\parallel{}^2 \cdot (s\gamma Y - \sin^2\theta)^2 / \sin^2\theta (s\gamma Y - 1)^2 \} / (A L Y^2 - 2)$$

$$L = \Big[ 2 A Y^2 D - (1 - A Y^2) \Big\{ 2 A Y^2 + Y^2 \sin^2\theta - B^{-\frac{1}{2}} \cdot \{ - Y^4 \sin^4\theta + 4 A Y^4 \cos^2\theta (1 - A Y^2) - 2 Y^2 \cos^2\theta (1 - A Y^2) \} \Big\} \Big] / D^2$$

$$D = 1 - A Y^2 - \tfrac{1}{2} Y^2 \sin^2\theta - B^{\frac{1}{2}}$$

$$B = \tfrac{1}{4} Y^4 \sin^4\theta + (1 - A Y^2)^2 Y^2 \cos^2\theta$$

where $\sigma = \omega_p^2/\omega_o^2$ = density of stream / density of ambient plasma

$$A = X/Y^2$$

$$x = n\beta_\perp \sin\theta/\gamma Y$$

then $$\mathrm{Im}(\frac{\delta}{\omega}) = \pm \tfrac{1}{2}\sqrt{3}\,(M^{\frac{1}{3}} - C^{\frac{1}{3}})$$

where $$M = -\tfrac{1}{2} d + (\tfrac{1}{4} d^2 + b^3/27)^{\frac{1}{2}}$$

and $$C = -\tfrac{1}{2} d - (\tfrac{1}{4} d^2 + b^3/27)^{\frac{1}{2}}$$

Hence the power radiated by a helical stream of N electrons is

$$W' = N\, W(\theta)\, \exp\{\mathrm{Im}(\delta)\, t\}$$

where t is the time taken for the wave to propagate through the stream.

## 5.6 Summary.

The propagation and emission of radio waves in a plasma has been examined. The only emission mechanisms which give polarisation and narrow band characteristics similar to Jupiter's decametric emissions are plasma Cerenkov and cyclotron radiation. Expressions for the power radiated by a single electron and the amplification by a helical stream are given for both processes. These will be used in later chapters to derive the properties of the emission from models based on these radiation processes.

## 5.7 References.

ASTROM, E. (1950) Arkiv f. Fysik, 2, 443

DENISSE, J.F. and D.L. DELCROIX (1963) Plasma Waves, Interscience

EIDMAN, V. Ia (1958) Soviet Physics, J.E.T.P., 7, 91

FUNG, P.C.W. (1966) Unpublished Ph.D. Dissertation, University of Tasmania.

GINZBURG, V.L. and J.N. FRANK (1947) C.R. Acad. Sci U.S.S.R. 56, 583

GINZBURG, V.L., V.V. ZHELEZNYAKOV and V. Ia EIDMAN (1962) Phil Mag 7, 451

LIEMOHN, H.B. (1965) J. Res. Nat. Bur. Standards 69D, 741

McKENZIE, J.F. (1966) Proc. Phys. Soc. 87, 349

NEWFELD, J. and H. WRIGHT (1964) Phys. Fluids 7, 1527

PIDDINGTON, J.H. (1955) Phil. Mag. 46, 1037

POEVERLEIN, H. (1949) Z. Angew Phys. 1, 517

POEVERLEIN, H. (1950) Z. Angew Phys. 2, 152

RATCLIFFE, J.A. (1959) The Magnetoionic Theory and its Applications to the Ionosphere, Cambridge.

SCHEUER, P.A.G. (1960) M.N.R.A.S., 120, 231

SCHWINGER, J. (1949) Phys. Rev. 75, 1912

SESHADRI, S.R. and H.S. TUAN (1965) J. Res. Nat. Bur. Standards 69D, 767

STEPANOV, K.N. and A.B. KITSENKO (1961) Soviet Phys. Tech. Phys. 6, 120

WARWICK, J.W. and M.A. GORDON (1965) J. Res. Nat. Bur. Standards 69D, 1537

WILD, J.P., S.F. SMERD and A.A. WEISS (1963) Ann. Rev. Ast. and Astrophys. 1, 291

# CHAPTER 6.

# CERENKOV EMISSION AS THE SOURCE OF JUPITER'S DECAMETRIC EMISSIONS

## 6.1 Introduction.

Cerenkov emission is generated when particles exceed the phase velocity of emission in the medium, so that radiation can only be generated where the refractive index exceeds unity. For example moderately relativistic electrons (energy < 250 kev) can only emit Cerenkov radiation when the refractive index is greater than 1.3.

Figure (6.1) shows the variation of refractive index with height in Jupiter's magnetosphere for a frequency of 20 MHz and a wave normal angle at $30^{o}$. The maximum electron density is assumed to be $5_{10}6$ $cm^{-3}$ with a polar field strength of 18 gauss and a temperature of $10^{4^{o}}$ K. The only region where the Cerenkov condition can be satisfied under these conditions is over a small range of heights near 1.35 radii where the wave frequency is close to the electron gyrofrequency. Reduction of the maximum electron density or the electron temperature has the effect of narrowing the possible region of generation.

Cerenkov radiation may be in the form of longitudinal or transverse waves depending on the temperature of the ambient plasma. If the geometric mean of the velocity of light and the thermal velocity of the ambient plasma electrons is greater than the longitudinal velocity of the radiating electrons, the majority of the emission will be in the form of plasma waves (McKenzie, 1966). For typical particle streams with $v_{\parallel} > 0.05c$, the condition for plasma rad-

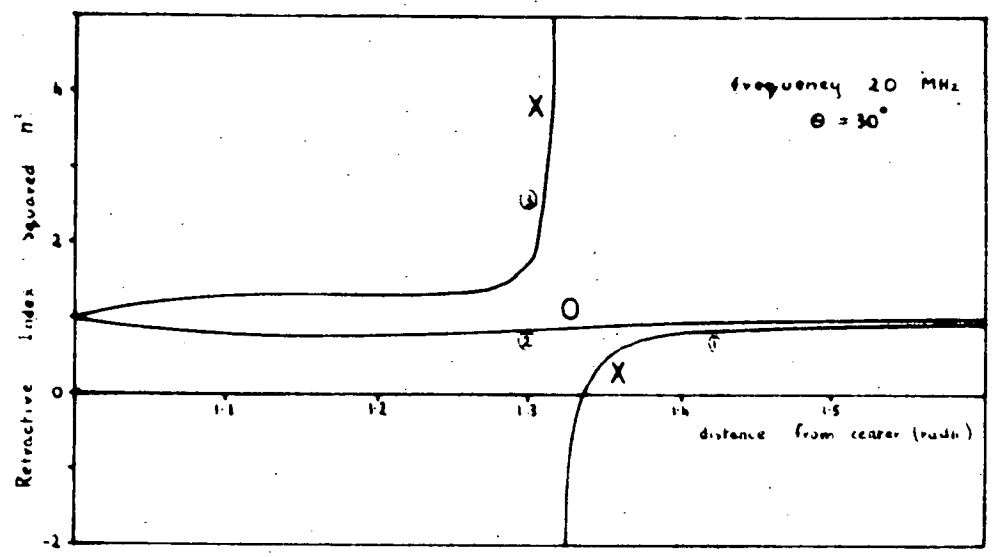


Figure 6.1 Variation of refractive index with height in Jupiter's magnetosphere for a frequency of 20 MHz and a wave normal angle of $30^{\circ}$. The maximum electron density is assumed to be $5_{10}6$ cm$^{-3}$ with a polar field strength of 18 gauss and electron temperature of $10^{4}_{8}$ K.

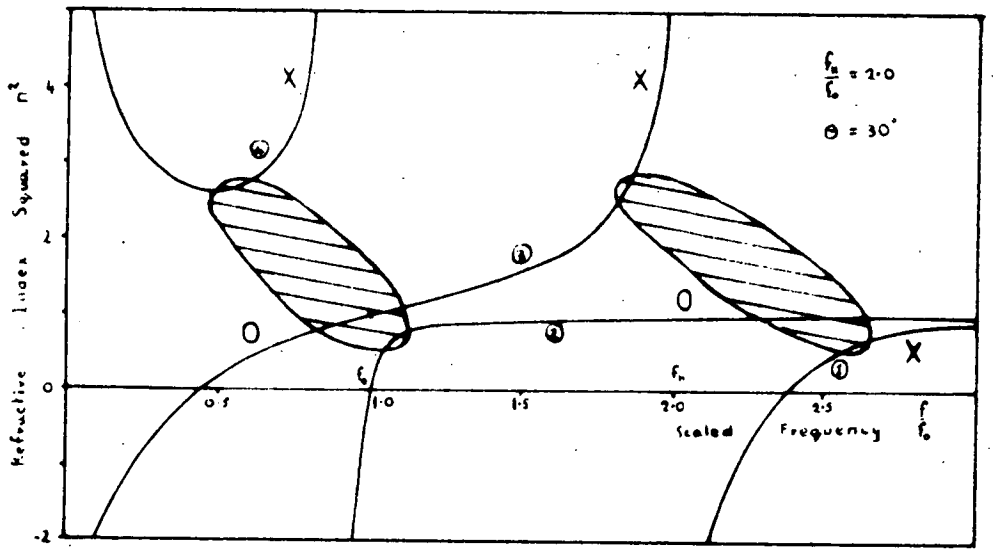


Figure 6.2 Variation of refractive index with frequency in a plasma for a wave normal angle of $30^{\circ}$ and a value of $f_H/f_o = 2$. The regions where coupling between modes occur are circled.

iation is that $T \geq 1.5_{10}4^{\circ}K$. This may not be an unreasonable temperature to find in the magnetosphere of Jupiter so that both forms of emission are possible. The ambient plasma plays an integral part in the motion of plasma waves, so that if the disturbance is to propagate from Jupiter to Earth coupling between the plasma waves and electromagnetic waves must occur.

Cerenkov radiation has been investigated as a mechanism for Jupiter's decametric emissions by Warwick (1961, 1963, 1964, 1967) and a model proposed.

## 6.2 Warwick's Model.

Warwick has developed a model of Jupiter's magnetosphere aimed at explaining the observed low time resolution dynamic spectra using Cerenkov radiation. He proposed emission at a frequency slightly below the electron gyrofrequency in agreement with the conditions imposed above which places it on the x-mode branch of the dispersion curve labelled (3) in Figure (6.2).

Warwick assumed that the radiation is emitted inwards and is beamed in a narrow cone ($< 15^{\circ}$) about the magnetic field direction, finally reaching the Earth after reflection from Jupiter's ionosphere or surface. In order to construct a dynamic spectrum that corresponds to the observed frequency-longitude drifts Warwick was forced to conclude that Jupiter's magnetic field is displaced from a symmetrical position as shown in Figure (6.3).

Warwick has made no attempt to explain the observed longitude profiles at low frequencies.

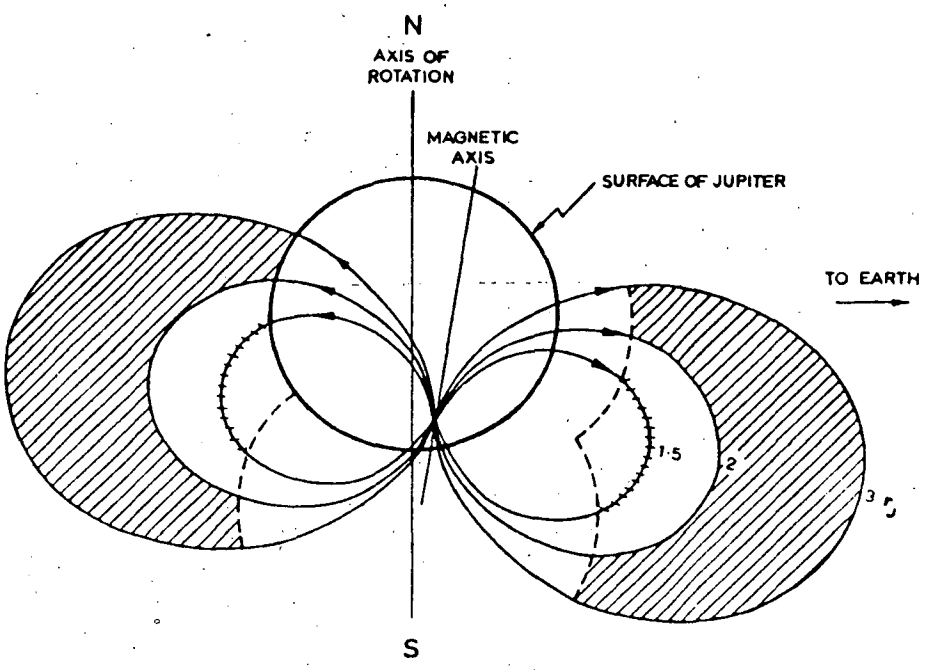


Figure 6.3 The configuration of the Jovian magnetic field and the radiation belts according to the theory of Warwick. The section shown is at a longitude of 200°.

## 6.3 Discussion of Warwick's Model.

Warwick's theory has been criticised by Ellis and McCulloch (1963) and Ellis (1965) on two main points. Firstly that Cerenkov radiation is not confined to a narrow cone about the field as assumed but may be emitted over a wide range of directions depending on the velocity distribution of the radiating particles. Secondly, that any radiation generated in the x-mode below the electron gyrofrequency has to pass through a region of the magnetosphere where the refractive index is imaginary in order to reach the Earth. It was suggested that the associated attenuation would be large and hence prevent sufficient power reaching the Earth.

Warwick (1967) has replied to the first objection by referring to an article by McKenzie (1966) on Cerenkov emission in a plasma in a magnetic field. He refers to McKenzie as follows, "McKenzie (1966) shows that in this case (with restriction on the magnetic field) emission concentrates along the field lines." The paper referred to is called 'Cerenkov radiation in a warm plasma under the action of an infinite magnetostatic field'. As the title implies the paper is concerned with Cerenkov emission in the presence of an infinite magnetic field. The frequency range of transverse waves in this case is below the plasma frequency while for plasma waves the generation frequencies occupy a small range about the plasma frequency. McKenzie states that the plasma waves are confined to a cone of semi-angle $\pi/2 - \chi$ perpendicular to the field direction while the transverse waves are confined to a cone of semi-angle $\chi$ about the field direction. The angle $\chi$ depends

on the velocity of the radiating electrons and the temperature of the ambient plasma, but provided the particles are moderately relativistic and the temperature does not approach $10^6$° K, the angle $\chi$ will be very close to $\pi/2$. The assumption of an infinite magnetic field implies that the gyrofrequency must be much higher than both the wave frequency and the plasma frequency in the emission region. This situation is not applicable to Warwick's theory of the Jovian magnetosphere since Warwick requires the wave frequency to be close to the gyrofrequency. Furthermore the maximum plasma frequency in Jupiter's magnetosphere is unlikely to be as large as the highest wave frequencies observed, so that the infinity in the refractive index near the plasma frequency does not occur. Hence the conclusions of McKenzie are not applicable to Warwick's model because McKenzie and Warwick are referring to emission on two different branches of the dispersion curve.

Warwick has suggested two possible ways in which the radiation may pass through the stop-zone without appreciable attenuation. One requires Jupiter to have a very special electron distribution throughout its magnetosphere. The distribution required is such that at the generation region where the wave frequency is slightly below the local gyrofrequency the electron density is moderately high (many electrons /cc), but at the stop-zone region the electron density is very low (about 1/cc or less). In these circumstances the width of the stop-zone is very small and the radiation escapes without attenuation.

The second possible way in which radiation might pass through the stop-zone, as suggested by Warwick, is by scattering

on irregularities of the electron density in the magnetosphere as might result from shock waves.

Warwick's theory can also be criticised on the grounds of the large displacement of the dipole field from the centre of the planet. Whether or not such assymetries are possible theoretically they are ruled out by the observations of Roberts and Ekers (1966), McAdam (1966) and Branson (1968) who all find that the centroid of the decimetric radio emission is close to the physical center of Jupiter.

## 6.4 Limitations on the Parameter of a Model for Jupiter's Decametric Emissions.

The observations of Jupiter at microwave frequencies place severe limitations on the Jovian magnetic field. It must be closely centered on the disc of Jupiter, deviation less than 0.1 $R_J$, and almost dipolar in character with some evidence for a distortion near longitude $220^{\circ}$ with a polar field strength in the range 1 to 50 gauss.

Further restrictions are obtained by considering the decametric observations. The sizes of the individual sources of the decametric emissions are smaller than 3" arc and probably nearer 1" arc, while the intensity of the emission from these regions often exceeds $10^{-20}$ $Wm^{-2}$ $Hz^{-1}$.

If the Cerenkov emission is in the form of longitudinal waves these must be transformed into electromagnetic waves in order to reach the Earth. The efficiency of the known transformation processes is low, which makes the high observed intensities even

more of a problem. On the other hand if the emission is generated in the form of electromagnetic waves they must pass through a region where the refractive index is imaginary in order to reach the Earth. This in turn involves large attenuations in general. A final difficulty is that Cerenkov radiation is generated where the refractive index n is greater than one, and the radiation will be defocussed when leaving the magnetosphere. The dilution factor is approximately $\frac{1}{n^2}$.

## 6.5 The Transformation of Plasma Waves into Electromagnetic Waves.

Two mechanisms have been proposed (Ginzburg and Zheleznyakov, 1958, 1959) for transforming plasma waves into electromagnetic waves or, more generally, for converting from one possible wave mode in a plasma to another. One is coupling between two normal modes in a plasma and is analogous to the quantum tunnelling effect. This will be discussed in detail with regard to the escape of transverse waves from the exosphere. The second method of mode conversion involves the scattering of plasma waves on small-scale fluctuations of plasma density. Ginzburg and Zheleznyakov point out that because the ion mass is much larger than the electron mass, scattering by the ions and electrons are independent. The scattering component due to the ions gives rise to a quasi-neutral plasma density fluctuation which can only occur slowly and is not accompanied by an appreciable change in wave frequency. This type of scattering is called Rayleigh scattering

and the flux scattered in volume V into the normal mode, refractive index $n(\omega)$, is given by

$$P'(\omega) = \frac{n(\omega)\, e^4\, N\, V\, Eo^2}{6\, m^2\, c^3}$$

where Eo is the electric field amplitude of the plasma wave. The motion of the electrons gives rise to space charge fluctuations which themselves comprise plasma waves. The scattering of plasma waves by charge fluctuations can give rise to an electromagnetic wave at twice the frequency of the plasma wave; this process is called combination scattering. The flux scattered in volume V by combination scattering is given by

$$P''(\tilde{\omega}) = \frac{n(\tilde{\omega})\, e^4\, N\, V\, Eo^2}{6\, m^2\, c^3} \frac{\tilde{\omega}^2}{\omega^2} \frac{v_T^2}{v_{ph}^2}$$

where $\omega$ is the frequency of the plasma wave, $v_{ph}$ is its phase velocity and $v_T$ is the thermal velocity of the background plasma electrons.

Rayleigh scattering in the Jupiter magnetosphere could take place into both o and x-modes, the relative fluxes in the two modes being given by

$$\frac{\text{Flux (x)}}{\text{Flux (o)}} = \frac{n_x(\omega)}{n_o(\omega)}$$

At the frequency $\omega$ of the plasma wave the o-mode refractive index is close to unity while the x-mode refractive index is very small, so Rayleigh scattering would give predominantly o-mode radiation, contrary to observations. We conclude that Rayleigh scattering of plasma waves cannot explain the decametric emissions from Jupiter.

Combination scattering can also produce electromagnetic radiation in both modes, the relative fluxes being proportional to

the refractive indices of the two modes at twice the frequency of the plasma wave. Both refractive indices are near unity at that frequency so that combination scattering would produce emission of equal intensities in the two modes. The two scattering processes occur at the same time in the plasma and the ratio of their effectiveness for producing o-mode radiation is given by

$$\frac{P''(\tilde{\omega})}{P'(\omega)} = \frac{n_o(\tilde{\omega})}{n_o(\omega)} \frac{\tilde{\omega}^2}{\omega^2} \frac{v_T^2}{v_{ph}^2}$$

For plasma waves to be generated we must have $v_T \simeq v_{ph}$ and so the ratio P'' to P' is of the order of unity. Scattering of plasma waves by both processes is heavily biased in favour of producing o-mode electromagnetic waves and hence cannot satisfactorily explain Jupiter's decametric emissions.

## 6.6 Transmission Through an Infinity and an Adjacent Zero in the Refractive Index.

The second way in which plasma waves may escape, and the way in which transverse waves escape involves tunnelling through a region where the refractive index is imaginary.

The radiation is generated in a region below the height where the refractive index becomes imaginary (Figure 6.1), and in order to reach the Earth must pass through this barrier. In general infinities in the refractive index can occur in two regions, one near the plasma frequency and one near the gyrofrequency (Figure 6.2). The escape of radiation from regions below either of these infinities involves coupling between different branches of the refractive index curves at the regions which are circled in

Figure (6.2). Coupling near the plasma frequency takes place from branch (4) to branch (2) of the refractive index curves. The polarisations corresponding to these branches are opposite, so that coupling is accompanied by a polarisation change, which is only possible when X is very close to 1. The emitted radiation in this case would be o-mode, and hence this process could not explain the observed polarisation of the radiation. The second coupling region occurs near the electron gyrofrequency between branches (3) and (1) which have the same polarisation, x-mode, and hence the emission would have the observed polarisation sense. Coupling can also occur near the plasma frequency between branches (4) and (3), but radiation on branch (3) is still trapped and must couple to branch (1) near the gyrofrequency in order to escape. This requires two coupling processes and is considered unlikely in comparison with generation on branch (3) and coupling to branch (1). Generation on branch (4) is also unlikely because for moderate electron densities, this branch does not exist in the Jovian magnetosphere (Figure 6.1). Coupling cannot take place between mode (3) and (2) near the gyrofrequency unless $X \simeq 1$ also occurs at that region, since the branches correspond to opposite polarisations and polarisation changes only occur near $X = 1$.

We now have to calculate the transmission coefficient between branch (3) and (1) in the neighbourhood of the electron gyrofrequency. The refractive index changes rapidly with distance (z) near the pole and zero in the refractive index, and the geometrical optical approximation does not apply. The transmission coefficient can only be obtained by solving the wave equation

$$\frac{d^2E}{dz^2} + \frac{\omega^2}{c^2} n^2(\omega,z)\, E = 0$$

This has been done for various cases by Budden (1961) and Ginzburg (1960). Their results can be expressed in the form

$$\text{transmission coefficient } T = \exp\left( -\tfrac{1}{2} \pi \omega \mid \Delta z \mid /c \right)$$

$$= \exp\left( -\pi^2 \mid \Delta z \mid /\lambda \right)$$

where $\mid \Delta z \mid /\lambda$ is the width of the attenuating region in wavelengths.

If the electron density in the Jovian exosphere is small and the wave normal angle is small the quasi-longitudinal (QL) approximation is valid, and

$$n^2 \simeq 1 - X/(1 - Y_L) \quad \text{for } \tfrac{1}{4} Y_T^4 / Y_L^2 \ll (1 - X)^2$$

where $Y_L$ and $Y_T$ are the longitudinal and transverse components of Y respectively. The refractive index has a pole at $Y_L = 1$ and a zero when $Y_L = 1 - X$. The width of the attenuating region depends only on the rate of change of $Y_L$ with height and the value of X at the zero. We can regard X as constant in this case and the rate of change of n with Y is

$$2n \frac{dn}{dY} = \frac{(n^2 - 1)^2}{X} \left[ \frac{1}{1 - \tfrac{1}{2} \sin^2\theta} \right] \text{ for Y near 1}$$

and the width of the attenuating region is given by

$$\left| \frac{\Delta z}{z} \right| \quad \frac{\Delta Y}{3Y} = \int_{\infty}^{0} \frac{2\, n\, X}{3(n^2 - 1)^2} (1 - \tfrac{1}{2} \sin^2\theta)\, dn$$

$$= -\tfrac{1}{3} X (1 - \tfrac{1}{2} \sin^2\theta) \left[ \frac{1}{n^2 - 1} \right]_{\infty}^{0}$$

$$= \tfrac{1}{3} X (1 - \tfrac{1}{2} \sin^2\theta)$$

The width of the attenuating region in wavelengths is

$$\left| \frac{\Delta z}{\lambda} \right| = \tfrac{1}{3} X \left(1 - \tfrac{1}{2} \sin^2\theta\right) z/\lambda \qquad 6.6.1$$

where z is the distance of the attenuating region from the center of the planet.

If the wave normal angle is large the quasi-transverse (Q.T.) approximation may hold and

$$n^2 \simeq 1 - X(1 - X) / (1 - X - Y_T^2)$$
$$\text{for } \tfrac{1}{4} Y_T^4 / Y_L^2 \gg (1 - X)^2$$

In this case the refractive index has a pole when $Y_T = (1 - X)^{\frac{1}{2}}$ and a zero when $Y_T = 1 - X$. The width of the attenuating region can be made small if X changes rapidly, i.e. X must change by a factor of 2 in a distance less than a wavelength. This requires an improbably large exponential change in density with height. The required law takes the form

$$N \simeq N_o \exp\{(1 - R)\, 10^6/R^3\} \quad \text{where R is in radii.}$$

The likely ratio of maximum to minimum electron density in the magnetosphere is less than $10^{10}$ so that this decrease in density could only be maintained over a distance $\sim 2_{10}{-5}\ R_J$, and only a narrow frequency band $\Delta f \simeq 10^{-4} f$ could escape by this means. We must conclude that the width of the attenuating region is controlled by the rate of change of Y and hence equation 6.6.1 holds.

Emission in Jupiter's magnetosphere has a high frequency cutoff near 40 MHz so we can make the approximation

$$z^3/R_J^3 \simeq 4_{10}7\ \lambda/c$$

and hence

$$z/\lambda = \{4_{10}7 / (\lambda^2 c)\}^{\frac{1}{3}} R_J$$
$$= 7.0_{10}6$$

The transmission through the stop zone becomes

$$T \simeq \exp \{ -\tfrac{1}{3}\pi^2 X (1 - \tfrac{1}{2}\sin^2\theta)\, 7.0_{10}6 \}$$

If we take $T = 0.1$ as an acceptable value we get

$$X \simeq 2.0_{10}-7$$

and hence $N \simeq 2.5_{10}-15\ f^2$ /cc.

This implies an electron density of about 1 per cc at a frequency of 20 MHz. If the attenuation is to be kept within reasonable limits the density in the stop zone and hence the density in the generating region must not greatly exceed this figure. The variation of electron density throughout the regions of the magnetosphere where generation takes place must be such that $X \leq 2.0_{10}-7$.

## 6.7 Cerenkov Radiation from a Stream of Electrons.

The expressions for the power radiated in the Cerenkov mode by a single electron and for the amplification by a helical stream are given in Chapter 5.

The polar diagram of the relative power radiated by a single electron for parameters appropriate to Jupiter's magnetosphere is shown in Figure (6.4). The power increases sharply as the wave normal angle tends to $\pi/2$ although it must drop to zero at $\pi/2$ because of the effect of the thermal motion of the ambient plasma electrons. The corresponding ray directions for maximum power are close to $\pi$ i.e. the radiation is strongest for initial ray directions opposite the direction of motion of the radiating particle.

The extremely high flux densities received at the Earth indicate that the emission must be the result of coherent radiation

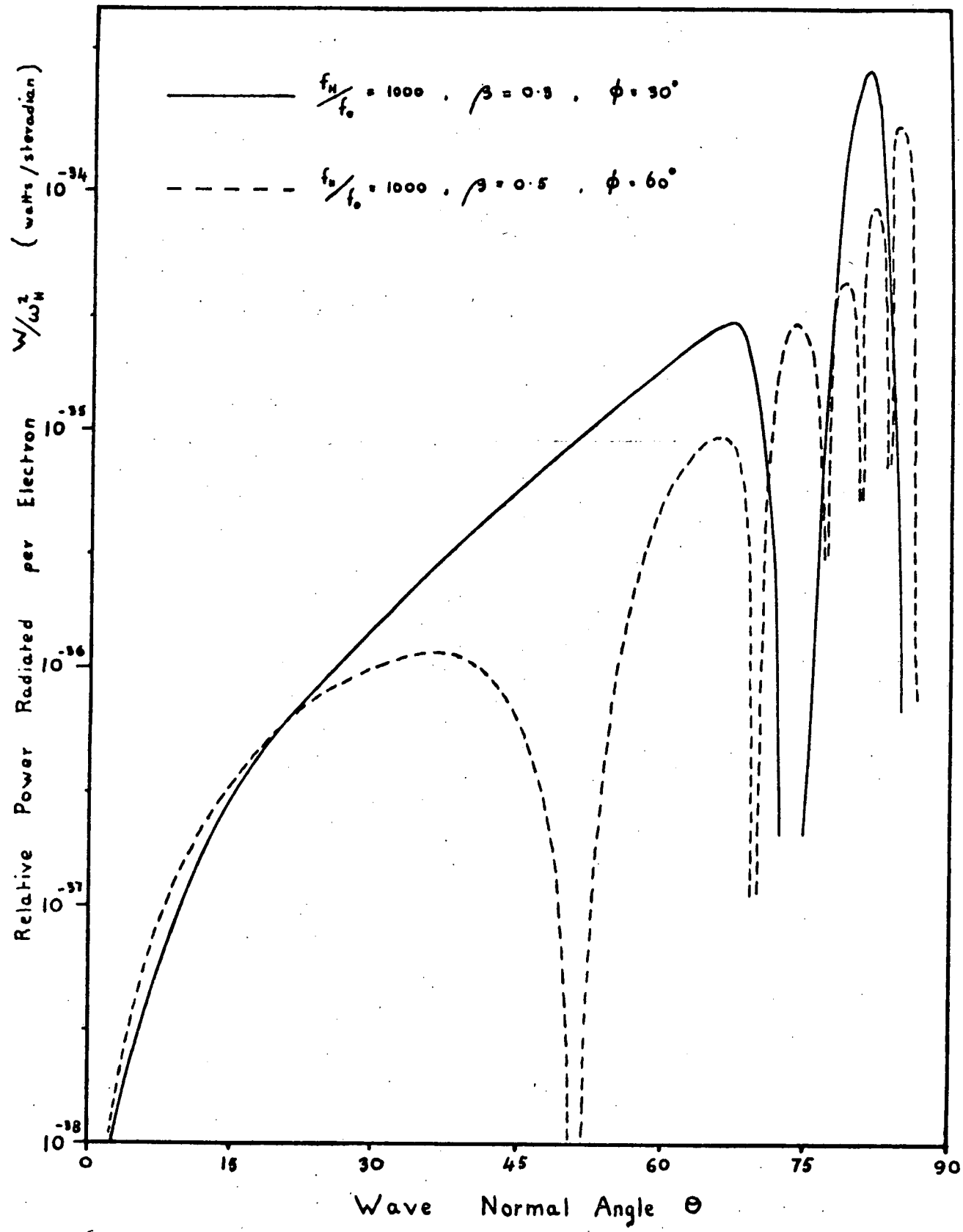


Figure 6.4 Variation of the relative Cerenkov emission from a single electron as a function of wave normal angle for parameters appropriate to Jupiter's magnetosphere.

from a large number of electrons. The radiation from a single electron is amplified as it passes through a helical stream so that the radiated power from N electrons is between N and $N^2$ times the power from one electron. The growth of the wave depends upon the wave normal angle and the parameters of the electron bunch as given in Chapter 5. The resultant polar diagram of radiation from the bunch may be very different from the polar diagram of the single electron. The growth of the wave is given by

$$\exp(\delta t)$$

where t is the time the radiation spends in the stream. Near the region of cyclotron resonance in a low density plasma the group refractive index is large so that the ray velocity is small. The time interval during which the wave grows

$$t = n_{gp} R \cos\alpha / c$$

where $n_{gp}$ is the group refractive index, $\alpha$ is the angle between the wave normal and ray directions, c is the velocity of light, and R is the characteristic dimension of the amplifying region. We will use

$$\eta = n_{gp} \cos\alpha \, | \delta/\omega_H |$$

as a measure of the relative growth of the wave. The amplification factor is

$$A = \exp(\eta R \omega_H / c)$$

The relative growth rate $\eta$ is plotted as a function of wave normal angle for various values of the parameter $f_H/f_o$, the electron velocity $\beta$ and pitch angle $\varphi$ in Figures (6.5) and (6.6) for a ratio of stream density to ambient plasma density $\sigma$ of $10^{-7}$. The growth rate is zero for small wave normal angles in all cases. The angle of maximum growth varies slowly with the density of the background plasma (Figure 6.5a) and is independent of the electron energy

(Figure 6.6a) but decreases monotonically with increasing pitch angle (Figure 6.6b). The value of the growth rate increases with decreasing plasma density being proportional to $N^{-\frac{1}{2}}$ and increases linearly with electron velocity, and also increases rapidly as the pitch angle tends to $\pi/2$.

The attenuation of the wave in escaping from the exosphere depends on the width of the region of imaginary refractive index at the appropriate wave normal angle. The amplification of the wave in the generating region depends upon the time the wave takes to propagate through that region. This in turn depends upon the width of the amplifying region, the group velocity, and the direction of ray propagation in the medium. We can estimate the width of the amplifying region as follows. The plots of growth rate against wave normal angle show that radiation can only be generated coherently over a small range of wave normal angles, from $\theta_1$ to $\theta_2$ say. These limiting wave normal angles correspond to refractive indices $n_1$ and $n_2$ and hence coherent radiation can only be generated in a region where the refractive index is in the range $n_1$ to $n_2$.

We have

$$n^2 = 1 - \frac{X\,(1 - X)}{1 - X - \frac{1}{2} Y_T^2 \pm \{\frac{1}{4} Y_T^4 + (1 - X)^2 Y_L^2\}^{\frac{1}{2}}}$$

For X constant $\quad 2n \frac{dn}{dY} \simeq \frac{(n^2 - 1)^2}{X} \{1 - \frac{1}{2} \sin^2\theta\}^{-1}$ for $Y \simeq 1$

and the distance over which amplification takes place corresponding to a change dn in n is

$$\frac{dz}{z} = \frac{dY}{3Y} = \frac{2\,n\,X}{3(n^2 - 1)^2} (1 - \tfrac{1}{2} \sin^2\theta)\, dn$$

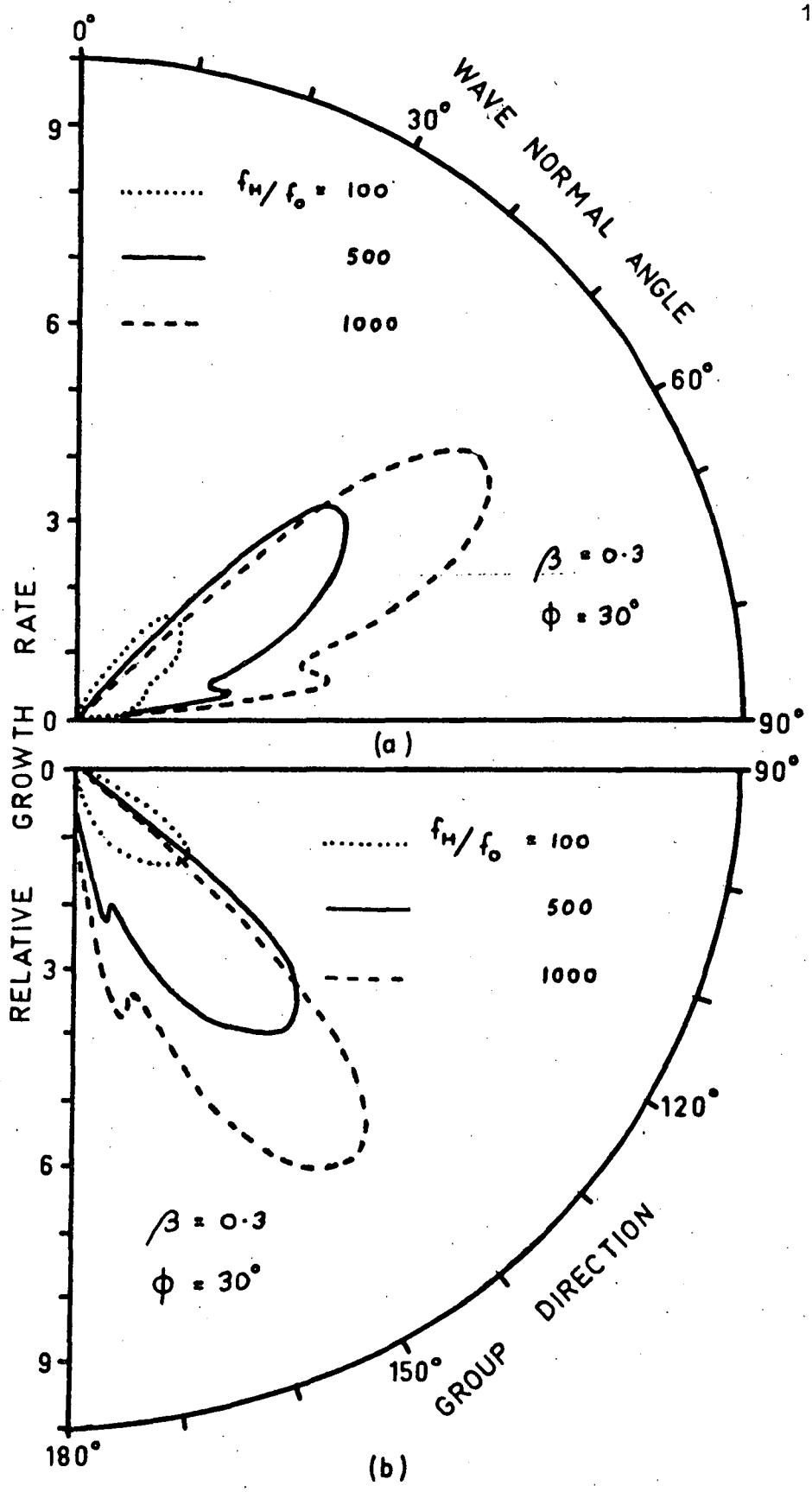


Figure 6.5 (a) Variation of the relative growth rate as a function of wave normal angle for various values of electron energy, pitch angle and $f_H/f_o$.

(b) The same curves as in (a) plotted as a function of the group direction.

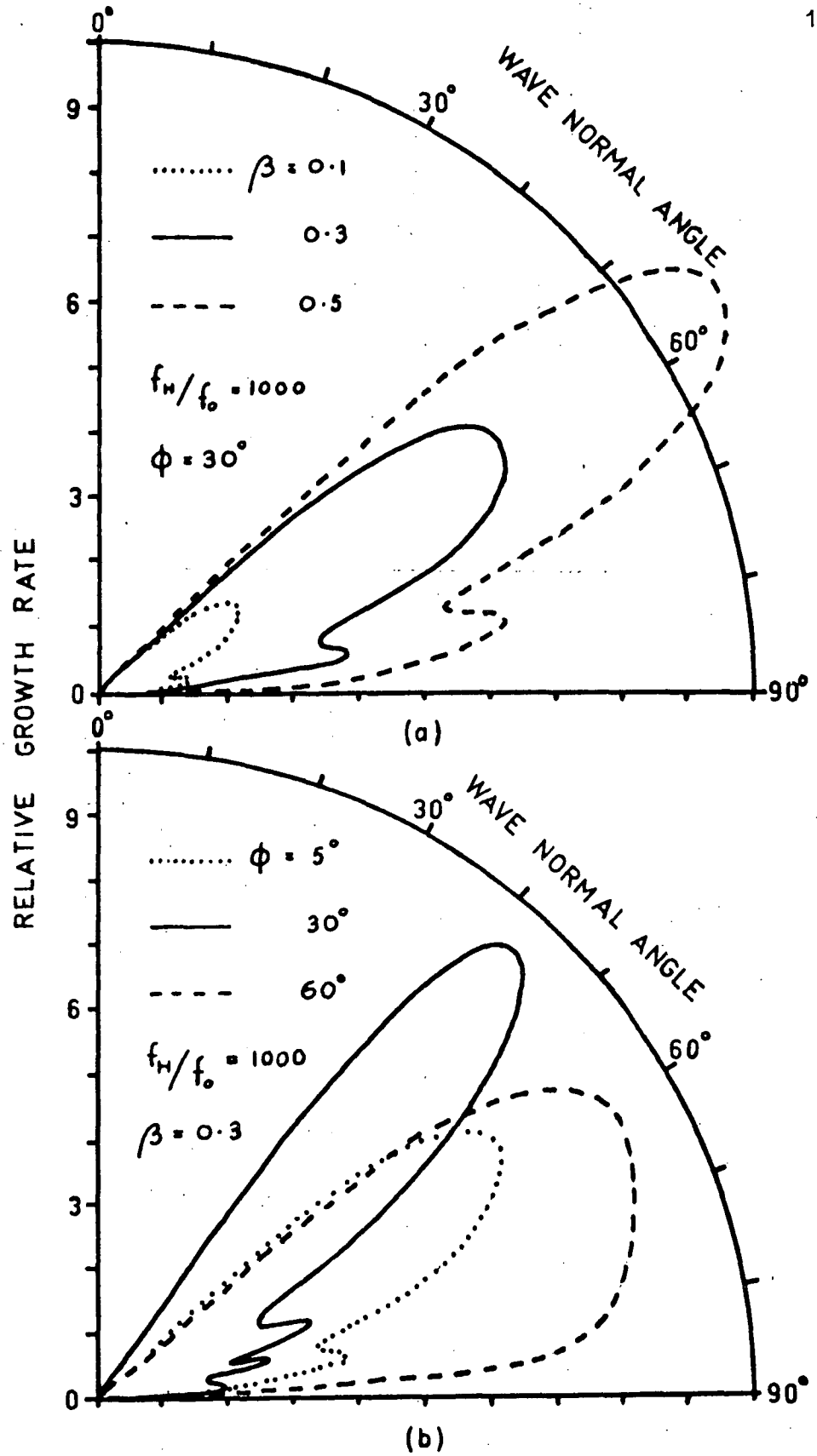


Figure 6.6 Variation of relative growth rate as a function of wave normal angle for $f_H/f_o$ = 1000 and (a) a pitch angle of 30° and various electron energies, and (b) an electron energy of 25 kev and various pitch angles.

since for a dipole field $Y \propto z^{-3}$

The width of the region in which n changes from $n_1$ to $n_2$ is

$$\frac{\Delta z}{z} = \int_{n_1}^{n_2} \frac{2 n X}{3(n^2 - 1)^2} (1 - \tfrac{1}{2} \sin^2\theta)\, dn$$

$$= \tfrac{1}{3} X (1 - \tfrac{1}{2} \sin^2\theta)\left[\frac{-1}{n^2 - 1}\right]_{n_1}^{n_2}$$

The width of the attenuating region is then

$$D = \tfrac{1}{3} X (1 - \tfrac{1}{2} \sin^2\theta)\, z$$

and the width of the amplifying region R is

$$R = D\left[\frac{-1}{n^2 - 1}\right]_{n_1}^{n_2} = D\left[\frac{1}{n_1^2 - 1} - \frac{1}{n_2^2 - 1}\right]$$

If the ray direction in the amplifying region makes an angle $\varepsilon$ with the equipotential surfaces the gain will be

$$\exp\left(\frac{2 \pi \eta R}{\lambda \sin \varepsilon}\right)$$

The overall gain upon escaping from the exosphere will be

$$G = \exp\left[\frac{\pi D}{\lambda}\left\{\frac{2 \eta}{\sin \varepsilon}\left(\frac{1}{n_1^2 - 1} - \frac{1}{n_2^2 - 1}\right) - \pi\right\}\right]$$

The refractive index near the resonance region is dependent mainly on the variable Y, so that layers of constant Y will coincide with layers of constant n. The direction of the gradient of Y remains constant throughout the resonance region and the medium is made up of plane parallel layers on which the refractive index is constant. The direction of a ray through the medium can be traced using a Poererlein construction. The refractive index surfaces are drawn so that the direction of grad Y is vertical, then a ray which is generated at a point $(n, \theta)$ on the diagram can be traced by foll-

owing a vertical line, AB in Figure (6.7), through that point. The wave normal and ray directions are given for each level (corresponding to a particular value of Y) by the radius vector and normal to the refractive index surface at the intersection of AB and the refractive index surface. A ray is traced by moving from refractive index surface to refractive index surface up or down the line AB depending on the initial ray direction. The curves inside the unit circle correspond to the region above the attenuating layer while the curves outside the unit circle correspond to the region below the attenuating layer. Propagation will only be possible between these two regions if the vertical line through the point of emission passes through the unit circle. As we pass from the point of generation down the line towards the unit circle a point of reflection is reached so that according to geometrical optics the ray can never reach free space. However, close to the discontinuity in the refractive index the approximations of geometrical optics do not hold and tunnelling may take place, the final direction of the ray after tunnelling being obtained from the refractive index surfaces at their intersection with the line AB.

As a consequence of the escape conditions, the power which is radiated into a solid angle $\Omega$ where the refractive index is n is spread over a solid angle $\Omega n^2$ upon reaching free space. The angle between the field direction and the vertical in Figure (6.7) is just the angle $\alpha$ between the field direction and the gradient of the field. The way in which this varies with magnetic latitude is shown in Figure (6.8) for a dipole field. The angle $\alpha$ is small for high latitudes and since the growth rate is zero

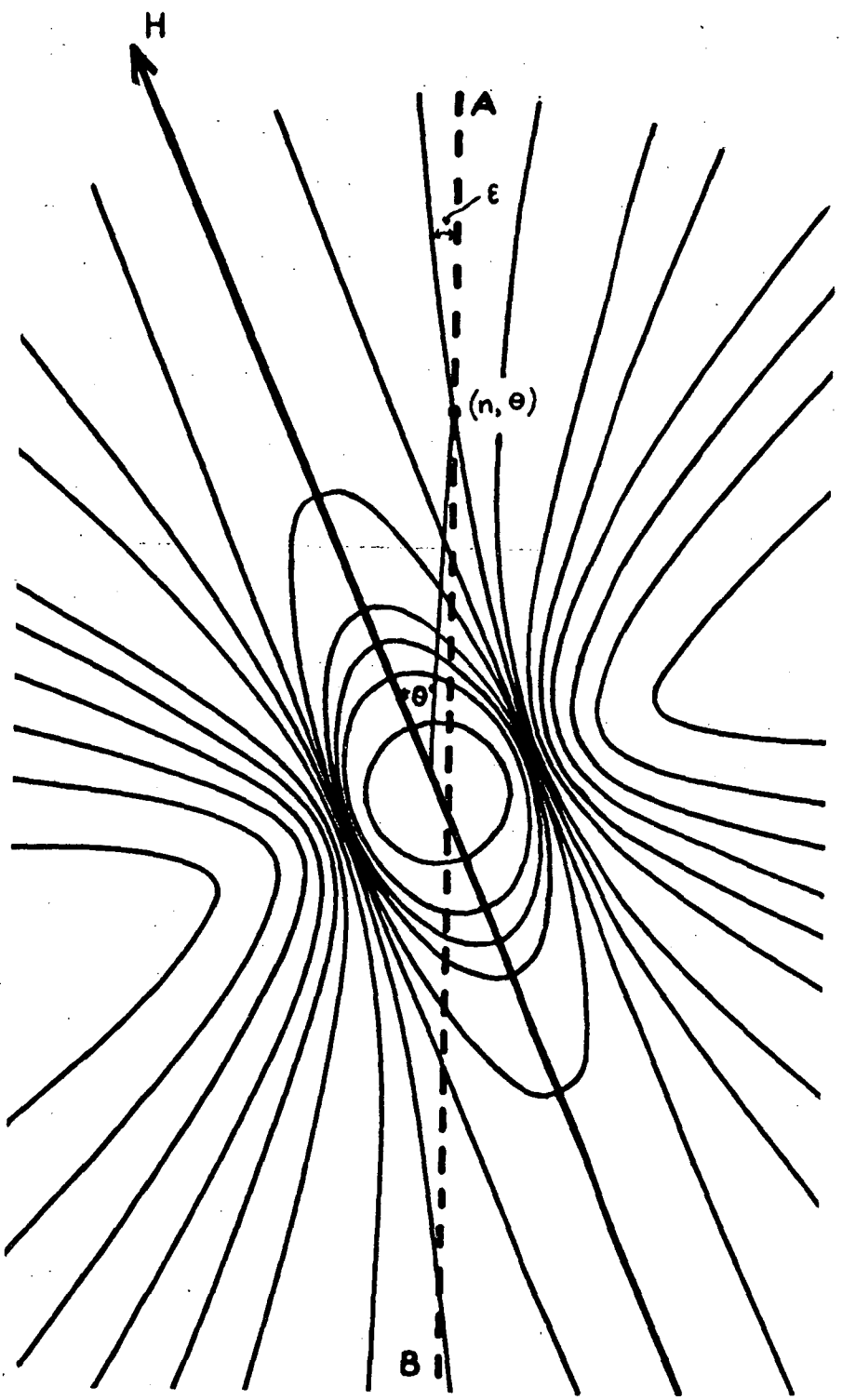


Figure 6.7 Refractive index surfaces for frequencies near the gyrofrequency. The vertical line AB is in the direction of grad Y.

for small wave normal angles, Cerenkov emission will only escape if it is generated at low magnetic latitudes.

## 6.8 The Direction of the Emitted Radiation.

The relation between the wave normal angle $\theta$ at which the radiation is generated and its final wave normal angle $\theta'$ upon escape is

$$\theta' = \arcsin \{n \sin (\theta - \alpha)\} - \alpha$$

The final propagation direction with respect to the particle direction depends on the sign of sin $\varepsilon$ while the magnitude of the amplification depends on $\left| \frac{1}{\sin \varepsilon} \right|$. Calculations of $\theta'$ and $\varepsilon$ for various emission configurations show that about 96% of the rays generated by moderately relativistic electrons propagate in the same general direction as the electrons. Hence the radiation from outward moving electron streams, which decreases in frequency with time, propagates directly to the Earth and is not reflected from Jupiter's ionosphere or surface. Warwick and Gordon (1967) have observed fast drift bursts which have the same time scales as the bursts which Slee and Gent (1967) have shown to originate from Jupiter. These indicate that the majority of the radiation reaching the Earth is generated by outgoing electron streams. In this case the emission which reaches the Earth is emitted initially into a small range of wave normal angles whose values depend on the magnetic latitude of the emission point. This is plotted in Figure (6.9).

## 6.9 The Intensity of the Emitted Radiation.

The radiation emitted from this range of wave normal angles is spread out over a $20^{\circ}$ range between magnetic declinations

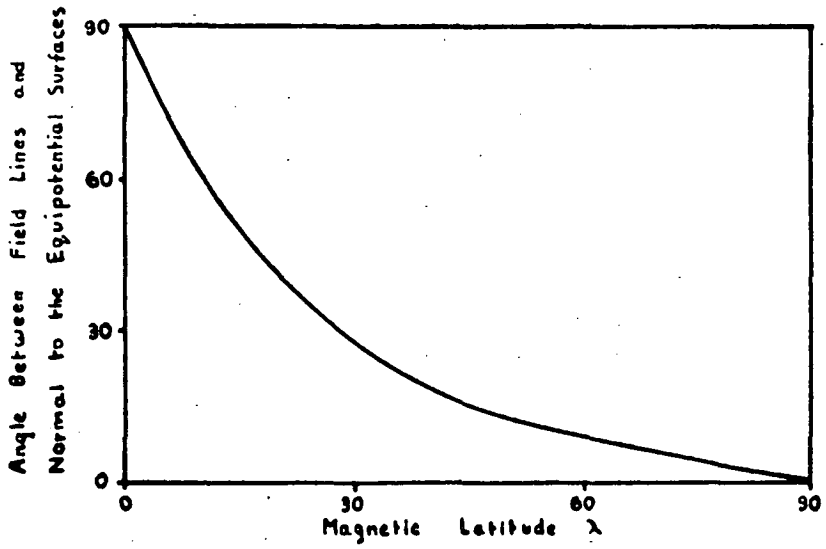


Figure 6.8 Variation of the angle between the direction of the field and the normal to the equipotential surfaces as a function of magnetic latitude for a dipole field.

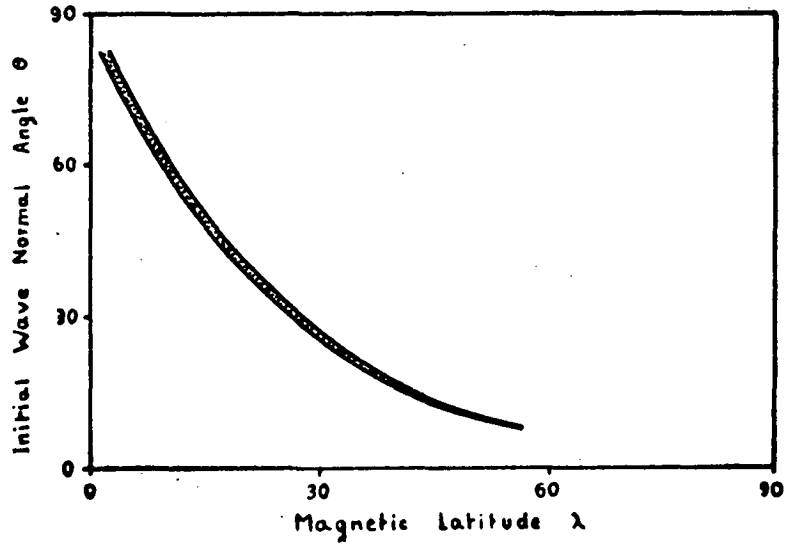


Figure 6.9 The shaded region shows the initial range of wave normal angles from which radiation can reach the Earth.

$\pm 10^{o}$ by defocussing upon escape into free space. The variation of the intensity of the radiation over this interval is determined by the magnitude of sin $\varepsilon$ in each direction.

The minimum detectable flux density for the majority of observations of Jupiter in the decametric range is about $10^{-22}$ $Wm^{-2}$ $Hz^{-1}$. We can use this to estimate the minimum flux that must be emitted at Jupiter. A power of $10^{-22}$ $Wm^{-2}$ $Hz^{-1}$ at the Earth represents a power of approximately 42 W/steradian/Hz at Jupiter.

If W is the power emitted per electron per steradian, G is the amplification factor and N the number of radiating electrons then the power emitted at Jupiter is

$$\frac{N\ W\ G}{B} \quad \text{watts/steradian/Hz}$$

where B is the bandwidth of the emission. The radiation is diluted by a factor of $n^2$ in reaching free space, so the power outside Jupiter's exosphere is $\frac{N\ W\ G}{n^2 B}$.

The length of the emission region $\Delta z$ corresponding to a bandwidth B at height z and frequency f is given by

$$\frac{3\Delta z}{z} \simeq \frac{B}{f}$$

If we choose f = 20 MHz and assume an 18 gauss field for Jupiter

we have $$z \simeq 1.26\ R_J$$

then $$\Delta z \simeq \frac{1.26\ B\ R_J}{3\ f}$$

The maximum angular size of the emitting region has been estimated by Slee and Higgins to less than 1" arc. This implies a maximum diameter of the bunch of about 0.03 $R_J$.

The densities of electrons in the energy range 40 kev

to 100 kev observed in the Earth's magnetosphere is about $5_{10}$-3 /cc (Frank et al, 1963). If we assume that densities of the same order are applicable to Jupiter's magnetosphere we can estimate an upper limit on the density of monoenergetic electrons of $5_{10}$-4 /cc. This is a very optimistic estimate and requires about 10% of the total energetic electron content to be monoenergetic. A more realistic estimate would probably be an order of magnitude lower. We then obtain an upper limit on the number of electrons that can radiate coherently

$$N \simeq 3.4_{10}13 \frac{B R_J}{f}$$

$$\therefore \quad \frac{N}{B} \simeq 1.2_{10}16$$

To obtain a detectable burst we require that

$$WG \simeq 8.9_{10}\text{-}14 \qquad \text{for} \qquad n = 5$$

The minimum growth rate required is plotted in Figure (6.10) as a function of electron velocity for frequencies of 5, 10, 20 and 40 MHz. The values used for the power per electron are typical values calculated for small wave normal angles.

The expression for G was given in Section (6.7)

$$G = \exp\left[\frac{\pi D}{\lambda}\left\{\frac{2\eta}{\sin\varepsilon}\left(\frac{1}{n_1^2 - 1} - \frac{1}{n_2^2 - 1}\right) - \pi\right\}\right]$$

If $n_2 >> n_1 >> 1$ we can make an approximation by replacing $\left(\frac{1}{n_1^2 - 1} - \frac{1}{n_2^2 - 1}\right)$ by $\frac{1}{n_1^2}$ where $n_1$ is the minimum refractive index for which growth is possible. We have the Cerenkov condition, $\frac{1}{n_1^2} = \beta^2 \cos^2\theta \cos^2\varphi$ where $\theta$ is the minimum wave normal angle for which growth is possible. Empirically we find that the

growth rate increases rapidly as the pitch angle tends to $\pi/2$ but increases linearly with $\beta$. Hence to a good approximation

$$2\eta/n_1^2 = 4\eta'\beta^3\cos^2\theta$$

where $\eta'$ is the value of $\eta$ where $\beta = 0.5$. The growth rate then becomes $G = \exp\{\pi D (4\eta'\beta^3\cos^2\theta/\sin\varepsilon - \pi)/\lambda\}$

The thickness of the attenuating region is directly proportional to the electron density of the ambient plasma, while $\eta'$ is inversely proportional to the square root of the density. Hence provided the overall gain is large, G varies with electron density $N_e$ according to

$$G = \exp(\text{const } N_e^{\frac{1}{2}})$$

We can then obtain any desired overall gain by increasing the electron density sufficiently. However this also increases the attenuation in the stop zone and the final limit is placed by the available energy of the radiating electrons.

The maximum value of $|\varepsilon|$ for which a burst can be observed is plotted against electron velocity in Figure (6.11) for various values of the parameter $f_H/f_o$. For a given value of refractive index the angle $\varepsilon$ for which radiation can escape in the direction of the Earth increases with the magnetic latitude of the emission point. This relationship has been used in conjunction with the data of Figure (6.11) to calculate the minimum electron velocity required to give a detectable burst as a function of the magnetic latitude of the emission point. This is plotted in Figure (6.12) for refractive indicies of n = 6 and 10 and for values of $f_H/f_o$ = 1200 and 5000. The required electron energy increases rapidly as the magnetic latitude is increased above $10^o$ and is most favourable for the smallest values of $f_H/f_o$ i.e. for high values

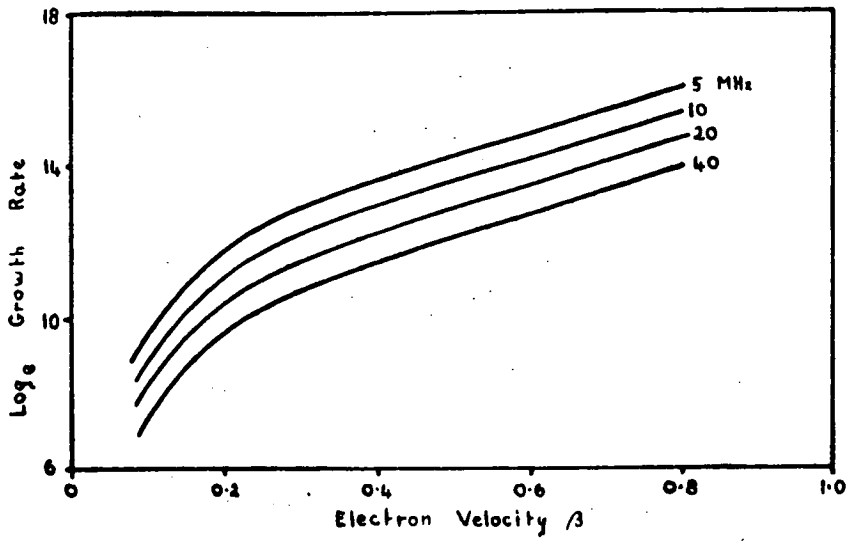


Figure 6.10 The log of the minimum growth rate required to give a burst of intensity $10^{-22}$ $Wm^{-2}$ $Hz^{-1}$ at the Earth for various wave frequencies as a function of electron energy.

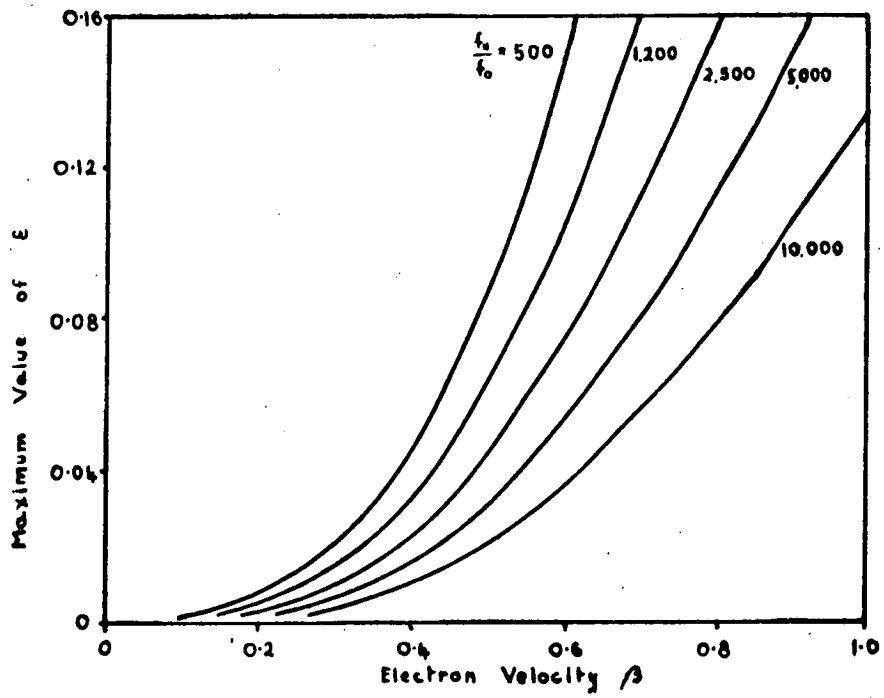


Figure 6.11 The maximum angle of $|\varepsilon|$ for which a burst of $10^{-22}$ $Wm^{-2}$ $Hz^{-1}$ can be obtained, plotted as a function of electron energy for various values of $f_H/f_o$.

of the ambient plasma density. The range of wave normal angles for which radiation can reach the Earth is plotted as a function of magnetic latitude in Figure (6.9). This allows us to calculate the electron velocity which satisfies the Cerenkov condition for a given refractive index at each magnetic latitude. For example, if we take n = 10 and $\lambda = 10^{\circ}$ we find $\theta \simeq 60^{\circ}$ and $\beta_{\parallel} \simeq 0.2$. This is lower than the minimum velocity given in Figure (6.12) and hence radiation will not be observed under these conditions. If we reduce the refractive index $\beta_{\parallel}$ will increase but so does $\beta_{min}$ and the condition still cannot be satisfied. For higher magnetic latitudes than $10^{\circ}$, $\beta_{min}$ increases (Figure 6.12) while $\theta$ decreases and hence $\beta_{\parallel}$ decreases. Hence we cannot satisfy the conditions for an observable burst for $n \lesssim 10$ and $\lambda \gtrsim 10^{\circ}$. This leaves us with two alternatives, to increase the refractive index or decrease the magnetic latitude.

To satisfy the radiation conditions we have to reduce $\lambda$ to less than $5^{\circ}$ and hence the range of frequencies that can be radiated by an electron moving along the field is less than 1.09 : 1. Dynamic spectra of inidividual bursts observed by Gordon (1966) occur over a frequency range from at least 24 to 31 MHz, a range of 1.3 : 1 and show only negative frequency time slopes. This rules out the possibility that $\lambda \lesssim 5^{\circ}$ on the grounds that the observed frequency range is much larger than could be obtained theoretically, and only negative frequency slopes are observed while theoretically we would expect equal number of positive and negative slopes.

We must then consider the one remaining possibility that the refractive index $n > 10$. For n sufficiently large $\beta_{min}$ can be

made as small as we like and hence we can satisfy the radiation conditions and obtain a sufficiently large growth with low energy electrons since $\beta = \frac{1}{n \cos\theta \cos\varphi}$

## 6.10 Power Available from the Electron Streams.

The total energy of a bunch containing N electrons each of energy $E_e$ is given by $E_T = N E_e$

The maximum number of electrons that can radiate coherently has been given in Section (6.9) as $N = 1.2_{10}16\ \Delta f$

where $\Delta f$ is the bandwidth of the emission.

Then $E_T = 1.2_{10}16\ E_e \Delta f$

Individual dynamic spectra of bursts indicate durations of about 0.1 seconds, so that the available power is

$$W = \frac{10\ E_T}{\Delta f} \quad \text{watts/Hz}$$

$$= 1.2_{10}17\ E_e \quad \text{watts/Hz}$$

where $E_e$ is expressed in watts.

This power is initially radiated into a solid angle at about 1 steradian but that part which escapes from the magnetosphere is diluted by a factor of $n^2$. Hence the maximum available power just outside the magnetosphere of Jupiter is

$$W = 1.9_{10}-2\ \frac{E_e}{n^2} \quad \text{watts/steradian/Hz}$$

where $E_e$ is now expressed in electron volts. However the radiation is attenuated by a factor of

$$\exp\left(\frac{\pi^2 D}{\lambda}\right) \text{ in passing through the stop zone}$$

where $D/\lambda = \frac{1}{3} X (1 - \frac{1}{2} \sin^2\theta)\ z/\lambda$

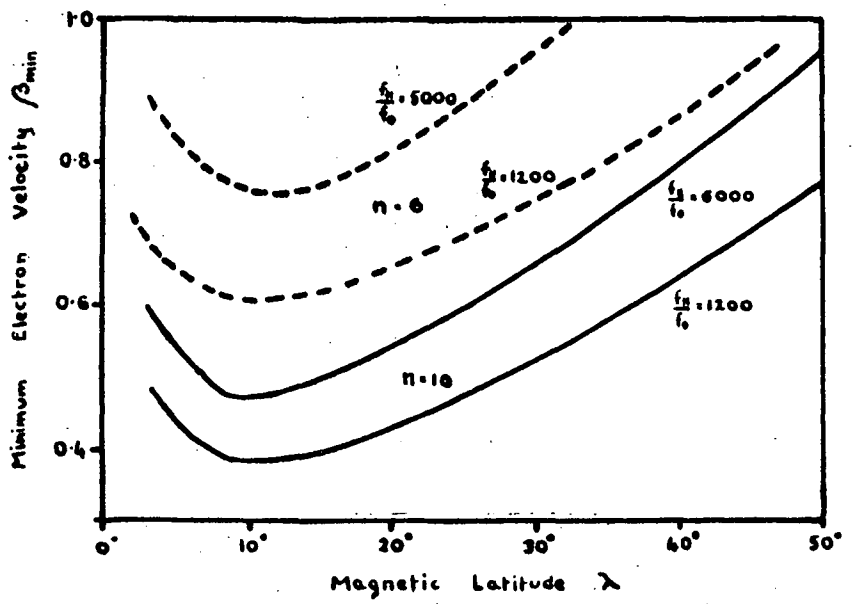


Figure 6.12 Variation of the minimum electron energy to give a burst of $10^{-22}$ $Wm^{-2}$ $Hz^{-1}$ as a function of magnetic latitude for various combinations of refractive index and $f_H/f_o$.

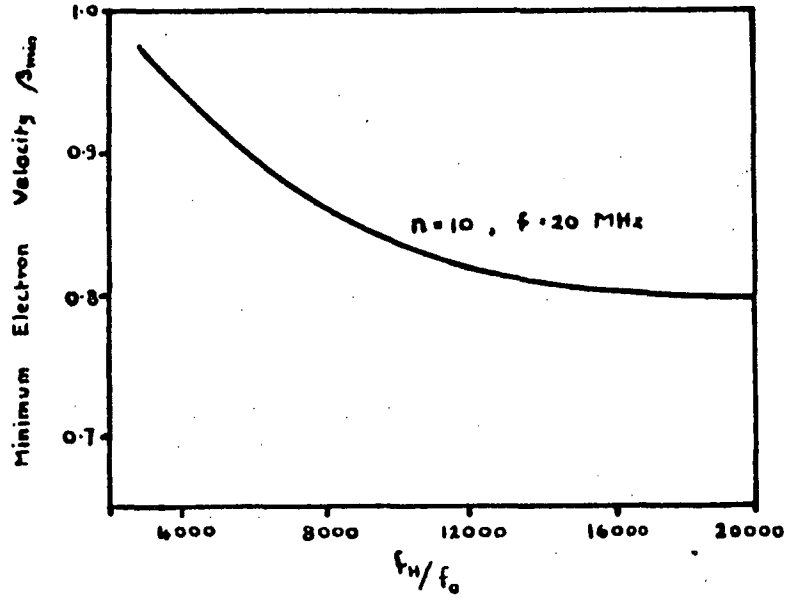


Figure 6.13 Variation of the minimum electron energy needed to give radiation of $10^{-22}$ $Wm^{-2}$ $Hz^{-1}$ at the Earth as a function of $f_H/f_o$ for emission where the refractive index is 10.

and z is the distance of the emission point from the center of Jupiter. Figure (6.13) shows the minimum value of $\beta$ for which a burst at 20 MHz emitted where the refractive index is 10 reaches the Earth with an intensity of $10^{-22}$ $Wm^{-2}$ $Hz^{-1}$.

For emission where n = 10 we have $\beta \simeq 0.2$ which is much smaller than the minimum $\beta$ required to give an observable burst. Even if all the energy of the bunch was radiated in about 0.01 seconds $\beta_{min}$ would be about 0.15 and radiation could only just be detected. Under no circumstances could bursts having flux densities as high as $10^{-20}$ $Wm^{-2}$ $Hz^{-1}$ be received at the Earth. Hence we must conclude that Cerenkov radiation is not a suitable emission process to explain the decametric radio emissions from Jupiter.

## 6.11 Conclusions.

The model of Warwick's based on Cerenkov radiation has been examined. We find that the assumptions made are inconsistent with the observations and properties of Cerenkov radiation on three counts. These are the displacement of Jupiter's magnetic field from the symmetrical position, and the confinement of Cerenkov radiation to a small cone of angles about the field direction. Thirdly the assumption that emission occurs near the gyrofrequency where the electron density is high but passes unattenuated through a neighbouring stop zone because the electron density has decreased to zero only allows a very narrow band of frequencies to escape.

The general properties of Cerenkov emission as applied to Jupiter have been examined to determine whether an alternative model could be found. If we accept the estimates of Slee and

Higgins for the maximum angular diameter of the source as $\simeq$ 1" arc and take the maximum density of monoenergetic electrons in a helical stream to be $5_{10}{}^{-4}$ /cc then no alternatives can be found. The conditions for the escape of radiation and for the growth of the wave to be sufficiently high for the radiation to be detected on Earth require emission where the refractive index n > 10. This in turn implies low electron energies so that the limits on the size and density of the stream prevent sufficient energy being contained within the bunch.

Hence we must conclude that the attenuation in escaping from Jupiter's magnetosphere and the defocussing that accompanies it places such severe limitations on the properties of the radiating particles that it is impossible for Cerenkov emission to explain the observed intensities of Jupiter's emissions at the Earth.

## 6.12 References.

BRANSON, N.J.B.A. (1968) Mon. Not. R. Astr. Soc. 139, 155

BUDDEN, K.G. (1961) Radio Waves in the Ionosphere. Cambridge

ELLIS, G.R.A. (1965) J. Res. Nat. Bur. Standards 69. D., 1513

ELLIS, G.R.A. and P.M. McCULLOCH (1963) Aust. J. Phys. 16, 380

FRANK, L.A., J.A. VAN ALLEN and E. MACAGNO (1963) J. Geophys. Res. 68, 3543

GINZBURG, V.L. (1960) Propagation of Electromagnetic Waves in Plasmas North Holland

GINZBURG, V.L. and V.V. ZHELEZNYAKOV (1958) Soviet Astronomy, A. J. 2, 653

GINZBURG, V.L. and V.V. ZHELEZNYAKOV (1959) Soviet Astronomy, A. J. 3, 235

GORDON, M.A. (1966) Ph. D. Thesis, University of Colorado

McADAM, W.B. (1966) Planet Space Sci. 14, 1041

McKENZIE, J.F. (1966) Proc. Phys. Soc. 87, 349

ROBERTS, J.A. and R. EKERS (1966) Icarus 5, 149

SLEE, O.B. and H. GENT (1967) Nature 216, 235

SLEE, O.B. and C.S. HIGGINS (1968) Aust. J. Phys. 21, 341

WARWICK, J.W. (1961) Annals N.Y. Acad. Sci. 95, 39

WARWICK, J.W. (1963) Astrophys. J. 137, 41

WARWICK, J.W. (1964) Ann. Rev. Ast. Astrophys. 2, 1

WARWICK, J.W. and M.A. GORDON (1965) Astron. J. 70, 332

# CHAPTER 7.

# CYCLOTRON RADIATION AS THE SOURCE OF JUPITER'S DECAMETRIC EMISSIONS

## 7.1 Introduction.

Cyclotron radiation was first proposed as the source of Jupiter's decametric emissions by Ellis (1962, 1963). A detailed model of the emission region was developed by Ellis and McCulloch (1963), it was based on the need for coherent radiation from many electrons but the properties of the emission were assumed to be identical to the emission from a single electron. This model was reviewed and developed by Ellis (1965). Recently Fung (1966) developed a theory for the amplification of a wave by a helical electron stream, and compared this with the theory used by Ellis and McCulloch. He concluded that the properties of the radiation assumed by Ellis and McCulloch were justified by the amplification theory.

However, there are differences in these two theories which lead to a different emission model. The following discussion is based on the amplification theory of Fung and on more recent observations of Jupiter's emissions.

## 7.2 The Conditions for Cyclotron Radiation in a Plasma.

Cyclotron radiation from moderately relativistic electrons is emitted mainly at the fundamental of the relativistic Doppler shifted cyclotron frequency,

$$f = f_H (1 - \beta)^{\frac{1}{2}} / \{1 - n \beta \cos \theta \cos \varphi\} \qquad 7.2.1$$

where $f_H = eH/2\pi mc$ is the cyclotron frequency

$\beta = v/c$

$\gamma = (1 - \beta^2)^{\frac{1}{2}}$

$v$ = electron velocity

$\theta$ = wave normal angle

$\varphi$ = electron pitch angle

into a medium whose refractive index is given by the Appleton-Hartree equation

$$n^2 = 1 - \frac{X (1 - X)}{1 - X - \frac{1}{2}Y_T^2 \pm \{\frac{1}{4}Y_T^4 + (1 - X)^2 Y_L^2\}^{\frac{1}{2}}}$$

where $X = f_o^2/f^2$

$f_o = (N_e^2/\pi m)^{\frac{1}{2}}$ is the plasma frequency

$Y_T = Y \sin \theta$

$Y_L = Y \cos \theta$

$Y = f_H/f$

Jupiter's emissions are predominantly x-mode radiations so the minus sign is appropriate in the Appleton-Hartree equation. The refractive index is imaginary for frequencies between $\gamma f_H$ and $fx = (f_o^2 + \frac{1}{4} f_H^2)^{\frac{1}{2}} + \frac{1}{2} f_H$, and is less than one for frequencies above fx. Only if the electron velocity is sufficiently large to Doppler shift f above fx can radiation be generated. In general equations 7.2.1 and 7.2.2 have two solutions for a given wave normal angle, Figure (7.1), but there exists some wave normal angle $\theta_c$ above which no solutions exist. Radiation at the fundamental is confined to a cone of half angle $\theta_c$. The emission is generated where $n < 1$ so that the radiation is focussed into a narrower cone

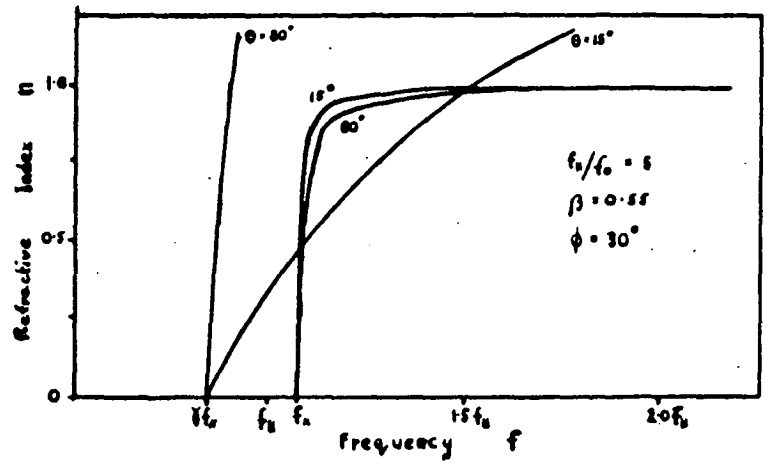


Figure 7.1 The graphical solution of the Appleton-Hartree equation and Doppler equation for wave normal angles of 15° and 80°.

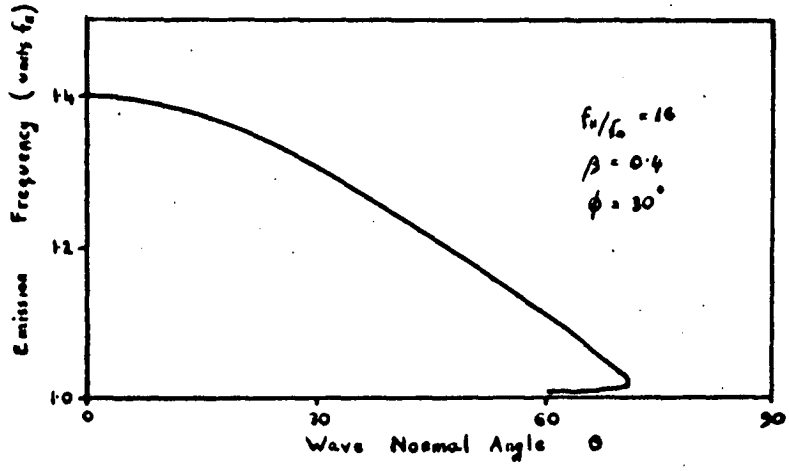


Figure 7.2 Variation of the emitted frequency with wave normal angle for 45 kev electrons, pitch angle 30° and $f_H/f_0 = 16$.

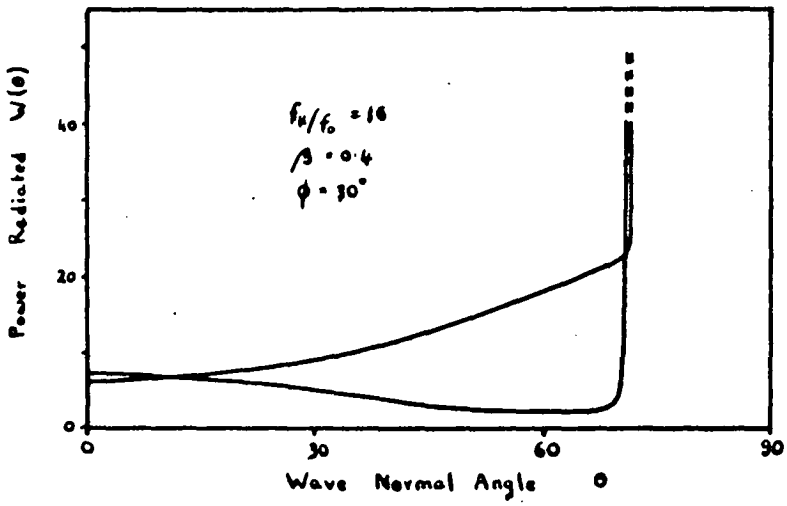


Figure 7.3 Variation of the relative power emitted by a single electron as a function of wave normal angle for the same conditions as Figure 7.2.

upon propagating to free space. This is just the opposite of Cerenkov radiation which is diverged when escaping from the magnetosphere. Figure (7.2) shows the variation of the emitted frequency with wave normal angle.

For radiation at the second and higher harmonics, by moderately relativistic electrons, there is always one and only one solution to the equations for a given value of $\theta$. Emission occurs for all wave normal angles and is generated where $n \simeq 1$ so that focussing is negligible.

## 7.3 Cyclotron Radiation from a Stream of Electrons.

The power W radiated by a single electron is amplified by the helical stream of N electrons by a factor A, so that the emitted power is

$$P = N W A$$

where $$A = \exp \{ Im(\delta)\ t \}$$

and t is the propagation time of the wave in the stream. Expressions for W and $Im(\delta)$ for cyclotron radiation were given in Chapter 5.

The variation of W with wave normal angle $\theta$, is shown in Figure (7.3) for values of electron energy and pitch angle which are likely to occur in Jupiter's magnetosphere. The power is found to peak sharply over a small range of wave normal angles where the denominator of the expression for W vanishes, i.e. when $n_{gp} \beta \cos \theta \cos \varphi = 1$ where $n_{gp}$ is the group refractive index. The power can never go to infinity and will be limited because of the finite temperature of the ambient plasma, although it could be several orders of magnitude larger at its maximum than at neighbour-

ing wave normal angles.

The polar diagram of the power emitted by a stream of electrons will be dominated by the amplification effects so unless the power at the maximum adds coherently throughout the stream the maximum will be insignificant.

The way in which the maximum angle of emission $\theta_c$ varies with electron energy, pitch angle and ambient plasma density is plotted in Figure (7.4).

It is convenient to take a quantity which we will call the growth rate defined by $\eta = \left| \frac{Im(\delta)}{\omega_H} \right| = \frac{1}{Y} \left| \frac{Im(\delta)}{\omega} \right|$ as a measure of the amplification of the wave. The variation of $\eta$ with wave normal angle, and frequency is shown in Figures (7.5) and (7.6) respectively. The growth rate increases slowly with wave normal angle and reaches a broad maximum at about $\frac{3}{4}$ of the maximum wave normal angle $\theta_c$, it then drops off rapidly as $\theta$ tends to $\theta_c$. The 3 db bandwidths and beamwidths of the radiation are plotted as a function of the amplification in Figures (7.7) and (7.8). The beamwidth changes on the average about $2^\circ$ for every order of magnitude change in the amplification while the bandwidth changes by only a few per cent for the same change in amplification.

The variation of 3 db bandwidth with electron energy, pitch angle and $f_H/f_o$ is shown in Figure (7.9) for an amplification of $10^8$. The observed bandwidths of 1 to 2 MHz at 20 MHz for the fast drift bursts are consistent with radiation from low energy ($\beta \leqslant 0.4$) electrons with pitch angles $\varphi \geqslant 30^\circ$.

The angle at which the growth rate is a maximum, $\theta_m$ is

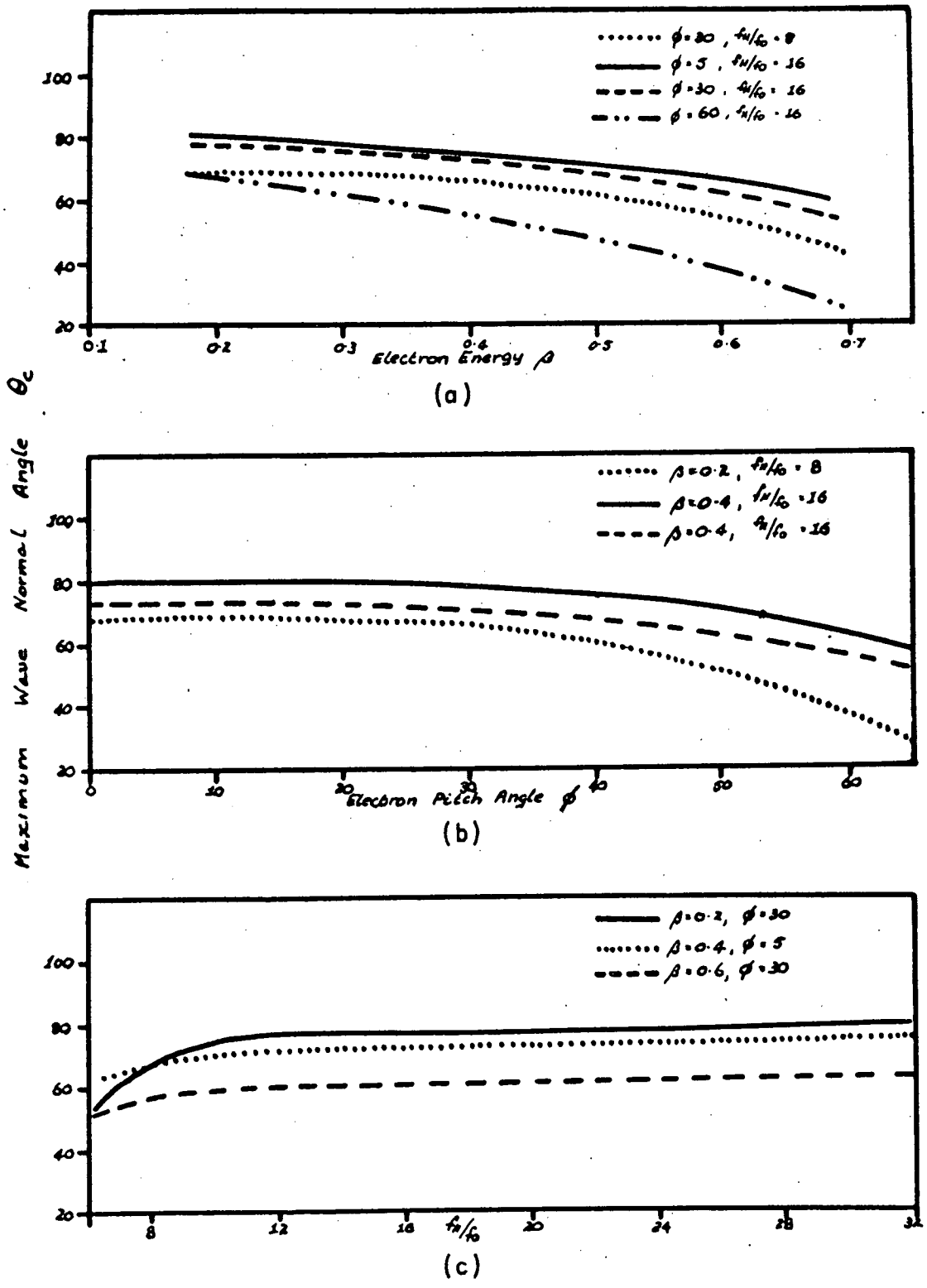


Figure 7.4 Variation of the maximum angle of emission with (a) electron energy (b) electron pitch angle, and (c) with the parameter $f_H/f_o$.

plotted as a function of electron energy, pitch angle and $f_H/f_o$ in Figures (7.10) to (7.12) while the maximum value of $\eta$ is plotted in Figures (7.13) to (7.15) against the same parameters for a ratio of stream density to ambient plasma density of $10^{-7}$.

## 7.4 The Intensity of the Emitted Radiation.

The observed intensities of the radiation bursts vary widely, from peak powers of about $10^{-18}$ $Wm^{-2}$ $Hz^{-1}$ downwards, the lower limit being provided by the receiver threshold. This lower limit is usually around $10^{-22}$ $Wm^{-2}$ $Hz^{-1}$, which is equivalent to a radiated power of about 42 W/steradian/Hz at Jupiter.

The radiated power is given by $P = N W A$ where N is the number of electrons radiating coherently, W is the power radiated by a single electron and A is the amplification factor. The observations of Slee and Higgins (1968) indicate that the maximum dimension of the emitting electron bunch is about $0.03\ R_J$, which gives a maximum cross sectional area of about $0.001\ R_J^2$. The length L of the coherent region will be determined by the bandwidth $\Delta f$ of the emitted burst. For a dipole field

$$L \simeq \frac{R}{3}\left(\frac{\Delta f}{f_H}\right)$$

where R is the distance of the emission point from the center of Jupiter. Then $N = \frac{1}{3} N_s R \left(\frac{R_J}{30}\right)^2 \left(\frac{\Delta f}{f}\right)$ where $N_s$ is the electron density in the stream.

For emission on a high latitude field line having a maximum gyrofrequency of $f_{max}$ $R^3 \simeq \left(\frac{f_{max}}{f_H}\right) R_J^3$

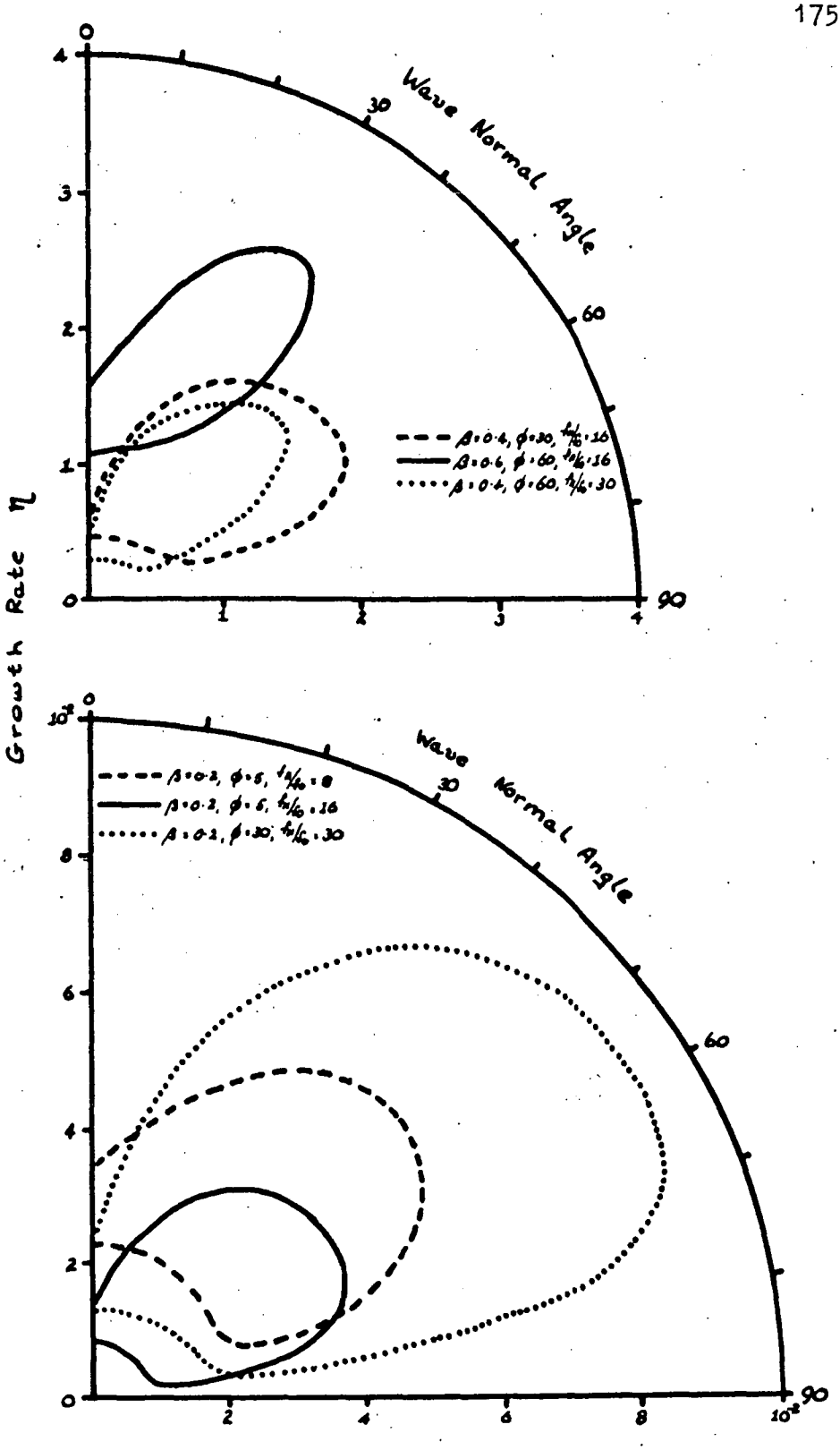


Figure 7.5 Variation of the growth rate as a function of wave normal angle for various values of electron energy, pitch angle and $f_H/f_o$.

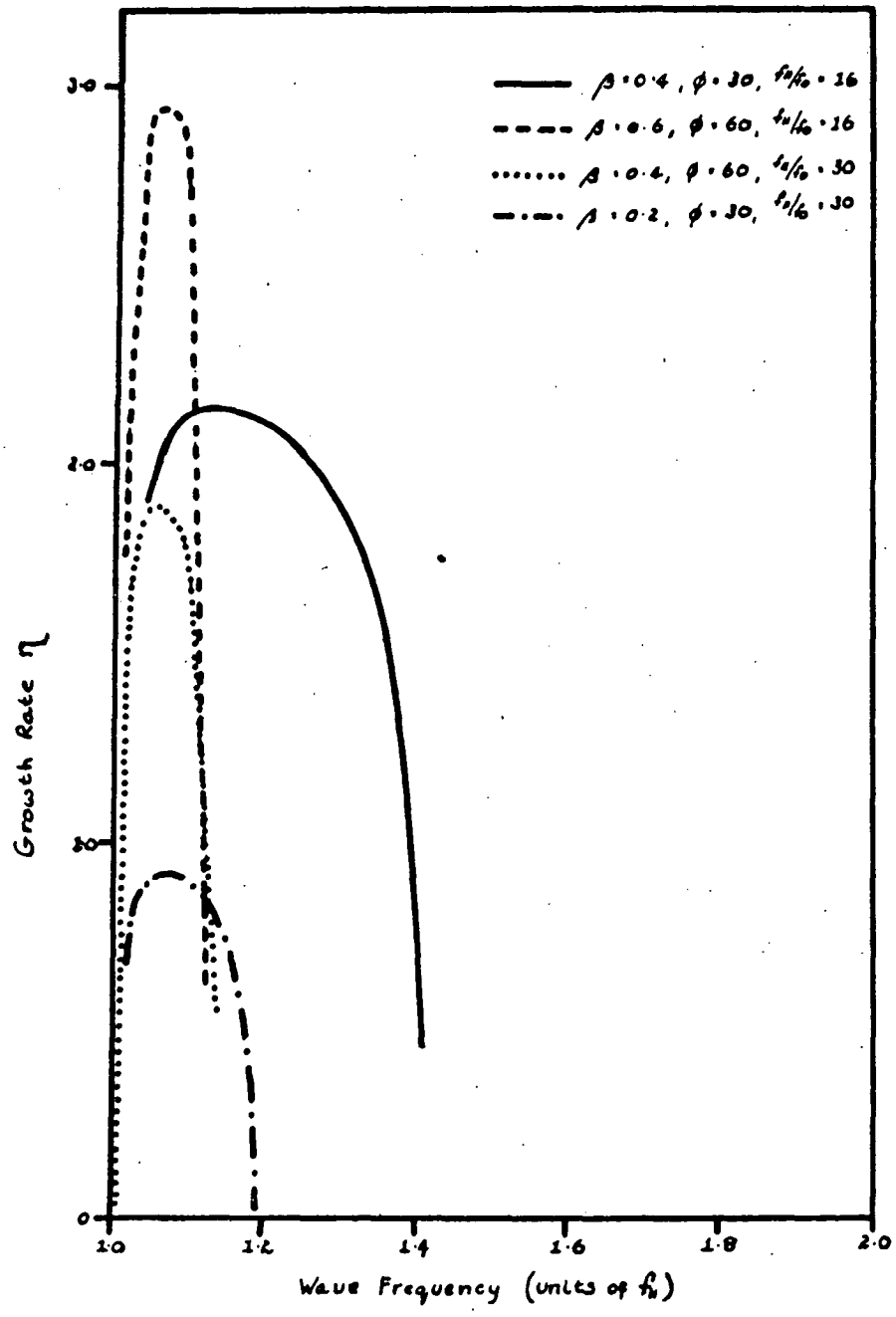


Figure 7.6 Variation of the growth rate as a function of the wave frequency for various values of electron energy, pitch angle and $f_H/f_o$.

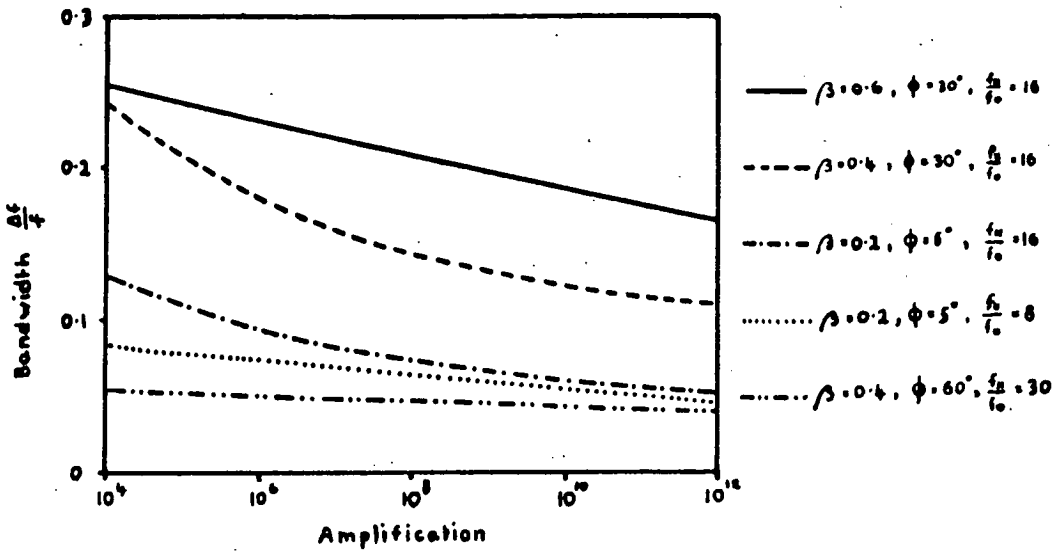


Figure 7.7 The 3 db bandwidth $\Delta f/f$ of the emitted radiation plotted as a function of the amplification for various combinations of energy, pitch angle and $f_H/f_o$.

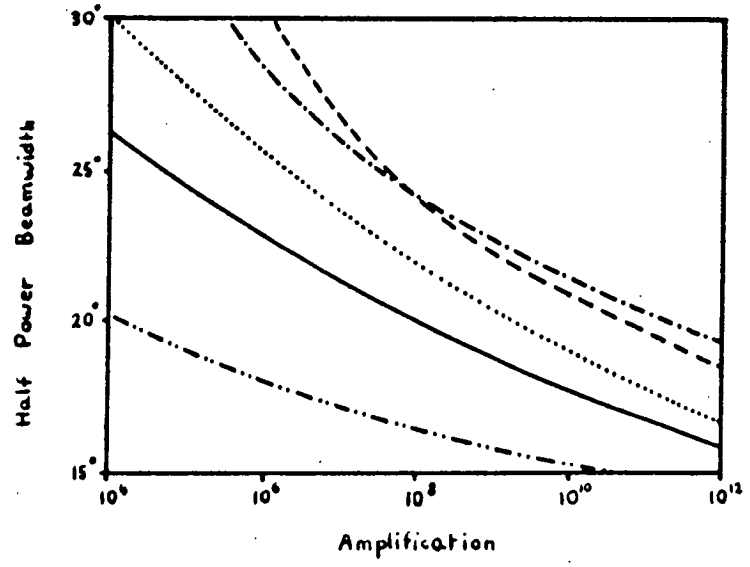


Figure 7.8 Variation of the 3 db beamwidth of the emission cone as a function of the amplification. The legend is the same as for Figure 7.7.

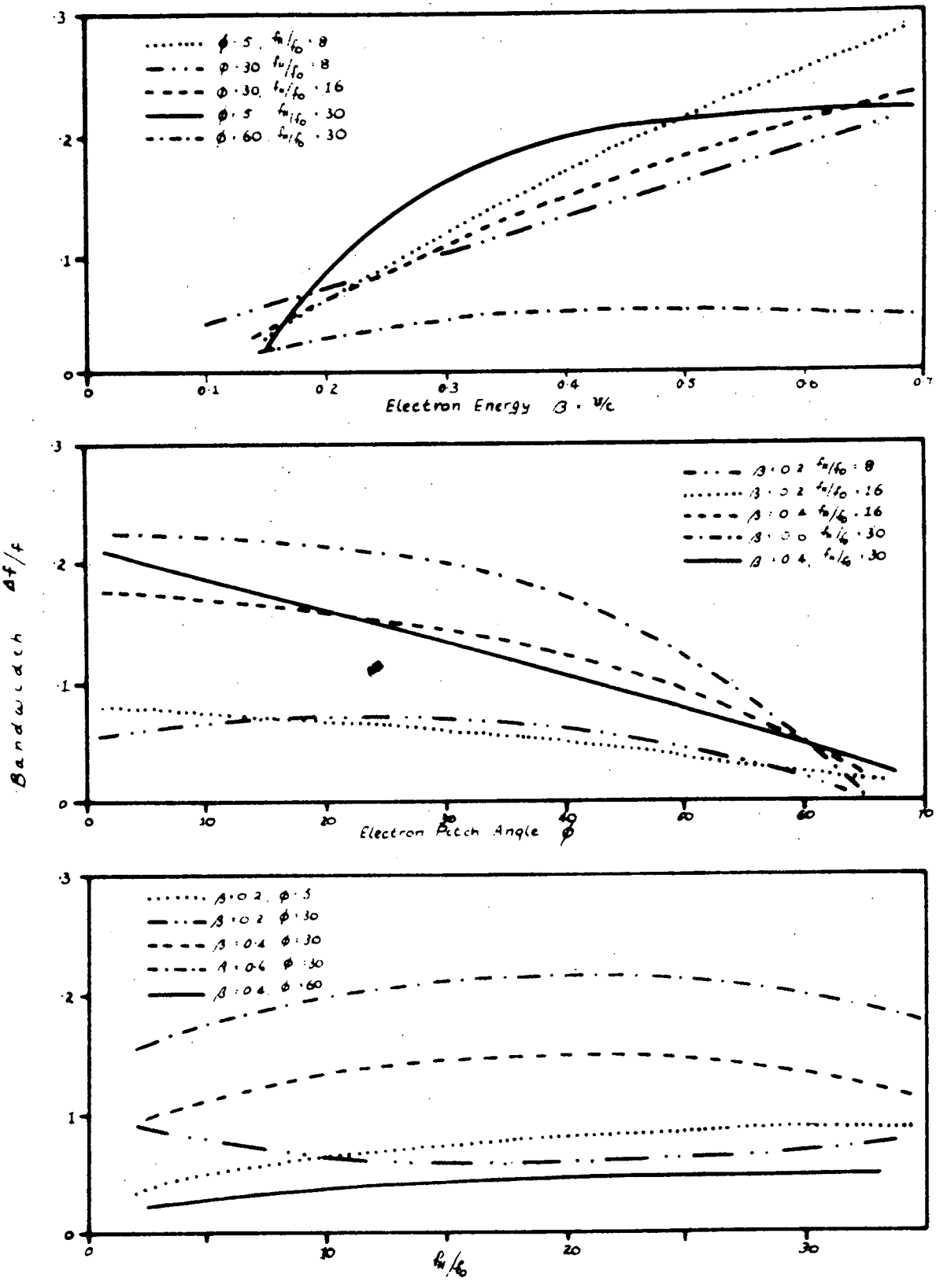


Figure 7.9 Variation of the 3 db bandwidth of the radiation for an amplification of $10^8$ as a function of (a) electron energy (b) electron pitch angle, and (c) $f_H/f_o$.

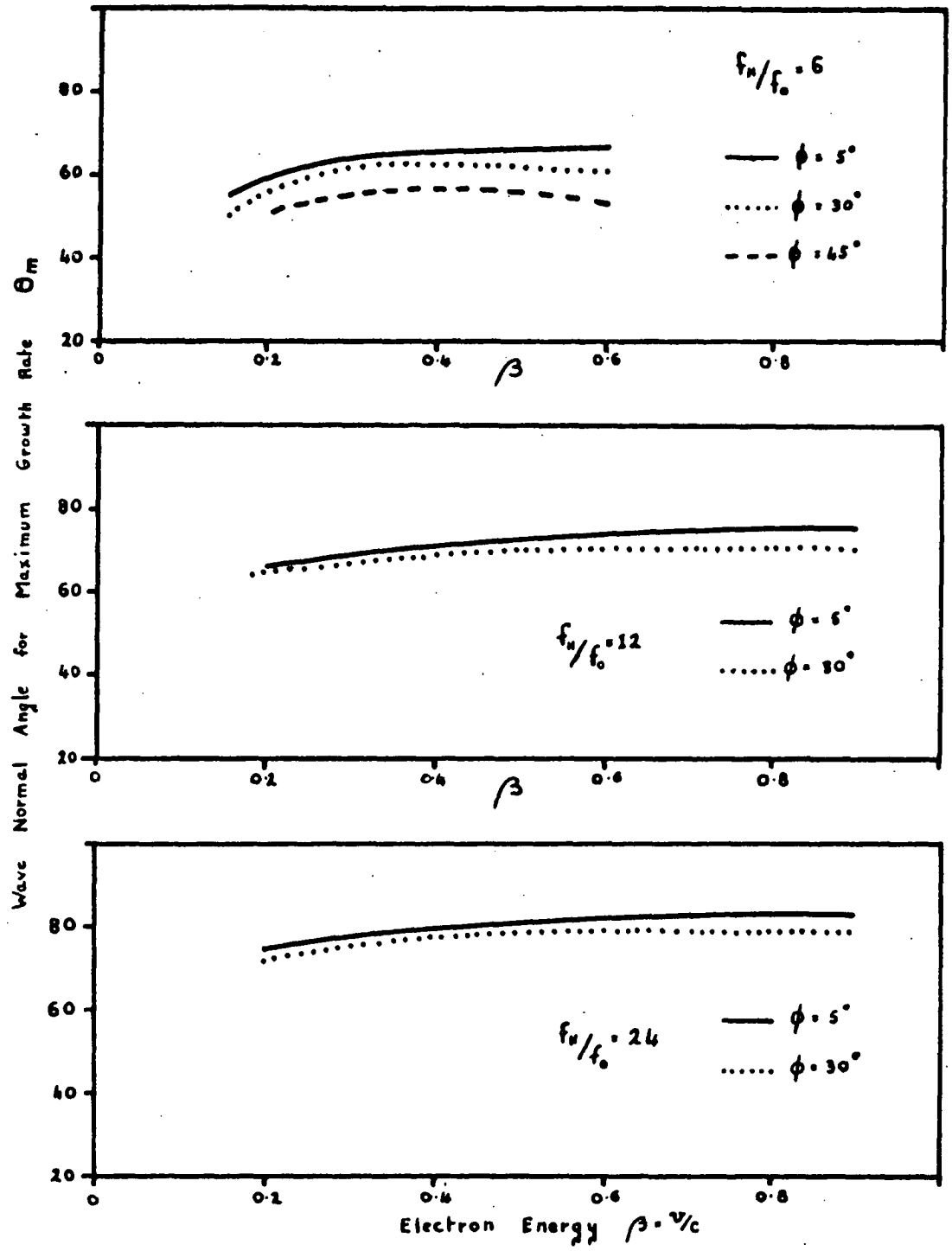


Figure 7.10 The wave normal angle for which the growth rate is a maximum plotted as a function of electron energy for various values of pitch angle and $f_H/f_o$.

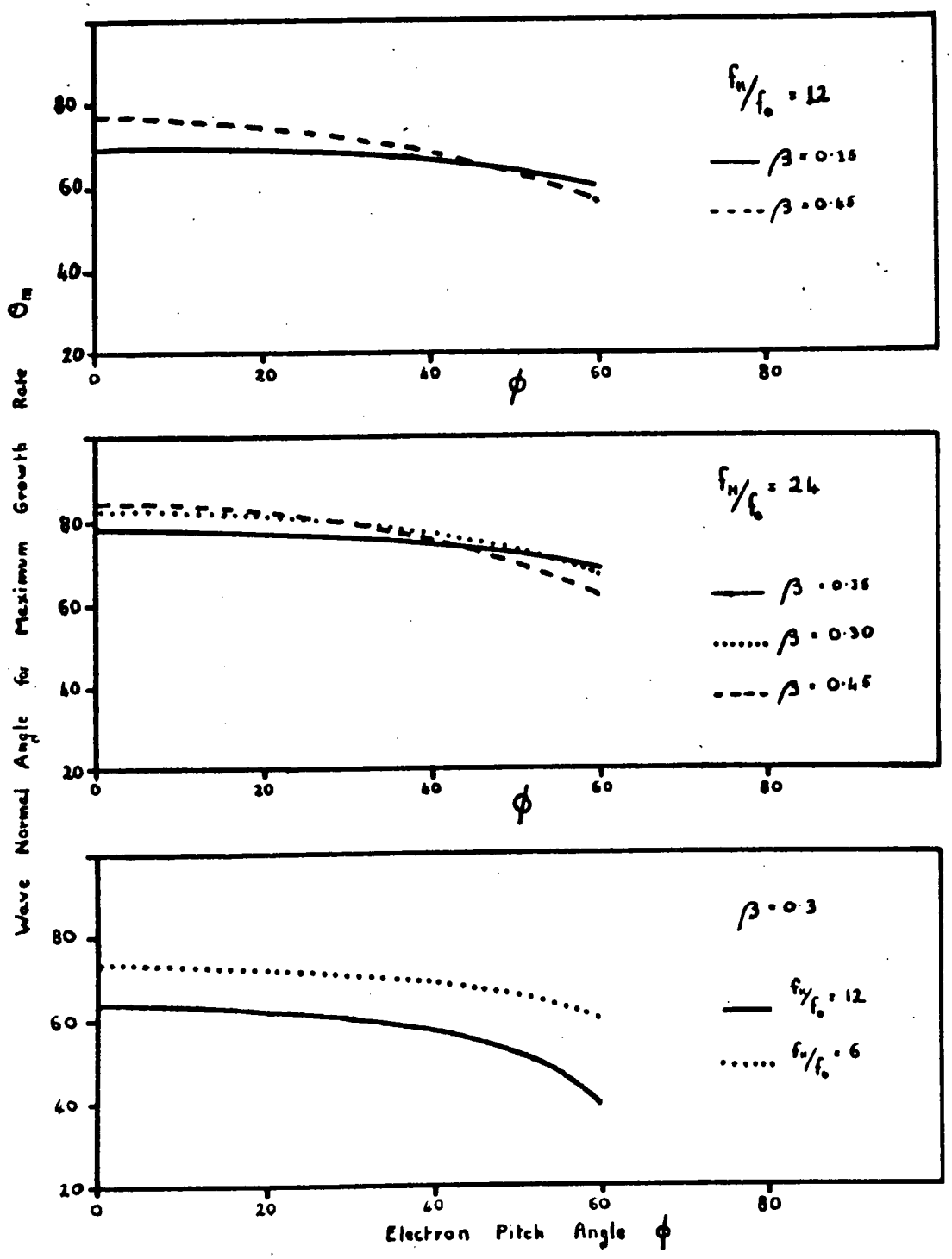


Figure 7.11 The wave normal angle for which the growth rate is a maximum plotted as a function of electron pitch angle for various values of energy and $f_H/f_0$.

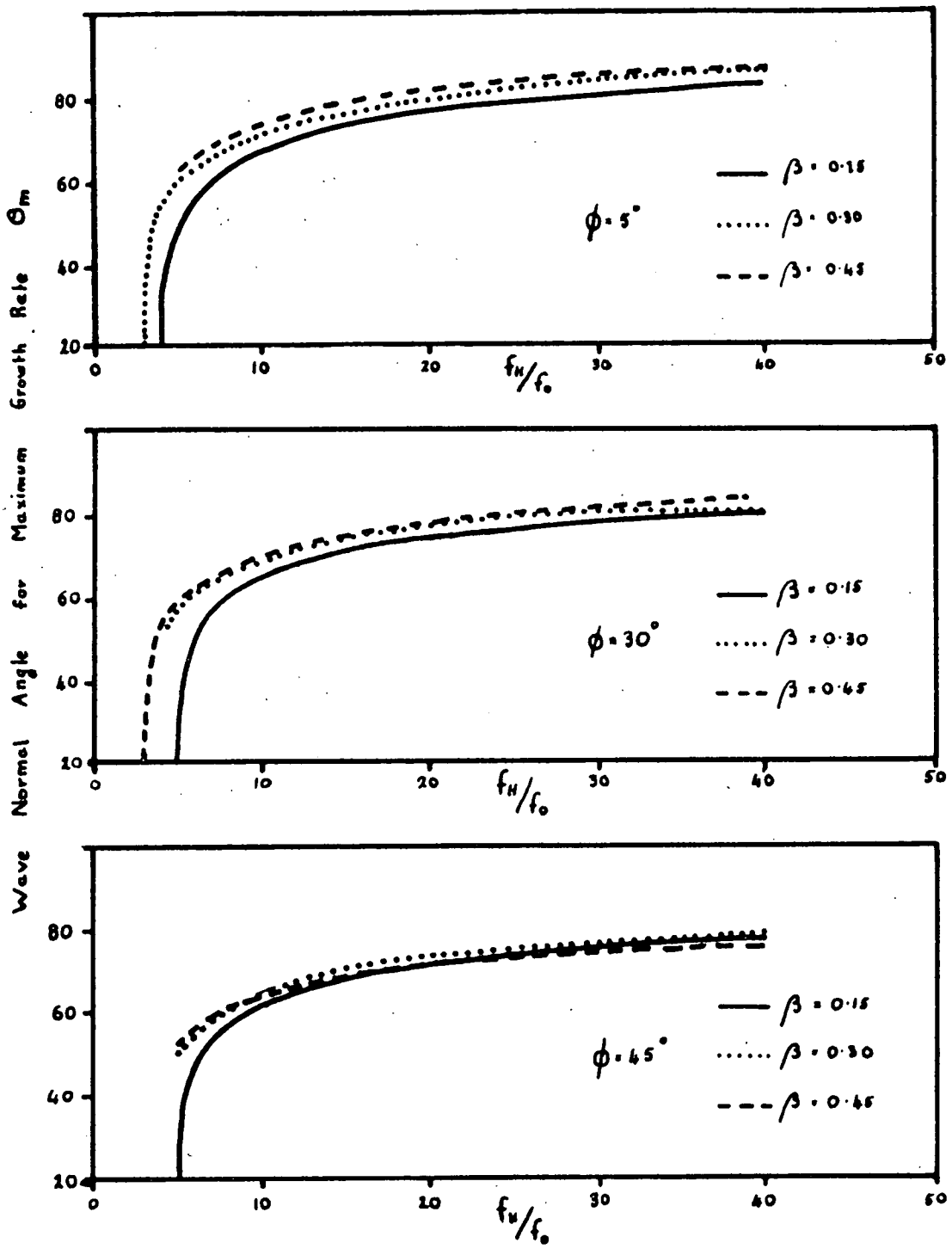


Figure 7.12 The wave normal angle for which the growth rate is a maximum plotted as a function of $f_H/f_o$ for various values of electron energy and pitch angle.

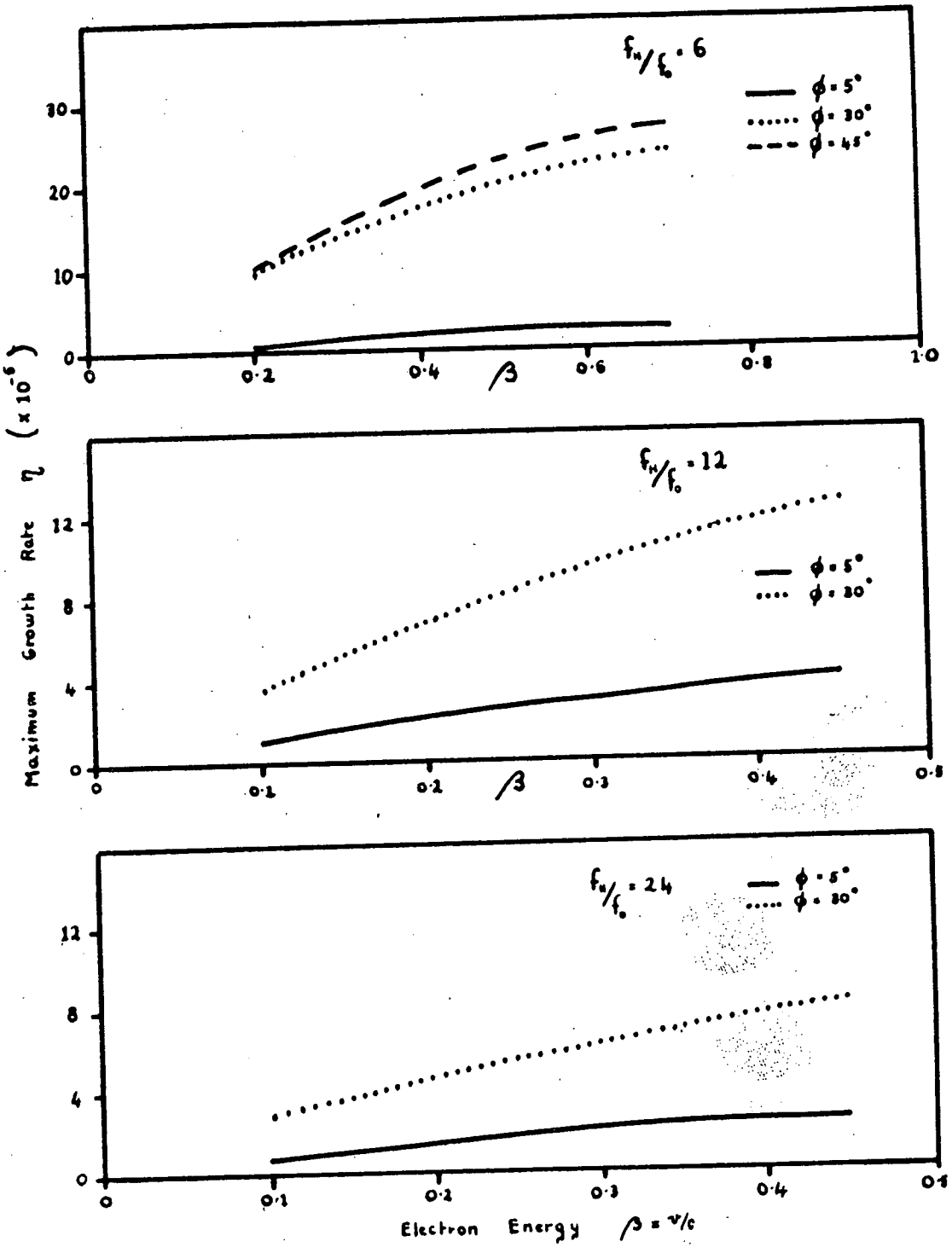


Figure 7.13 Variation of the maximum growth rate as a function of electron energy for various values of pitch angle and $f_H/f_o$. The ratio of stream density to ambient electron density is $10^{-7}$.

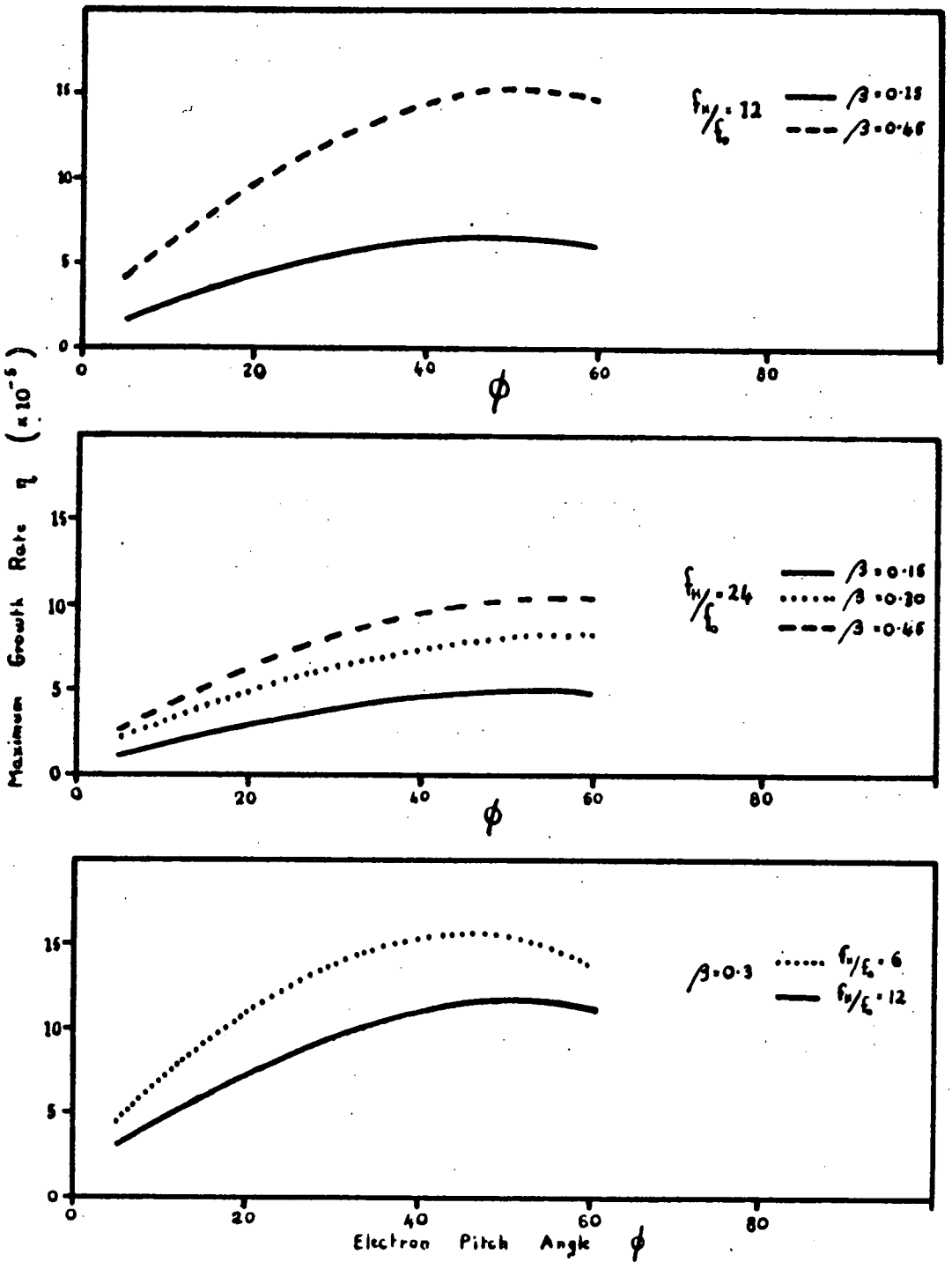


Figure 7.14 Variation of the maximum growth rate as a function of electron pitch angle for various values of energy and $f_H/f_o$. The ratio of stream density to ambient electron density is $10^{-7}$.

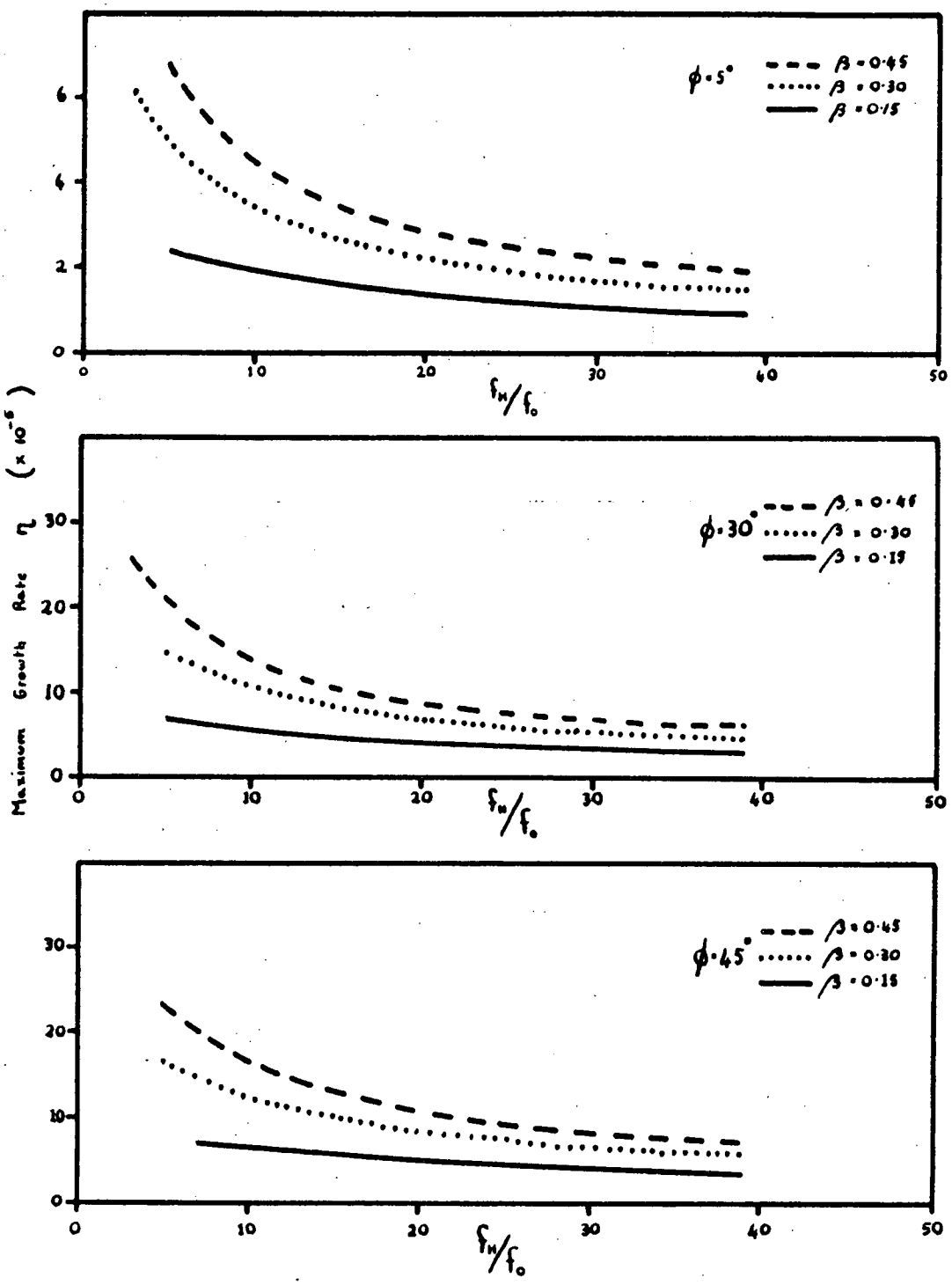


Figure 7.15 Variation of the maximum growth rate as a function of $f_H/f_o$ for a ratio of stream density to ambient plasma density of $10^{-7}$ and various values of electron energy and pitch angle.

The power radiated per unit solid angle per Hz by a single electron is

$$W = \frac{4 \pi^2 f^2 W'}{\Delta f}$$

then the maximum power emitted is given by

$$P_{max} = 4 \pi^2 f_H^{2/3} f_{max}^{\frac{1}{3}} R_J^3 N_s W' A / 3000$$

The amplification coefficient A can be written

$$A = \exp (\sigma^{\frac{1}{3}} \eta, \omega_H t)$$

where $\eta$, is the value of $\eta$ corresponding to $\sigma = 1$, and t is the propagation time through the amplifying region.

$$t \simeq \frac{L}{c}$$

and

$$\sigma = \frac{N_s}{N_e}$$

where $N_e$ is the ambient plasma density.

If at the emitting region $f_H / f_o = \alpha$

$$\sigma = 8_{10}7 \, N_s \alpha^2 / f_H^2$$

then $$A = \exp \left\{ \tfrac{1}{3} \eta, R_J \left(\frac{f_{max}}{f_H}\right)^{\frac{1}{3}} \left(\frac{8_{10}7 \, N_s \alpha^2}{f_H^2}\right)^{\frac{1}{3}} \left(\frac{\Delta f}{f_H}\right) \frac{2 \pi f_H}{c} \right\}$$

$$= \exp \left\{ \frac{2 \pi \eta, R_J}{c} \left(\frac{\Delta f}{f_H}\right) \left(8_{10}7 \, N_s \alpha^2 f_{max}\right)^{\frac{1}{3}} \right\}$$

The density of moderately energetic electrons (40 kev < E < 200 kev) within the Earth's magnetosphere has been studied by Frank et al (1963), who found densities between $2_{10}$-4 and $5_{10}$-3 /cc on the sunlit side of the magnetic equatorial plane. If these densities are assumed to hold for Jupiter, a maximum density of monoenergetic electrons of $5_{10}$-4 /cc could be reasonable. However if we assume a similar ratio of the energetic particle density to ambient particle density as occurs in the Earth's exosphere, this max-

imum density of monoenergetic electrons could be increased to $10^{-3}$ /cc. If we assume that emission occurs on field lines where the maximum gyrofrequency is 50 MHz we can calculate the minimum amplification needed to produce a burst of radiation of $10^{-22}$ $Wm^{-2}$ $Hz^{-1}$. This minimum amplification is nearly independent of $f_H / f_o$ but is strongly dependent on the electron pitch angle (Figure 7.16) and energy.

The fast drift bursts observed by Warwick and Gordon (1967) can be interpreted as emission from single bunches of electrons in the Jovian magnetosphere, we can use their properties to calculate a maximum amplification for the bunch. The fast bursts had durations of about 100 m sec so that if the linearised amplification theory of Fung is to apply, the electrons must not radiate more than about 25% of their energy in this time. The energy available from N electrons each of energy E is 0.25 N E and if this is radiated in 100 m sec the power available is

$$P = 2.5 \, N \, E \text{ watts}$$

The actual power radiated is

$$P = N \, W' \, A \, \omega_H^{\,2} \, \Omega$$

where $\Omega$ is the solid angle of the emission cone, which is typically 1.0 steradian. The maximum amplification available is given by

$$A \simeq 2.5 \, E \, / \, (\omega_H^{\,2} \, W')$$

This is plotted as a function of electron pitch angle for a wave frequency of 20 MHz in Figure (7.17). The maximum amplification is found to be nearly independent of electron energy, and slightly dependent on $f_H / f_o$. It is about a factor of ten greater than the amplification required to give a burst of $10^{-22}$ $Wm^{-2}$ $Hz^{-1}$ for elec-

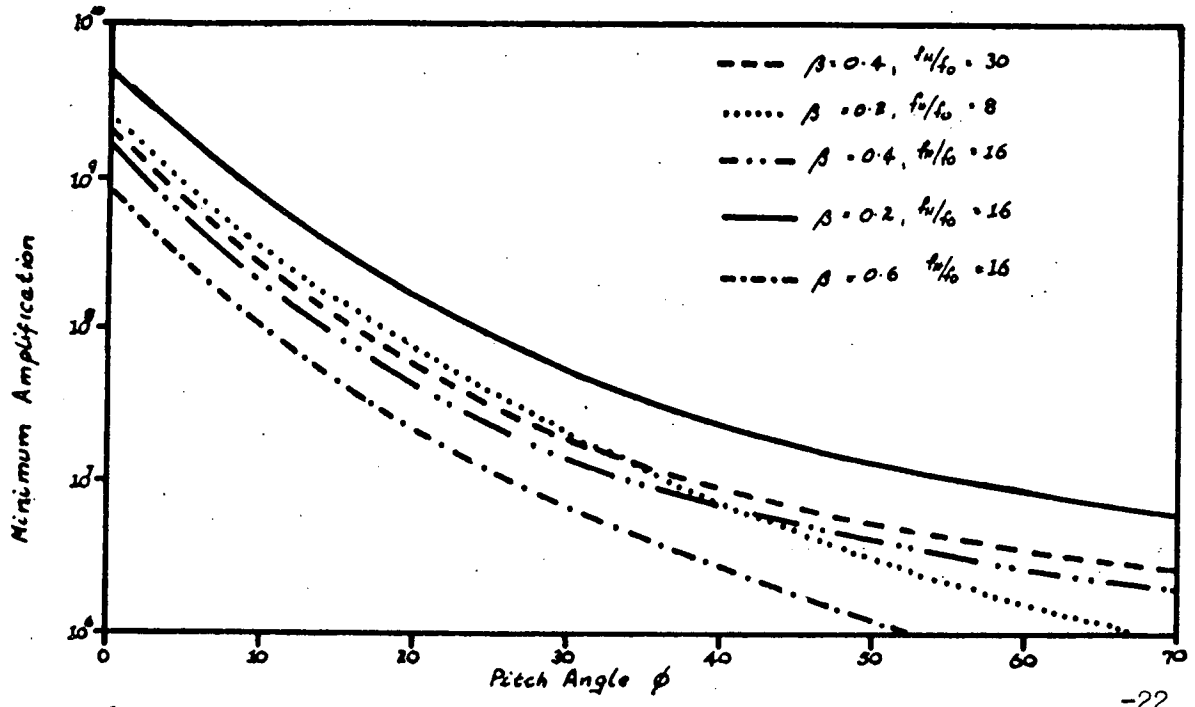


Figure 7.16 The minimum amplification needed to produce radiation of $10^{-22}$ $Wm^{-2}$ $Hz^{-1}$ at the Earth as a function of electron pitch angle, for various values of energy and $f_H/f_o$. The assumed stream density is $10^{-3}$/cc with emission on magnetic field lines where the maximum gyrofrequency is 50 MHz.

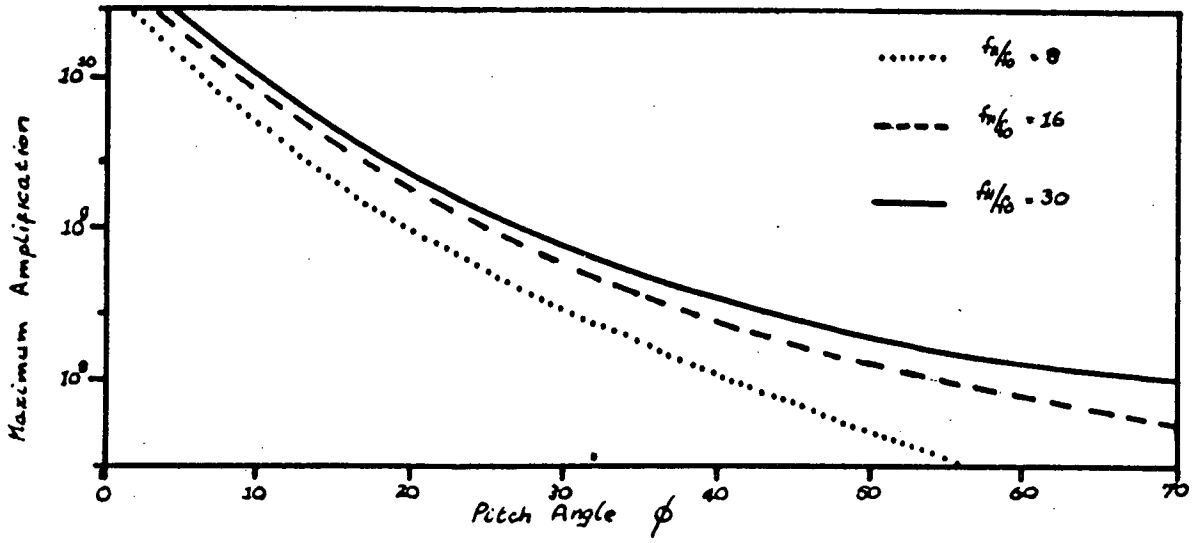


Figure 7.17 The maximum amplification that can be obtained from a stream of electrons, density $10^{-3}$/cc, plotted as a function of pitch angle for various values of $f_H/f_o$. Assumed wave frequency 20 MHz. Based on the assumption that the electrons cannot radiate more than 25% of their energy in 100 msec and the maximum diameter of the emitting bunch is 0.03 $R_J$.

tron energies of 10 kev and increases to about two orders of magnitude greater at 100 kev.

The minimum value of $\eta$, for emission to be visible for any particular emission configuration can be calculated from the minimum amplification and the bandwidth for that configuration. Comparison of these minimum values of $\eta$, with the computed values shows that emission would not be visible from electron streams having very small pitch angles ( $< 5^{o}$), and very small energies ($\beta < 0.1$). All other combinations of energy, pitch angle and $f_H/f_o$ produce detectable radiation provided the electron stream has sufficiently large dimensions, within the limit of a maximum diameter of 0.03 $R_J$.

## 7.5 Escape of the Radiation from Jupiter.

The radiation is generated in a region where the refractive index is less than one, so that in escaping from the magnetosphere it will be refracted. The final direction of radiation emitted outwards will be given by Snells law

$$\sin \chi' = n \sin \chi$$

where $\chi$ is the angle between the wave normal direction and the normal to the surfaces of constant refractive index. If X is small (i.e. $f_H/f_o$ large) surfaces of constant refractive index will coincide with the surfaces of constant magnetic field strength, which are nearly parallel to the planets surface. We then have

$$\chi = \theta + \beta$$

where $\beta$, the angle between the normal to the equipotential surfaces and the wave normal direction, is plotted as a function of magnetic latitude in Figure (7.18). The final wave normal angle after

refraction $\alpha = \chi' - \beta$, is plotted in Figure (7.19) as a function of $\theta$, for emission in the magnetic meridian plane where $\beta = 5^{o}$.

Radiation which is emitted inwards is reflected near the level X = 1 - Y and then propagates outwards. The final wave normal angle after refraction is

$$\alpha' = \alpha - 2\beta$$

where $\alpha$ is the final direction of the outward emitted ray. Rays which are emitted inwards in the magnetic meridian plane towards the magnetic equator have a final wave normal angle which is $2\beta$ smaller than the final wave normal angle of the corresponding rays emitted outwards. If the emission direction was inwards towards the magnetic poles the final wave normal angle is $2\beta$ larger than that for the corresponding rays emitted outwards. For rays not emitted in the magnetic meridian plane the change in wave normal angle varies between $-2\beta$ and $+2\beta$. The geometry of the emission is illustrated in Figure (7.20). The only rays which can reach the Earth are those emitted towards the equator for which the cone angles of the outward rays are approximately $2\beta$ larger than the cone angles for the inward rays.

The power radiated at angle $\theta$ is modified by refraction so that

$$P(\alpha) = \frac{\sin\theta}{\sin\alpha}\frac{d\theta}{d\alpha} P(\theta)$$

When $\theta = \theta_c$, $\frac{d\theta}{d\alpha} = 0$ and hence $P(\alpha) = 0$, this has the effect of suppressing the infinity in the power emitted near $\theta = \theta_c$. But when $\alpha = \alpha_c$ the maximum of $\alpha$, $\frac{d\alpha}{d\theta} = 0$ and $P(\alpha) \uparrow \infty$, i.e. the radiation in the neighbourhood of $\alpha_c$ is strongly focussed. For example for $f_H/f_o = 16$, radiation which was initially emitted into a $5^{o}$

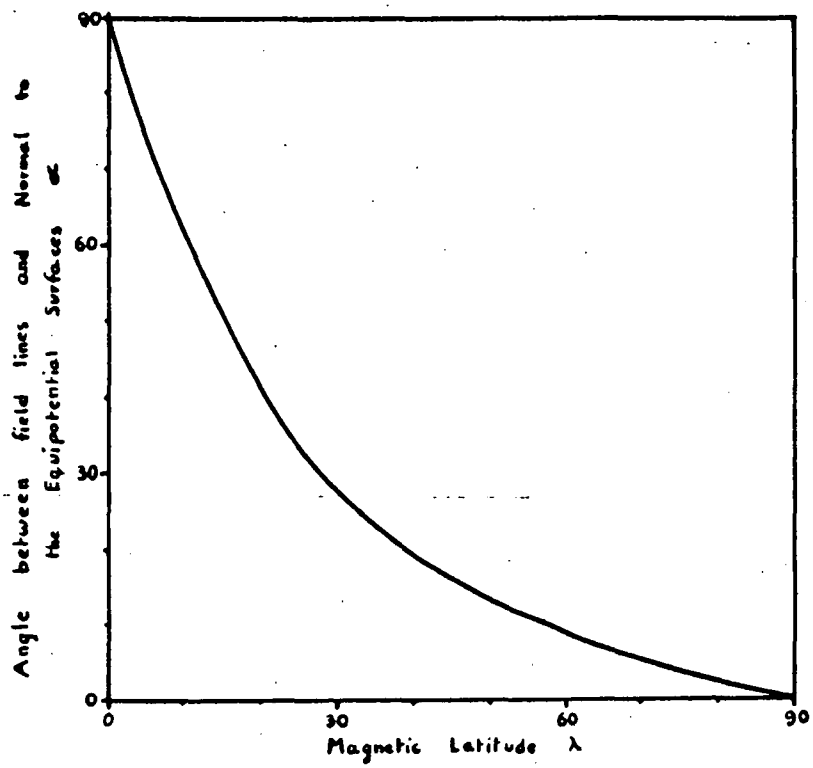


Figure 7.18 The angle between the field lines and the gradient of the field plotted as a function of magnetic latitude for a dipole magnetic field.

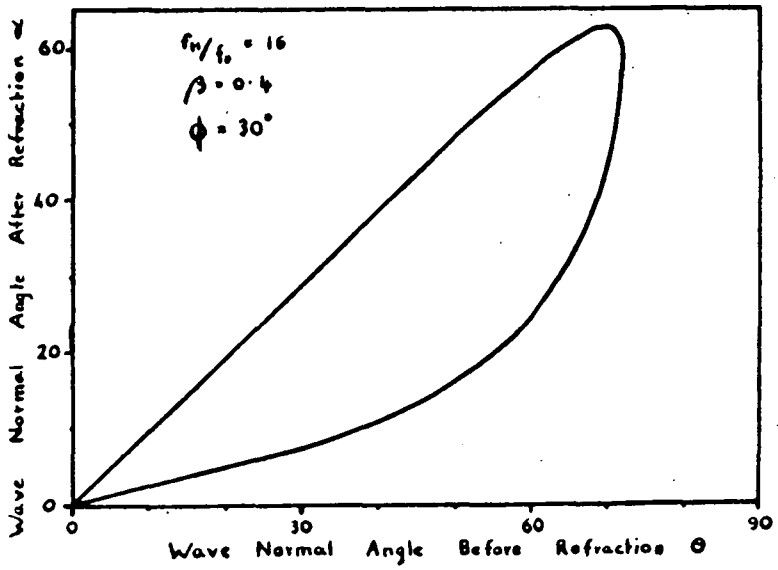


Figure 7.19 The wave normal angle of emission after refraction plotted as a function of the wave normal angle before refraction. Electron energy 45 kev, pitch angle 30°, $f_H/f_o = 16$, for emission at a magnetic latitude of 75°.

range of $\theta$ is focussed into less than $1^{\circ}$ range of $\alpha$. The gains which can be obtained depend on the final width of the focussed cone, for a $1^{\circ}$ range the gain is about 5 while for a $0.1^{\circ}$ range gains of about 100 can be obtained. In practice the gain obtained will depend upon the thinnest cone that remains stable over the whole emission region. The thickness of this cone will be limited by the effect of irregularities and curvature in the magnetic field. The curvature can be estimated. We have already assumed that the diameter of the emission region is about 0.03 $R_J$ and if we assume that emission occurs at a height of 1.5 $R_J$ from the center of Jupiter, the emission region subtends a range of magnetic latitudes of about $\frac{0.03}{1.5}$ radians or $1.3^{\circ}$. For high latitude field lines the corresponding range of field line inclinations is about $0.7^{\circ}$. Hence it would appear that focussing could not produce cones narrower than about $0.5^{\circ}$ with corresponding gains less than 20 unless the emission regions are significantly smaller than 0.03 $R_J$.

Hartz (1964) has examined a similar focussing effect in the Earth's ionosphere. He has found that radio emissions from the Sun are enhanced about 2 db when recorded near the edge of the receiving cone of a satellite in the Earth's ionosphere. This gain is much less than would be expected from the ray theory, Smith (1961). The lower gains obtained in this experiment may have been the result of electron density irregularities and curvature of the Earth's magnetic field. The curvature of Jupiter's magnetic field in the region where focussing may occur is an order of magnitude less than for the Earth. Also the electron density in the focussing region on Jupiter is relatively much smaller than for the corresponding

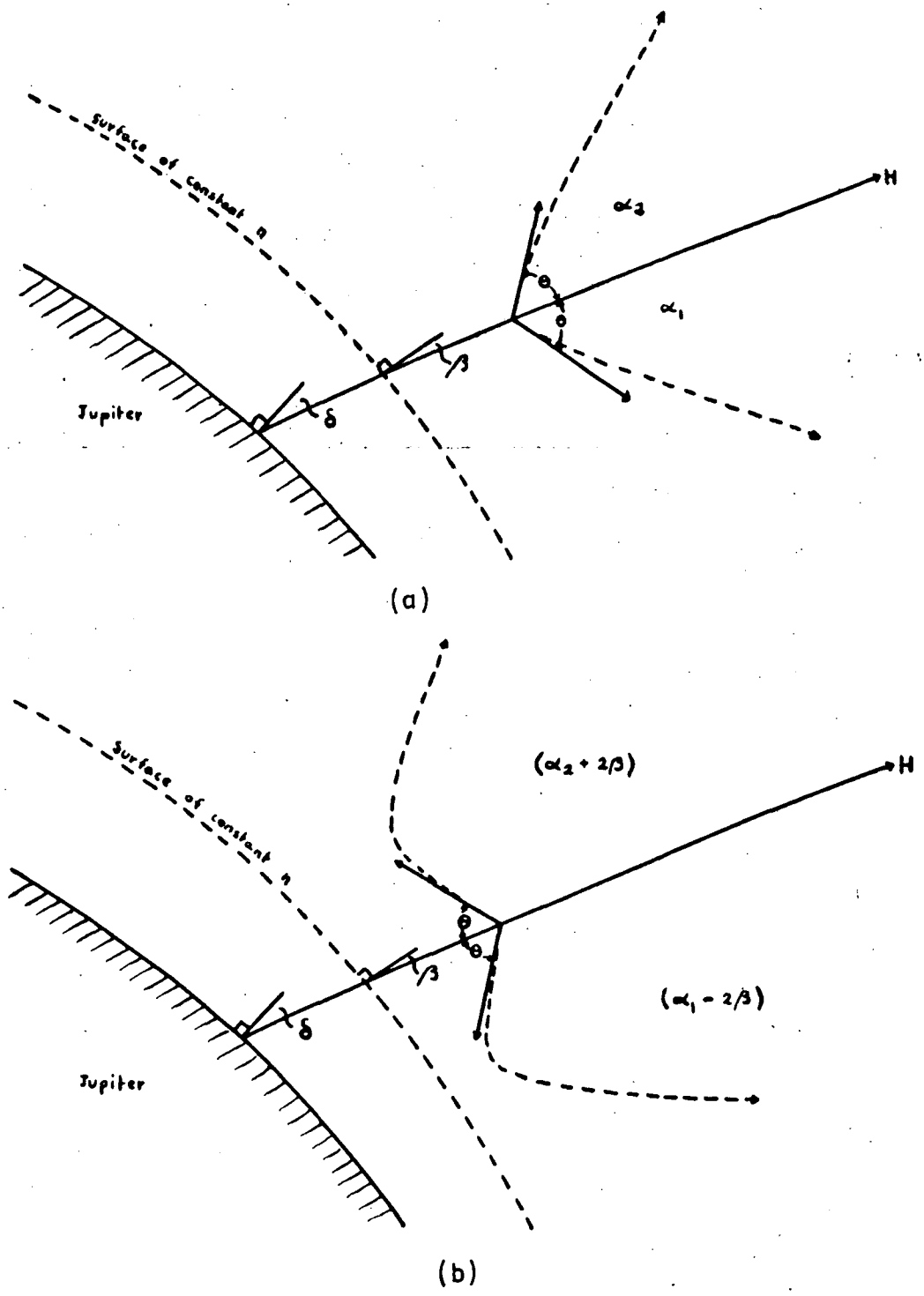


Figure 7.20 Diagrammatic representation of the relation between the angles of emission after refraction for (a) emission initially outwards, and (b) emission initially inwards.

situation on the Earth. Hence we would expect the effect to be much smaller on Jupiter. However, the conclusions regarding focussing in a magneto-ionic medium are not at all definite at present so we shall work on the assumption that significant focussing can be obtained on Jupiter.

## 7.6 Polarisation of the Radiation.

Cyclotron radiation is generated predominantly in the x-mode so that radiation associated with Jupiter's north magnetic pole will be right hand elliptically polarised, as observed. The axial ratio of the polarisation ellipse will be determined at the point where the limiting polarisation is attained. The condition for a wave to propagate without change of polarisation has been given by Budden (1960).

$$| \psi |^2 > | \tfrac{1}{4} (n_o - n_x)^2 - \frac{\pi i}{\lambda} \frac{d}{dz} (n_o - n_x) |$$

where the subscripts o and x refer to the refractive index modes and $\psi$ is the coupling coefficient defined by

$$\psi = \frac{1}{\rho_x^2 - 1} \frac{2\pi}{\lambda} \frac{d\rho x}{dz}$$

where $\rho_x$ is the polarisation of the wave. If we make the approximations $n_o \simeq 1$ and ignore collisions the condition reduces to

$$X > n_o - n_x$$

Now X is small and hence the limiting polarisation is attained when $n_x \simeq 1$ so that the appropriate wave normal angle is $\alpha$. The polarisation axial ratio is then $A_r = \pm \cos \alpha$

The observed axial ratios vary over a wide range but average between 0.4 and 0.6 for frequencies near 20 MHz, the corres-

ponding emission angles are between $66^{\circ}$ and $53^{\circ}$. Emission must therefore take place on high latitude field lines where the angle $\beta$ is around $4^{\circ}$. Plots of the maximum emission angle $\alpha_c$ at which radiation of $10^{-22}$ $Wm^{-2}$ $Hz^{-1}$ can be obtained for emission where $\beta = 4^{\circ}$ are shown in Figure (7.21). $\alpha_c$ depends strongly on $f_H/f_o$ and $\varphi$ but is relatively insensitive to $\beta$ provided $f_H/f_o$ is in the range of about 7 to 16.

## 7.7 Model of the Jupiter Magnetosphere.

In order to proceed further it is necessary to consider a more specific model of the Jupiter magnetosphere. Observations of the decimetric radiations have led to the conclusions that the polar magnetic field intensity is between 5 and 50 gauss, that the dipole axis is inclined about $10^{\circ}$ to the rotation axis of the planet, and that the longitude of the north magnetic pole is between $180^{\circ}$ and $200^{\circ}$ system III. The maximum observed frequency of the decametric radiation, about 40 MHz places a lower limit on the field strength of 14.5 gauss at the generation point.

The observed polarisation axial ratios of 0.4 to 0.6 imply that the radiating electrons are moving along field lines inclined at an angle of about $60^{\circ}$ to the magnetic equator. Hence the magnetic latitude of the field line must be about $70^{\circ}$. Radiation cone angles of $60^{\circ}$ or greater are only possible for electron bunches whose pitch angles are less than about $45^{\circ}$, Figure (7.21). Now observations of high time resolution dynamic spectra show bursts whose frequency decreases with time and hence must be produced by electron streams moving outwards along the field lines. The max-

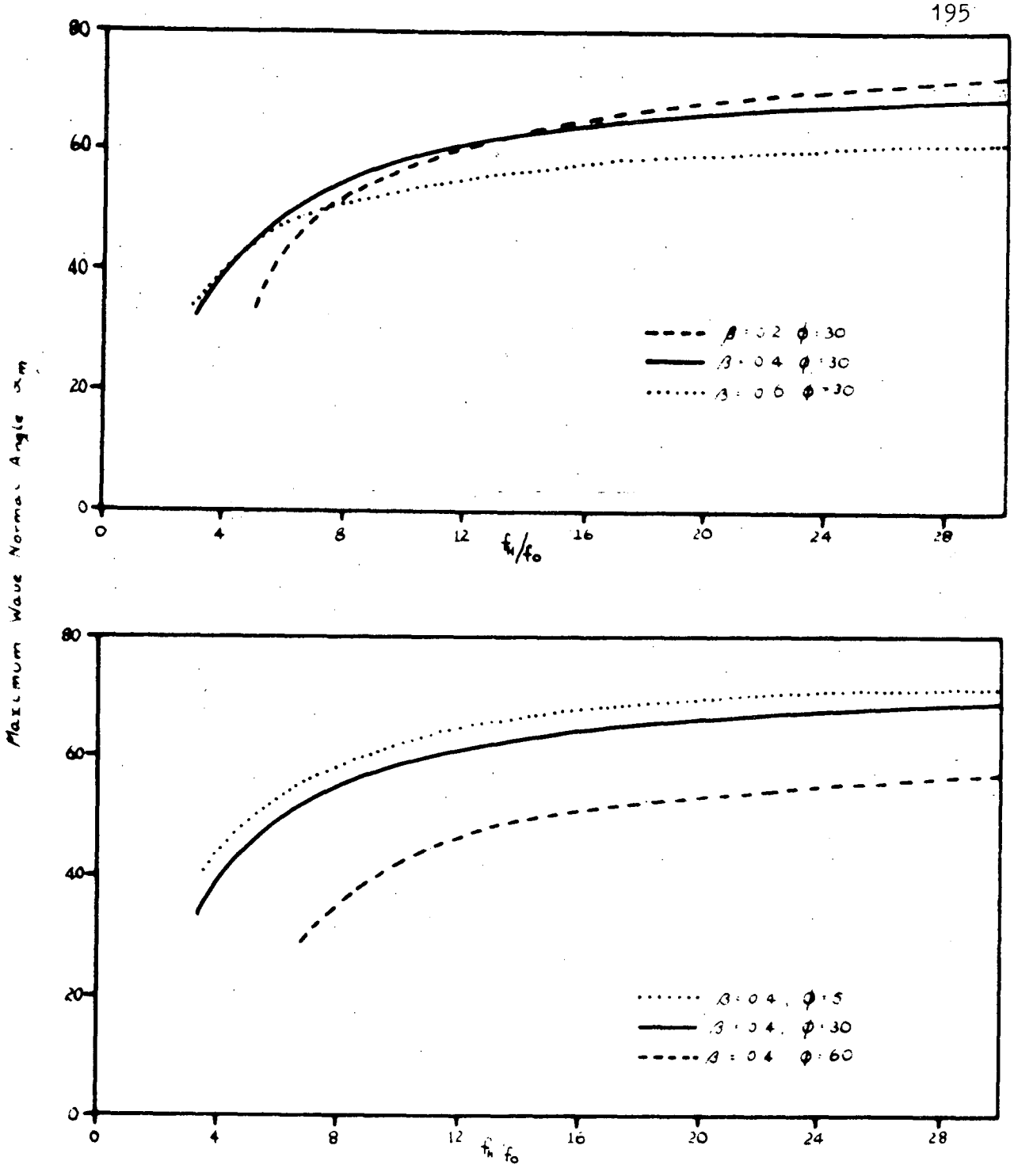


Figure 7.21 Variation of the maximum angle of emission after refraction at magnetic latitude 75° as a function of $f_H/f_o$ under the condition that the radiation is strong enough to give a burst of $10^{-22}$ $Wm^{-2}$ $Hz^{-1}$ at the Earth. Assumed maximum diameter of the electron stream 0.03 $R_J$, and maximum density $10^{-3}$/cc.

imum observed frequency is about 40 MHz and hence we must have electron streams with pitch angles of about $45^{o}$ near the 40 MHz gyrofrequency level. This implies a field strength at the ground on the appropriate field lines of about 30 gauss. We will assume that the polar field strength is 30 gauss and that the longitude of Jupiter's north magnetic pole is $175^{o}$.

The amplification theory requires the existence of bunches or streams of monoenergetic electrons all with the same pitch angle. We assume that the pitch angles of the electrons vary from bunch to bunch so that all pitch angles occur with equal probability except those in the loss cone that do not get mirrored. This excludes very small pitch angles. We also assume that the velocities of these electrons are in the range 0.2c to 0.7c as is observed for the Earth. We must also make some assumption about the distribution of electron bunches in latitude. We assume a linear increase with magnetic latitude above $75^{o}$.

## 7.8 Probability of Occurrence of Radiation Bursts.

To obtain the theoretical variation in the probability of observing radiation bursts as Jupiter rotates, we assume initially that electron bunches occur at a magnetic colatitude $\beta$ and all magnetic longitudes.

The angle of the radiation cone is strongly dependent on the electron pitch angle, Figure (7.21), but varies much more slowly with electron energy provided $f_H / f_o$ is in the range 7 - 16. Then for values of $f_H / f_o$ in this range we can ignore the variation of cone angle with energy, so that to a first approximation the cutoff

angle is a function of pitch angle only.

$$\alpha_c = f(\varphi)$$

Assuming that bunches of electrons with pitch angles greater than the minimum value required for mirroring occur with equal probability, we find the number dN of bunches with pitch angles in the range $\varphi$ to $\varphi + d\varphi$ to be

$$dN = \sin \varphi \, d\varphi \qquad \text{for } \varphi > \varphi_{min}$$

The value of $\varphi_{min}$ is given by

$$\sin^2 \varphi_{min} = \frac{f_H}{(f_H)_{max}}$$

where $(f_H)_{max}$ is the maximum gyrofrequency on the field line. At a cone angle $\alpha$ radiation can be seen from all bunches with pitch angles smaller than some critical value $\varphi_c$ given by $f(\varphi_c) = \alpha$ The number of bursts seen is

$$N_\alpha = \int_{\varphi_{min}}^{\varphi_c} \sin \varphi \, d\varphi$$

If the colatitude of the field line on which the bunches travel is $\beta$ and their longitude is $0^o$ we can find the number of bursts which can be seen in a particular magnetic latitude $\lambda$ and longitude L by using the transformation

$$\cos \alpha = \cos L \sin \beta \cos \lambda + \cos \beta \sin \lambda$$

Figure (7.22) shows plots of N against $\lambda$ for various values of L for electron bunches on the $75^o$ field line where $f_H / f_o = 14$. The shape of these curves does not depend greatly on the position of the emission point or the value of $f_H / f_o$, although the particular range of magnetic latitudes covered does. For this reason it is more convenient to plot N as a function of the angle $\varepsilon$ of penetration

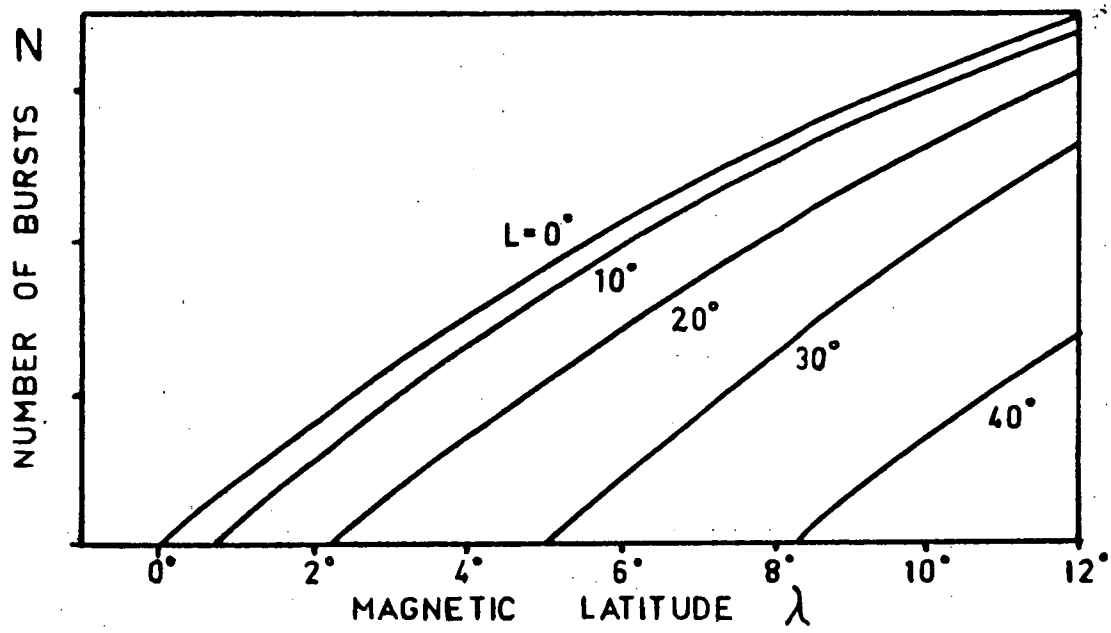


Figure 7.22 Variation of the relative number of bursts as a function of magnetic latitude for various values of L. Field line latitude 75°, $f_H / f_o = 14$, all pitch angles and energies included.

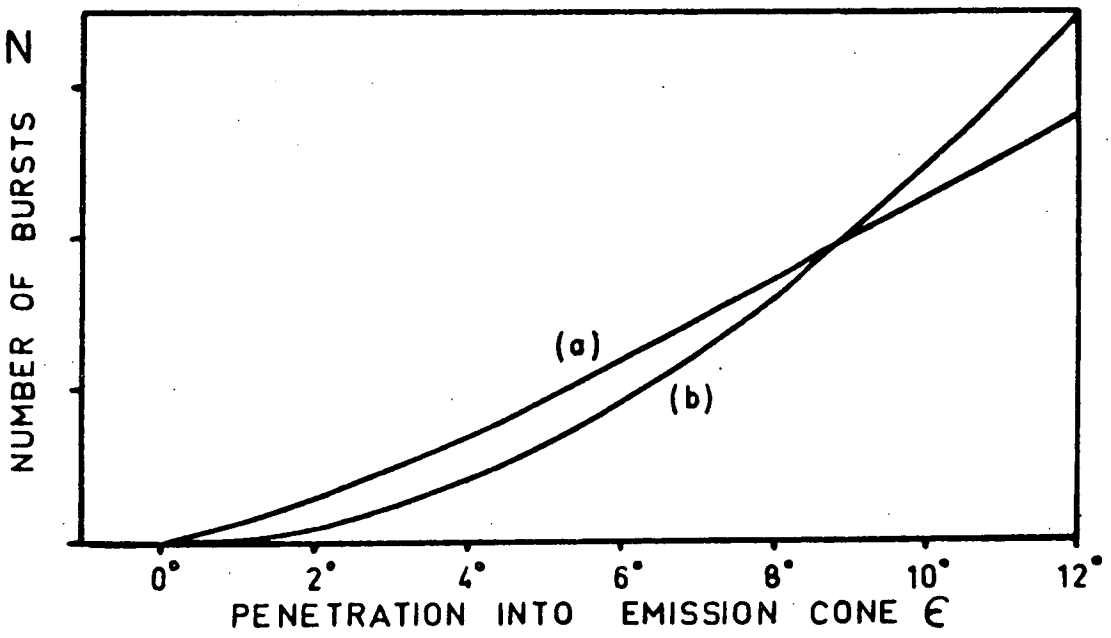


Figure 7.23 Variation of the relative number of bursts as a function of the angle of penetration of the observers line of sight into the emission cone (a) for emission on a single line, and (b) assuming that the number of emitting electron bunches increases linearly with magnetic latitude above 75°.

into the emission cone. This angle is just the magnitude of the difference in latitude between the outer edge of the radiation cone and a point inside the cone.

If electron bunches occur at all magnetic longitudes the relative number of bursts as a function of the angle of penetration into the emission cone is obtained by integrating over all values of L in Figure (7.22). The result is shown in Figure (7.23a). If we assume that the number of electron bunches increases linearly, from zero, with magnetic latitude above $75^{\circ}$ then the function is modified to the form shown in Figure (7.23b).

## 7.9 Power of the Radiation Bursts.

The power emitted by a particular bunch of electrons increases almost linearly as the wave normal angle changes from $\alpha_c$ to the angle where the power is a maximum, $\alpha_m$. The width of this linear region $(\alpha_c - \alpha_m)$ is typically greater than $15^{\circ}$. The maximum cone angle $\alpha_c$ depends upon the electron pitch angle $\varphi$ as shown in Figure (7.21).

It may be shown from Eidman's equation that the power emitted by a single electron varies with pitch angle according to $W \propto \sin^2\varphi$. The maximum growth rate also depends upon the electron pitch angle so that the slope of the linear region of the variation of W with $\alpha$ is given by

$$\text{slope} \propto \sin^2\varphi \; g(\varphi)$$

If we include radiation from all electron bunches with pitch angles in the range $d\varphi$ about $\varphi$, the slope becomes

$$\sin^3\varphi \; g(\varphi) \; d\varphi$$

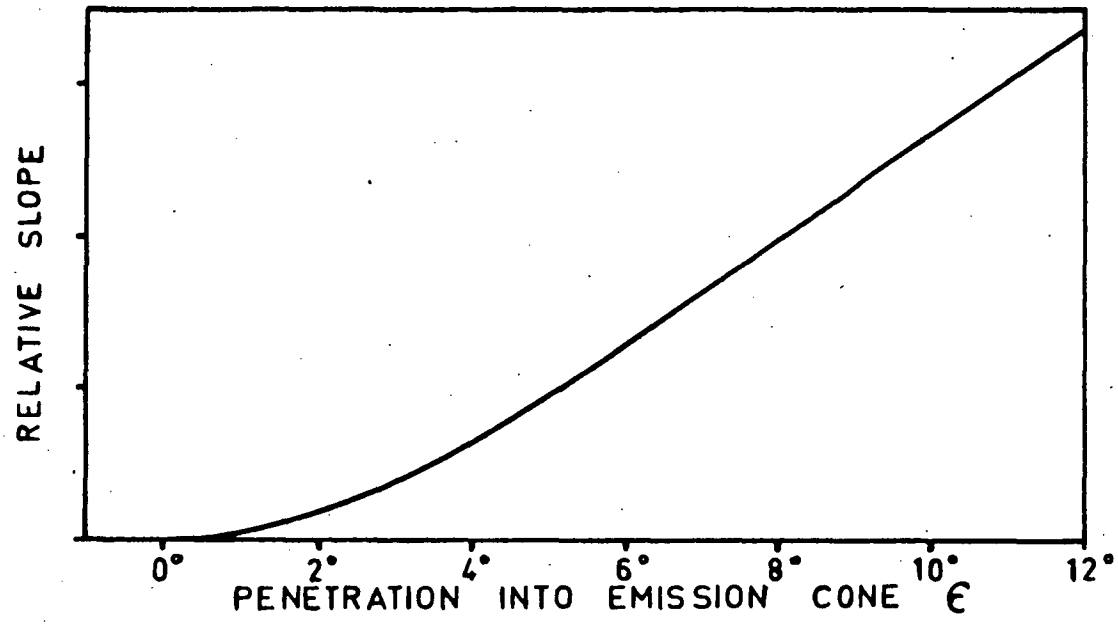


Figure 7.24 Variation of the slope of the linear part of the relationship between the emitted power and radiation angle as a function of the angle of penetration into the emission cone.

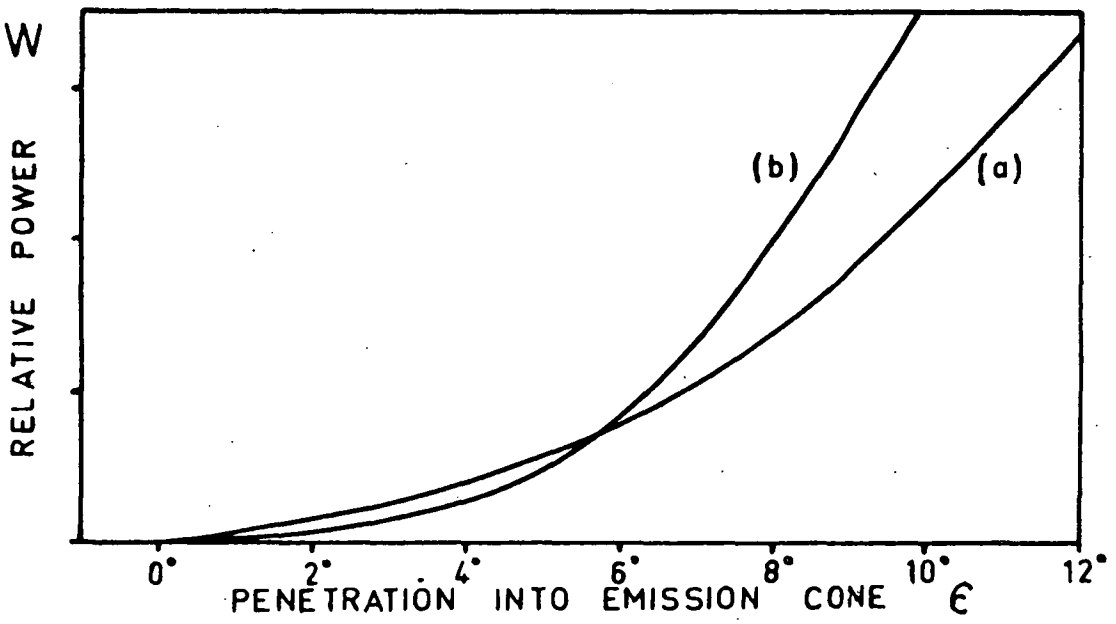


Figure 7.25 The relative power of emission as a function of the angle of penetration into the radiation cone for emission at all magnetic longitudes by electron bunches with all energies and pitch angles. (a) Radiation from a single field line latitude. (b) Under the assumption that the number of electron bunches increases linearly with latitude above $75^{o}$.

This is plotted in Figure (7.24) as a function of the angle of penetration into the radiation cone $\varepsilon$. If we integrate over all pitch angles and magnetic longitudes we find the variation of emitted power with $\varepsilon$ for emission on a single field line. This is shown in Figure (7.25a). Assuming that the number of electron bunches increases linearly, from zero, with magnetic latitude above $75^{\circ}$, the variation of emitted power with $\varepsilon$ takes the form shown in Figure (7.25b).

## 7.10 Longitude Profiles.

Microwave observations of Jupiter have shown that its dipole axis is tilted $10^{\circ}$ with respect to its rotation axis and as a result the magnetic latitude of an observer on Earth varies cyclically through $\pm 10^{\circ}$ as the planet rotates. This means that the angle the observer sees into the radiation cone varies cyclically and hence the probability of occurrence and mean power of the emission will also vary cyclically. Peaks in the emission will occur when either of Jupiter's magnetic poles is tilted furthest towards the Earth. The only observation which shows two peaks separated by about $180^{\circ}$ of longitude is the relative power profile at 4.7 MHz, Figure (3.3). The longitudes of the maxima on this curve are $175^{\circ}$ and $340^{\circ}$. These observations were made in 1961 and since there is an apparent inaccuracy in the system III period amounting to about $4^{\circ}$ of longitude per year, this position of the pole is consistent with that determined by Roberts and Komesaroff (1965) late in 1963.

Typical variations of mean power with system III longitude are shown in Figure (7.26) for values of the parameter $\xi$. For each value of $\xi$ the frequency of emission and the ratio $f_H/f_o$ are

related as shown in Figure (7.27).

The peaks in the observed power longitude profiles corresponding to emission when the magnetic poles are facing the Earth can be matched to a particular curve in Figure (7.26). The value of $\xi$ for that curve and the observing frequency can be used to obtain the appropriate value of $f_H/f_o$ from Figure (7.27). The gyrofrequency $f_H$ can be estimated from the observing frequency, then the plasma frequency $f_o$, and hence the electron density can be calculated. For a particular model of the magnetic field the radius corresponding to a particular $f_H$ is known which allows us to plot the electron density and plasma frequency as a function of radius, Figure (7.28). The density below 1.4 radii has been extrapolated to give a maximum density in the ionosphere of $10^6$/cc, which corresponds to an ionospheric temperature of about 5,000° K (see Figure 4.1).

The observed power longitude profiles do not vary in the quasi-sinusoidal way expected for a regular dipole magnetic field. Only at 4.7 MHz are there two pronounced maxima approximately 180° apart. To account for the additional maxima at higher frequencies it is necessary to modify the dipole field. The additional maxima in the total power profiles may clearly be produced by a deviation of the magnetic dip from that of a dipole in the latitudes and longitudes where the emission takes place. The dip anomalies needed to account for the observed variations of power with longitude are shown in Figure (7.29). Theoretical power longitude profiles are shown in Figure (7.30) and the corresponding probability of occurrence profiles in Figure (7.31). It should be noted that at the lower frequencies the probability of occurrence varies much less

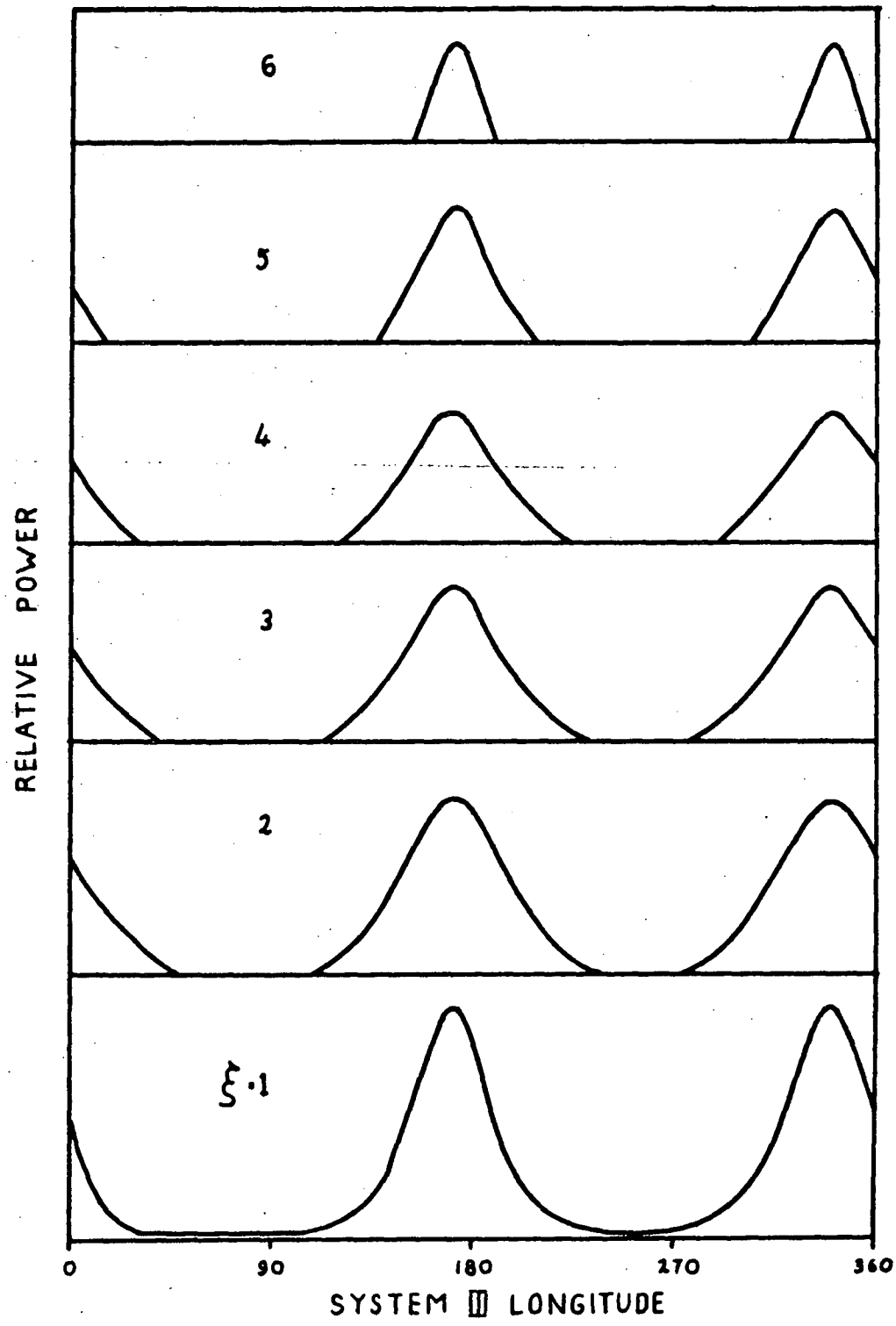


Figure 7.26 Variation of the relative power of emission against system III longitude for various values of a parameter $\xi$. The magnetic field is assumed to be a pure dipole.

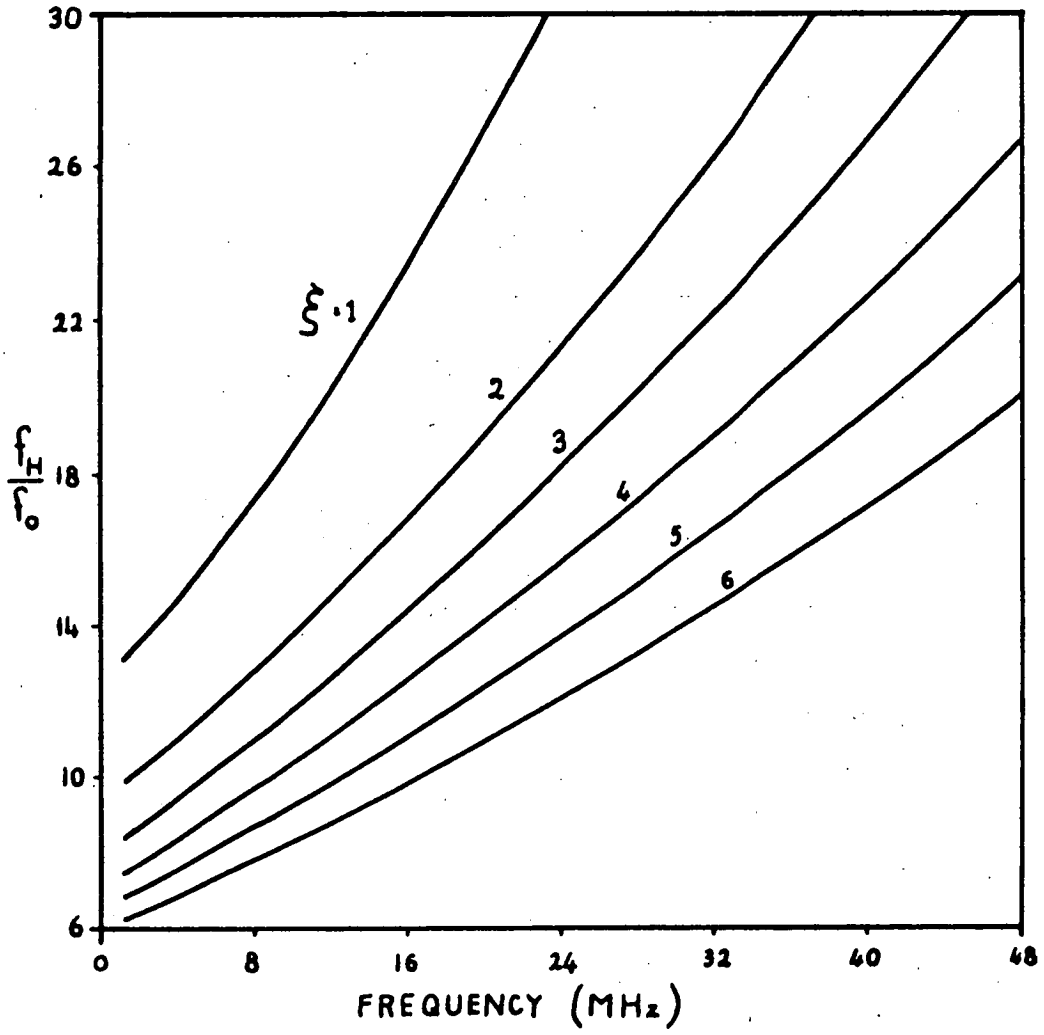


Figure 7.27 Variation of $f_H / f_o$ as a function of wave frequency for each value of $\xi$ shown in Figure 7.26.

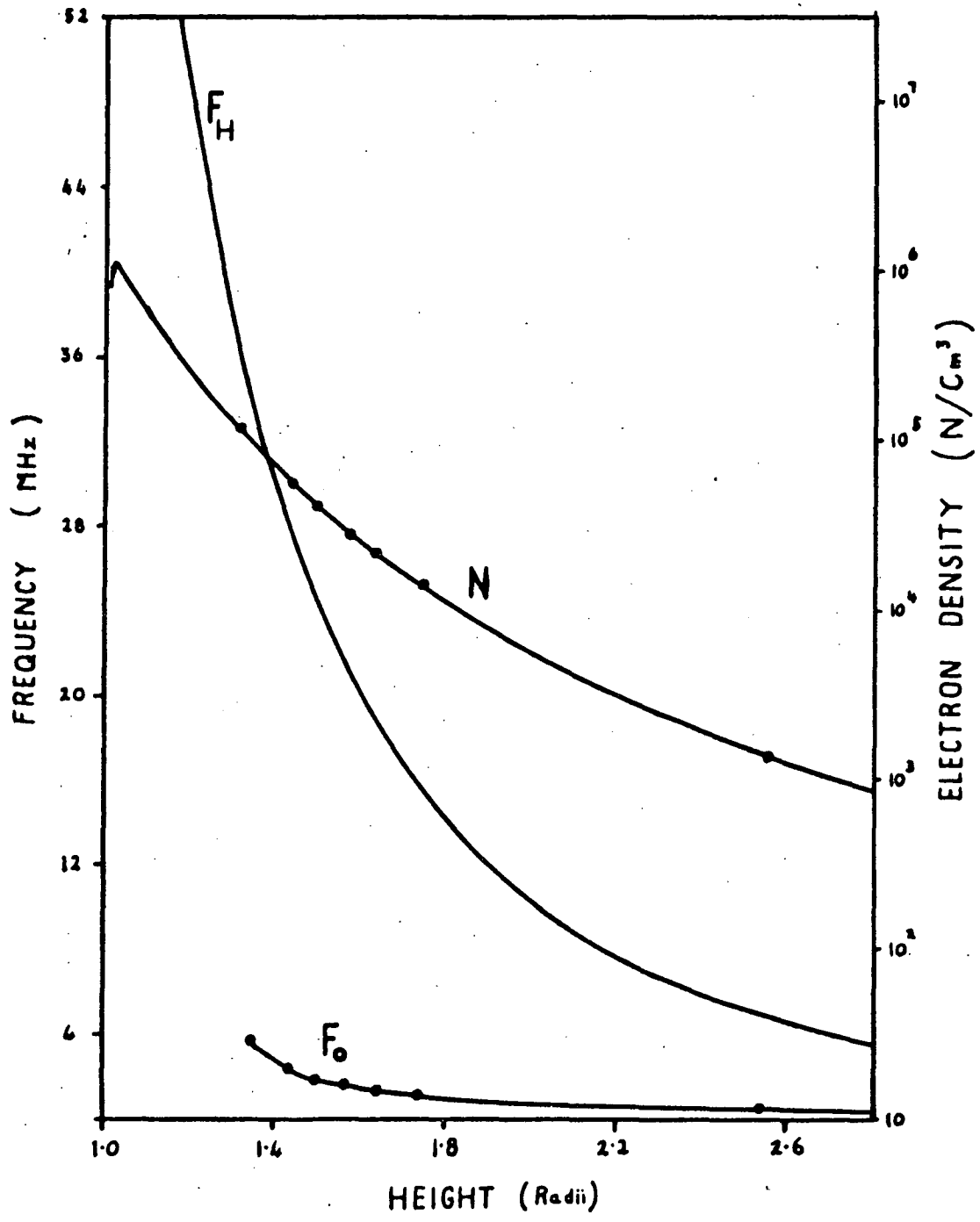


Figure 7.28 Variation of the gyrofrequency $f_H$, plasma frequency $f_o$ and electron density N with the height in radii from the center of Jupiter. The assumed polar field strength is 30 gauss.

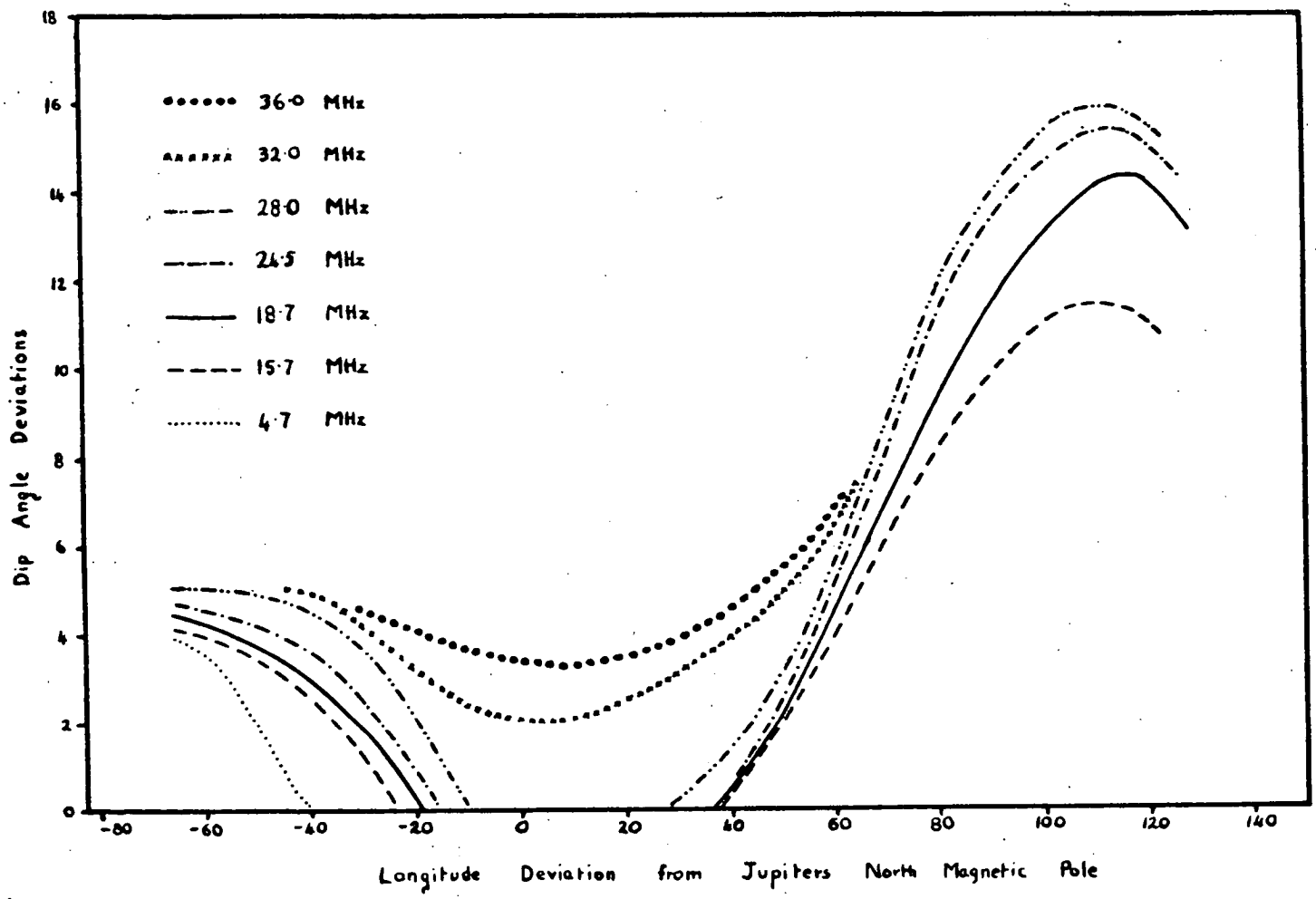


Figure 7.29 The variation in dip angle of Jupiter's magnetic field at a northern magnetic latitude of $75^{\circ}$ needed to account for the observed relative power longitude profiles. The height corresponding to each observing frequency can be obtained from Figure 7.28.

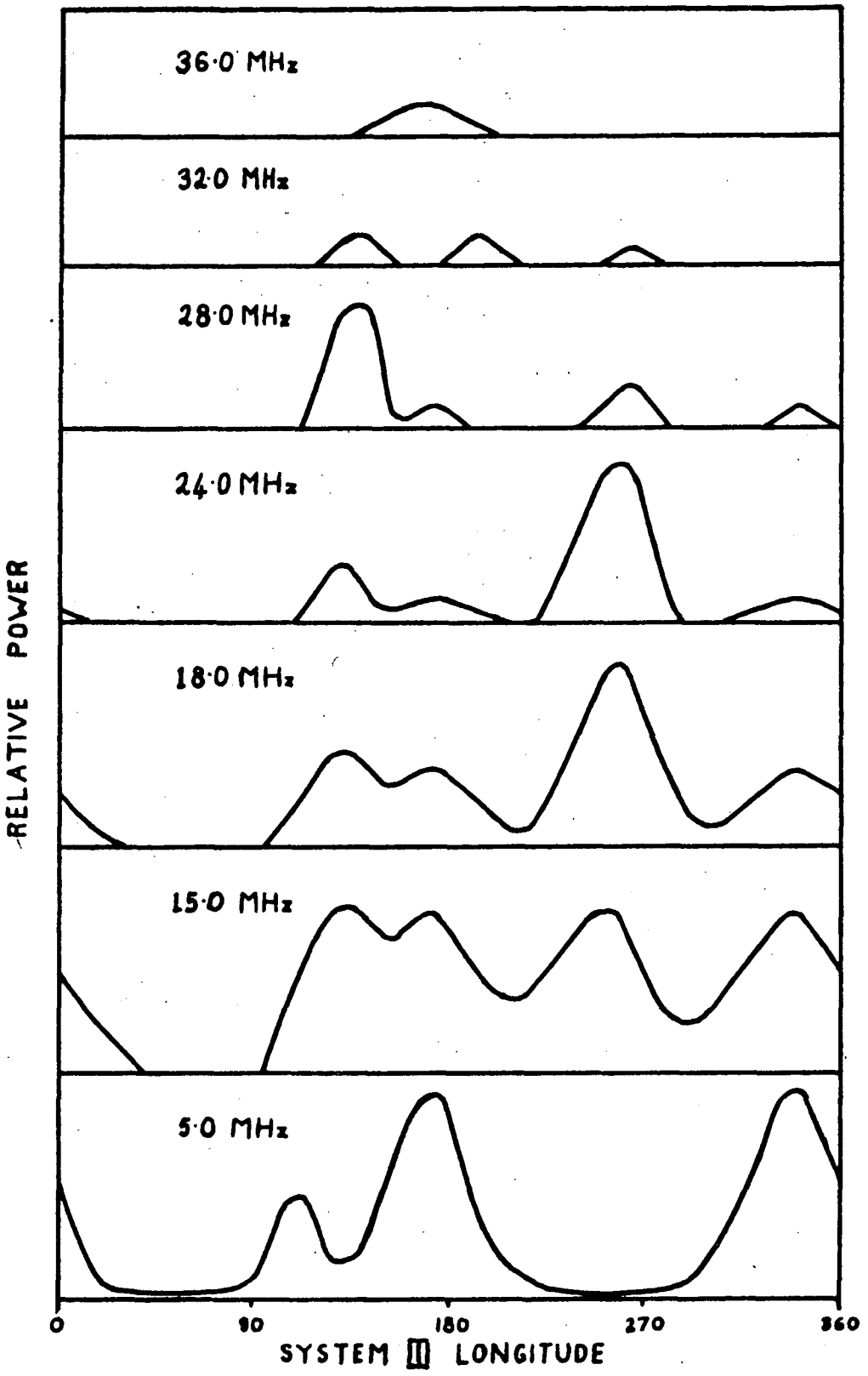


Figure 7.30 Theoretical longitude profiles of relative power at frequencies of 5, 15, 18, 24, 28, 32 and 36 MHz obtained using the field configuration of Figure 7.29.

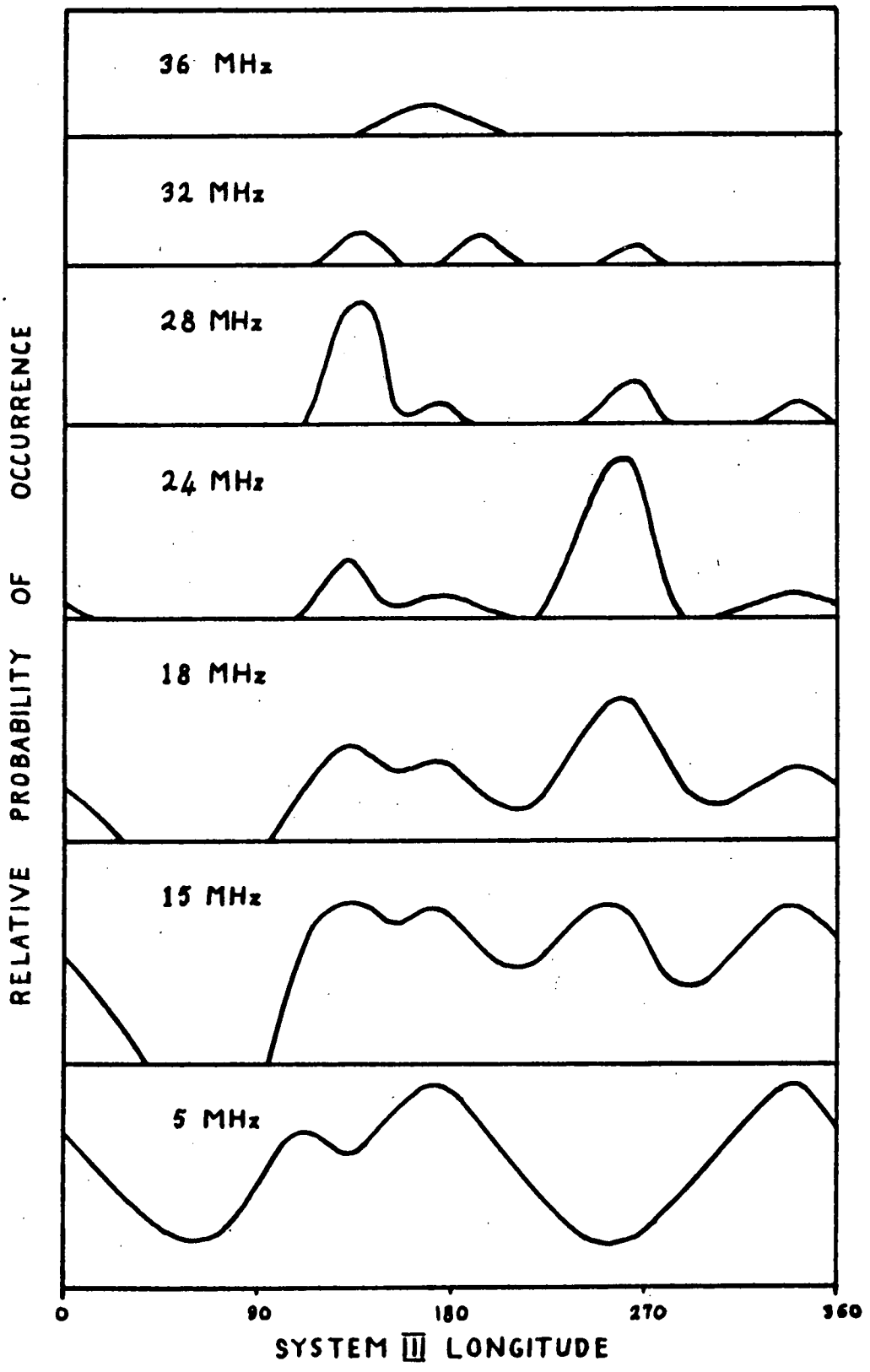


Figure 7.31 Theoretical relative probability of occurrence longitude profiles corresponding to the relative power profiles of Figure 7.30.

with longitude than the relative power. The theoretical profiles agree well with those observed in their general characteristics, although no attempt has been made to match all details as more complete data is needed to accurately define the observed profiles. In the cyclotron theory the observability and power from a given region depends upon the inclination of the field line at the point of emission, so that any observed profiles may be accounted for by suitable small adjustments of the magnetic dip angle.

The required dip angle deviations are found to increase with increasing frequency or decreasing radius. This is just the form a variation in the magnetic field would be expected to take. High above the surface it should approach a true dipole while close to the surface it could be severely distorted.

## 7.11 Polarisation of the Bursts.

The polarisation axial ratio of an individual burst is given to a good approximation by

$$A_r = \pm \cos \alpha$$

The relative probabilities of bursts with various axial ratios are shown in Figure (7.32), while the variation of the mean axial ratio with longitude at a number of frequencies is plotted in Figure (7.33) together with the observed variations. The theoretical curves have been plotted under the assumption that only one stream of electrons is radiating at any instant and that the ionised medium between the emission point and the observer does not effect the state of polarisation of the emission. The general form of the theoretical curves shown is in reasonable agreement with the observations, with

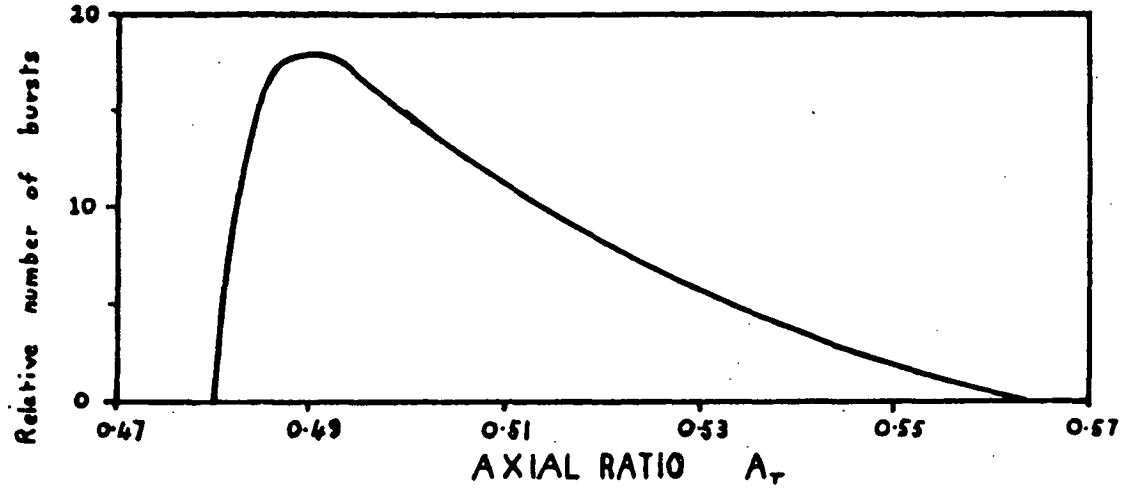


Figure 7.32 Relative probability of obtaining bursts of various axial ratios at a wave frequency of 18 MHz.

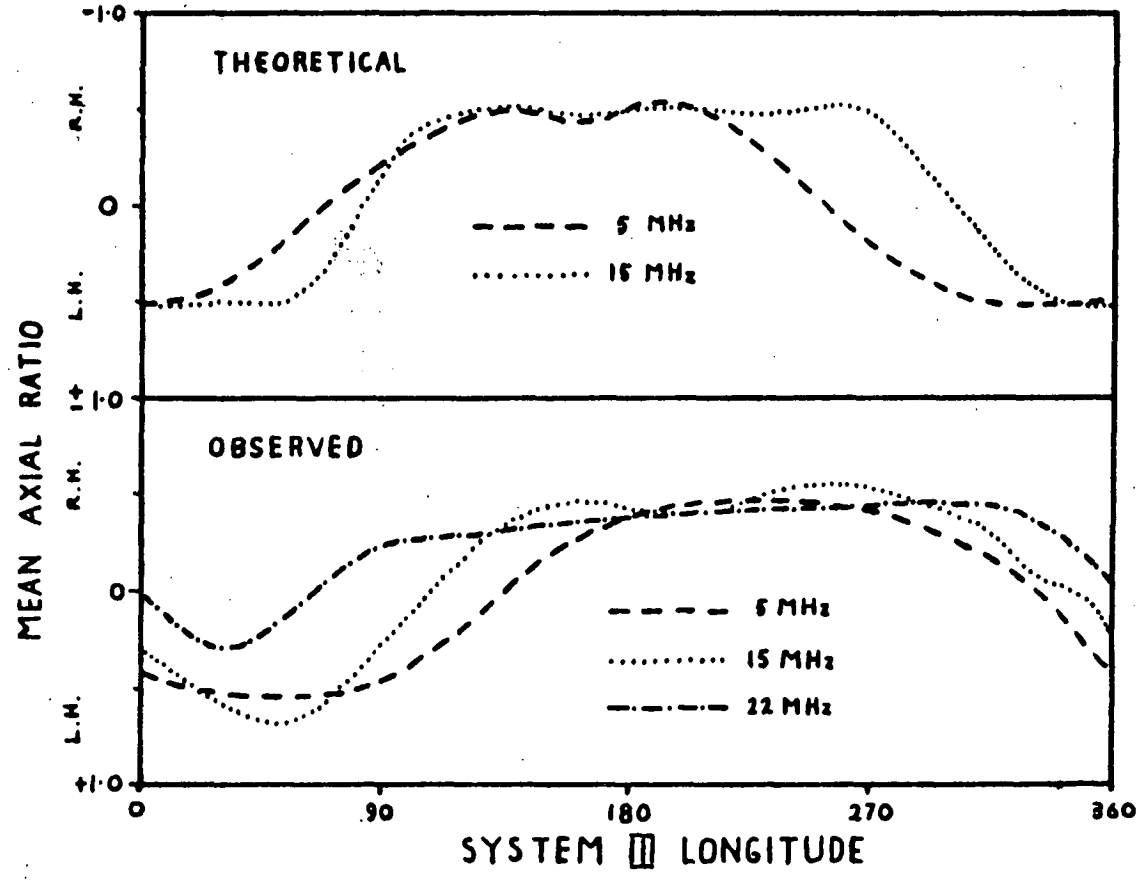


Figure 7.33 Theoretical and observed variations of the mean axial ratio of bursts at various frequencies as a function of longitude.

the exception that no circularly polarised or randomly polarised radiation is predicted. The radiation mechanism can only give completely polarised emission for individual bursts.

A possible explanation for these discrepancies lies in the simultaneous emission of a number of bursts from different parts of the planet, each at slightly different frequencies and having different amplitudes and polarisations. If the polarisation of all these bursts was right hand elliptical then the superposition observed at the antenna may appear as a right hand circular component, plus a random component, or possibly elliptical plus random. Hence circularly polarised emission which is received along with random polarisation may just be the sum of a number of elliptically polarised bursts.

We still have to explain however the observation of some pure circular polarisation which could occur because of anomalous propagation conditions in the Earth's ionosphere. Polarisation of signals transmitted by satellites is sometimes severely influenced by ionospheric scintillations, Roger (1965). The downcoming signal is split into its characteristic modes in the ionosphere; these can at times be scintillated separately so that an initially linearly polarised signal can be received as anything from pure right circular to pure left circular. The propagation of Jupiter's emissions through the ionosphere is essentially quasi-longitudinal so that the refractive index for the two modes is given by

$$n^2 = 1 - \frac{X}{1 \pm Y \cos \theta}$$

For emission near 20 MHz, $X \ll 1$, $Y \cos\theta \ll 1$ and

$$n^2 \simeq 1 - X(1 \mp Y \cos\theta)$$

The irregularities encountered by each mode are the same shape and size, but have different refractive indices. Hence we can treat the propagation of the two modes as propagation of two frequencies $f_1$ and $f_2$ such that

$$n^2(f_1) = n^2(\text{o-mode})$$
$$n^2(f_2) = n^2(\text{x-mode})$$

We then have the approximate relation

$$f_2 = f_1 + f_H \cos\theta$$

and the maximum separation of the two frequencies in the ionosphere is about 1.5 MHz. The correlation of scintillations at two neighbouring frequencies has been studied by Budden (1965). He finds that for a thin diffraction screen the correlation between frequencies of 20 MHz and 21.5 MHz is extremely small providing the irregularity scale size is smaller than about 250 meters. Hence if an elliptically polarised wave propagates through the ionosphere when such irregularities are present there is a strong probability that circularly polarised bursts will be recorded at times. Another result of this is that left hand polarised bursts will be observed from right hand emissions and vice versa. Hence a general spreading of right and left hand polarisations throughout all longitudes will result. This is in fact observed, as left hand bursts are found in predominantly right hand longitudes and vice versa. The observed axial ratios would also be expected to vary over a much wider range than the emitted axial ratios. The effect of the scintillations varies as the inverse cubes of the frequency and

should be proportional to the scale of the irregularities in the ionosphere, which in turn depends on the sunspot numbers. This frequency dependance is consistent with the percentage of L.H. bursts observed from the predominantly R.H. regions of the planet.

The fact that polarisation axial ratios can be severely modified by ionospheric scintillations implies that great care should be exercised in interpreting all polarisation measurements.

## 7.12 Dynamic Spectra of the Radiation.

The dynamic spectra of Jupiter's emission are of two types, very rapid variations of frequency with time of the order of tens of MHz/sec, and slow changes of frequency with time as the planet rotates.

The rapid time variations are much faster than variations produced by interplanetary scintillations and Slee and Gent (1967) have concluded that they originate on Jupiter. The most plausible explanation is that they are produced by individual streams of electrons radiating as they move along the field lines.

In Section (7.5) we saw that the emission cone for outward moving electron streams was about $8^{\circ}$ larger than for the corresponding inward moving electron streams. Hence we would expect to see many more bursts from the outward moving streams than from the inward streams. The corresponding emission decreases in frequency with time, as is in fact observed. The rate of change of frequency with time is given by

$$\frac{df}{dt} \simeq \frac{df_H}{dt} \simeq -\frac{3 f_H}{R} \frac{dR}{dt}$$

where R is the radius of the emission points

$$\frac{df}{dt} = -3 \beta c f_H / R$$

where R is the distance of the emission point from the center of the planet. For $f_H = 20$ MHz we have

$$\frac{df}{dt} \simeq -180\ \beta_{\parallel}\ \text{MHz/s}$$

where $\beta_{\parallel}$ is the longitudinal component of the electron velocity. This gives drift rates in the range 35 to 100 MHz/s for electrons with energies in the range 10 - 100 kev.

The predicted bandwidths of these bursts vary from a few tens of kHz to several MHz depending on the energy and pitch angle of the emitting electrons and the degree of focussing in Jupiter's magnetosphere. The durations of the resulting bursts observed on a narrow band receiver would be in the range of about 1 millisec to 0.1 sec. These drift rates, bandwidths and burst durations are consistent with the observed values. In particular, these burst durations are the same as the duration of bursts observed simultaneously at sites separated by large baselines, indicating that they originate on Jupiter and are not produced by scintillations.

Observations of the statistical distributions of bandwidths and drift rates of these fast bursts should provide information about the distribution of pitch angles and energies among the radiating electron bunches.

The slow drift spectra show variations with time scales of tens of minutes and are characteristic of certain longitudes on the planet. The high frequency emission stub which occurs between longitudes $90^{\circ}$ and $180^{\circ}$ has been built into the model as a permanent distortion of the magnetic field which allows radiation to be observed in the appropriate frequency-longitude regions. The theoretical

spectrum which is produced by radiation from electron streams in all magnetic longitudes having a wide range of pitch angles and energies is shown in Figure (7.34a). If the radiating electrons do not occur in all magnetic longitudes, or are not distributed over all energies and pitch angles the form of the spectrum will be changed. In particular it will occupy a narrower frequency and longitude range and hence will only occupy part of the figure. The actual frequency-longitude profile of each spectrum will depend on the longitudes of the emitting electrons, which provides a way in which Io could influence the shape of the spectrum.

There is another type of spectrum which can be produced within the frequency-longitude emission profiles governed by the configuration of the magnetic field. If stable focussing can be obtained, emission will occur on the edge of a cone. The angle of the cone and the inclination of its axis to the magnetic equator will depend on the emission frequency. A continuous stream of electrons on one field line will emit on a series of cones, whose angles and directions will vary smoothly with frequency. As the planet rotates the observers line of sight may pass through these cones in a regular way giving a smooth variation of frequency with longitude over many minutes. The geometry of the emission is shown in Figure (7.35) and typical spectra are drawn in Figure (7.34b). If the electrons are not monoenergetic or are not confined to a small range of magnetic longitudes and latitudes the spectrum may be broadened into forms similar to that shown in Figure (7.34c).

This type of spectrum is similar to the cusps of emission observed from the longitude range $200^{\circ}$ to $360^{\circ}$ by Dulk (1965).

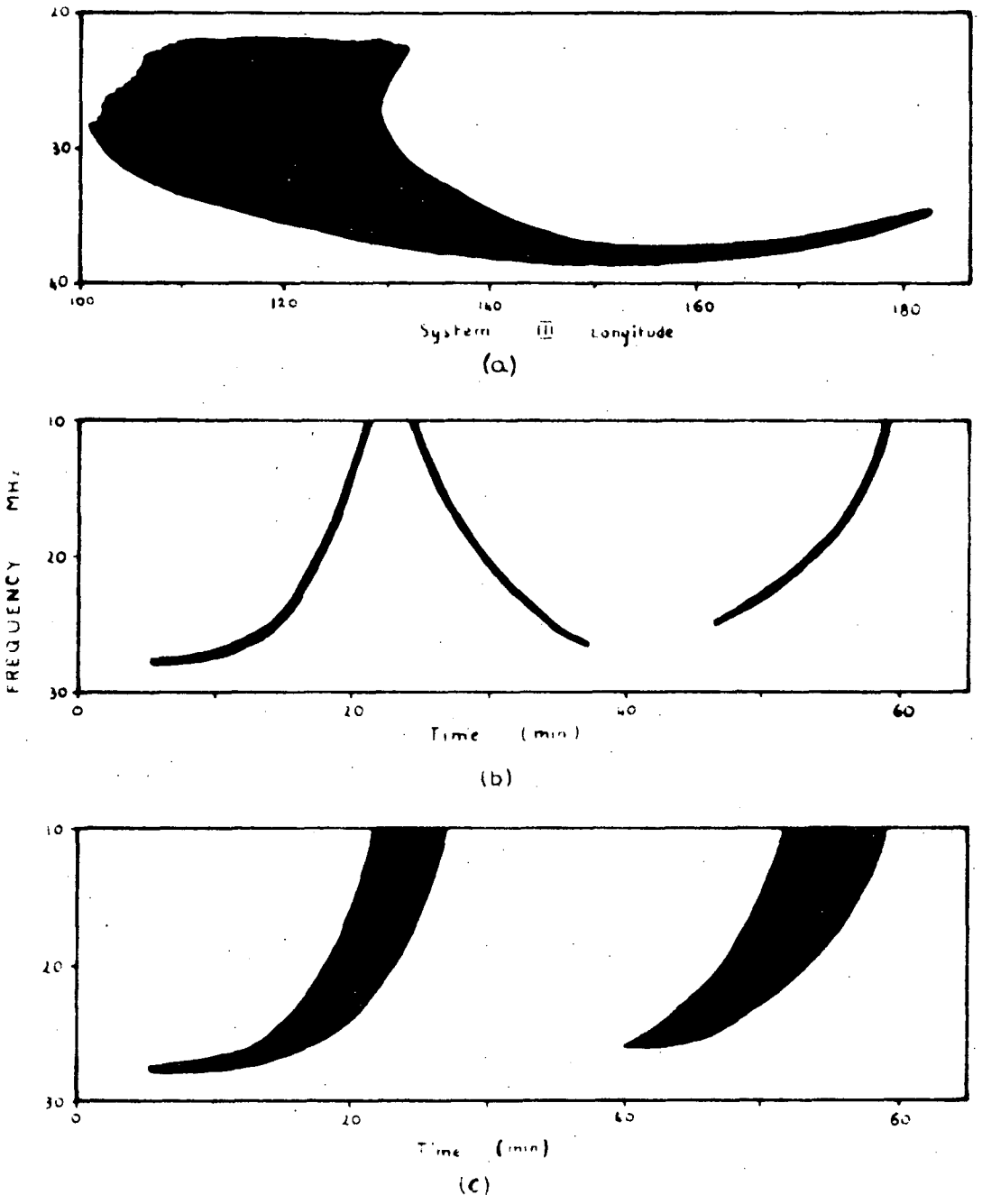


Figure 7.34 Theoretical dynamic spectra. (a) Low time resolution, resulting from emission by electron streams at all longitudes with all possible energies and pitch angles. (b) Spectra obtained from focussed emission by monoenergetic particles on a small range of field lines. (c) The spectra in (b) modified by emission from a wide range of field lines or by emission from bunches with a broad distribution of energies and pitch angles.

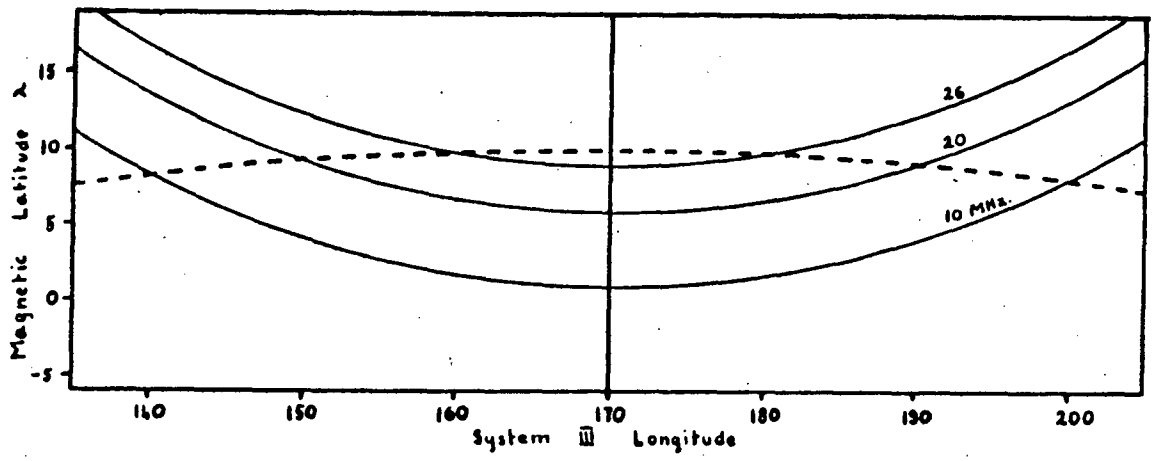


Figure 7.35 The geometry of the emission spectra of Figure 7.34b showing the edge of the focussed cone of emission at a number of frequencies. The dotted line shows the path of the observers line of sight.

Theoretically both positive and negative frequency slopes would seem equally likely, however, to date, only negative slopes have been reported. The exact shape of these emission cusps will depend upon the distribution of the radiating electrons in Jupiter's magnetosphere.

7.13 Power Spectrum of the Radiation.

In Section (7.4) it was shown that the maximum power emitted is given by

$$P = 4\pi^2 f_H^{2/3} f_{max}^{\frac{1}{3}} N_s W' A R_J^3 / 3000$$

Where the amplification factor A is given by

$$A = \exp\left\{\eta, R_J \frac{2\pi}{c} \left(\frac{\Delta f}{f_H}\right) \left(8_{10}7 N_s \alpha^2 f_{max}\right)^{\frac{1}{3}}\right\}$$

Substituting in the appropriate factors for each wave frequency, we find the maximum power radiated at each frequency at a given position in the radiation cone. Making allowance for the different maximum penetrations into the radiation cones at each frequency we obtain the peak power spectrum of the emission. This is plotted in Figure (7.36a). The theoretical and observed longitude profiles were matched by choosing suitable values of $\alpha = f_H / f_o$ at each observing frequency. At the low frequency end there could be a large inaccuracy in the value of $\alpha$ chosen as the shape of the profiles are not very sensitive to this parameter. As a result the points on the peak power spectrum at low frequencies could be significantly in error as $\alpha$ appears in the exponential term. Within the limits imposed on the spectrum by the choice of $\alpha$, the theoretical mean power spectrum is obtained by allowing for the ratio of mean to peak powers at each frequency and by allowing for the variation in the number of electron

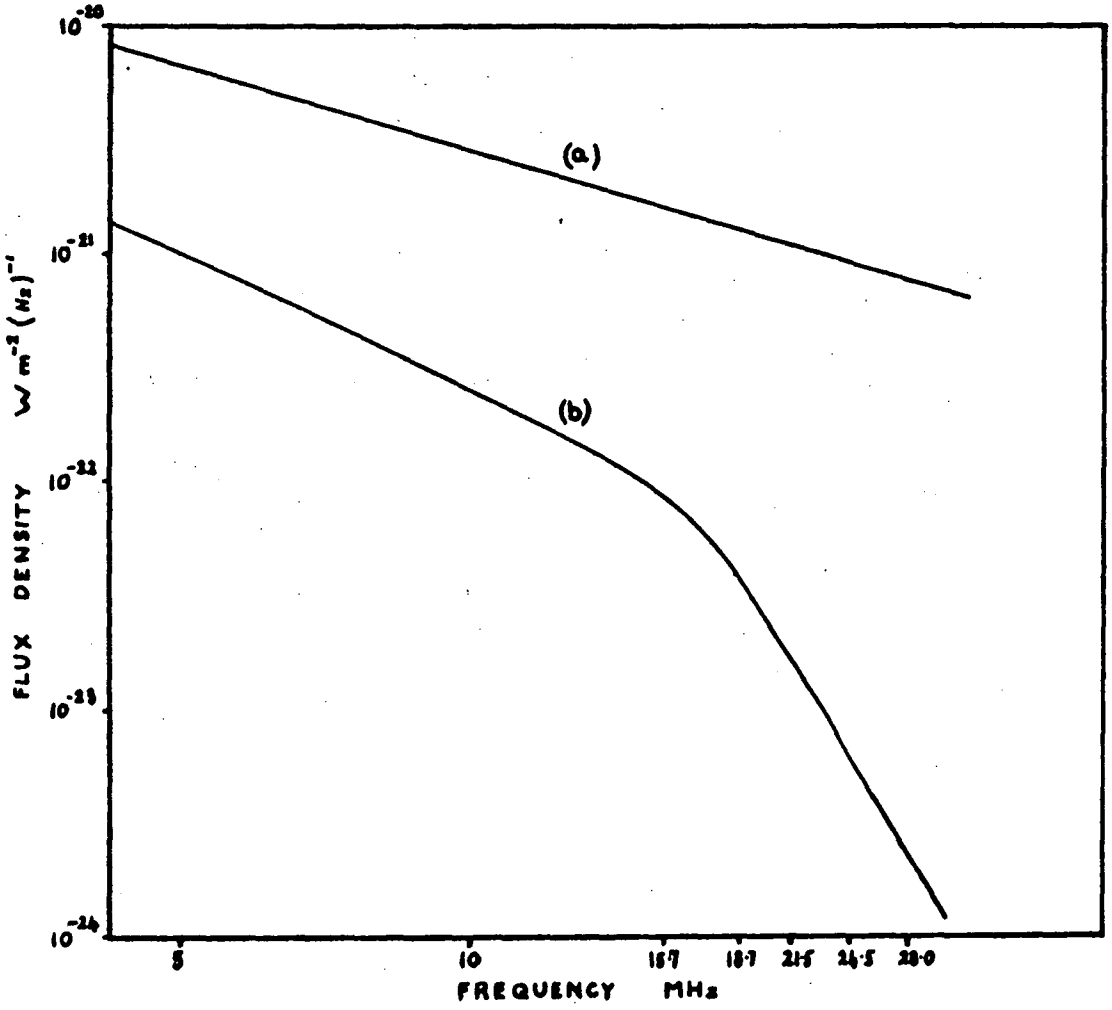


Figure 7.36 Spectra of Jupiter's decametric emission. (a) Peak power spectrum. (b) Mean power spectrum averaged over quiescent as well as active periods.

bunches present at each gyrofrequency level. The spectrum obtained is plotted in Figure (7.36b). This also agrees, within the errors, with the observed mean power spectrum.

## 7.14 Effects of Jupiter's Rotation Around the Sun.

As Jupiter moves in its orbit around the Sun the angle $D_E$ between Jupiter's rotation axis and the Earth-Jupiter line changes by $\pm 3^{\circ}$. The time taken for one complete cycle is Jupiter's orbital period about 11.9 years. Hence for one point on Jupiter's orbit we see much further into Jupiter's northern hemisphere than into the southern hemisphere while six years later the situation is reversed. This results in an 11.9 year period amplitude variation for the peaks in the longitude profiles which should be $180^{\circ}$ out of phase for the peaks associated with the north and south poles. Figure (7.37) shows the theoretical and observed variation of the ratio of the amplitudes of the peaks associated with Jupiter's poles as a function of the year of observation and the corresponding variation of $D_E$. The agreement between the theoretical and observed curves is quite good and adds further weight to the identification of the magnetic poles on Jupiter. Because the majority of the emission at frequencies of 18 MHz and above takes place in the northern hemisphere we would also expect to see a change in the shape of the longitude profiles with $D_E$ and an overall change in the emission probability. These are plotted in Figures (7.38) and (7.39). The variations of $D_E$ and sunspot numbers are also shown in Figure (7.39). The observed variation of emission probability is consistent with that expected on the basis of the cyclotron theory. In Figure (7.38)

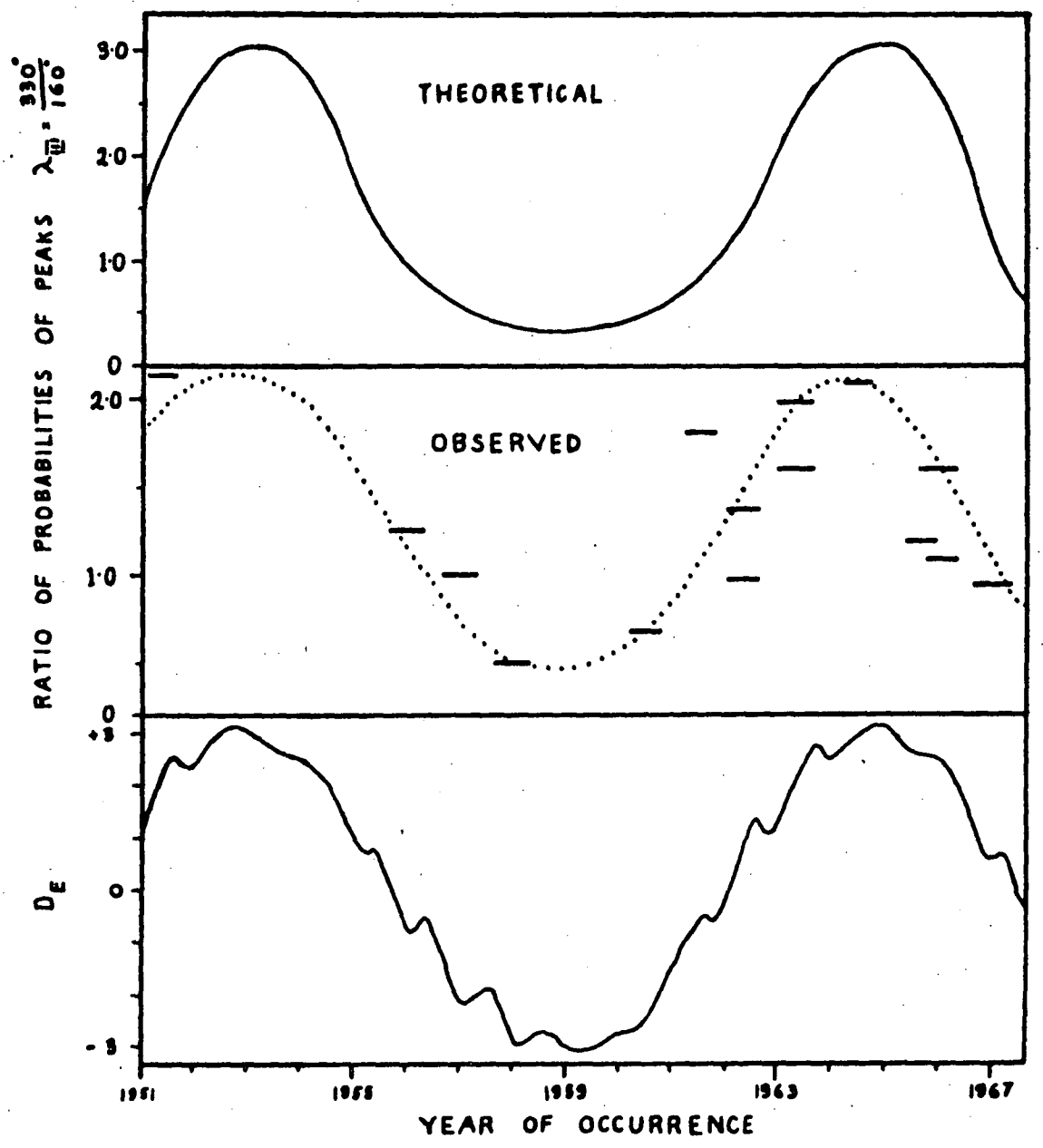


Figure 7.37 Theoretical and observed variation of the ratio of the probabilities of occurrence at longitudes 330° and 160° as a function of the year of observation for frequencies near 18 MHz. The variation of $D_E$ is plotted for comparison.

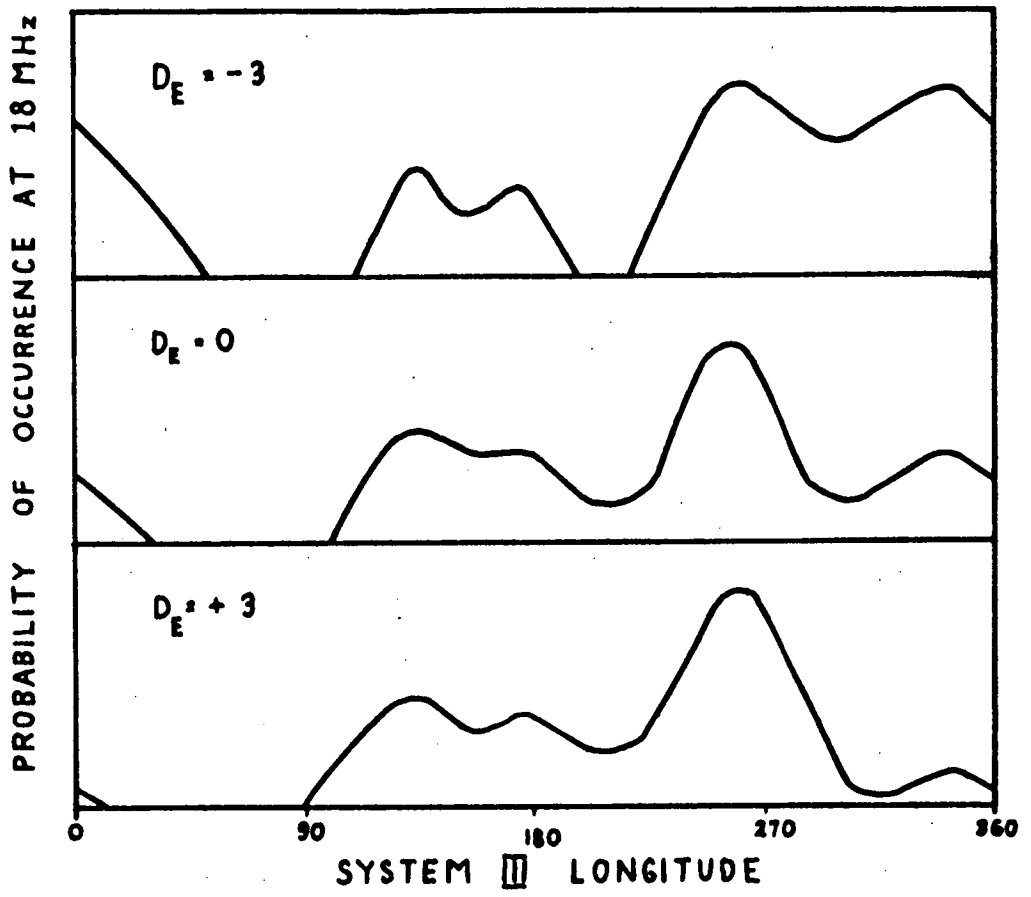


Figure 7.38 Longitude profiles of probability of occurrence at 18 MHz for different values of $D_E$. No attempt has been made to include the shift in position of the main peak in these profiles.

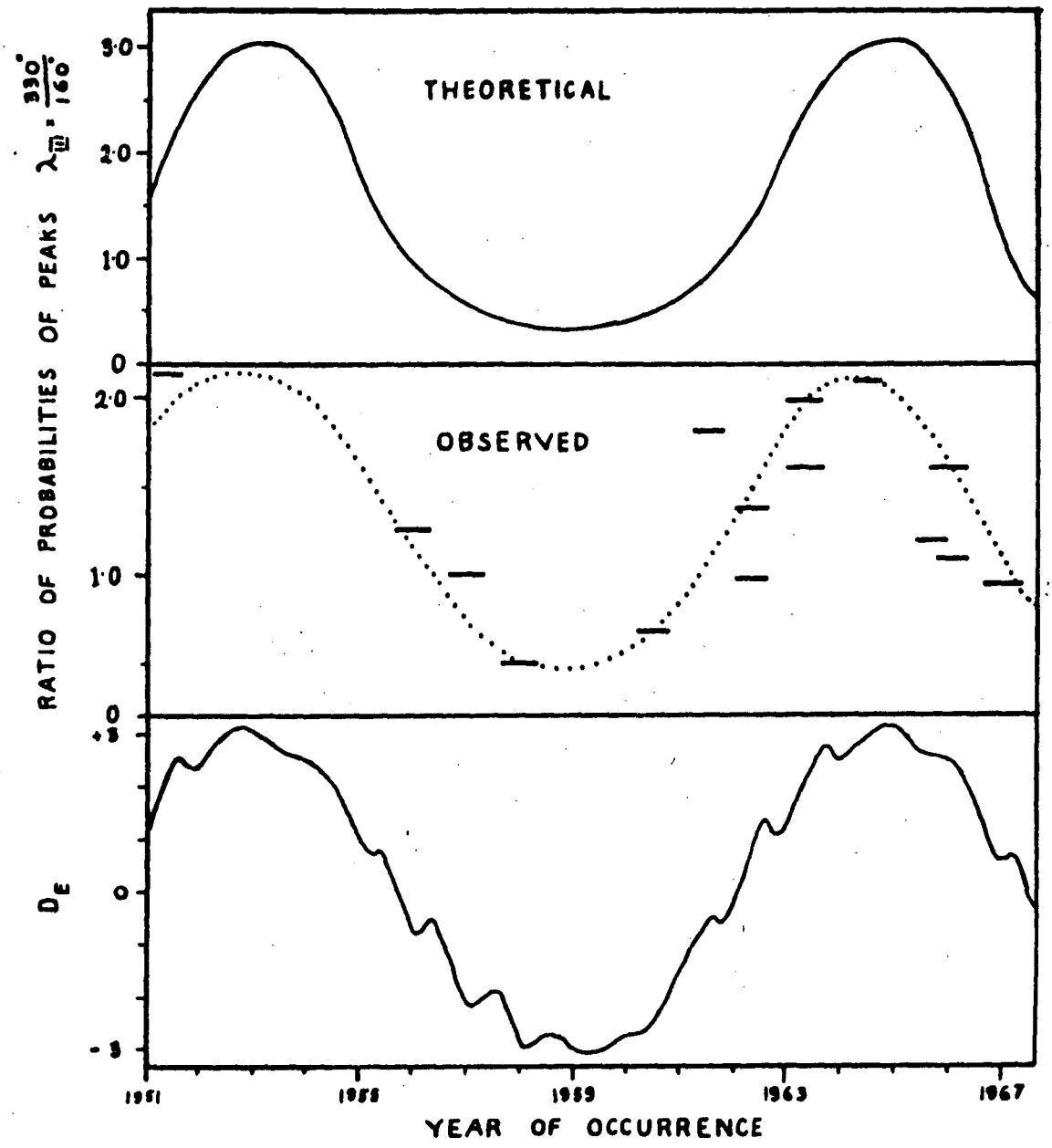


Figure 7.37 Theoretical and observed variation of the ratio of the probabilities of occurrence at longitudes 330° and 160° as a function of the year of observation for frequencies near 18 MHz. The variation of $D_E$ is plotted for comparison.

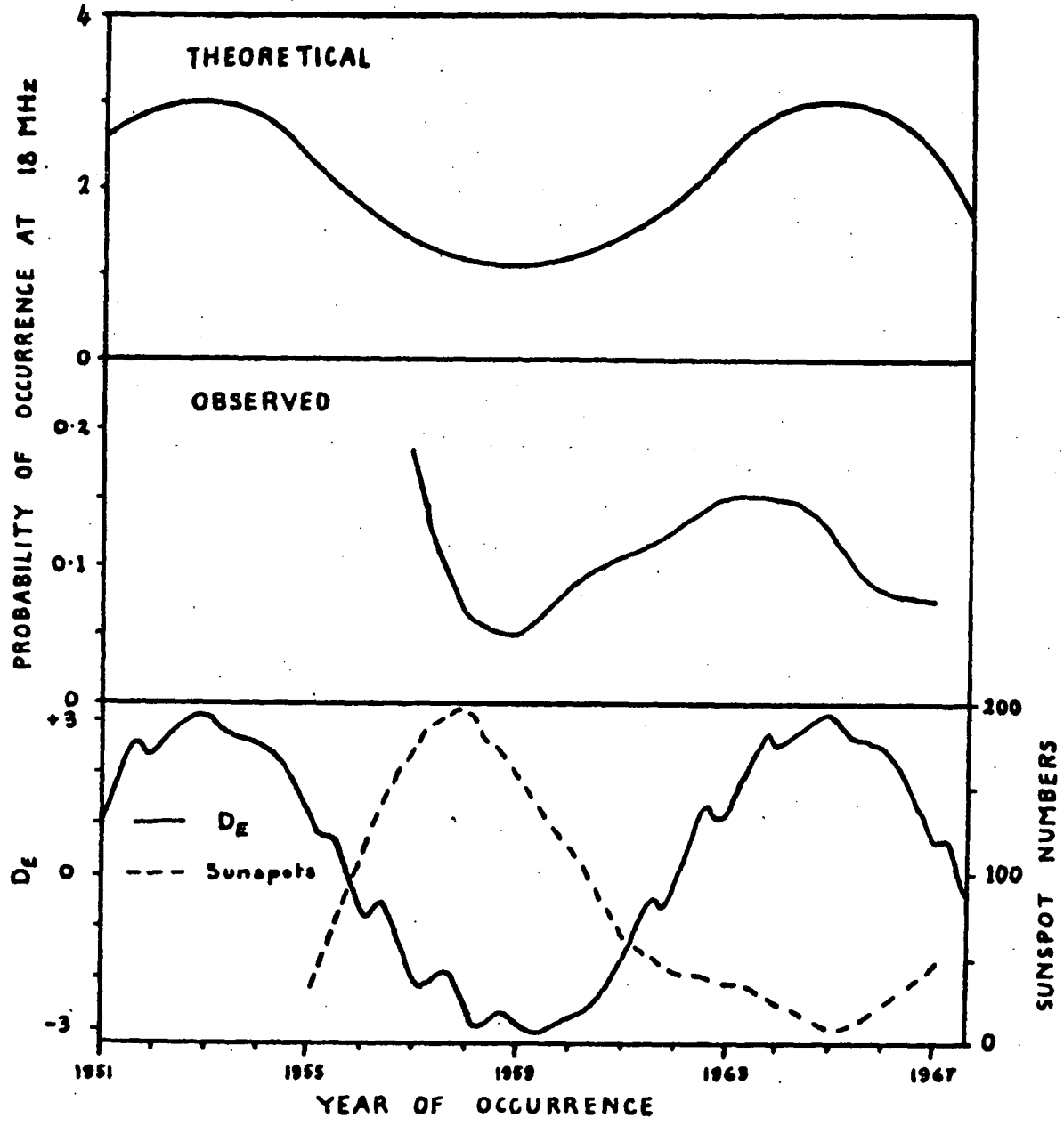


Figure 7.39 Theoretical and observed variation of probability of occurrence at 18 MHz. The variations of $D_E$ and sunspot numbers are included for comparison.

no attempt has been made to show the shift in position of the main source in the longitude profiles with $D_E$. This is discussed in detail in the next Chapter.

## 7.15 Burst Structure.

The observations of Douglas (1964) and Slee and Higgins (1963, 1966) have shown that burst structure with time scales from about 1 sec to 30 sec is produced by interplanetary scintillations. On the other hand, structure with time scales from 1 to 100 m sec has been shown to originate on Jupiter (Slee and Gent, 1967). These short durations are consistent with the durations that would be expected for the emission from electron streams when recorded on a narrow band receiver. The shorter durations, of about 1 m sec, could be produced by focussed emission from a small source.

Baart, Barrow and Lee (1966) have shown that the millisecond pulses originate mainly from the regions we have associated with the magnetic poles. These regions are the longitude ranges where there are no magnetic anomalies and hence the curvature of the magnetic field lines is smallest. It has been shown, Section (7.5), that the angular width of the emission cone produced by focussing is a minimum when the field curvature is smallest. Hence in the vicinity of the poles stronger focussing and hence narrower emission cones which could produce millisecond bursts would be expected.

## 7.16 Conclusions.

The properties of the decametric emissions from Jupiter appear to be explained adequately on the basis of cyclotron radiation

from electrons in a magnetosphere which is generally similar to that of the Earth. A necessary feature of this explanation is that Jupiter is surrounded by an ionised exosphere with a maximum electron density of about $10^6$/cc. Jupiter's magnetic field has a polar strength of about 30 gauss and deviates from a dipole in at least two areas of the planet. The density variations in the exosphere and the location and extent of the magnetic anomalies can be obtained from the model.

Measurements of polarisation axial ratio are shown to be subject to errors due to the effects of scintillations and hence a potentially powerful technique for investigating Jupiter's emissions produces results whose interpretation is ambiguous.

Observations of the fast drift dynamic spectra of the radiation are likely to provide specific information on the energy and pitch angle distributions of the electron bunches and streams.

## 7.17 References.

BAART, E.E., C.H. BARROW and R.T. LEE (1966) Nature 211, 808

BUDDEN, K.G. (1960) Radio Waves in the Ionosphere, Cambridge

BUDDEN, K.G. (1965) J.A.T.P. 27, 883

DOUGLAS, J.H. (1964) I.E.E. Trans Mil. Electronics MIL 8, 173

DULK, G.A. (1965) Ph. D. Dissertation, University of Colorado

ELLIS, G.R.A. (1962) Aust. J. Phys. 15, 344

ELLIS, G.R.A. (1963) Aust. J. Phys. 16, 74

ELLIS, G.R.A. (1965) J. Res. Nat. Bur. Standards 69D, 1513

ELLIS, G.R.A. and P.M. McCULLOCH (1963) Aust. J. Phys. 16, 380

FUNG, P.C.W. (1966) Unpublished Ph. D. Thesis, University of Tasmania

HARTZ, T.R. and R.S. ROGER (1964) Canadian J. Phys. 42, 2146

ROBERTS, J.S. and M.M. KOMESAROFF (1965) Icarus 4, 127

ROGER, R.S. (1965) J.A.T.P. 27, 335

SLEE, O.B. and H. GENT (1967) Nature 216, 235

SLEE, O.B. and C.S. HIGGINS (1963) Nature 197, 781

SLEE, O.B. and C.S. HIGGINS (1966) Aust. J. Phys. 19, 167

SMITH, F.G. (1961) Mon. Not. R. Astr. Soc. 122, 527

WARWICK, J.W. and M.A. GORDON (1965) J. Res. Nat. Bur. Standards 69D, 1537

# CHAPTER 8.

# THE RADIO ROTATION RATE OF JUPITER

## 8.1 Introduction.

Since 1961, the most intense source of Jovian decametric emission has drifted with respect to system III longitude at a rate of about + $10^{\circ}$ per year (Douglas and Smith, 1963; Smith et al, 1965). Interpreted as a change in the rotation rate, this would imply that the period increased by approximately $1.1^{s}$ around 1960. Since it is felt that this period is the period of the rotation of the magnetic field of Jupiter, which in turn is thought to be associated with the solid body of the planet a sudden change in rotation period involves considerable theoretical difficulty from the point of view of energy conservation.

A more plausible interpretation has recently been advanced by Gulkis and Carr (1966). They show that the results are consistent with a constant rotation period about 0.3 sec longer than the system III period, together with a cyclic drift in the longitude of Source A.

Late in 1966 it was decided to try and check the rotation period of Jupiter by observing the rocking of the plane of polarisation of the radiation at a wavelength of 11 cm and comparing the observed phase of this variation with that observed by Roberts and Komesaroff in 1963.

This Chapter describes a series of 11 cm polarisation observations made at Parkes, N.S.W., in January, 1967, and the subsequent interpretation of the decametric observations in terms of

the cyclotron theory. The 11 cm observations were made in co-operation with Mr. M.M. Komesaroff, of the C.S.I.R.O. Division of Radiophysics, and the results have been published in Astrophysical Letters. The interpretation of the rotation period in terms of the cyclotron theory has been published in the Australian Journal of Physics.

## 8.2 11 cm Linear Polarisation Observations of Jupiter.

The observations were made with an 11 cm parametric receiver and 'scalar' feed described respectively by Cooper et al (1964) and Simmons and Kay (1966).

Thirty seven complete linear polarisation determinations were made over a period of fifteen Jupiter rotations. Each consisted of six flux density measurements, with the feed orientation (with respect to the telescope structure) advanced by $30^{\circ}$ between successive measurements. The results were recorded on punched tape and analysed by computer. In the analysis a sine wave was fitted to each set of six points by the method of least squares to yield the degree and position angle of the polarisation.

The flux density was calibrated by comparison with the source 3C-161, for which the flux density was taken as 11.5 f.u. (a preliminary value supplied by J.A. Roberts and B. Harris).

Figure (8.1) shows the derived position angles as a function of system III longitude. The crosses represent the January, 1967, observations and the filled circles represent the observations made by Roberts and Komesaroff (1965) in November, 1963. The large gaps in the 1967 data are the result of observing time being lost due to adverse weather, while the larger scatter of points is prob-

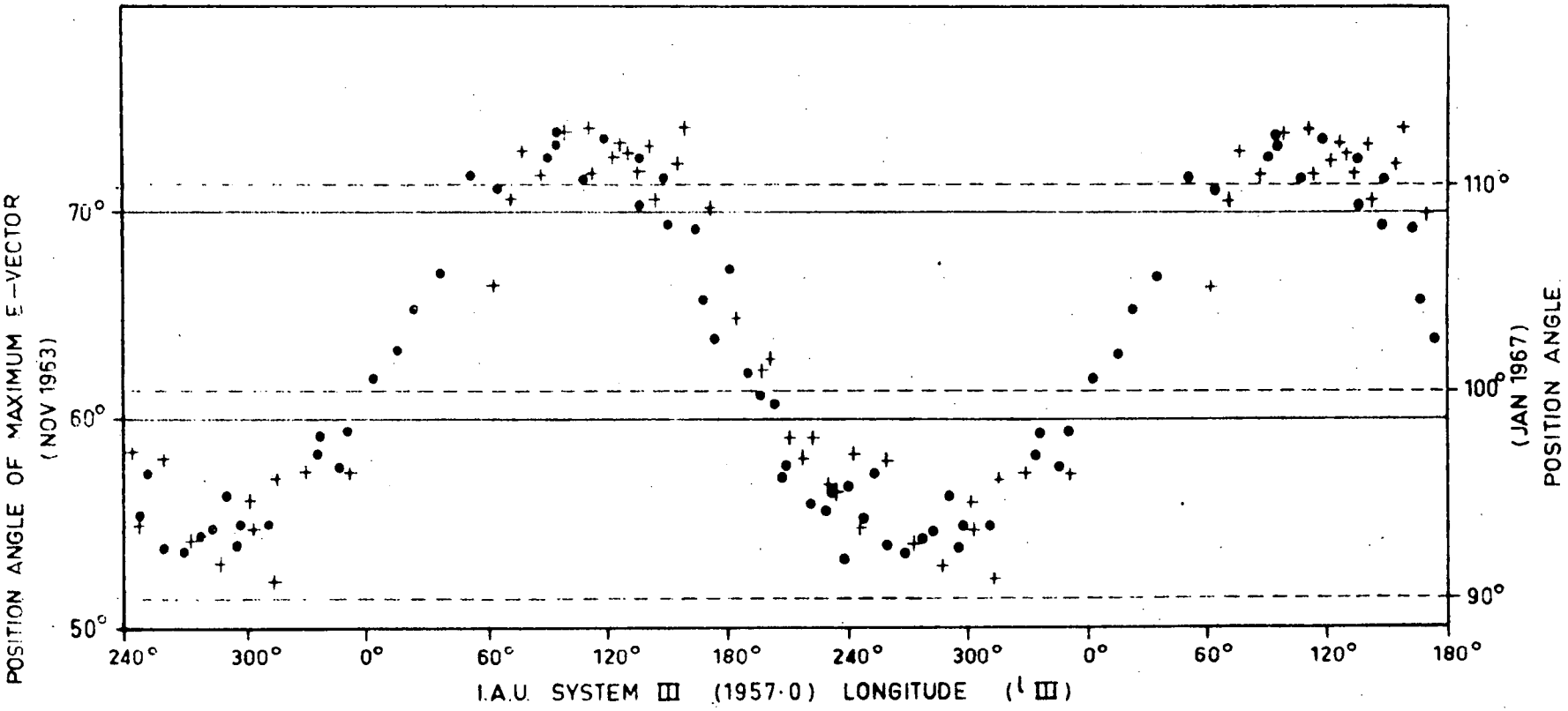


Figure 8.1 Position angle of the maximum electric vector as a function of system III (1957.0) longitude for January 1967 (crosses) and November 1963 (filled circles).

ably due to the greater zenith angles ( $> 55^{\circ}$) of Jupiter at this time. Inspection of the figure suggests that the 1967 points are at systematically higher longitudes which is confirmed by fitting curves to the two sets of data.

The four term Fourier series which yields the least squares best fit to the 1967 data is

$$\text{P.A.} = 101.9^{\circ} + 9.6^{\circ} \sin (\lambda_{III} - 21.8^{\circ}) + 1.0^{\circ} \sin 2 (\lambda_{III} - 81.9^{\circ}) + 0.5^{\circ} \sin 3 (\lambda_{III} - 14.6^{\circ})$$

For november, 1963, the series is

$$\text{P.A.} = 63.3^{\circ} + 9.8^{\circ} \sin (\lambda_{III} - 8.6^{\circ}) + 0.7^{\circ} \sin 2 (\lambda_{III} - 68.6^{\circ}) + 0.6^{\circ} \sin 3 (\lambda_{III} - 9.5^{\circ})$$

The first and second harmonic terms both show a phase change of about $13.2^{\circ}$ which corresponds to a rotation period that exceeds the system III period by 0.46 sec.

There are several sources of errors in the position angle measurements. There is an uncertainty in the zero position of the feed rotator, this is a consistent error and its only effect is to shift the vertical scale in Figure (8.1). Faraday rotation in the terrestrial ionosphere is also a possible source of error, its magnitude of about $1^{\circ}$ may have changed slightly due to changes in the ionospheric critical frequency over the observing period. However the fluctuations are unlikely to be more than about $0.25^{\circ}$. The other main source of error is random noise fluctuations. None of these effects can produce a systematic change in the longitude dependent terms of the Fourier series.

The ninety percentile error in the phase of the fundamental term in the Fourier series for 1967 is $6.9^{\circ}$ and for 1963 it

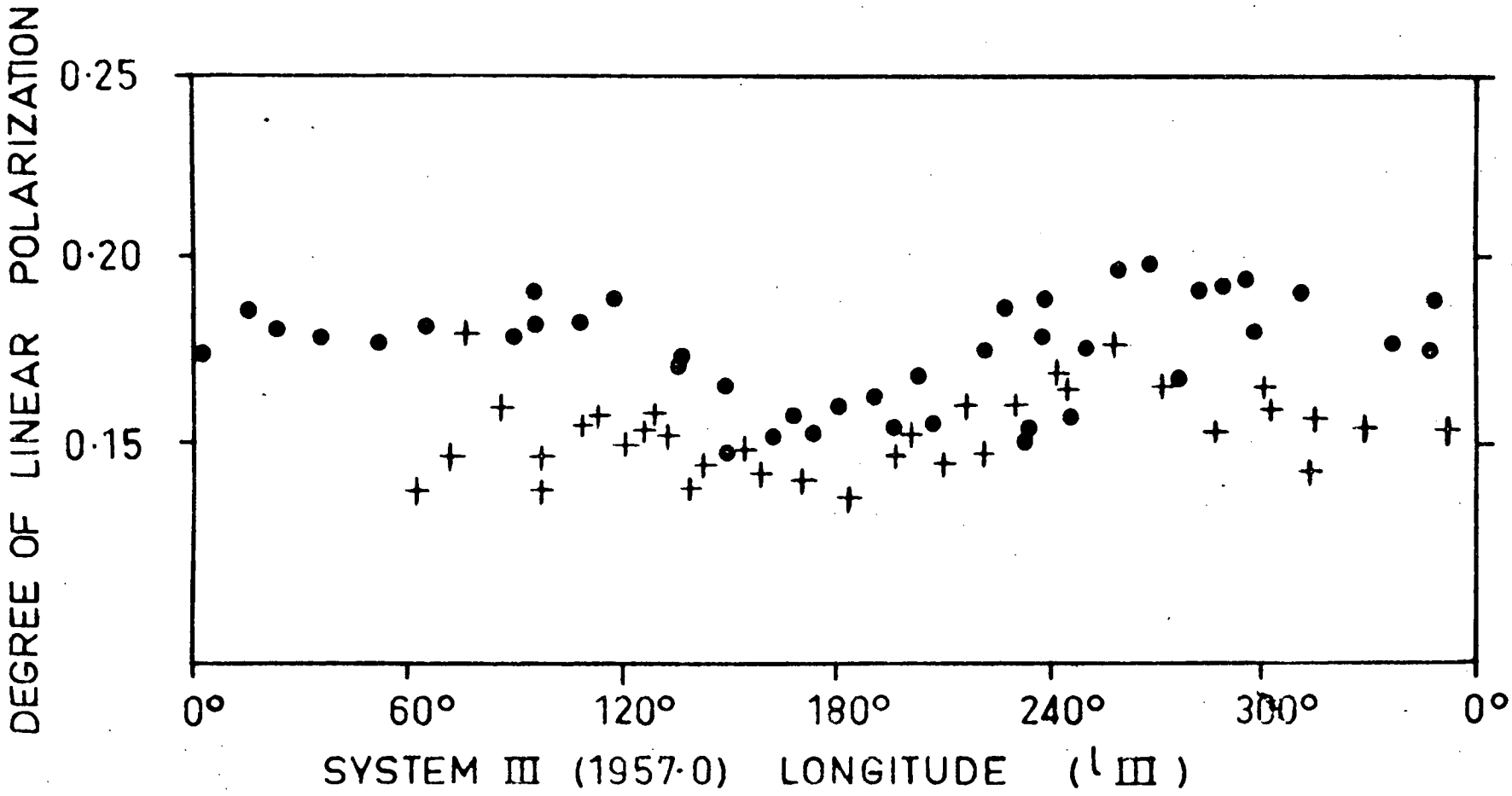


Figure 8.2 Degree of polarisation as a function of system III longitude for January 1967 (crosses) and November 1963 (filled circles).

is $2.7^{o}$. We may therefore say that between November, 1963, and January, 1967, the drift in the position angle curve relative to system III longitude is $13.2^{o}$ with a ninety percentile error of $\pm 7.5^{o}$. This is equivalent to saying that the rotation period between 1963 and 1967 exceeded the system III period by $0.46^{s} \pm 0.26^{s}$ agreeing, within the quoted errors, with the results of Gulkus and Carr. Further observations are proposed with the aim of reducing the errors.

Figure (8.2) shows the degree of linear polarisation as a function of system III longitude for 1963 and 1967. The only significant difference between the two sets of data is that the 1967 values are consistently lower. The polarised flux from Jupiter at 11 cm appears to have dropped by about 20% since November, 1963. The possibility that the difference is a spurious effect due to receiver non-linearities has been examined. This seems ruled out by the fact that the measured values of Jovian flux density for the two periods show good agreement despite the fact that the intensity calibrator for 1963 was very much weaker than Jupiter and that for 1967 was almost twice as strong.

The flux density as a function of system III longitude is plotted in Figure (8.3). The same general variation is apparent as for the 1963 data but the spread of points was much larger. This was probably because on most nights we did not have time to observe the calibration source more than twice and on a few nights it was only observed once. Despite the fluctuations we can say that the maximum flux density which is observed when the Earth lies in the zenomagnetic equator is $7.30 \pm 0.1$ f.u. Corresponding

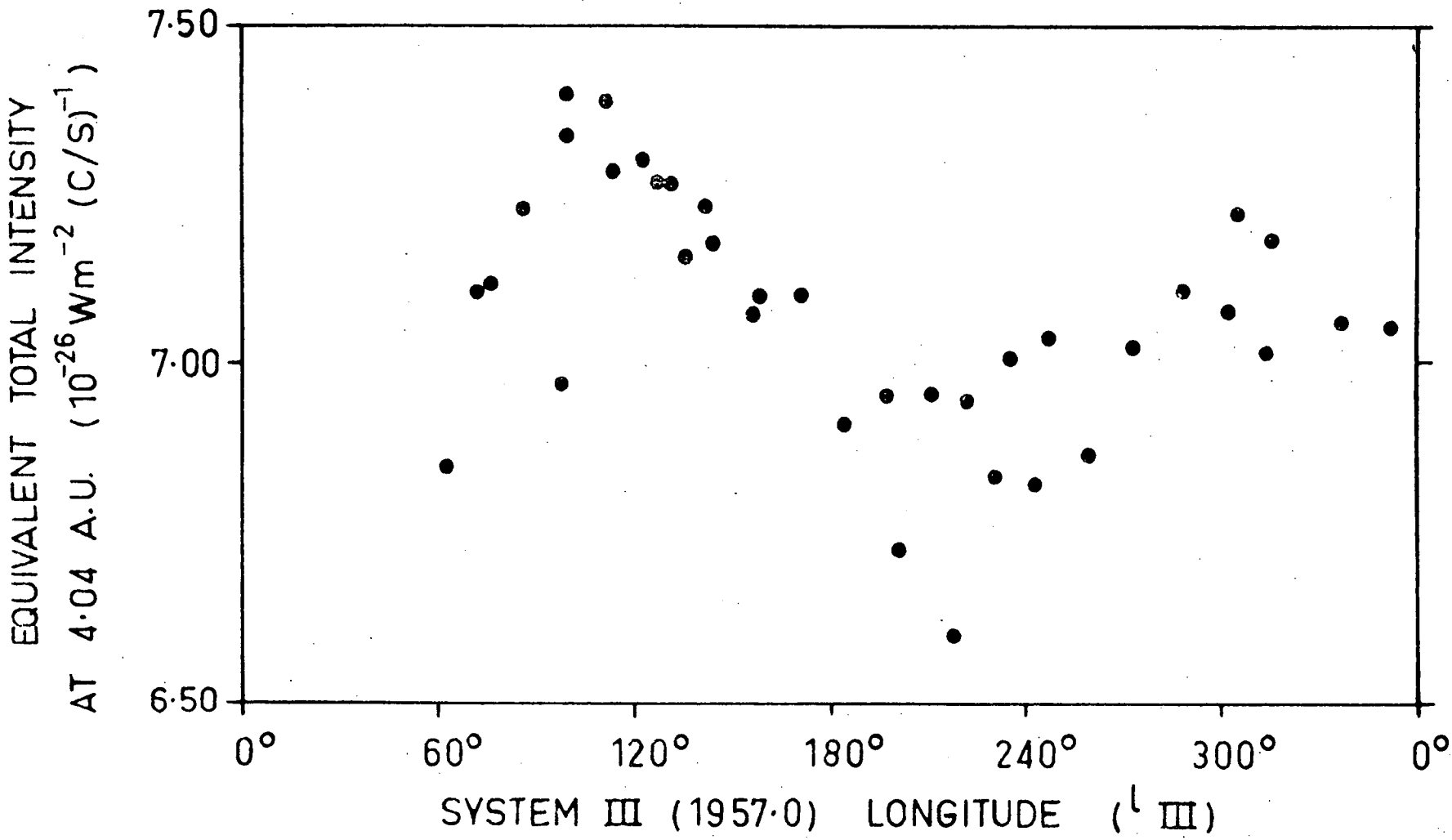


Figure 8.3 Received flux density (normalised to a distance of 4.04 A.U.) for January 1967 as a function of system III longitude.

values for 1963 and 1964 (Roberts and Komesaroff, 1965; Roberts and Ekers, 1967) are 7.50 $\pm$ 0.1 and 7.60 $\pm$ 0.1 respectively. Because it was necessary to use different calibrator sources for the different observing periods there may be some errors in scaling. However, even if this is as large as 10% the total variation over three years did not exceed about 15%. These results indicate a fairly continuous replenishment of the van Allen belt electrons over the period of the observations.

## 8.3 The Change in Position of the Decametric Sources.

The analysis of Douglas (1960) and Carr et al (1961) of data obtained prior to 1961 indicated that the rotation period was constant at about $9^h\ 55^m\ 29.37^s$. Observations made since 1961 indicate that between 1961 and 1965 the rotation period has fluctuated, the mean period being approximately $1.0^s$ longer than the system III period quoted above. Since 1965 the period appears to have decreased to somewhere near its former value. Figure (8.4) shows the estimated positions of the three main sources in the longitude profiles at 18 MHz since 1951. The drift in the main source A is quite distinct while the points for sources B and C are not as consistent.

Gulkis and Carr (1966) have suggested that the apparent rotation period of Jupiter drifts cyclically about a constant mean value which is about $0.3^s$ longer than system III. Figure (8.5) shows the data of Figure (8.4) for sources A and C replotted on a system III (1965.0) longitude scale which is defined to coincide with system III (1957.0) at $0^h$ U.T. on 1st January, 1965, and has

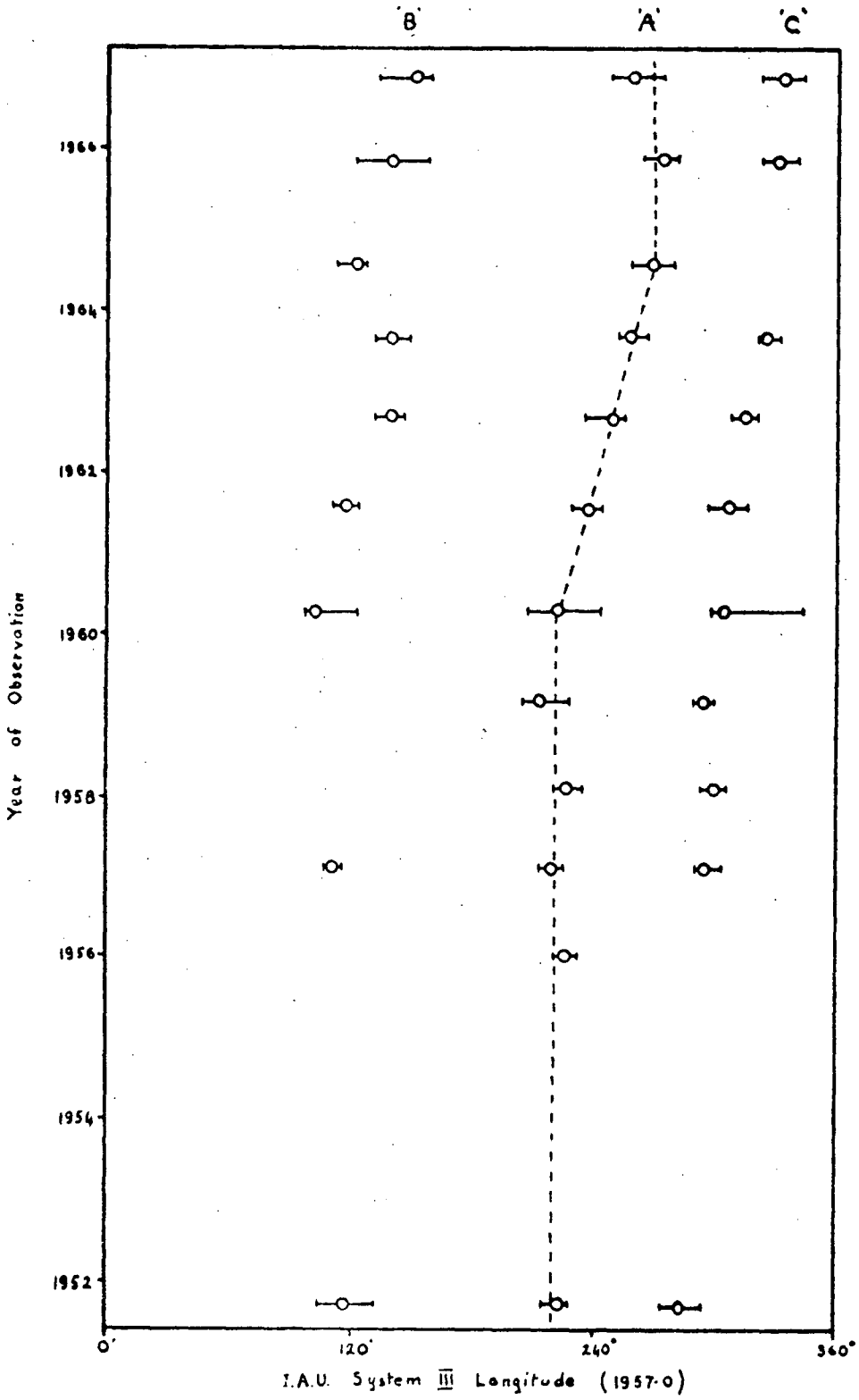


Figure 8.4 Estimated system III longitude positions of the three main sources in the longitude profiles at 18 MHz are plotted for each year of observation since 1951.

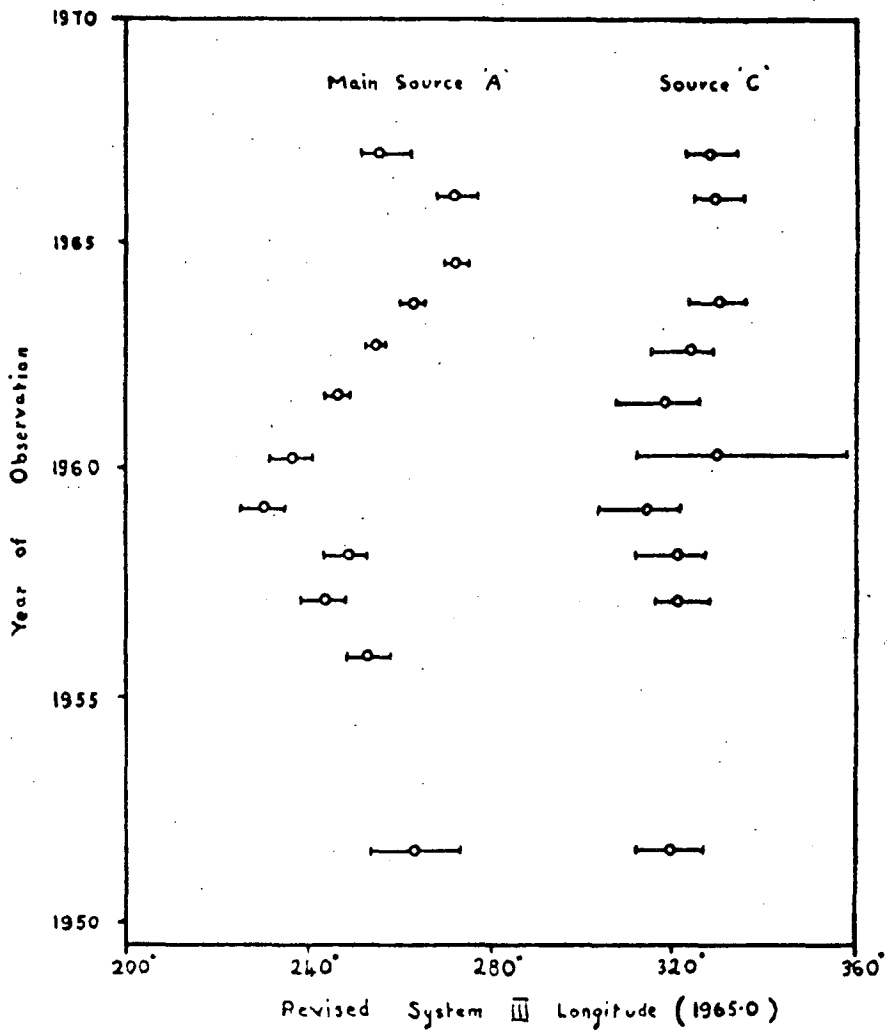


Figure 8.5 Data of Figure 8.4 for sources A and C replotted on a revised system III (1965.0) longitude which coincides with system III (1957.0) at $0^h$ U.T. on January 1, 1965, and has a rotation period of $9^h\ 55^m\ 29.67^s$.

a rotation period of $9^h\ 55^m\ 29.67^s$. The points for source A define a sine wave with an amplitude of about $18^\circ$ and a period of about 12 years, in close agreement with Jupiter's orbital period and the length of the sunspot cycle. The points for source C also define a sine wave which is in phase with that defined by source A but only has an amplitude of about $8^\circ$. The data from the two early sources B1 and B2 has not been analysed in this way because they are not well defined on the majority of longitude profiles.

## 8.4 Interpretation of the Change in Source Positions in Terms of the Cyclotron Theory.

The cyclotron theory of the Jupiter decametric emissions has been developed in detail in Chapter 7. Radiation is emitted at the local electron gyrofrequency by electron streams in Jupiter's magnetic field. The observed frequency is Doppler shifted due to the longitudinal motion of the electrons. The propagation of the radiation is controlled by the medium so that only radiation in the extraordinary mode in the forward direction escapes. In this case the observed frequency is slightly above the local gyrofrequency. The emission is concentrated onto the surface of a cone about the magnetic field direction, where the cone angle depends on the ratio of the gyrofrequency to plasma-frequency at the emission point and the pitch angle of the electrons.

The electron streams are assumed to be confined to field lines that intersect the surface of Jupiter at latitudes greater than $75^\circ$, with the probability of finding an electron stream at $75^\circ$ being zero but increasing linearly with magnetic latitude. All

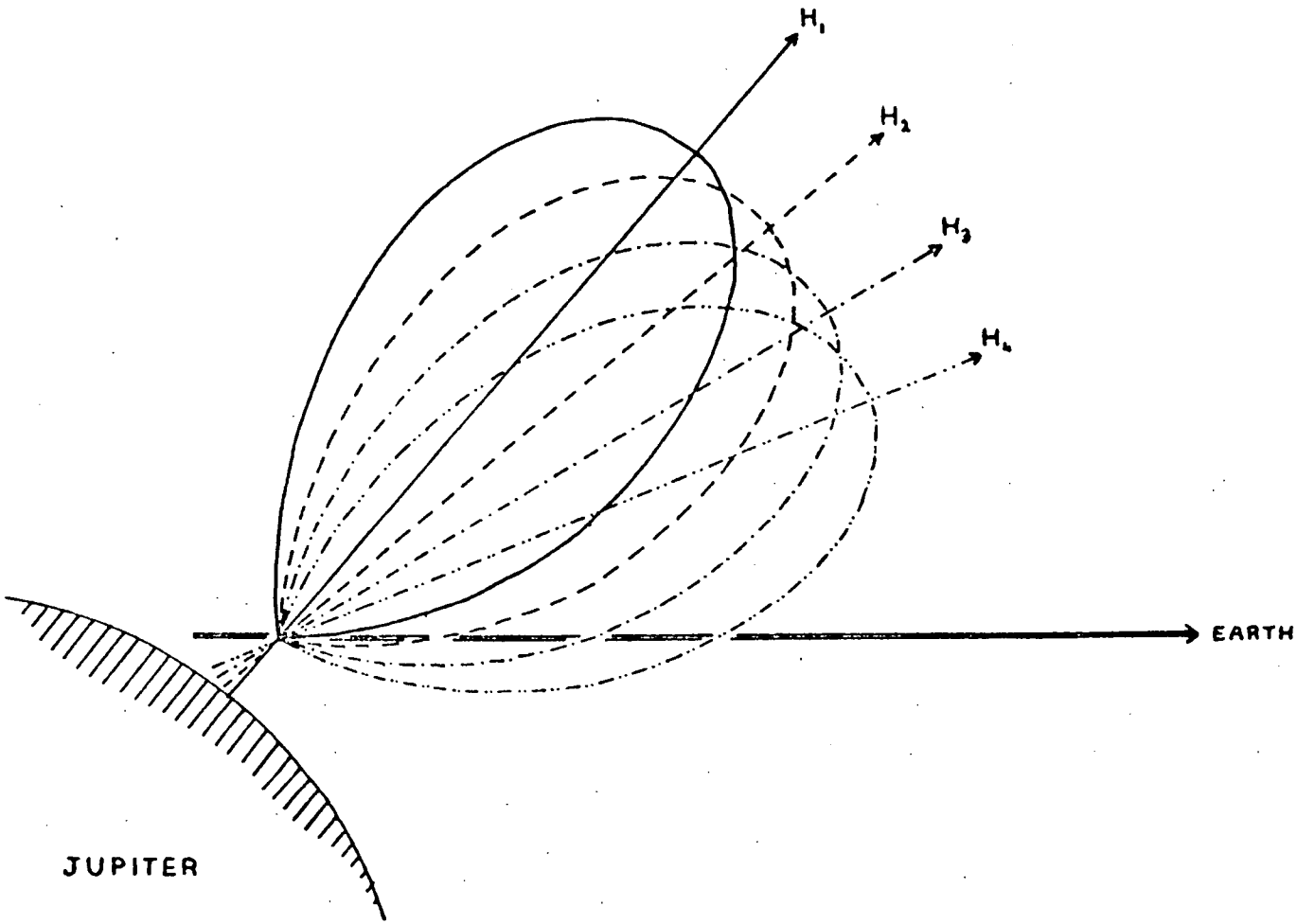


Figure 8.6 Probability of occurrence emission cones are illustrated for four different inclinations of Jupiter's magnetic field. The relative probability of occurrence at any time is given by the intersection of the cones with the Earth-Jupiter line.

magnetic longitudes are assumed to be equally probable. The characteristics of the model are such that the probability of occurrence and power of the emissions depends on the angle between the observers line of sight and the axis of the emission cone. As the cone angle is fixed for a given distribution of electron streams the probability of occurrence as a function of longitude can only be varied by changing the inclination of the magnetic field (Figure 8.6).

The main peak in the longitude profiles for frequencies above 15 MHz was explained by a local dip anomaly in Jupiter's magnetic field. The maximum tilt of the field lines from those of a dipole necessary to account for the observations was found to be about $15^{o}$.

As Jupiter revolves about the Sun the tilt of its rotation axis $D_E$ to the Earth-Jupiter line changes cyclically. This results in a cyclic variation in the range of magnetic latitudes from which emission can be seen at any time. Hence if the longitude of the maximum dip deviation changes with magnetic latitude we would expect to see a cyclic change in the longitude of the corresponding emission region. The change in main source position can then be interpreted as a change in longitude of the maximum dip angle deviation with magnetic latitude. The dip anomalies needed at different latitudes to explain the observed main source positions are shown in Figure (8.7).

The consequence of this explanation of the main source position drift is that each of the four individual sources in the longitude profiles could change positions in different ways depending on the local dip anomalies. The sources associated with the

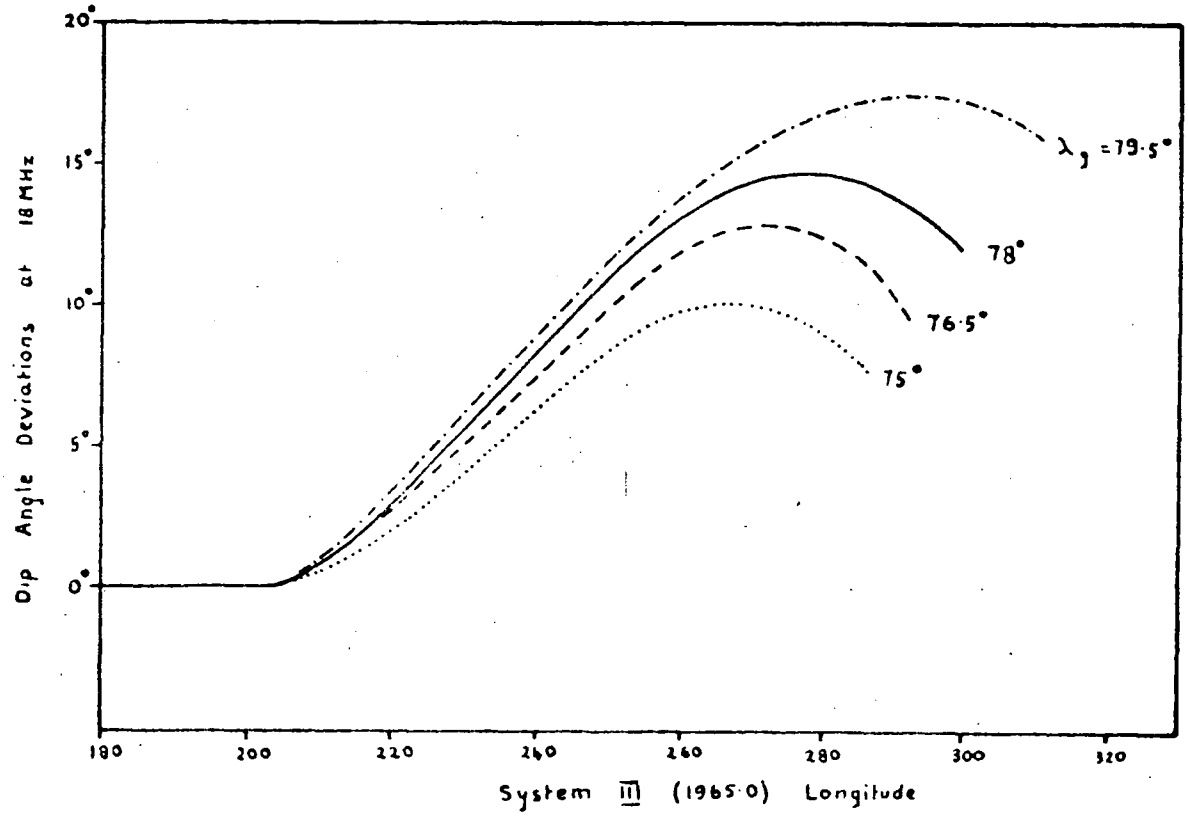


Figure 8.7 The proposed dip angle deviations at 18 MHz in the vicinity of source A are plotted for various values of $\lambda_g$, the magnetic latitude at which the undisturbed field line intersects the surface of Jupiter.

magnetic poles would not be expected to change their positions appreciably. The small in-phase variation of source C can be explained on the basis of overlapping by source A, which is much larger and has a larger position variation. The earlier of the two B sources could change in position with appropriate dip angle deviations similar to those for source A. However the present observations are not sufficiently accurate to demonstrate any such variation.

The different rotational periods determined by Dulk (1965) by analysing spectral data in different ways may be explained on the basis of the above discussion. The correlation or comparison of longitude profiles give periods which are dominated by the period of the strongest source A in the longitude profiles. Comparison of individual features on dynamics spectra on the other hand are biassed in favour of the early B source as this is the region where the majority of repeatable dynamic spectra are obtained. We have seen that there is no need for the periods of sources A and B to be the same according to the cyclotron theory. These two types of observation give information about the configuration of Jupiter's magnetic field in two different longitude ranges.

Duncan (1967) has recently done a statistical analysis of Jupiter data at frequencies above 20 MHz (where possible) for the period 1957-66. He has found that the commencement of main source storms has recurred with a period which has been constant from 1951-1966. The period being $9^h\ 55^m\ 29.70^s \pm 0.05^s$, in good agreement with that obtained by Gulkis and Carr.

The cyclotron theory predicts that the width in longitude of an emission peak depends on the penetration of the observers

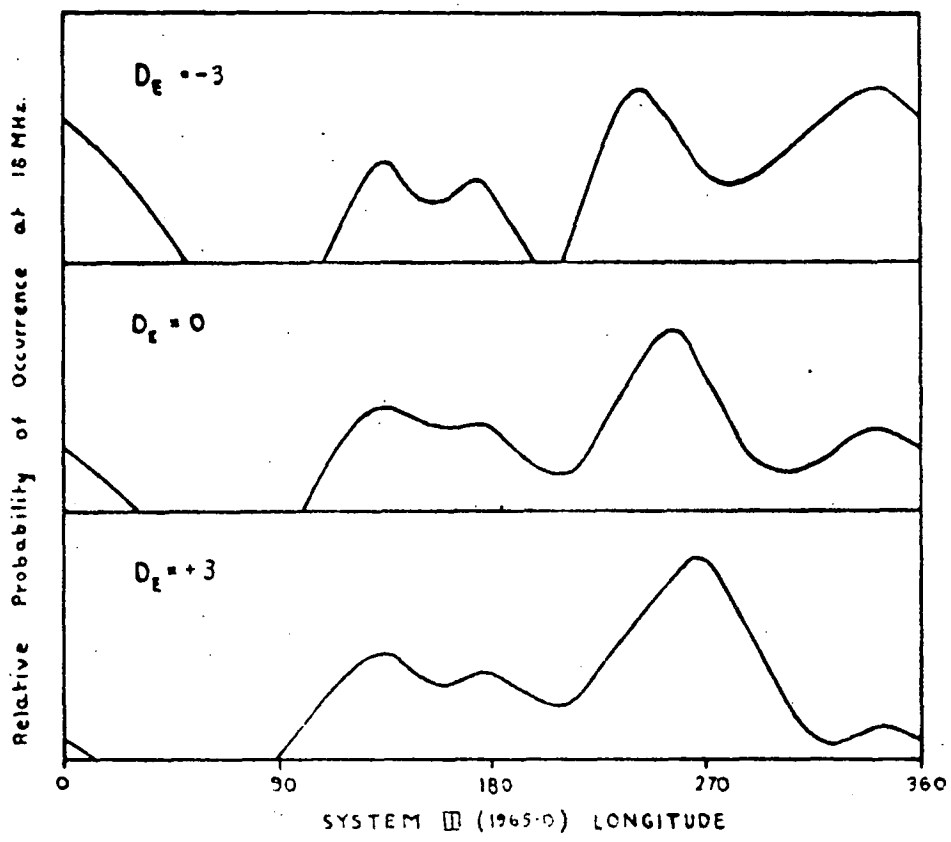


Figure 8.8 Theoretical profiles showing the relative probability of occurrence at 18 MHz are plotted for various values of $D_E$, the inclination of Jupiter's rotation axis to the Earth-Jupiter line.

line of sight into the emission cone. The width of the emission regions then vary cyclically with $D_E$. Figure (8.8) shows probability of occurrence longitude profiles of source A for various values of $D_E$. A most interesting feature of these profiles is that the increase in width of the peak is just sufficient to compensate for the change in longitude of the peak. Hence the leading section of the source always occurs at the same longitude regardless of the value of $D_E$. There is then no contradiction between the observations of Duncan and Gulkis and Carr as the starting times are exactly compensated by the change in source width. Hence the center of the emission region is the important feature and not the storm commencement. This is further emphasised by the observation of Duncan (1966) that Io's influence is sharpest for the peak in the emission region, and is not as well correlated with the commencement time.

## 8.5 References.

CARR, T.D., A.G. SMITH, H. BOLLHAGEN, N.F. SIX, Jr, and N.E. CHATTERTON (1961) Astrophys. J. 134, 105

COOPER, B.F.C., T.E. COUSINS and L. GRUNER (1964) Proc. Inst. Rad. Elec. Eng. Aust. 25, 221

DOUGLAS, J.N. (1960) Ph. D. Dissertation, Yale University

DOUGLAS, J.N. and H.J. SMITH (1963) Astron. J. 68, 163

DULK, G.A. (1965) Ph. D. Dissertation, University of Colorado

DUNCAN, R.A. (1966) Planet Space Sci. 14, 1291

DUNCAN, R.A. (1967) Planet Space Sci. 15, 1687

GULKIS, S. and T.D. CARR (1966) Science 154, 257-259

ROBERTS, J.A. and R.D. EKERS (1967) Icarus (in press)

ROBERTS, J.A. and M.M. KOMESAROFF (1965) Icarus 4, 127-156

SIMMONS, A.J. and A.F. KAY (1966) I.E.E. Conference (G.B.) Publication No. 21

SMITH, A.G., G.R. LEBO, N.F. SIX, T.D. CARR, H. BOLLHAGEN, J. MAY and J. LEVY (1965) Astrophys. J. 141, 457

# CHAPTER 9.

# THEORY OF IO'S INFLUENCE ON JUPITER'S DECAMETRIC EMISSIONS

## 9.1 Introduction.

The innermost Gallilean satellite of Jupiter, Io, has been observed to strongly modulate the intensity and probability of Jupiter's decametric emissions (Bigg, 1966; Duncan, 1966), the effect being most pronounced at frequencies greater than 30 MHz. Radiation occurs mainly from two configurations of Jupiter and Io. The first is when Io is $90^{\circ}$ from superior geocentric conjunction (S.G.C.) and Jupiter's longitude is near $120^{\circ}$, and the second when Io is $240^{\circ}$ from S.G.C. and Jupiter's longitude is near $230^{\circ}$. The observed features of the modulation have been discussed in detail in Sections (2.11) and (3.7).

Two classes of theories have been proposed to explain the modulation. The first due to Gledhill (1967 a, b) requires the radiation to be generated near Io, with the emission probabilities and frequencies depending upon the position of Io within Jupiter's magnetosphere. The second class of theories (Dulk, 1965; Warwick, 1967) requires the radiation to be generated close to the surface of Jupiter. This implies that there must exist some coupling mechansim between Io and the region close to Jupiter where the radiation is generated.

In this Chapter we give a brief discussion of the two classes of theories as they have been presented. A theory of the second type is developed which explains the observed characteristics

of the modulation.

## 9.2 Gledhill's Theory.

Gledhill has proposed a model of Jupiter's magnetosphere in which the plasma is confined to a narrow disc by the rapid rotation of the planet. He finds that on the assumption that Jupiter has a 30 gauss dipolar magnetic field tilted $10^{o}$ to the rotation axis the plane of the plasma is inclined about $7^{o}$ to the rotation axis. Contours of plasma density are shown in Figure (9.1). As the plasma disc co-rotates with Jupiter it passes across Io twice per relative rotation. Gledhill has scaled the electron density contours so that the variation of electron plasma frequency at Io matches the high frequency sections of the dynamic spectra recorded by Warwick. This leads to a maximum electron density at Io's orbit of $2.0_{10}7$/cc. The density increases inwards reaching a maximum of about $10^{8}$ or $10^{9}$/cc depending on the rates of recombination and diffusion in the lower magnetosphere.

Gledhill does not go into the details of the emission mechanism but suggests plasma radiation excited by a shock wave generated by Io's motion through the magnetosphere. To produce the observed narrow emission profiles with respect to Io's position the radiation would have to be strongly beamed in a direction normal to the magnetic field. Known beaming mechanisms tend to favour radiation along the field direction although ray tracing techniques would be needed to determine the final direction of the radiation.

The main objections to the theory arise from the extremely high density magnetosphere required to give a 40 MHz plasma frequen-

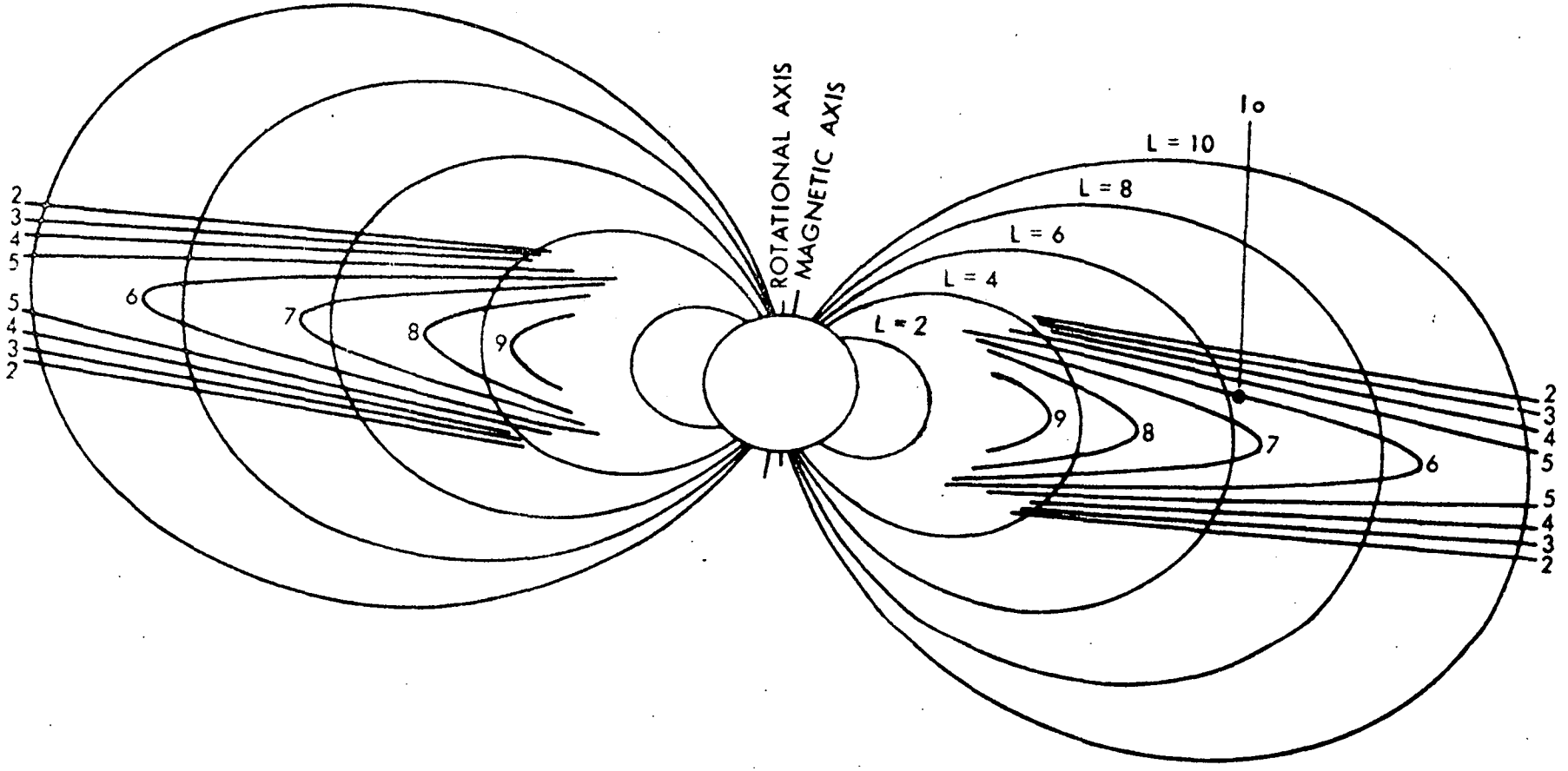


Figure 9.1 Contours of electron density in Jupiter's magnetosphere according to the theory of Gledhill (1967).

cy at Io. The calculations of Section (4.2) place an upper limit of about $5_{10}6$/cc on the electron density in Jupiter's magnetosphere while Gledhill requires densities greater than $10^8$/cc. A more reliable estimate for the maximum electron density in Jupiter's magnetosphere was obtained in Section (4.5) on the basis of Faraday rotation of the decimetric radiation, this gave a limit of about $5_{10}5$/cc. Hence we must conclude that Gledhill requires an unreasonably high density in Jupiter's magnetosphere and his model is inconsistent with other observations.

## 9.3 Coupling Theories.

The second class of theories mentioned earlier could be classified as coupling theories as they require a coupling mechanism between Io and a point near Jupiter's surface. Many different coupling mechanisms have been proposed among which the most promising are:-

hydromagnetic or electromagnetic waves, Ellis (1965)

low frequency hydromagnetic waves, Warwick (1967)

magnetic coupling along tubes of force, Piddington and Drake (1967)

ring currents, Bigg (1966)

tidal effects, Shever (1967).

The only mechanism which has been considered in any detail is the magnetic coupling of Piddington and Drake. In this model the tube of flux passing through Io is assumed to be frozen in, and hence revolves about Jupiter with Io. The motion of the base of this flux tube through Jupiter's ionosphere is assumed to excite electrons from the ambient plasma to radiate at decametric frequen-

cies. To explain the observed longitudes of emission at high frequencies the radiation must be beamed into a cone so as to be visible $75^{o}$ from the meridian plane.

The only known process which can account for the intensity of the observed emission is cyclotron radiation by moderately relativistic electrons. Cone angles of $75^{o}$ and larger can be obtained with cyclotron radiation and the general characteristics of the longitude profiles could be obtained using Piddington and Drake's theory. However the complicated changes in the location and intensity of the emission regions at low frequencies as illustrated in Figure (3.9) can not be accounted for in this way. Hence coupling by magnetic tubes of force can not be incorporated into any known theory of the decametric emissions to explain the influence of Io.

The other possibilities that we are left with for coupling mechanisms involve wave propagation in either the hydromagnetic or electromagnetic modes. We will now examine these possibilities and derive a detailed theory to explain the influence of Io on Jupiter's decametric emissions.

## 9.4 The Cyclotron Resonance Theory of the Io Effect.

This theory falls into the second class of theories described above and hence could be called a coupling theory. There are three processes which must take place in any such theory, they are:-

(a) The generation of a disturbance in the vicinity of Io.

(b) The propagation of this disturbance from Io to a

point near Jupiter where the decametric emission originates.

(c) The coupling of the disturbance to the outgoing decametric emissions.

The cyclotron theory has been shown to successfully explain the observed properties of Jupiter's decametric emissions not directly associated with Io. It is therefore reasonable to assume that the magnetic field configuration of Jupiter as derived from the cyclotron theory dominates the radiation properties as a function of system III longitude. Superimposed on this variation due to the field configuration must be another variation directly attributable to the position of Io. Hence in investigating any theory of Io's influence it is reasonable to start with the model of Jupiter's magnetosphere derived from the cyclotron theory. The model obtained consists basically of a centered dipole, polar field strength 30 gauss, with dip anomalies close to the surface in certain longitude ranges. The variation of electron density with height was obtained for magnetic field lines intersecting the planet at a magnetic latitude of $75^{\circ}$. This variation of density with height was fitted to the magnetosphere proposed by Melrose (1967) to give a trial model.

This theory of Io's modulation is based on coupling by low frequency electromagnetic waves, for which a large number of possible generating mechanisms exist as well as several possible propagation modes. We will examine propagation through the model magnetosphere outlined above in an attempt to restrict the number of possible modes. Since the Io effect is predominant at frequencies above 30 MHz we will define the coupling region as that part of Jupiter's

magnetosphere where the gyrofrequency exceeds 30 MHz.

Tiuri (1967) has discussed the similarities between the effects of artificial satellites in the Earth's magnetosphere and the effect of Io. He finds that artificial satellites effect the orbits of electrons many thousands of km away, evidently by the propagation of a disturbance generated by the satellite to the auroral zones. The effect is most pronounced when the satellite is near its maximum magnetic latitude. The marked similarities between the effect of artificial satellites and the effect of Io provide circumstantial evidence for the existence of some coupling mechanism in the case of Io.

## 9.5 Propagation of Electromagnetic Waves Between Io and Jupiter.

The model magnetosphere we have chosen is characterised by a monotonic decrease in the magnetic field strength and the electron density as we move away from the surface of Jupiter. The resultant gyrofrequency at Io is about 195 kHz and the corresponding plasma frequency is about 350 kHz, corresponding to a density of about 1500/cc. The variation of refractive index with frequency near Io is illustrated in Figure (9.2) for a wave normal angle of $30^{o}$.

The two high frequency modes, i.e. the o-mode above $f_o$ and the x-mode above $f_x$ are not suitable as propagation modes for this effect. The reason is that in order to propagate as far as the coupling region, the propagation frequency would have to exceed 30 MHz for the x-mode and about 2 MHz for the o-mode. Both these frequencies are many times greater than any resonant frequency of the plasma at Io, and hence they would have to be generated as high har-

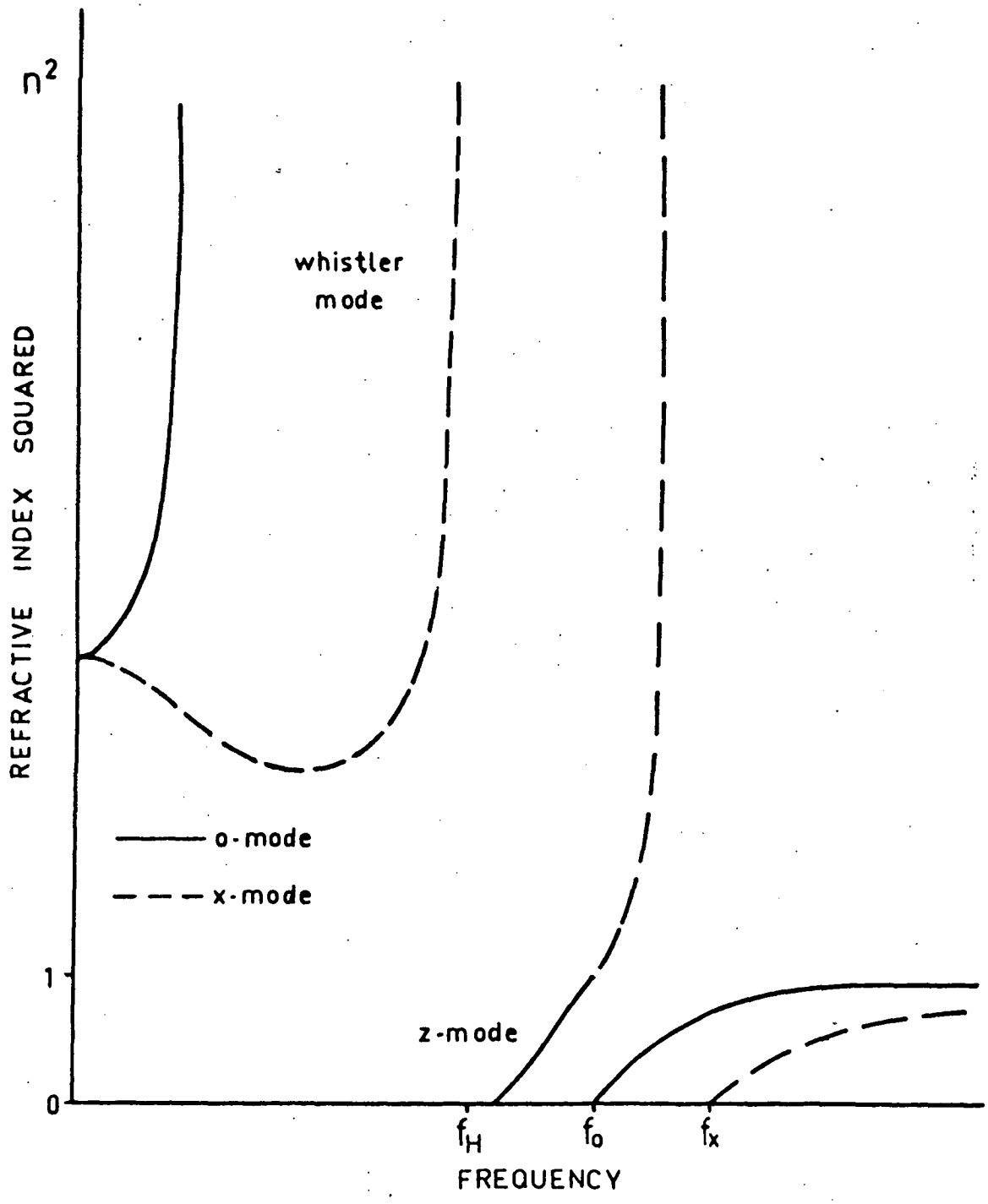


Figure 9.2 Variation of refractive index with frequency in the neighbourhood of Io. Wave normal angle $30^{\circ}$.

monics. If this were to happen we might expect even higher harmonics to be generated, which could propagate directly to Earth and would be seen as a series of narrow band emissions separated by several hundred kHz. No such emission has been observed from the direction of Jupiter. Furthermore generation at high harmonic numbers requires ultra-relativistic particles which are unlikely to be accelerated by Io.

The next branch of the refractive index surfaces is the x-mode branch between $f_x$ and $f_o$, occupying the frequency range 350 kHz to 460 kHz at Io. This range disappears when the propagation frequency equals the plasma frequency. Hence radiation cannot reach the coupling region on this mode.

The whistler mode is the x-mode branch of the curves below the plasma frequency and gyrofrequency. This occupies the frequency range up to 190 kHz at Io and up to 2 MHz near the coupling region. Clearly any radiation generated in this mode at Io can propagate inwards to the surface of Jupiter.

Another branch of the refractive index curves is the z-mode branch, which is the o-mode section in the frequency range between $X = 1$ and $X = 1 + Y$ where $X = f_o^2/f^2$ and $Y = f_H/f$. At Io this range is approximately 250 - 350 kHz, while in the coupling region the appropriate frequency range is 110 kHz - 2 MHz. These frequency ranges overlap so that propagation appears possible on this mode.

The remaining branch of the curves is the o-mode branch below the ion-gyrofrequency. This corresponds to frequencies below 100 Hz and is in the hydromagnetic range. Waves can propagate from Io to Jupiter in this mode.

There are only three modes out of the six considered by which radiation may propagate between the desired regions. In order to decide which of these is the most suitable we will have to examine the generation and coupling of the waves.

## 9.6 Generation of Electromagnetic Waves Near Io.

The three main processes which have been discussed previously are possible mechanisms for generation of electromagnetic waves near Io; they are cyclotron radiation, Cerenkov radiation and plasma radiation. Cyclotron radiation may be generated in either the forward or backward normal modes or the forward anomalous mode. The frequency and wave normal angle of emission must simultaneously satisfy the Appleton-Hartree equation $n = n(X, Y, \theta)$ and the Doppler equation

$$n = \frac{1 - s\gamma Y}{\beta \cos\theta \cos\varphi}$$

where the harmonic number $s = 1$ for the normal modes and $s = -1$ for the anomalous mode. The solutions of these equations are illustrated diagrammatically in Figure (9.3). Cerenkov and plasma radiation are generated at frequencies and wave normal angles which simultaneously satisfy the refractive index equation and the Cerenkov condition

$$n = \frac{1}{\beta \cos\theta \cos\varphi}$$

These solutions are also illustrated in Figure (9.3). The distinction between the generation of longitudinal plasma waves and transverse electromagnetic waves depends upon the relative velocity of the radiating electrons and the R.M.S. thermal velocity of the ambient plasma electrons.

Solutions exist on the whistler mode for backward and

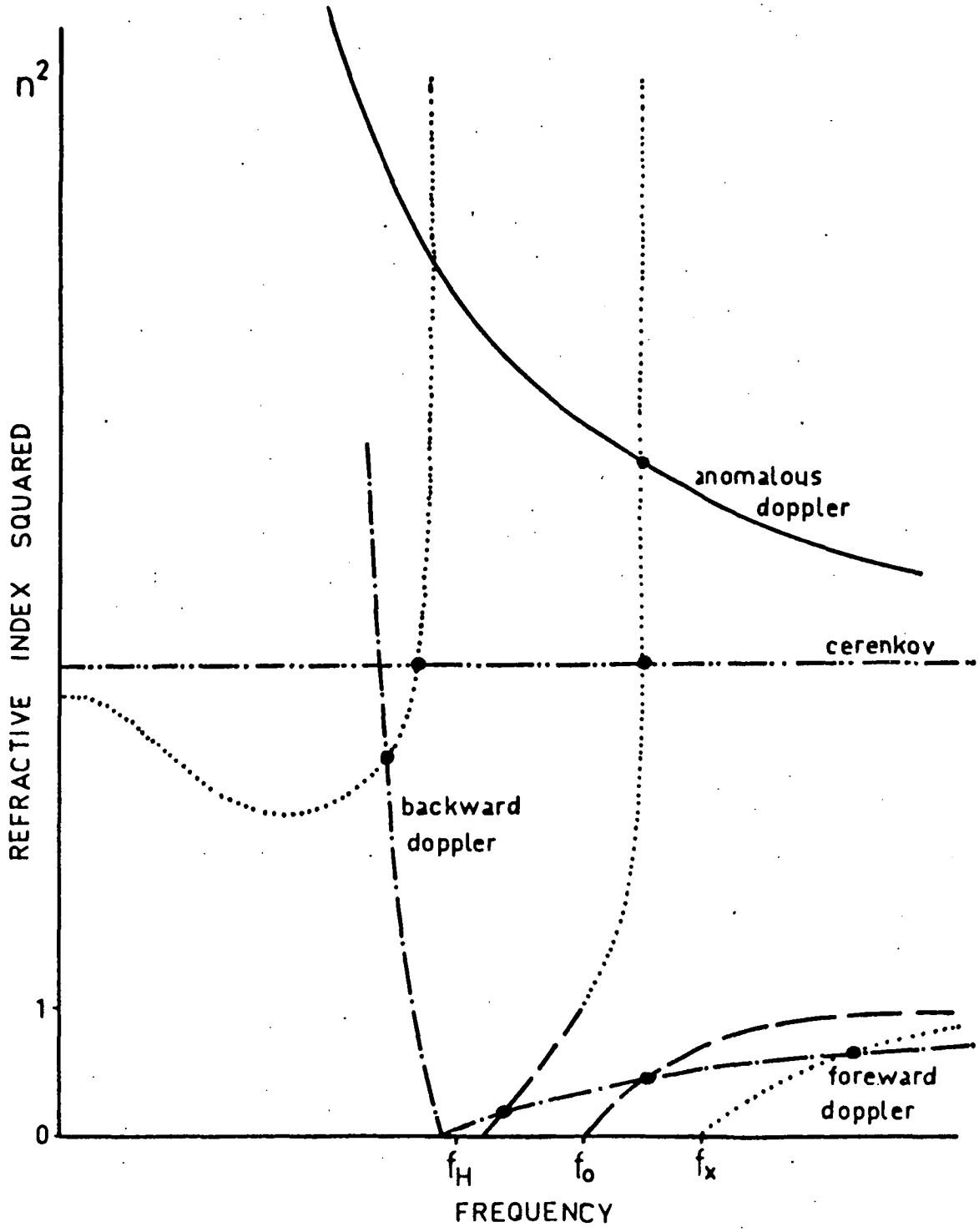


Figure 9.3 Graphical solution of the refractive index equation and Doppler and Cerenkov conditions near Io.

anomalous Doppler radiation, Cerenkov and plasma radiation. On the z-mode however the only possibilities are Doppler radiation, or plasma radiation initially generated on the whistler mode being transformed into electromagnetic waves on the z-mode by Rayleigh scattering.

The generation mechanisms which are available do not eliminate any of the possible propagation modes, although it appears to be far easier to generate radiation on the whistler mode.

## 9.7 Coupling of Low Frequency Waves to the Outgoing Decametric Emission.

The combination of the requirements for the generation and propagation of radio waves from Io to Jupiter limits the possible modes to the whistler mode, the z-mode and the ion cyclotron mode. In all cases the frequency of emission is likely to be about 200 kHz or below. The effect of Io is however most predominant at frequencies above 30 MHz, hence we require a mechanism whereby waves at frequencies less than 200 kHz can influence waves at frequencies greater than 30 MHz.

The analysis of the previous Chapters indicates that Jupiter's decametric emissions are best explained by cyclotron radiation from moderately relativistic streams of monoenergetic electrons. The coupling mechanism could therefore take the form of an interaction between the low frequency incoming wave and an electron stream; the wave supplying energy to the stream to convert it from a non-radiating condition to a radiating condition.

A suitable mechanism has been proposed to explain the interchange of energy between V.L.F. waves and high energy electron streams

in the Earth's exosphere. This process is referred to as the gyroresonant interaction (Brice, 1964; Cornwall, 1964; Gendrin, 1965). The requirements for the gyroresonant interaction to take place between a beam of particles and waves of the two polarisation modes are:-

(a) The wave frequency and particle velocities must simultaneously satisfy the Doppler equation and refractive index equation.

(b) The sense of polarisation of the wave and particle stream must be the same.

To understand the second point we can define the polarisation of the particles and waves as follows. An electromagnetic wave is R.H. circularly polarised if the field vector rotates clockwise looking along the field. A particle is defined to be R.H. circularly polarised if it circles to the right looking along the field. Hence electrons are right-hand polarised and protons are left-hand polarised.

In this normal mode of interaction particles and waves of the same polarity can interact, i.e. electrons and whistler mode waves or protons and z-mode or ion cyclotron mode waves. There is an exception to this rule however which occurs when the particles have a superluminal motion. In this case electrons and L.H. waves or protons and R.H. waves could interact, corresponding to the anomalous Doppler effect.

The condition for an electron z-mode interaction to take place is that the velocity of the electrons exceeds the phase velocity of the wave. However the phase refractive index for the z-mode is always less than unity so that this interaction is impossible.

The only interaction remaining is the normal whistler mode

electron interaction in which the particles and waves are travelling in opposite directions. Hence the generation, propagation and coupling mechanisms rule out all combinations except whistler mode waves which interact with outgoing electron streams.

No adequate theory of the quantitative effect of the incoming signal on the electron streams is available. However observations made by Kimura (1968) show that V.L.F. emissions in the Earth's magnetosphere can be triggered by a low power transmitter ($\simeq$ 100 watts). The actual power at the triggering point must have been significantly lower than 100 watts, hence we may conclude that the intensity of the incoming signal need not be large for significant coupling to take place.

## 9.8 Generation of Whistler Mode Waves Near Io.

The generation of waves in the whistler mode near Io requires the existence of streams of energetic electrons. Since Io is the source of the modulation of the decametric emissions it is reasonable to assume that Io must accelerate these electron streams in some way.

The main source of energy associated with Io is its kinetic energy due to its rapid rotation around Jupiter. Io's linear velocity is approximately 17 km/sec, however since Jupiter and Io are both moving in the same direction, Io has a relative velocity of approximately 56 km/sec in the opposite direction.

If the electron density at Io's orbit is $N_e$ /cc, then Io interacts with $N = N_e \pi r^2 V$ electrons/sec where r is the radius of Io and V is its velocity relative to the magnetosphere.

Then $N = 5_{10}23\ N_e$ electrons/cc.

At Io the electron gyrofrequency is about 190 kHz while the electron-ion collision frequency is given by $\nu = 31\ N_e\ T^{-3/2}$ Providing the electron density is less than about $10^5$/cc the gyrofrequency will be much greater than the collision frequency for reasonable temperatures. Hence the conductivity along the magnetic field will be much greater than transverse to it, and electrons disturbed by Io's progress through the magnetosphere will be directed along the magnetic field.

This can be verified by the alternative argument. The energy density of the magnetic field at Io is

$$\frac{B^2}{8\pi} = 1.4_{10}{-4}\ \text{erg/cc}$$

while the kinetic energy density associated with the particles disturbed by Io is

$$\tfrac{1}{2}\ M_i\ V^2\ N_e = 2.4_{10}{-11}\ N_e\ \text{erg/cc}$$

where $M_i$ is the mass of the ions. Hence provided $N_e \ll 10^7$ the energy density of the field dominates and the particles are constrained to move along the field.

The minimum velocity that can be obtained by these particles must be sufficient to move them out of Io's way. This implies a minimum mean velocity of 54 km/sec for both the electrons and ions, however after a short period of time equipartition of energy will be approached and the electron velocities may be many times higher than the proton velocities. In this way Io could accelerate electrons to velocities of several hundred km/sec.

If we assume the electron density at Io's orbit to be 1500/cc then Io will disturb approximately $8.5_{10}26$ electrons and ions

per second. The kinetic energy imparted to these particles is

$$= 2.2_{10}16 \text{ erg/sec}$$

$$= 2.2_{10}9 \text{ watts}$$

Once equipartition is attained approximately half this energy will have been given to the electrons. Hence the maximum power that can be transferred from Io to the coupling region is of the order of $10^9$ watts.

During a noise storm the power emitted at Jupiter is in excess of 100 watts/Hz bandwidth of the emission. The radiation that is most strongly effected by Io occurs above 30 MHz where the active bandwidths are about 2 MHz. Hence the Io related power emitted by Jupiter is about $2_{10}8$ watts, slightly lower than the maximum power that could be supplied by Io. We conclude that it is unlikely that Io could concentrate enough power in a particular region to accelerate the electron streams responsible for the decametric emission, however the power could be sufficient to strongly modify the energy distribution of existing electron streams.

There are three possible ways in which these electron streams can radiate; backward Doppler radiation, anomalous Doppler radiation and Cerenkov radiation. The velocity of the electron stream is low ($\simeq$ 100 km/sec) so that the refractive index would need to be correspondingly high. The attenuation of the rays in the cold magneto-plasma approximation depends upon the refractive index, so it is convenient to use the generation mechanism which gives the lowest refractive index. We have

$$n = \frac{Y - 1}{\beta_{\parallel} |\cos \theta|} \qquad \text{backward Doppler radiation}$$

$$n = \frac{1 + Y}{\beta_{\parallel} \cos \theta}$$ anomalous Doppler radiation

$$n = \frac{1}{\beta_{\parallel} \cos \theta}$$ Cerenkov radiation

The refractive index will clearly be greatest for anomalous Doppler radiation, while for $Y \gtrsim 2$ the values of the refractive index for backward Doppler radiation and Cerenkov radiation will be about equal. There is no firm reason for discounting any of the radiation processes and they are all likely to lead to similar results. In order to discuss the emission in more detail we will confine our attention to backward Doppler radiation, although this is purely an arbitrary choice.

The power radiated per electron in this process is given by the Eidman equation

$$W = W(n, X, Y, \theta, \beta, \varphi)$$

and the amplification coefficient in a monoenergetic stream is given by (Fung, 1966)

$$\eta = \left| \frac{\mathrm{Im}(\delta)}{\omega_H} \right| = \eta(n, X, Y, \theta, \beta, \varphi, \sigma)$$

where $\sigma$ is the ratio of stream density to ambient plasma density. The power radiated per electron is plotted in Figure (9.4) for various combinations of electron velocity and pitch angle. The corresponding values of the relative growth rate are plotted in Figure (9.5).

For small pitch angles the power W is radiated into a small range of wave normal angles near $\theta = 90^{\circ}$. As the pitch angle is increased the range of wave normal angles increases (Figure 9.4a) until at $\varphi = 85^{\circ}$ a significant amount of power is radiated at wave

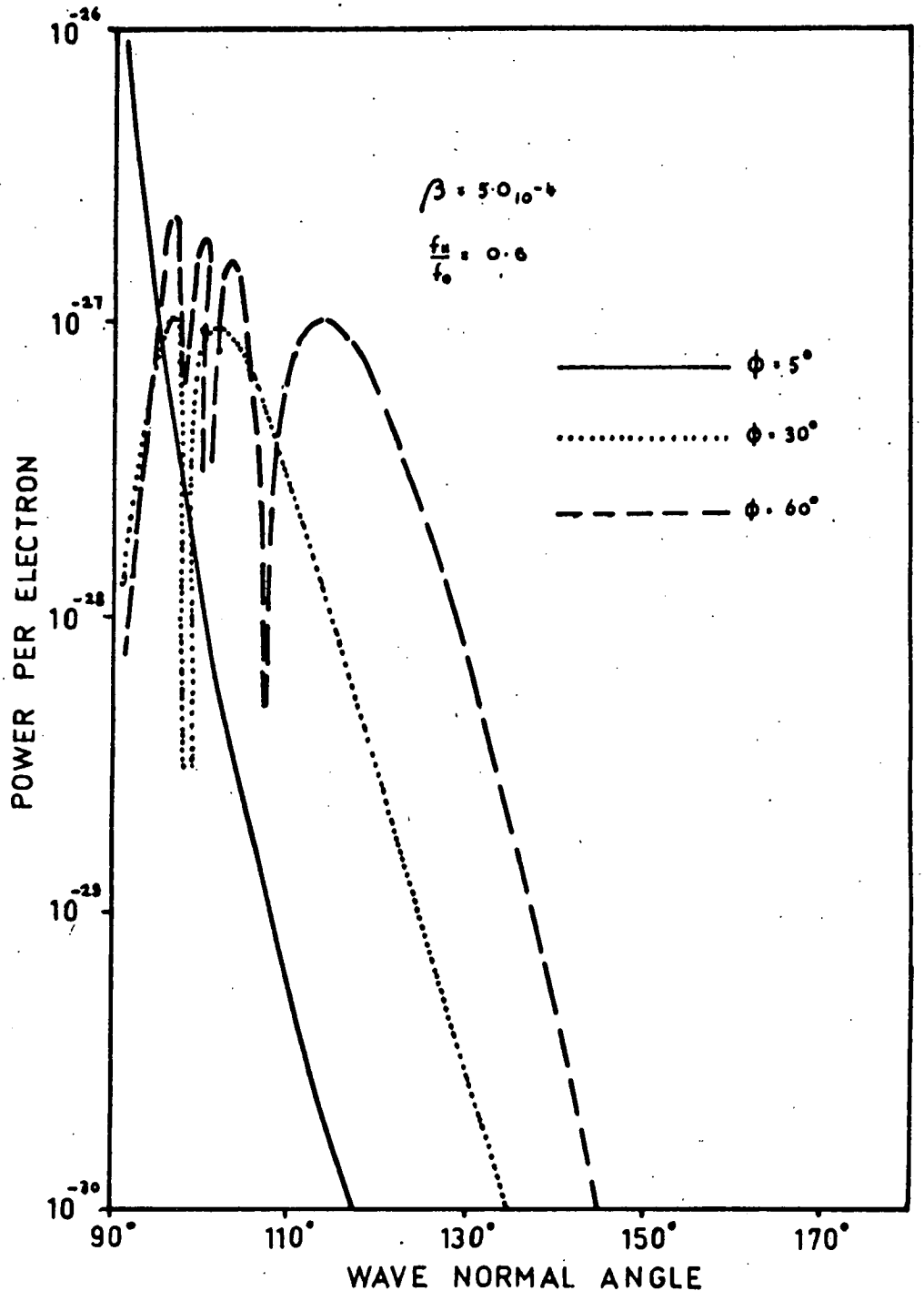


Figure 9.4a Power radiated by a single electron as a function of wave normal angle for various pitch angles.

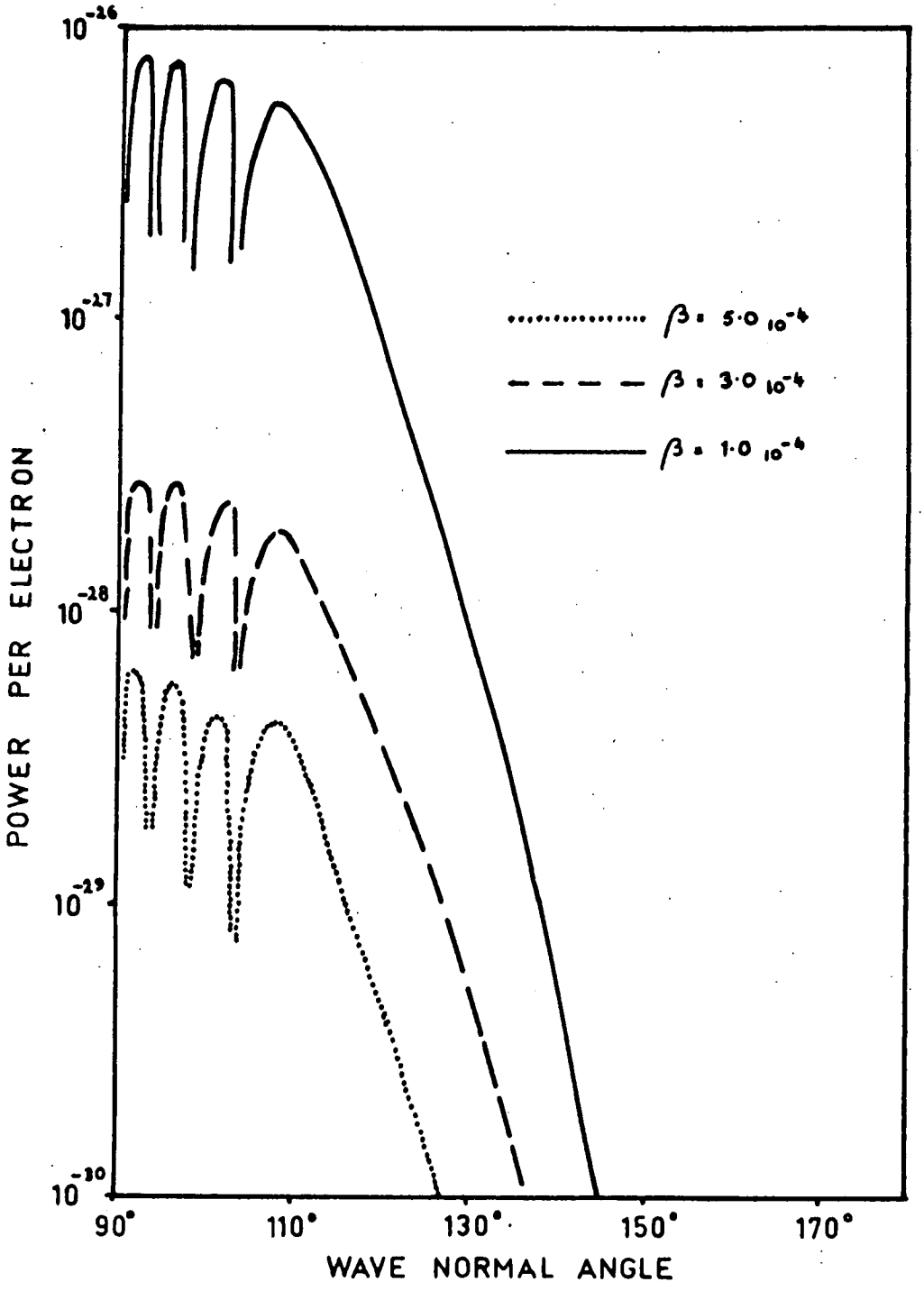


Figure 9.4b Power radiated by a single electron as a function of wave normal angle for various electron energies.

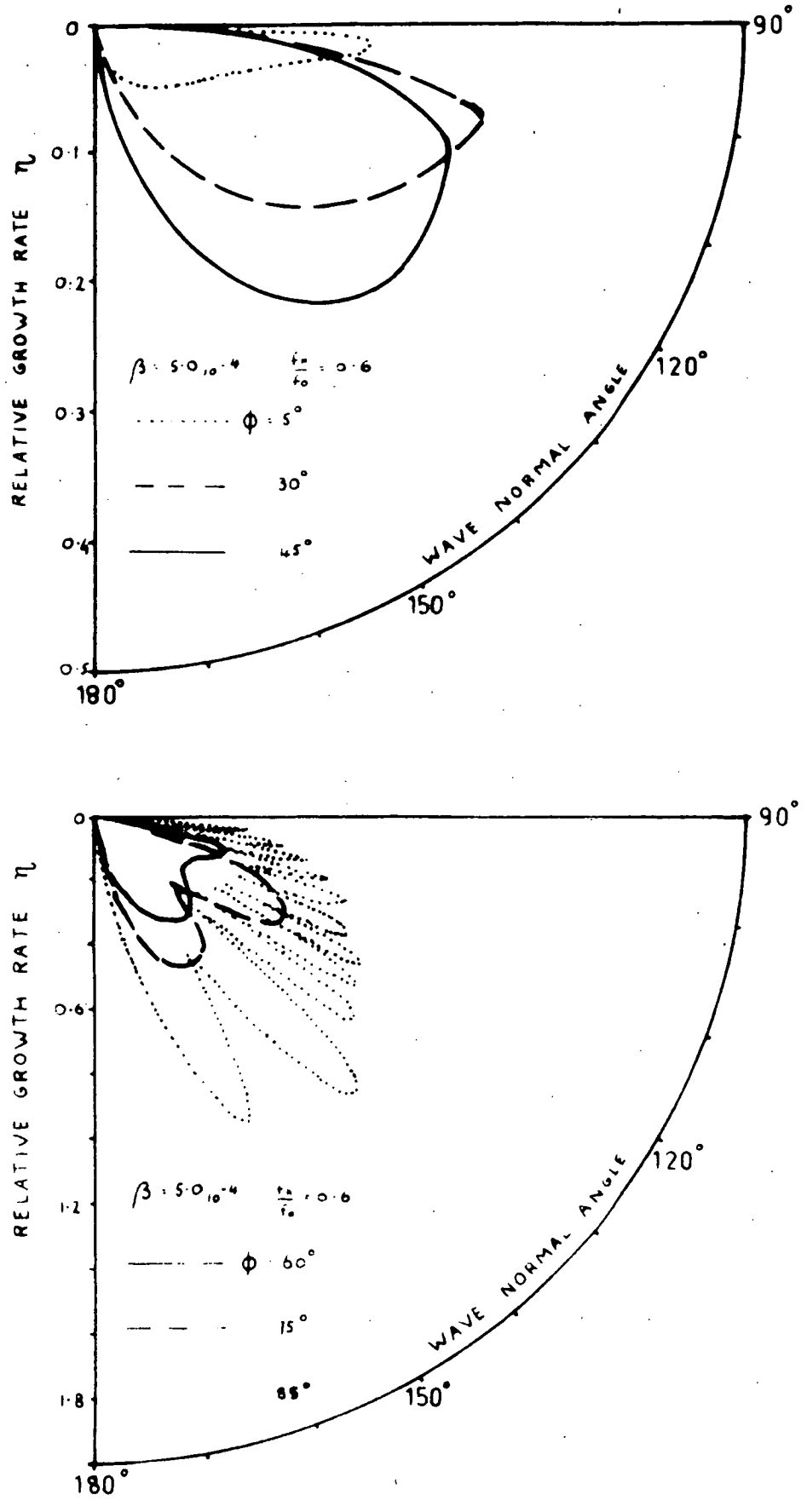


Figure 9.5a Polar diagrams of the relative growth rate as a function of wave normal angle for various electron pitch angles.

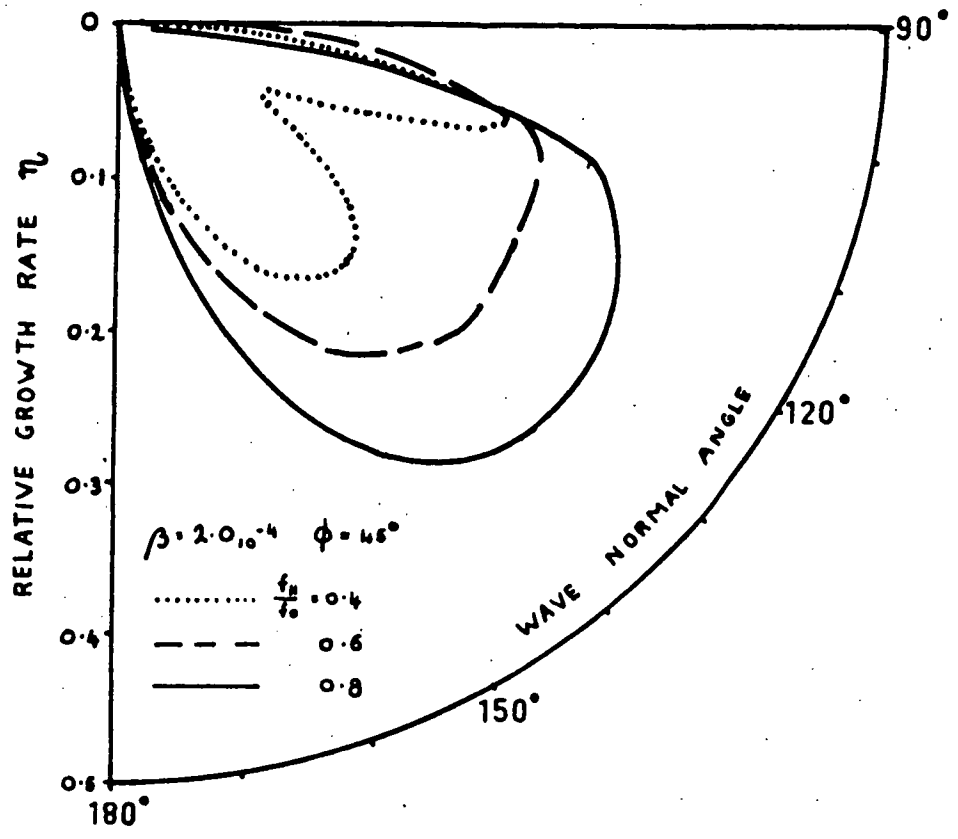


Figure 9.5b Polar diagram of the relative growth rate as a function of wave normal angle for various values of $f_H/f_o$.

normal angles above $150^{\circ}$. The actual maximum value of the power per electron is not a strong function of the pitch angle, although there is a minimum near $\varphi = 45^{\circ}$. The form of the variation of W with $\theta$ does not change with electron velocity between 30 km/sec and 150 km/sec, Figure (9.4b), but the value of W increases as $\beta$ decreases.

The wave normal angle at which the relative growth rate $\eta$ is a maximum increases from close to $90^{\circ}$ for small pitch angles to about $135^{\circ}$ at $\varphi = 85^{\circ}$. The maximum value of $\eta$ increases with $\varphi$ over this range, whereas the wave normal angle for maximum growth and the maximum value of $\eta$ do not vary with electron velocity in the range specified above.

The growth rate increases with the parameter $f_H/f_o$, while the wave normal angle of maximum growth remains constant. For some combinations of $f_H/f_o$ and $\varphi$, $\eta$ shows a large number of maxima at various wave normal angles, although their number and position change rapidly with small changes in the parameters.

The form of the curves of W and $\eta$ as a function of wave normal angle indicates that a maximum in the power radiated can be obtained at any wave normal angle by suitable choice of the parameters. However there is a tendency for the maximum to occur in the range $110^{\circ}$ to $150^{\circ}$ for values of $f_H/f_o$, $\beta$ and $\varphi$ likely to be associated with the electron streams excited by Io.

## 9.9 Limitations on the Ray Paths.

The most noticeable feature of Io's influence on Jupiter's decametric emissions is the modulation of the occurrence probability and intensity of the radiation as shown in Figure (9.6) from Bigg

(1964). The emission is enhanced when Io is in two positions about $90^{\circ}$ and $240^{\circ}$ from S.G.C. respectively. This implies that the sources are asymmetrically arranged with respect to the Earth-Jupiter line. One source is about $90^{\circ}$ earlier than this line and the other is about $60^{\circ}$ beyond it. The emission near Io must occur in a cone about the magnetic field direction and because of the symmetry of the magnetosphere the magnetic longitudes of the points of arrival of the rays at Jupiter will be symmetric about the longitude of emission. If the rays take an appreciable time to propagate from Io to Jupiter, Io will have changed its position in the magnetosphere by the time the rays arrive at Jupiter. Hence at the time of arrival of the rays at Jupiter, which in turn corresponds to the time of emission from Jupiter, the position of Io appears asymmetrical with respect to the arrival longitudes of the rays. This situation is illustrated diagrammatically in Figure (9.7). Io moves relative to Jupiter's magnetosphere at about $27.5^{\circ}$ per hour, hence to produce the required asymmetry the propagation time must be approximately 33 minutes. The radiation from Io must then intersect the coupling region $75^{\circ}$ either side of the position of Io at the time of emission.

The cyclotron theory of the decametric emission requires the emission to originate from electron streams that move along field lines which intersect the surface of Jupiter between magnetic latitudes $75^{\circ}$ and $80^{\circ}$. The emitted frequencies in the cyclotron theory are about 10% higher than the local gyrofrequency so that coupling must take place on the $75^{\circ}$ to $80^{\circ}$ field lines where the gyrofrequency exceeds 30 MHz.

We can now summarise the requirements for the ray paths

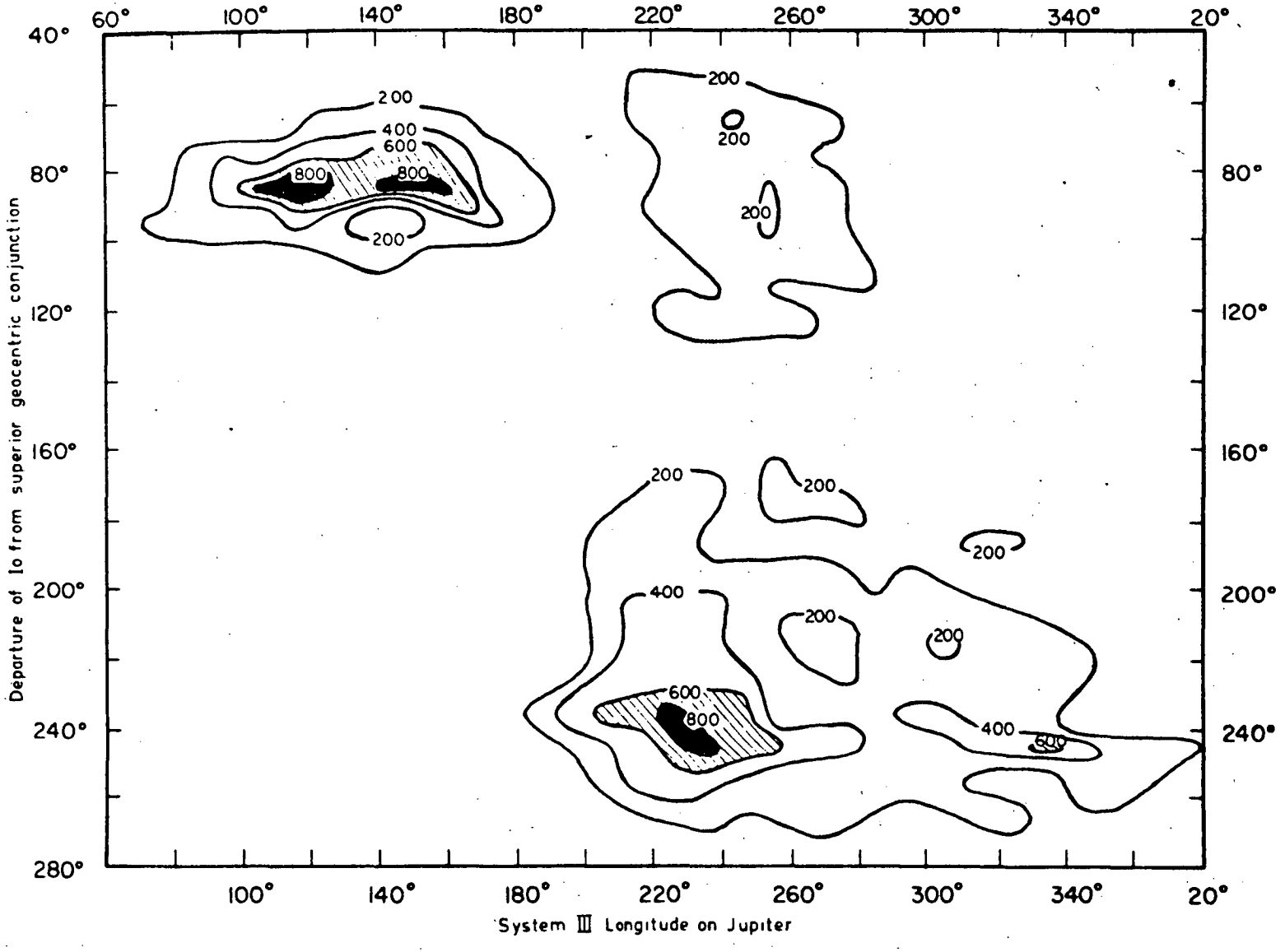


Figure 9.6 Contours of Jupiter's emission as a function of Io's position and Jupiter's longitude. (Bigg, 1964)

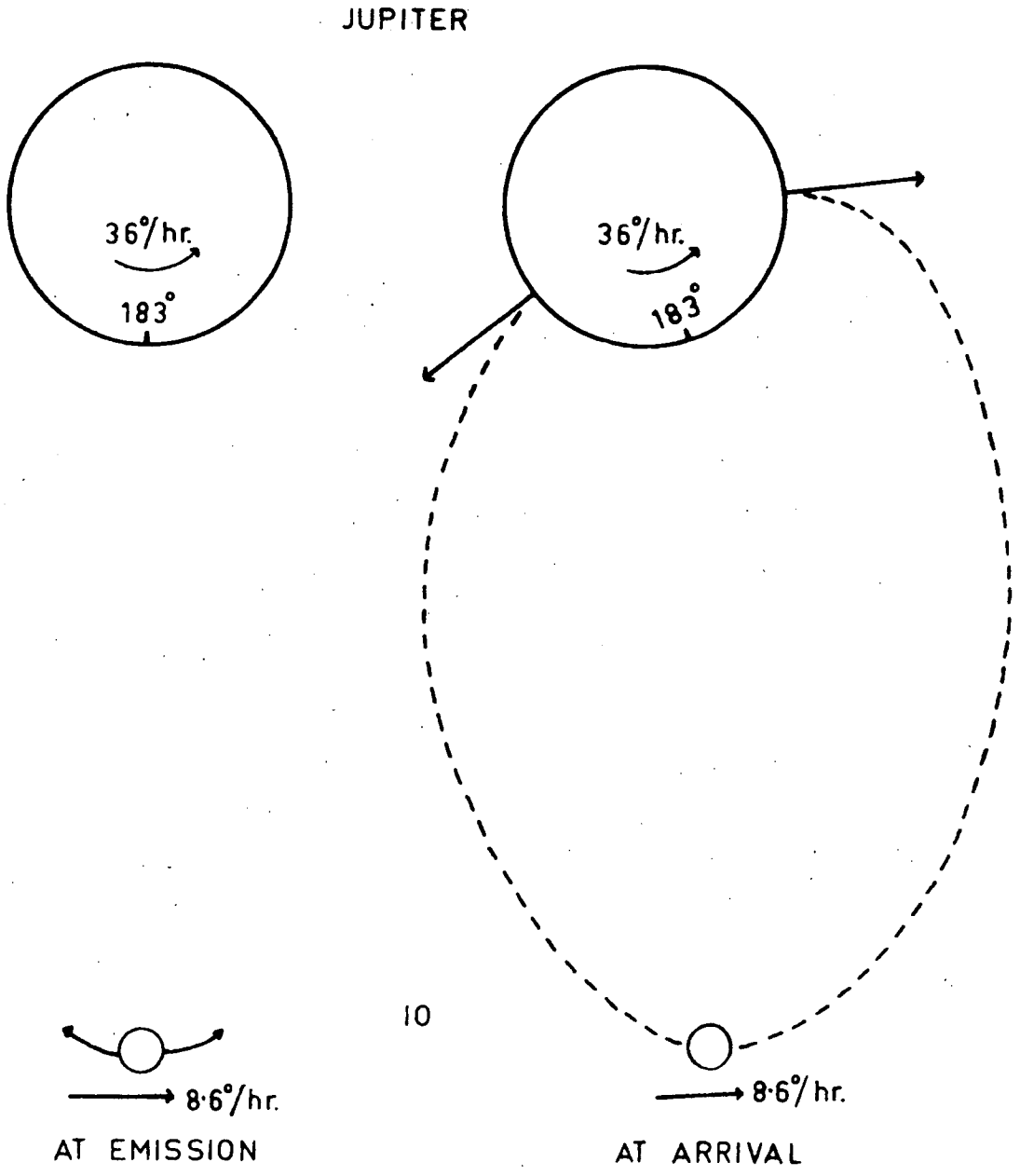


Figure 9.7 Diagrammatic representation of the orientation of Jupiter and Io at the time of emission from Io and arrival at Jupiter approximately 33 minutes later.

between Io and Jupiter as follows:-

(a) The rays must transmit the majority of their energy into the coupling region at points approximately $75^{\circ}$ of magnetic longitude each side of the longitude of Io at the time of emission.

(b) The transit time of these rays from the emission point near Io to the coupling region must be approximately 30 minutes.

(c) The energy transported to the coupling region must depend upon the magnetic longitude of Io, being a maximum when Io is adjacent Jupiter's north magnetic pole.

(d) The frequency and wave normal angle of the ray on arrival at the coupling point must be such that the ray can exchange energy with electrons in the energy range 30 - 250 kev.

(e) The rays should be emitted with wave normal angles in the range $110^{\circ}$ to $150^{\circ}$.

## 9.10 Propagation of Whistler Mode Waves in Jupiter's Magnetosphere.

Ray tracing in Jupiter's magnetosphere is complicated by the fact that the magnitude and direction of the field change continuously as does the electron density gradient. The only way in which the path of a ray can be determined in such a medium is by a full scale ray trace, which involves the simultaneous solution of six differential equations (the Haselgrove equations). The details of

this ray tracing method as applied to Jupiter's magnetosphere are given in Appendix A.

The conditions to be satisfied for generation by low energy electrons in the whistler mode imply that the refractive index should be high. In these circumstances the refractive index surfaces are relatively simple and we can make some general deductions about the path of the ray. As the ray penetrates closer to the surface of Jupiter the magnetoionic variables X and Y increase in value, and hence we pass in order through the refractive index surfaces shown in Figure (9.8a). The surfaces corresponding to the region close to the surface of Jupiter are very nearly straight lines normal to the magnetic field direction. Hence regardless of the direction in which a ray leaves Io it tends to propagate more closely along the magnetic field as it gets closer to Jupiter.

For wave frequencies below the ion-plasma frequency the refractive index surfaces become closed, and tend to become circles with a radius corresponding to the Alfven velocity (Figure 9.8b). Hence if the wave is propagating where the refractive index is much greater than that corresponding to the Alfven velocity, there is a reflection point in the neighbourhood of the ion-plasma frequency. For the model magnetosphere we are using this limits the minimum propagation frequency to about 60 kHz.

The exospheric model is based on that derived by Melrose (1967). The exosphere is divided into two regions with a boundary defined by

$$r_b = \left\{ \frac{7.76\, r}{\cos^2 \lambda} \right\}^{\frac{1}{4}}$$

$\lambda$ being the mag. lat.

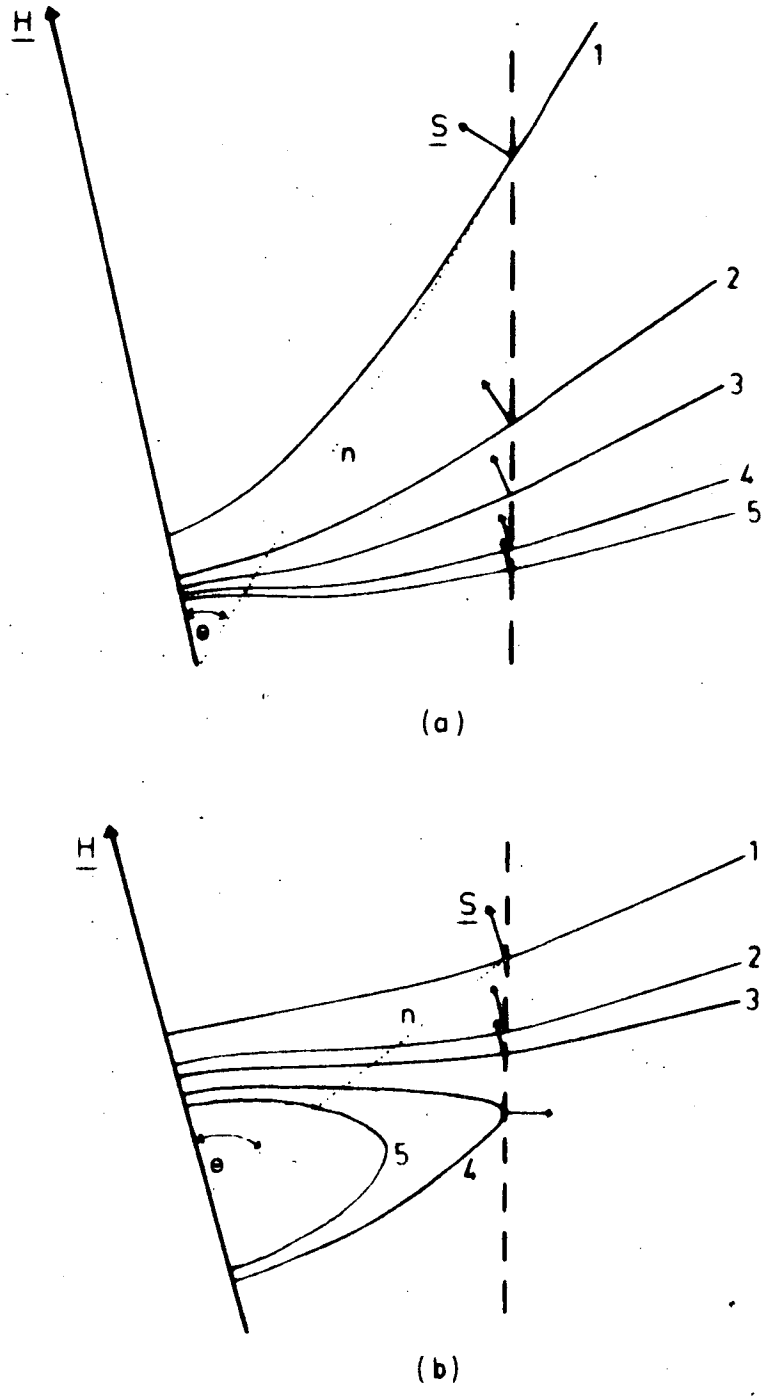


Figure 9.8 Refractive index surfaces for points between Io, curve 1, and Jupiter, curve 5. The dashed line represents an arbitrary path between Io and Jupiter, and $\underline{S}$ gives the ray direction at each intersection. (a) For a frequency of 120 kHz well above the ion-plasma frequency at Jupiter. (b) For 40 kHz, corresponding to the ion-plasma frequency at level 4. Note that the ray cannot reach Jupiter.

Inside this boundary the density varies according to

$$N = N_o \exp\left[ - \frac{A}{2} \left\{ 1 - \frac{1}{r} - 0.043 \cos^2 \lambda \left( r^2 - \frac{1}{r} \right) \right\} \right]$$

and beyond the boundary

$$N = N_{(r = r_b)} \left\{ \frac{r_b}{r} \right\}^{\beta} \qquad \text{where} \quad 3 \leqslant \beta \leqslant 4$$

The model contains three parameters $N_o$, A and $\beta$ where $N_o$ is the maximum electron density in Jupiter's ionosphere, A is the ratio of Jupiter's radius to the scale height and $\beta$ gives the power law in the outer region.

Each ray traced from Io to Jupiter is specified by two coordinates, its wave normal angle $\theta$ and the azimuth $\psi$ of the initial wave normal direction. The zero of azimuth is taken at the outward intersection of the wave normal cone with the magnetic meridian plane. For a particular magnetosphere, corresponding to a choice of $N_o$, A and $\beta$, a series of rays are traced for various values of $\theta$ and $\psi$. The intersection of each ray with the coupling region is specified by four coordinates ($\lambda$, **l**, T, E). $\lambda$ and **l** are the latitude and longitude of the intersection point, T is the propagation time in seconds and E represents the longitudinal energy of the electron stream which satisfies the conditions for coupling with the wave. We have

$$E = \beta_{\parallel} / (1 - \beta^2)^{\frac{1}{2}}$$

To satisfy the requirements on the ray paths specified previously we must have

$$T \simeq 2000$$

$$\text{and} \quad 0.1 \leqslant E \leqslant 1.0$$

The values of T and E depend on the assumed longitudinal velocity of the emitting electrons. However for a given model magnetosphere and

ray the product ET is constant so that varying the velocity of the emitting electrons only changes the ratio of E to T. Hence we can classify a suitable model magnetosphere as one in which

$$200 \leqslant ET \lesssim 2000$$

for rays which satisfy the conditions imposed on $\lambda$ and **l**.

For nearly all model magnetospheres investigated, it was possible to find some rays $(\theta, \psi)$ which satisfied the conditions on $\lambda$ and **l**. The most satisfactory models however were those for which the electrons were concentrated in a disc about the magnetic equator and the plasma frequency and gyrofrequency at Io were nearly equal. These models gave much more satisfactory values for the product ET although all models gave values towards the upper limit of this quantity.

The model magnetosphere which was derived from the cyclotron theory is as good as any investigated, and was used for a detailed investigation of the Io effect. The parameters of the model are

$$N_o = 2.0_{10}6 \cos^{\frac{1}{2}} \lambda$$

$$A = 22.0$$

$$\beta = 4$$

Contours of electron density in this model magnetosphere are plotted in Figure (9.9) for latitudes below $80^o$.

## 9.11 Attenuation of the Rays.

The magnetosphere of Jupiter is a region where large numbers of high energy particles are present as well as the thermal background plasma. The theory for the attenuation of low frequency radio waves in a cold plasma cannot be applied to this medium. We must consider

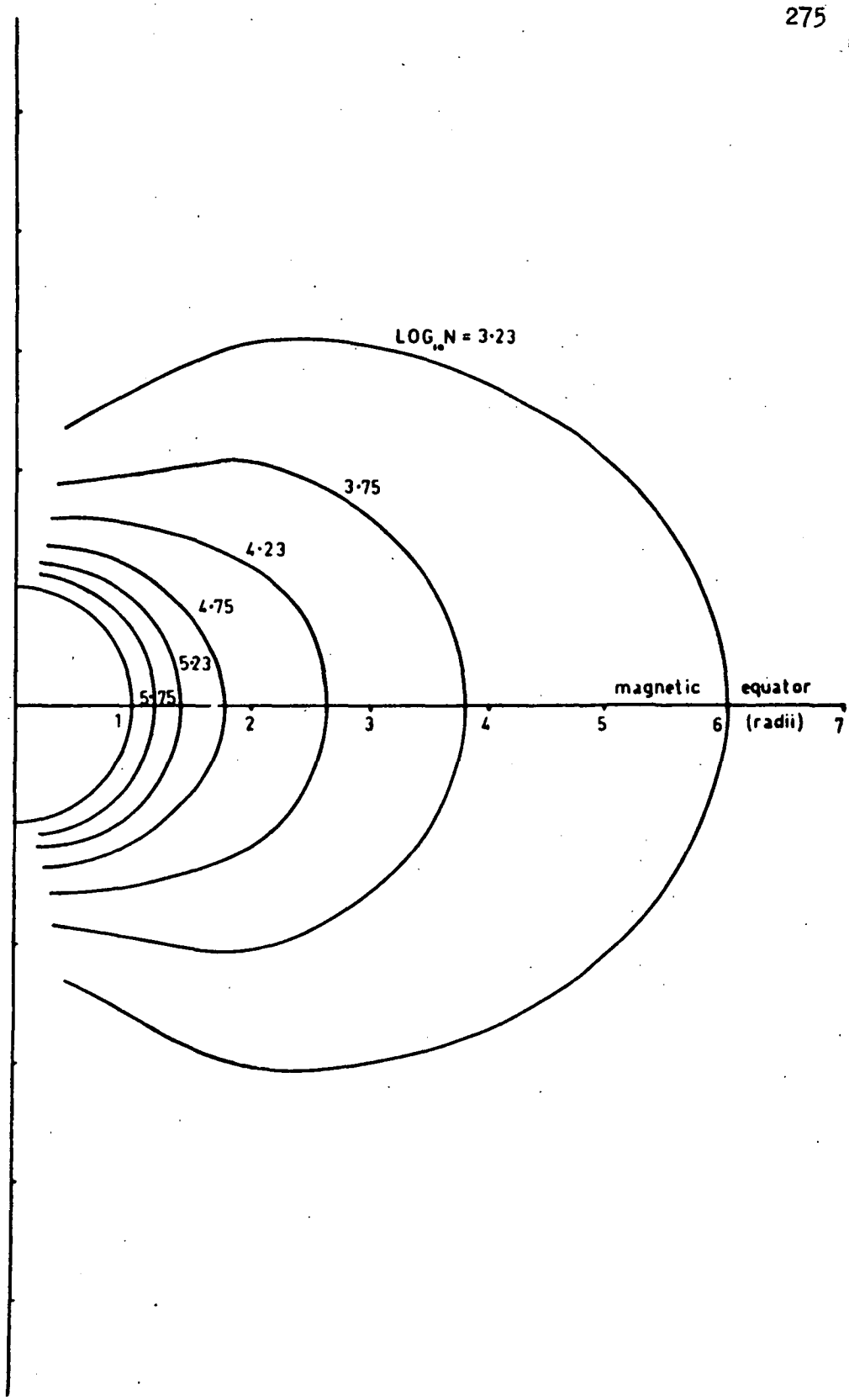


Figure 9.9 Contours of electron density in the model of Jupiter's magnetosphere.

propagation in a two component plasma consisting of a dense cold background propagation medium and a diffuse energetic nonthermal "tail". This nonthermal tail can give rise to resonant growth or damping of electromagnetic waves.

The growth rate $\gamma$ for waves propagating in such a medium has been given by Kennel (1966).

$$\gamma \frac{\partial D^{o}}{\partial \omega} = 2\pi^2 \sum_{+\,-} \frac{(\omega_o^{\pm})^2}{\omega\, k_{\parallel}} \int_0^{\infty} v_{\perp}\, dv_{\perp} \int_{-\infty}^{\infty} dv_{\parallel} \sum_s \delta\left(v_{\parallel} - \frac{\omega - s\,\omega_H^{\pm}}{k_{\parallel}}\right)$$

$$\Bigg[ G_1^{\pm} \Bigg\{ (P - n^2 \sin^2\theta) \{ 2(L - n^2) v_{\perp} J_{s+1}^2$$

$$+ 2 v_{\perp}(R - n^2) J_{s-1}^2 + n^2 \sin^2\theta\, v_{\perp} (J_{s+1} - J_{s-1})^2 \}$$

$$- n^2 \cos\theta \sin\theta \{ 2 v_{\parallel} J_s \Big( J_{s+1} (L - n^2)$$

$$+ J_{s-1} (R - n^2) \Big) + n^2 \cos\theta \sin\theta\, v_{\perp} (J_{s+1} - J_{s-1})^2 \} \Bigg\}$$

$$+ G_2^{\pm} \Bigg\{ 4 v_{\parallel} J_s \{ (L - n^2)(R - n^2) + n^2 \sin^2\theta (S - n^2) \}$$

$$- 2 n^2 \cos\theta \sin\theta \{ (R - n^2) v_{\perp} J_{s-1}$$

$$+ (L - n^2) v_{\perp} J_{s+1} \} \Bigg\} \Bigg]$$

where $D^{o}$ is the dispersion equation for the wave in the background plasma and $S = \frac{1}{2}(R + L)$

where $L = 1 - \sum_{+\,-} \frac{\omega_o^2}{\omega(\omega - \omega_H)}$ $\quad R = 1 - \sum_{+\,-} \frac{\omega_o^2}{\omega(\omega + \omega_H)}$

$$P = 1 - \sum_{+\,-} \left\{ \frac{\omega_o}{\omega} \right\}^2$$

and $n^2 = \frac{c^2 k^2}{2}$ is the square of the refractive index.

$v_{\parallel}$ and $v_{\perp}$ are the particle velocities parallel and perpendicular to the magnetic field and k is the wave number, $\delta$ is the Dirac delta function and s is the harmonic number.

The terms $G_1^{\pm}$ and $G_2^{\pm}$ are given by

$$G_1^{\pm} = \frac{\partial F^{\pm}}{\partial v_{\perp}} - \frac{k_{\parallel}}{\omega} \left( v_{\parallel} \frac{\partial F^{\pm}}{\partial v_{\perp}} - v_{\perp} \frac{\partial F^{\pm}}{\partial v_{\parallel}} \right)$$

and $$G_2^{\pm} = J_s \left\{ \frac{\partial F^{\pm}}{\partial v_{\parallel}} + \frac{s\,\omega_H}{\omega\, v_{\perp}} \left( v_{\parallel} \frac{\partial F^{\pm}}{\partial v_{\perp}} - v_{\perp} \frac{\partial F^{\pm}}{\partial v_{\parallel}} \right) \right\}$$

where the $F^{\pm}$ are the equilibrium velocity distribution function of the ionised particles.

The argument of the Bessell function is $\left\{ \frac{-\, k_{\perp}\, v_{\perp}}{\omega_H} \right\}$

For the waves under consideration we have

$$L \ll n^2, \qquad R \ll n^2 \qquad \text{and} \qquad S \ll n^2$$

and if we can neglect the effect of resonant ions the expression for $\gamma$ can be simplified. For $s \neq 0$

$$\gamma \frac{\partial D^o}{\partial \omega} = 2\pi^2 \frac{\omega_o^2}{\omega\, |k_{\parallel}|} \int_0^{\infty} v_{\perp}\, dv_{\perp} \int_{-\infty}^{\infty} dv_{\parallel} \sum_s \delta\left( v_{\parallel} - \frac{\omega - s\,\omega_H}{k_{\parallel}} \right) \theta_s$$

where $\theta_s = n^4 \left( \frac{\partial F}{\partial \alpha} \right) \left\{ J_{s+1} + J_{s-1} \right\}^2 \sin^2\theta \left( 2 - \frac{1}{sY} \right) (sY - 1)$

$$\left\{ 1 + \frac{\sin \alpha}{\cos \theta \cos \alpha} \right\}$$

is the weighting function for each resonance and $\alpha$ is the electron pitch angle, $\theta$ is the wave normal angle and $Y = \omega_H / \omega$.

For $s = 0$ we have $\theta_o = 0$.

Hence in this approximation the $s = 0$ Landau resonance does not contribute to the attenuation of the wave. However the cyclotron resonances $s \neq 0$ and $k_{\parallel} v_{\parallel} = \omega - s \omega_H$ do contribute.

There are two resonances for each value of $|s|$ corresponding to s +ve and -ve. We can find the contribution to the growth rate of both these resonances.

$$\gamma_s = (\gamma_{s\ +ve} + \gamma_{s\ -ve})$$

$$\text{then} \quad \gamma_s \frac{\partial D}{\partial \omega} = 2\pi^2 \frac{\omega_o^2}{\omega |k_{\parallel}|} \int_0^{\infty} v_{\perp}\, dv_{\perp} \int_{-\infty}^{\infty} dv_{\parallel} \{\theta_s \delta_s + \theta_{-s} \delta_{-s}\}$$

At a particular point on the path of the ray the quantities $\theta$, $\omega$, n and Y are fixed. For the low frequency whistler mode $Y \gg 1$ so that

$$\beta \cos \alpha = -(|s| Y + 1) / (n \cos \theta) \qquad s\ +ve$$

$$\beta \cos \alpha = (|s| Y + 1) / (n \cos \theta) \qquad s\ -ve$$

Hence the sign of $\cos \alpha$ is opposite for the two values of s and $|\beta \cos \alpha|$ is greater for s -ve, while the difference between $|\beta \cos \alpha|$ for the two values of s decreases as $|s|$ increases. Then

$$\{\theta_s \delta_s + \theta_{-s} \delta_{-s}\} \simeq \{J_{s+1} + J_{s-1}\}^2 \sin^2\theta\, n^4 \left[ \left\{ \frac{\partial F}{\partial \alpha} \left(2 - \frac{1}{|s| Y}\right) (|s| Y - 1) \left(1 + \frac{\sin \alpha}{\cos \theta \cos \alpha}\right) \right\}_{s\ +ve} \right.$$

$$\left. + \left\{ \frac{\partial F}{\partial \alpha} \left(2 + \frac{1}{|s| Y}\right) (-|s| Y - 1) \left(1 + \frac{\sin \alpha}{\cos \theta \cos \alpha}\right) \right\}_{s\ -ve} \right]$$

For particles in a van Allen belt configuration the pitch angle distribution is likely to peak in the neighbourhood of $\alpha = \pi/2$ and decrease on either side. Then it is reasonable to expect $\frac{\partial F}{\partial \alpha}$ to be +ve for $0 \leqslant \alpha \leqslant \pi/2$ and -ve for $\pi/2 \leqslant \alpha \leqslant \pi$. Then the positive cyclotron resonances (s +ve) will be unstable while the negative cyclotron resonances will be damping provided

$$\left| \frac{\sin \alpha}{\cos \theta \cos \alpha} \right| > 1$$

The net effect depends on the magnitudes of the two terms, which for s -ve are slightly greater than for the corresponding s +ve. Hence the net effect will be damping. We may write

$$\gamma_s = - f_s(n)\, g_s(\alpha)$$

$$\gamma = \sum_{s=1}^{\infty} \gamma_s$$

where $f_s(n)$ is a function of the refractive index and $g_s(\alpha)$ is a function of the velocity distribution of the radiating particles. Clearly the magnitude of $g(\alpha)$ may be made as small as we like by postulating a suitable distribution for the resonant electrons. Hence the rays are attenuated over their path by an amount that may be made sufficiently small by appropriate modifications of the medium. Since all rays propagating in to the coupling region travel through approximately the same distribution of electrons, the relative attenuation will be given to first order by $\int f(n)\, dt$ over the ray path.

## 9.12 The Io Effect.

The intersection points of rays emitted over a small range of wave normal angles about $130^{\circ}$ with the coupling region are shown

in Figure (9.10). The three diagrams (a), (b) and (c) show the intersection points of rays emitted when Io was above $\lambda_{III} = 183^{\circ}$, $200^{\circ}$ and $220^{\circ}$ respectively. The dotted line shows the apparent position of Io when the rays intersect the coupling region. Clearly such a cone of waves will satisfy the majority of the requirements specified in Section (9.9). Coupling occurs in the correct longitude and Io phase relations and is only significant when Io is near the north magnetic pole. The propagation times and coupling energies also agree with the requirements. However the model requires emission to be limited to a narrow cone of wave normal angles and the discussion in Section (9.8) indicates that all wave normal angles are likely, hence we must look for a different model.

The attenuation of the rays in propagating from Io to Jupiter provides a method of selecting the rays which will contribute to the disturbance near Jupiter. We consider propagation in any direction and select the rays which intersect the coupling region between $75^{\circ}$ and $80^{\circ}$ magnetic latitude. The ranges of wave normal angles $\theta$ and their azimuths $\psi$ which satisfy this condition are shaded in Figure (9.11) for various initial positions of Io. The ranges of $\theta$ and $\psi$ are much larger when Io is near the north magnetic pole than in any other position. Because of the symmetry of the magnetosphere the figures apply to positions of Io on either side of the magnetic pole. We can neglect the effect of rays which penetrate the corresponding position when Io is above the south magnetic pole, because polarisation measurements show that no emission originates from that hemisphere at frequencies above 30 MHz.

The paths of rays originating from a uniformly spaced grid

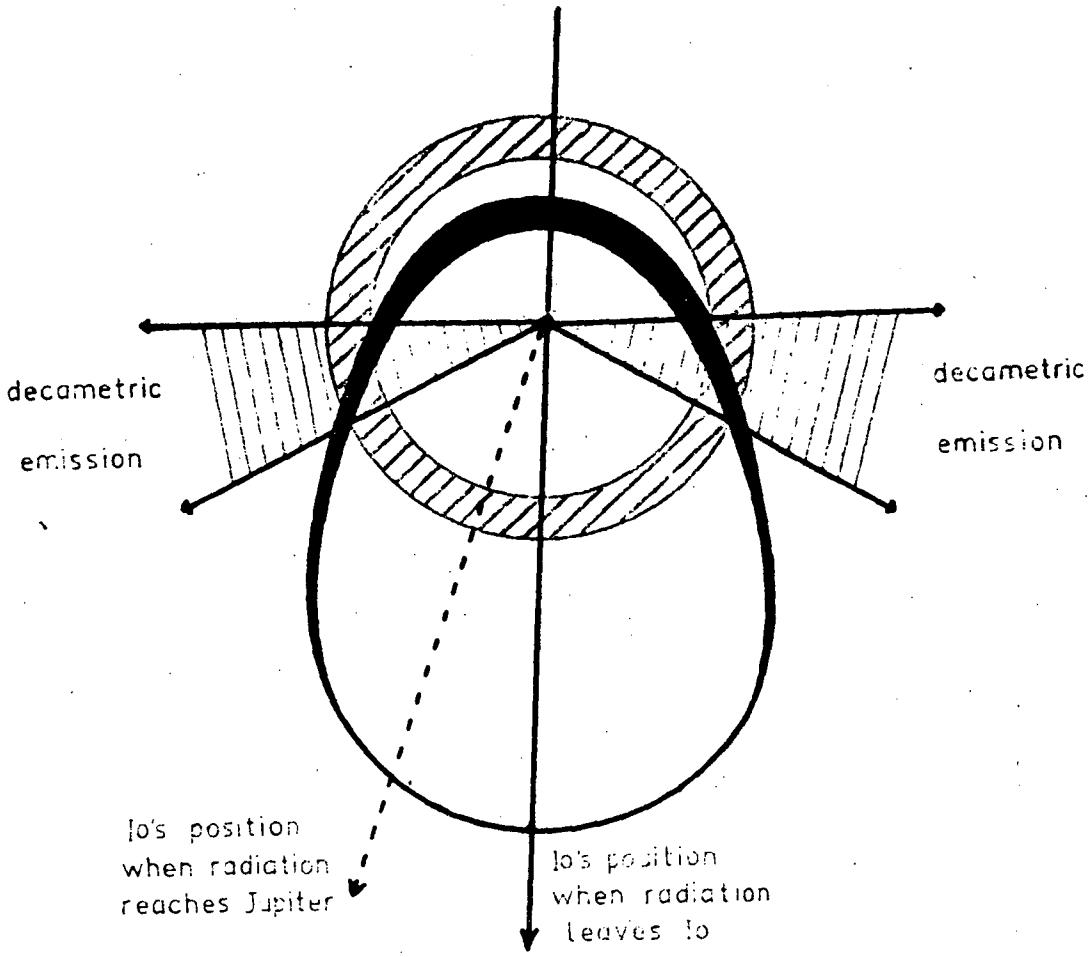


Figure 9.10a Projection on the 30 MHz gyrofrequency level in Jupiter's magnetosphere of emission from a narrow cone of wave normal angles when Io is above a longitude of 183°. The shaded ring shows the latitudes of electron bunches derived from the cyclotron theory. The intersection of this ring with the radiation cone gives the longitudes of decametric emission at frequencies above 30 MHz.

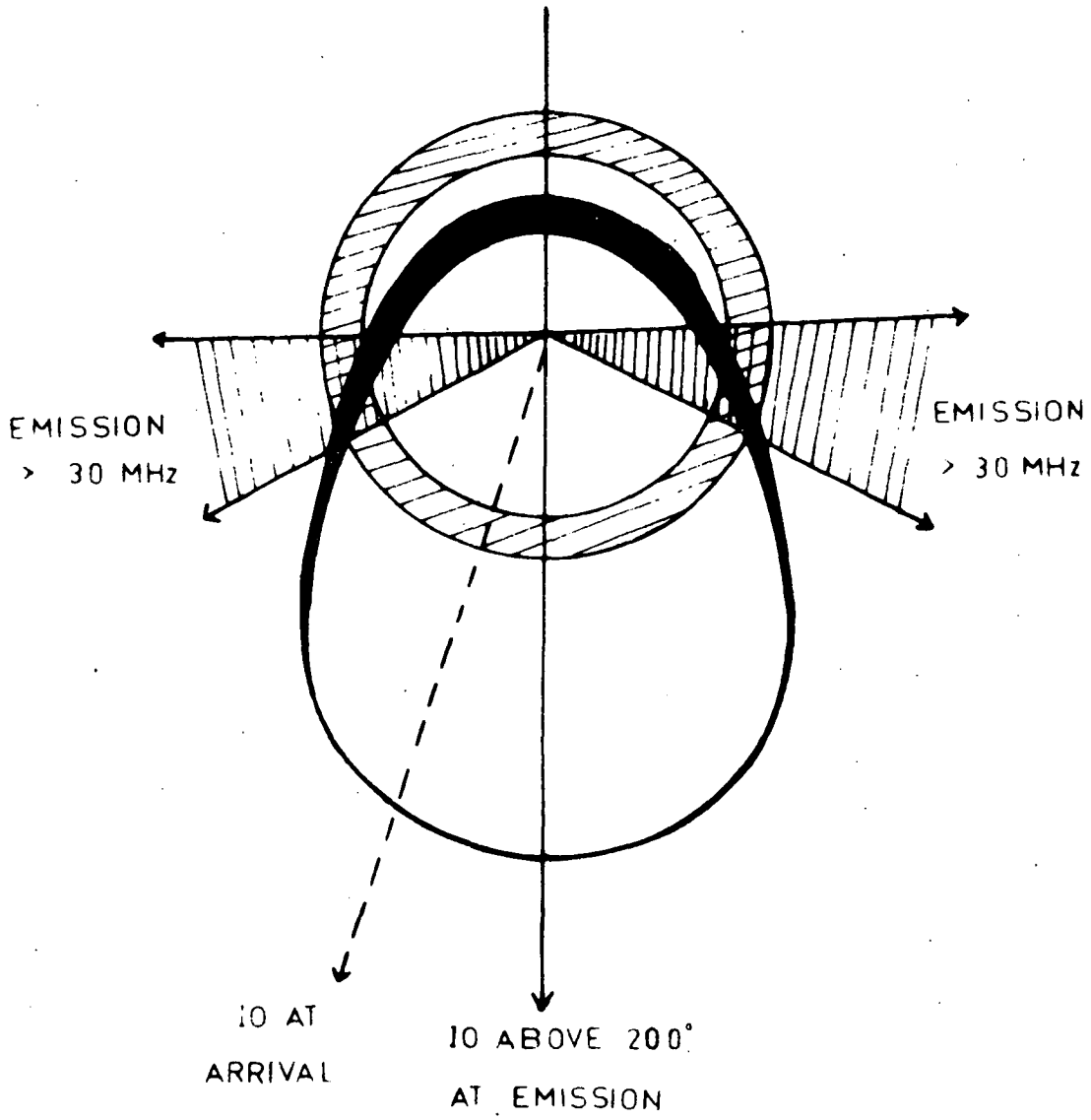


Figure 9.10b Projection on the 30 MHz gyrofrequency level in Jupiter's magnetosphere of emission from a narrow cone of wave normal angles when Io is above a longitude of 200°. The shaded ring shows the latitudes of electron bunches derived from the cyclotron theory. The intersection of this ring with the radiation cone gives the longitudes of decametric emission at frequencies above 30 MHz.

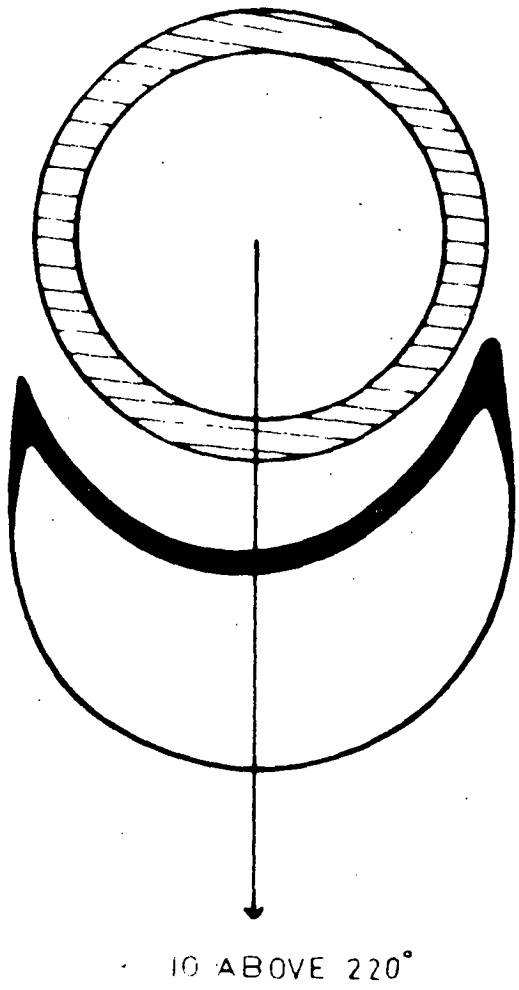


Figure 9.10c Projection on the 30 MHz gyrofrequency level in Jupiter's magnetosphere of emission from a narrow cone of wave normal angles when Io is above a longitude of 220°. Note that there is no decametric emission in this case.

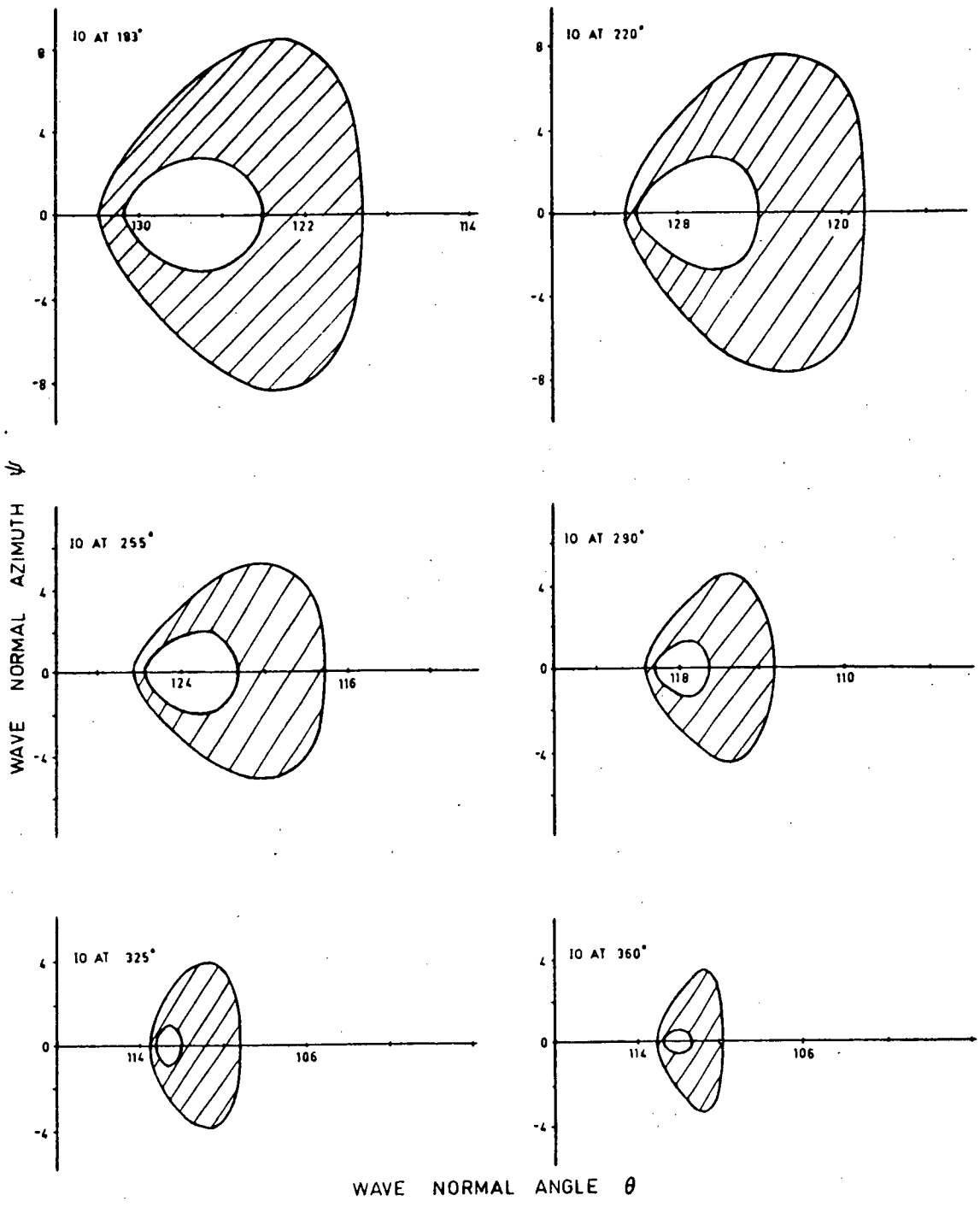


Figure 9.11 The shaded areas show the range of initial wave normal angles and azimuths for which rays intersect the 30 MHz gyrofrequency level between magnetic latitudes 75° and 80°.

over the shaded region in Figure (9.11) have been traced to their intersection points with the coupling region. The points of intersection are shown on spot diagrams in Figure (9.12) for each position of Io. These diagrams are plotted for Io at higher longitudes than the north pole, but apply equally well to longitudes below the pole.

Perspective diagrams of a pencil of rays emitted when Io was above the pole are shown in Figure (9.13). The set of rays (a) is viewed from directly above Jupiter's north magnetic pole while the set (b) is viewed from a point $45^{\circ}$ around from the pole above latitude $45^{\circ}$.

Each ray in Figure (9.11) takes in excess of 20 min to propagate from Io to Jupiter so that the position of Io when the rays reach the coupling region will have changed. Figure (9.14) shows the spot diagrams of Figure (9.12) replotted to show the deviation of the longitude of the ray from the longitude of Io when the ray reaches the coupling region. The allowance made for the propagation time produces a distinct asymmetry in the figure. If we make allowance for the attenuation of the rays we obtain the intensity of the radiation (number times strength of each ray) as a function of the deviation in longitude from Io's position at the time of arrival at the coupling region. The diagrams shown in Figure (9.15) are based on an assumed minimum attenuation between Io and Jupiter of 90%. Each plot shows two peaks of approximately equal amplitude asymmetrically placed with respect to the position of Io. As the initial position of Io gets further away from the pole the amplitude of the peaks decreases until about $60^{\circ}$ away from the pole the intensity is reduced to 2%. Hence we can neglect all rays which originate when

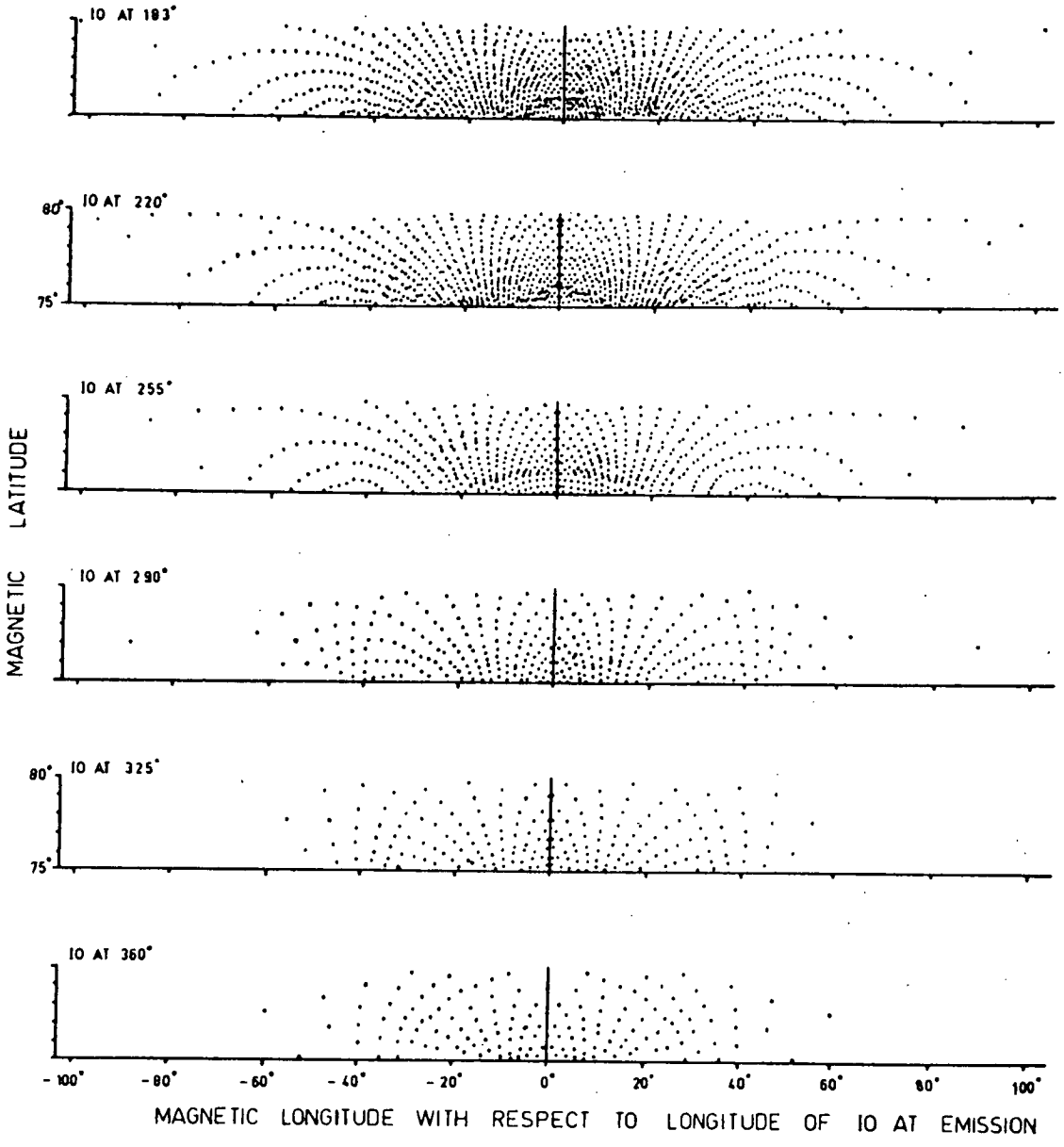


Figure 9.12 Spot diagrams showing the points of intersection with the 30 MHz gyrofrequency level of rays originating from a uniformly spaced grid over the shaded regions in Figure 9.11.

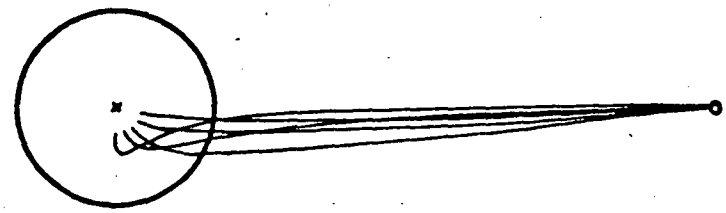

(a)

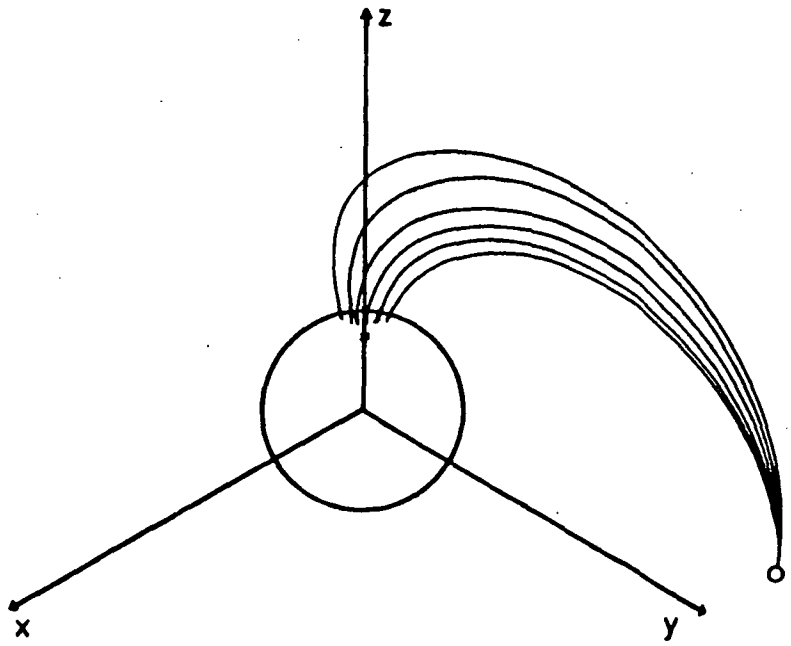


(b)

Figure 9.13 Perspective diagrams of a pencil of rays emitted when Io was adjacent Jupiter's north magnetic pole (marked "x"), (a) viewed from directly above the pole, and (b) viewed from a point $45^{\circ}$ around from the pole above latitude $45^{\circ}$.

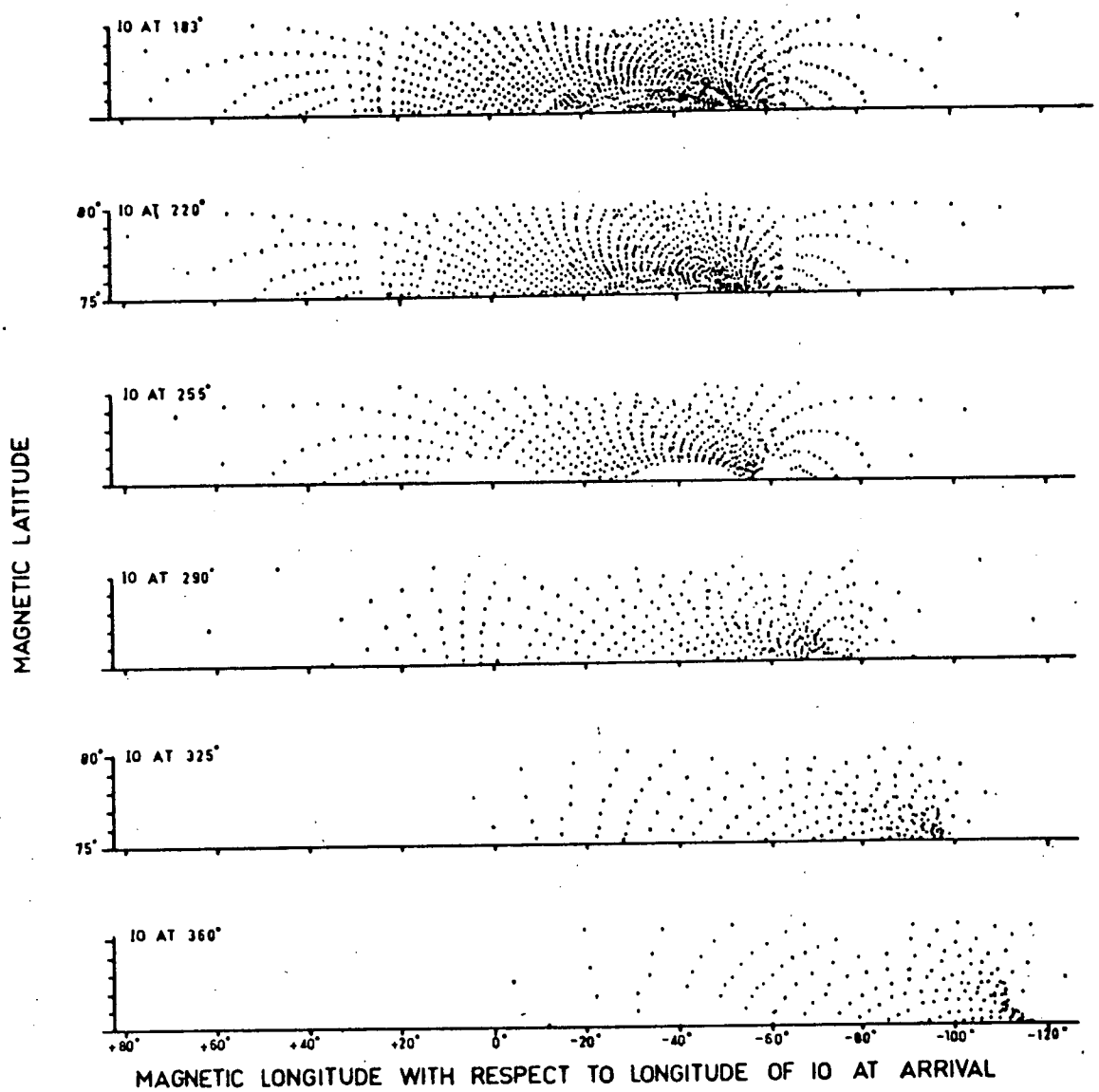


Figure 9.14 The spot diagrams of Figure 9.12 replotted as a function of the deviation in magnetic longitude from the longitude of Io at the time of arrival at the coupling region.

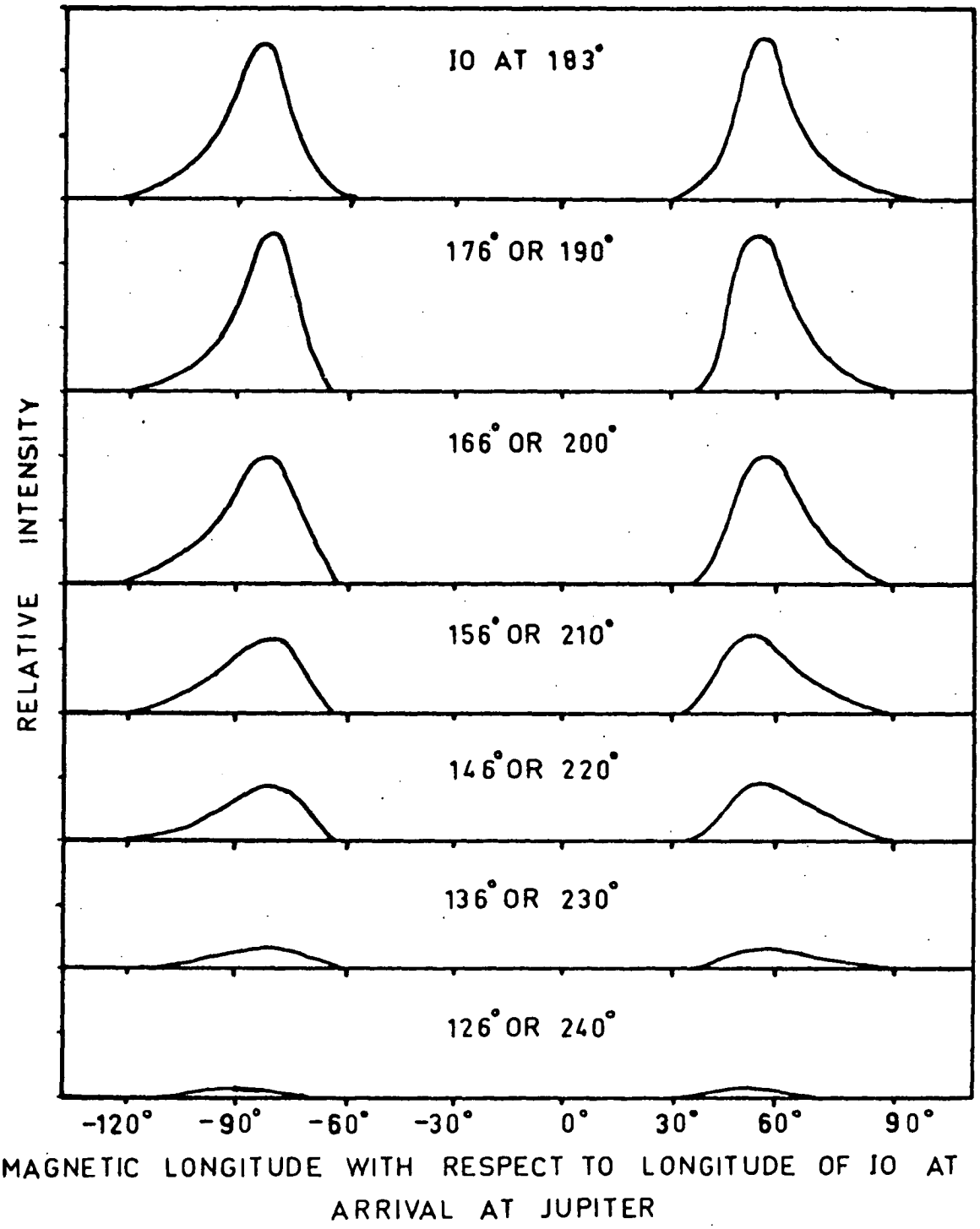


Figure 9.15 Relative intensity of Io's effect plotted as a function of the deviation in magnetic longitude with respect to the longitude of Io at the time of arrival at the coupling region. Assumed minimum attenuation 90%.

Io is further than $60^{o}$ from the pole. Note that the effect of the influence is to produce emission at longitudes $90^{o}$ lower and $60^{o}$ higher than the longitude of Io.

Figure (9.16) shows the intensity of the radiation from Io as a function of Io's longitude at the time of arrival at the coupling region. There is a strong maximum near a longitude of $200^{o}$ even though the position of the pole was assumed to be $183^{o}$. This shift of about $17^{o}$ is a result of the propagation time and must occur in order to produce the required asymmetry with respect to Io's departure from S.G.C. The position of this peak is in good agreement with the observations of Duncan (1966).

The data has been plotted as contours of intensity as a function of the system III longitude and Io's departure from S.G.C. in Figure (9.17) for frequencies greater than 30 MHz. In order to obtain a contour diagram showing the intensity received at the Earth we have to take account of the modulation of emitted power as a function of system III longitude due to Jupiter's magnetic field configuration. The resultant diagram for frequencies greater than 30 MHz is shown in Figure (9.18). The position of the peaks on this contour diagram agree fairly well with those obtained by Bigg, Figure (9.6) although Bigg's diagram refers to all frequencies observed by Warwick at Boulder.

The results shown in Figure (9.18) have been compressed onto the Io axis to give the distribution of radiation as a function of Io's departure from S.G.C., Figure (9.19). There are two peaks at about $98^{o}$ and $235^{o}$ in very good agreement with the results obtained by Bigg for frequencies greater than 30 MHz.

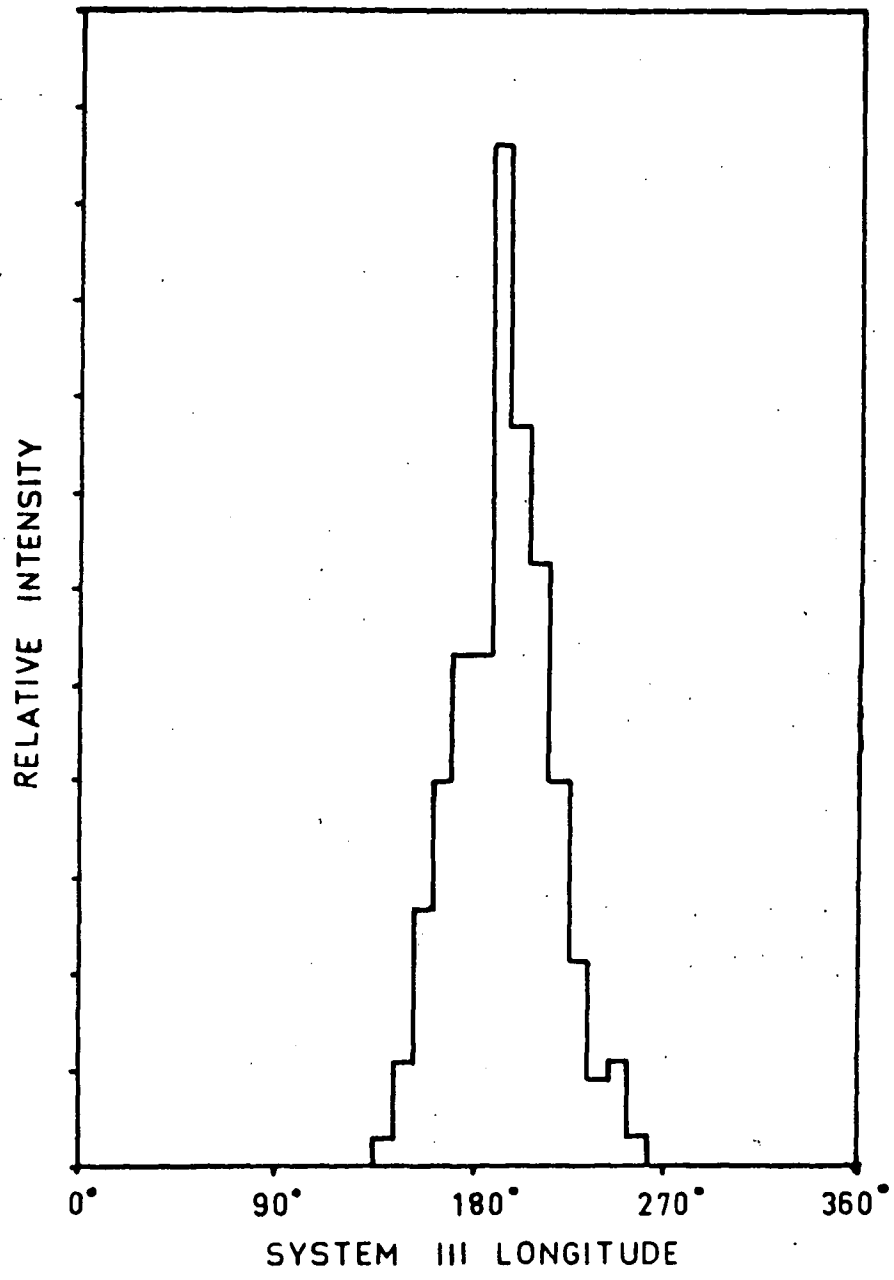


Figure 9.16 Relative intensity as a function of Io's longitude at the time of arrival of the rays at the coupling region.

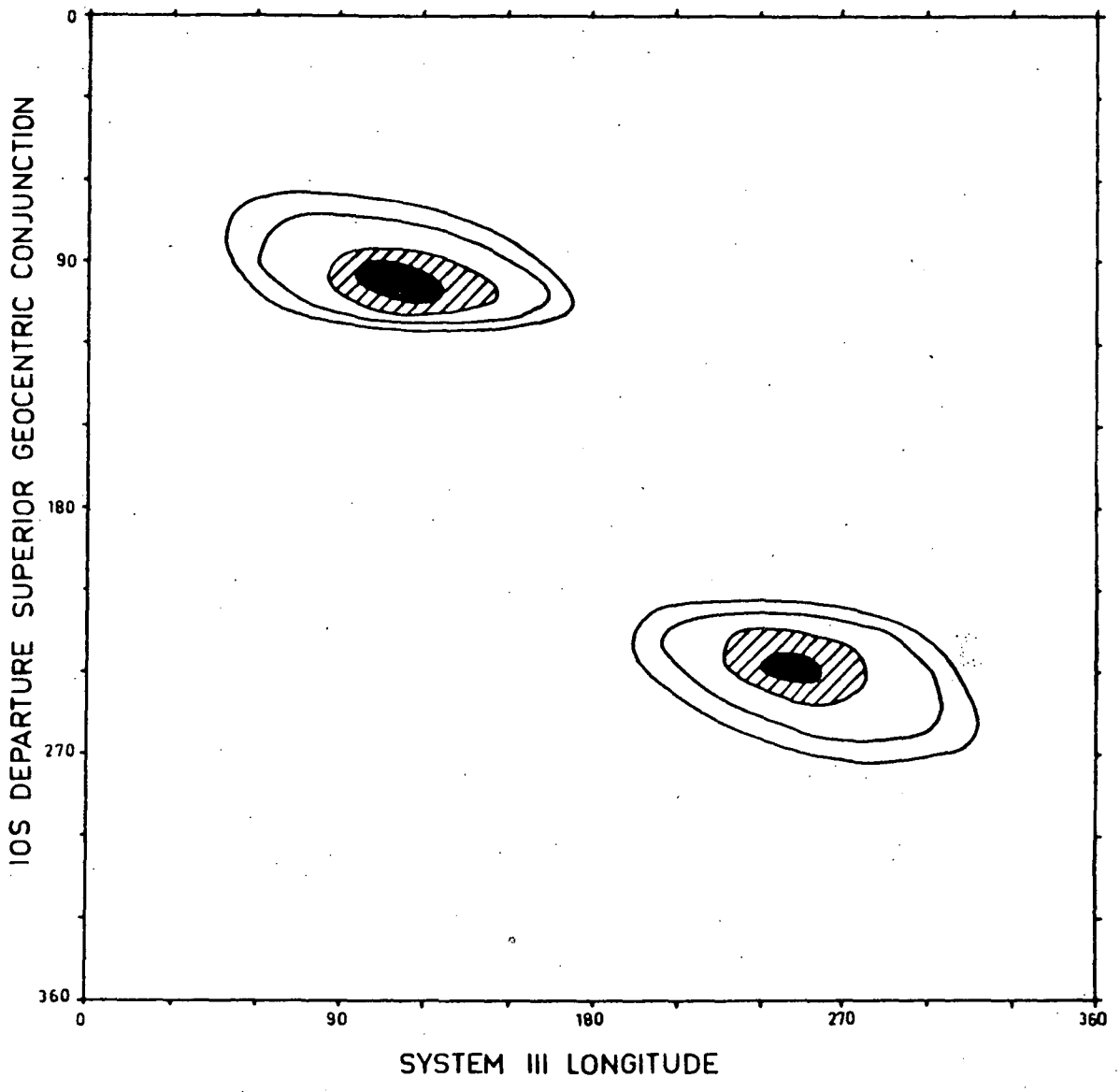


Figure 9.17 Contour diagram of the strength of Io's influence at the coupling region as a function of Io's position and Jupiter's longitude.

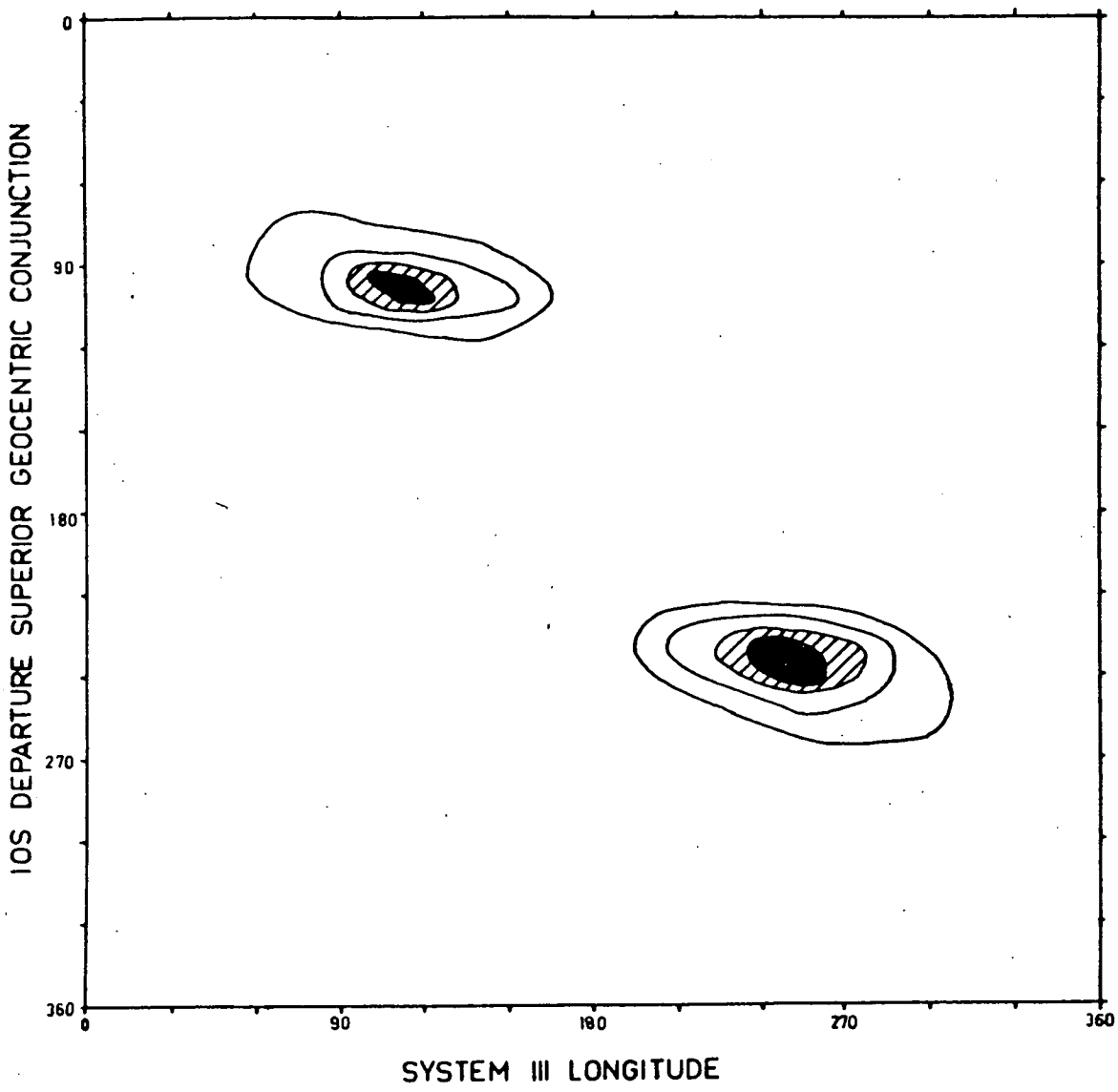


Figure 9.18 Contour diagram of the theoretical emission intensity at the Earth for frequencies above 30 MHz. The effect of Jupiter's magnetic field configuration has been taken into account.

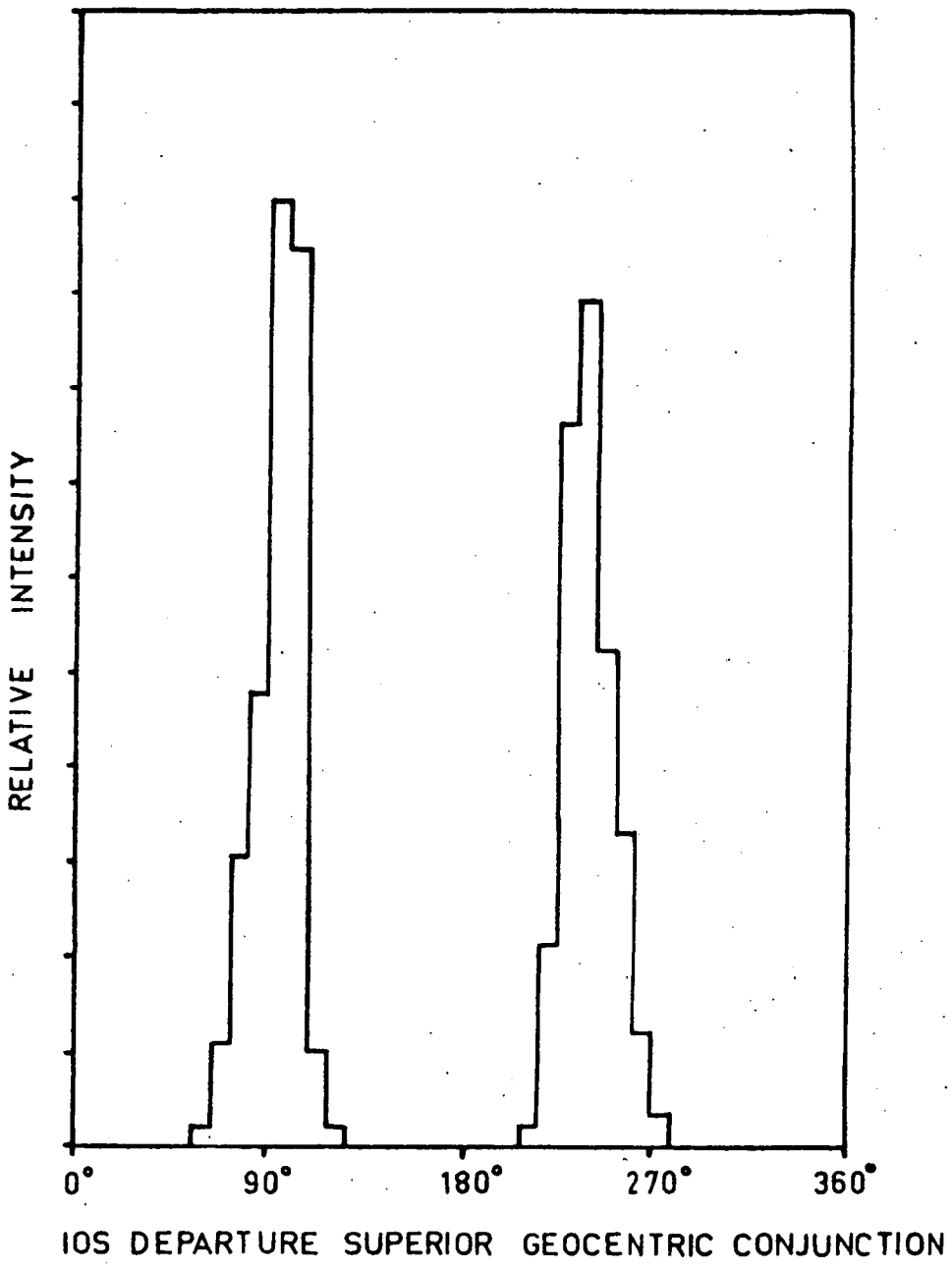


Figure 9.19 Relative intensity of Io's effect on the radiation at frequencies greater than 30 MHz as a function of Io's departure from S.G.C.

## 9.13 The Effect of Io on Early Source Dynamic Spectra.

The data of Figure (9.14) shows that Io's influence on the emission is only marked when Io is near either of two positions, viz $95^{\circ}$ or $235^{\circ}$ from S.G.C. The effect is strongest when Io is simultaneously close to the longitude of Jupiter's north magnetic pole. Hence we would expect the position of Io to effect the intensity and shape of the early source dynamic spectra as observed by Dulk (1965). The main feature of this effect is that the spectrum starts at lower longitudes when Io reaches $90^{\circ}$ from S.G.C. earlier. Figure (9.20) shows four theoretical early source dynamic spectra constructed for different positions of Io. They are based on the assumption that the intensity of the emission at a given longitude is proportional to the energy density of the radiation from Io at that longitude. This in turn implies the existence of electron streams in all longitudes that can be stimulated by this radiation. This condition is unlikely to be met in practice for individual storms, so that each spectra may differ from those shown. However the diagrams should represent an average of a large number of storms occurring when Io is in the appropriate position.

## 9.14 Conclusions.

Using the model of Jupiter's magnetosphere developed from the cyclotron theory in Chapter 7 we have developed a theory to explain the influence of Io on the radiation. This theory requires that Io's motion relative to Jupiter's magnetosphere accelerates large numbers of electrons which in turn emit electromagnetic waves.

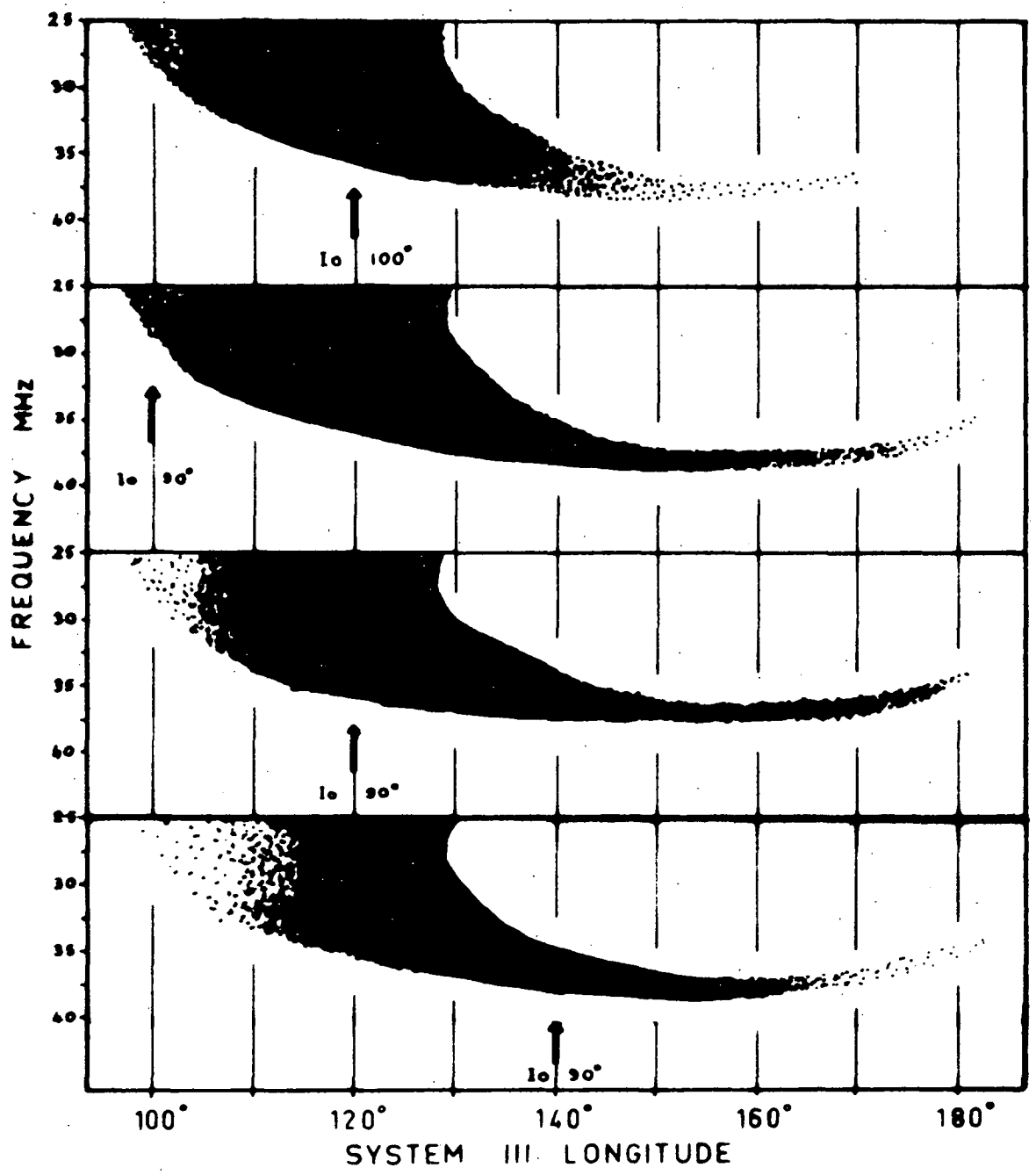


Figure 9.20 Four theoretical early source dynamic spectra corresponding to different positions of Io at the time of emission.

These waves propagate in the whistler mode towards the lower regions of Jupiter's magnetosphere where they interact with electron streams by means of the gyroresonant interaction causing them to emit the decametric radiation. When allowance is made for the ray paths and attenuation of these waves the strength of the interaction is sufficient to account for the observed properties of the Io modulation. In particular it accounts for the enhanced emission at the appropriate orientations and longitudes of Io and explains the change in character of individual dynamic spectra with Io's position.

In order to develop this theory further, more detailed observational data is required. The most convenient form of this for analysis is contour diagrams of emission as a function of Io's position and Jupiter's longitude. Separate diagrams are needed at a number of frequencies between 20 and 40 MHz.

## 9.15 References.

BIGG, E.K. (1964) Nature 203, 1008

BIGG, E.K. (1966) Planet Space Sci. 14, 741

BRICE, N. (1964) J. Geophys. Res. 69, 4515

CORNWALL, J.M. (1964) J. Geophys. Res. 69, 1251

DULK, G.A. (1965) Ph. D. Dissertation, University of Colorado

DUNCAN, R.A. (1966) Planet Space Sci. 14, 173

ELLIS, G.R.A. (1965) J. Res. Nat. Bur. Standards 69D, 1513

FUNG, P.C.W. (1966) Ph. D. Dissertation, University of Tasmania

GENDRIN, R. (1965) J. Geophys. Res. 70, 5369

GLEDHILL, J.A. (1967a) Nature 214, 155

GLEDHILL, J.A. (1967b) Goddard Space Flight Center, Publication

KENNEL, C. (1966) Phys. of Fluids 9, 2190

KIMURA, I. (1968) J. Geophys. Res. 73, 445

MELROSE, D.B. (1967) Planet Space Sci. 15, 381

PIDDINGTON, J.H. and J.F. DRAKE (1967) Private Communication

SHEVER, I. (1967) Ph. D. Dissertation, University of Florida

TIURI, M.E. (1967) Planet Space Sci. 15, 1203

WARWICK, J.W. (1967) Space Science Reviews 6, 841

# CHAPTER 10.

# CONCLUSIONS

## 10.1 Observations.

Observations of the mean power of Jupiter's decametric radio emissions at six frequencies, 4.7, 15.7, 18.7, 21.5, 24.5 and 28.0 MHz, have been used to prepare histograms of relative power and probability of occurrence at each frequency. Comparison of these two forms of displaying the data demonstrates that the relative power profiles show more pronounced variations with longitude especially at the lower frequencies. The shape of the probability of occurrence profiles depend critically on the sensitivity of the equipment used to record the bursts.

The mean and peak power spectra of the radiation were determined and both showed monotonic increases with decreasing frequency. The mean power spectrum consisted of two parts, one having a spectral index of -2.5 between 4.7 MHz and 20 MHz, and the other a spectral index of -13.7 between 24 and 30 MHz. The peak power spectrum has a spectral index of -1.2 over the range 4.7 to 28 MHz.

The data at 4.7, 15.7, 24.5 and 28.0 MHz were examined for the influence of the Jovian satellite Io and contour diagrams of emission plotted. The diagrams at the three higher frequencies show the same two emission regions as were originally observed by Bigg; however at 4.7 MHz the diagram is entirely different, although it should be emphasised that this conclusion is based on only 50 nights observing.

Linear polarisation measurements of the 11 cm radiation

from Jupiter in 1963 and 1967 indicate that the rotation period is about 0.5 sec longer than the system III (1957.0) period. The 11 cm flux density has shown little or no variation since 1963 and the configuration of the magnetic field determined from the variation of the position angle of the polarisation vector with longitude has been stable over that period.

## 10.2 Theory.

The mechanism for Jupiter's decimetric emissions has been accepted as synchrotron radiation from highly relativistic electrons trapped in van Allen belts similar to those surrounding the Earth.

No general agreement has been reached on the mechanism for Jupiter's decametric emissions. However the analysis in this thesis shows that of the two most favoured mechanisms, Cerenkov and cyclotron radiation, only cyclotron radiation can explain the observed intensity of the emission from a small diameter source. Cyclotron radiation has been used to develop a model of Jupiter's magnetosphere, which will account for the observed properties of the emission. The radiation can be emitted either over a broad cone or from a narrow range of angles on the edge of a cone, depending on the conditions in Jupiter's magnetosphere at the time of emission. By using the directional properties of the emission and making suitable deviations in the magnetic dip angle it is possible to reproduce any observed longitude profiles. The refraction of the radiation upon escape from Jupiter's magnetosphere explains why only negative frequency-time slopes are observed on high time resolution dynamic spectra. Long term variations in the probability of emission and shape of the emission profiles

are adequately explained by the variation of the angle between Jupiter's rotation axis and the Earth-Jupiter line as Jupiter revolves around the Sun.

The main features of the proposed model of Jupiter's magnetosphere are that Jupiter is surrounded by an extensive ionised exosphere, with a maximum electron density of about $10^6$/cc decreasing to about 1500/cc when extrapolated to the orbit of Io. The magnetic field is basically a dipole closely centered on the disc of Jupiter with a polar field strength of about 30 gauss. The dipole axis is tilted $10^\circ$ to the rotation axis with the longitude of the north magnetic pole near $200^\circ$ system III in February 1967. The field deviates from a true dipole in at least two regions close to the surface of Jupiter, the maximum deviation being about $17^\circ$ between longitudes $250^\circ$ and $300^\circ$.

Using this model magnetosphere and the cyclotron process a theory has been developed to explain the influence of Io on the radiation. This theory proposes that Io's motion relative to Jupiter's magnetosphere accelerates large numbers of electrons which in turn emit low frequency electromagnetic waves. These waves propagate in the whistler mode towards the lower regions of Jupiter's magnetosphere where they interact with electron streams by means of the gyroresonant interaction causing them to emit the decametric radiation. Sufficient energy may be transferred from the incoming whistler waves to the electron streams to induce them to emit cyclotron radiation above the local gyrofrequency. When allowance is made for the ray paths and attenuation of these waves the strength of the interaction is sufficient to account for the observed prop-

erties of the Io modulation. In particular it accounts for the enhanced emission at the appropriate orientations and longitudes of Io and explains the change in character of individual dynamic spectra with Io's position.

## 10.3 Suggestions for Further Research.

There are two critical experiments that could be performed to test the cyclotron theory in the form given in this thesis.

The two main peaks observed in power longitude profiles at 4.7 MHz have been identified with the magnetic poles of Jupiter. The radiation from these two regions originates in different hemispheres and hence should be of different polarisations, so that polarisation measurements at about 5 MHz provide a test of the model. This would be a difficult experiment to perform due to the effects of the interplanetary medium and the ionosphere on polarisation axial ratios at low frequencies. Also, unless the ionospheric critical frequency is below about 3 MHz one polarisation mode will be completely absorbed.

The second experiment involves direction finding of the radiation at a frequency near 30 MHz. Gledhill has proposed that the emission originates from Io and since most emission at 30 MHz occurs when Io is near its maximum elongation an angular resolution of about 3' arc would decide this point. The model based on the cyclotron theory requires the emission to originate predominantly from the central meridian of Jupiter. Other theories require the emission to originate from longitudes beneath Io. If the magnetic latitude of the emission region is not too high a resolution of

about 5" arc could distinguish between these models. If the latter theories are correct the position of the decametric source should change by at least 20" arc between the two favourable positions of Io, while the position remains constant for the cyclotron model.

Both of the above experiments provide critical tests of the cyclotron model although neither of them are tests of the cyclotron emission process. The properties of radiation emitted on the x-mode branch of the refractive index curves above the gyrofrequency are going to be the same whatever the emission process. The only way in which emission mechanisms can be tested is through their predictions based on some specific model.

In order to develop the theory of the Io modulation further, more detailed observational data is required. The most convenient form this could take for analysis is in the form of contour diagrams of emission as a function of Io's position and Jupiter's longitude. Separate diagrams would be needed at a number of frequencies between 20 and 40 MHz. This data should allow us to determine the variation of electron density throughout Jupiter's magnetosphere.

## SECTION B

# FINE STRUCTURE IN SOLAR RADIO EMISSIONS

# CHAPTER 11.

# FINE STRUCTURE IN SOLAR RADIO EMISSIONS

## 11.1 Introduction.

Early in 1965 a program was set up to study high time resolution dynamic spectra of Jupiter's emissions in the frequency range 20 to 40 MHz. At that time Jupiter was close to $+22^{\circ}$ declination and hence was about $65^{\circ}$ north of the zenith at Hobart. The low angle of the antenna beam needed for these observations resulted in serious interference from northern transmitting stations during the evenings at frequencies below 30 MHz. This, combined with the sparseness of strong Jupiter events in the frequency range 30 to 40 MHz, made observing almost impossible.

However, it was decided to use the equipment to observe the Sun in the frequency range 24 to 28 MHz during the day, and this was rewarded in March, 1966, when a major solar outburst took place. At the same time Professor G.R.A. Ellis was operating equipment over the frequency range 20-200 MHz with high time resolution. A new type of solar radio burst was observed on both sets of equipment during this storm. These bursts were of short duration and showed fine frequency splitting. The properties of these bursts observed during this and subsequent storms when different configurations of the equipment were used have been discussed in two papers, Ellis and McCulloch (1966, 1967).

## 11.2 Observations.

Over the period June, 1965, to March, 1967, observations of the dynamic spectra of solar radio emissions were made using a number

of spectrographs in several different configurations.

The spectographs incorporated electronic frequency scanning and hence could operate with high time and frequency resolution. The details of the spectrograph used from 24 to 28 MHz during March, 1966, are as follows; bandwidth 30 kHz, sweep rate 100/sec and film speed in the range 3"/min to 30"/min. The effective time resolution was determined by the film speed which for most of the observing was better than 0.1 sec.

The event which began on March 16, 1966, was the first recorded which showed any bursts other than type III. A notable feature of this event was the fact that only a single spot group was visible on the Sun's surface. It's position at 2200 U.T. on 16th March was about $45^{\circ}$ north latitude and $60^{\circ}$ east of the meridian. Large numbers of type III and type I bursts were recorded as well as many drift pairs and reverse drift pairs.

The most interesting bursts, however, were of a type not previously reported which occurred below 50 MHz and showed fine frequency splitting. On a wide range spectrograph (8-230 MHz) they appeared as sharp lines of almost constant frequency lasting from 1-2 secs (Ellis and McCulloch, 1966), see Figure (11.1a). When seen on a narrow range spectrum analyser scanning from 24.5-25.5 MHz, they appeared as two components occurring almost simultaneously with negative frequency time slopes and separated by about 100 kHz (Figure 11.1b).

During subsequent storms the equipment was modified to incorporate four spectrum analysers scanning the frequency ranges 24-28, 28-36, 36-46 and 46-60 MHz respectively. The scan rate of each was 50/sec and the bandwidths were about 30 kHz.

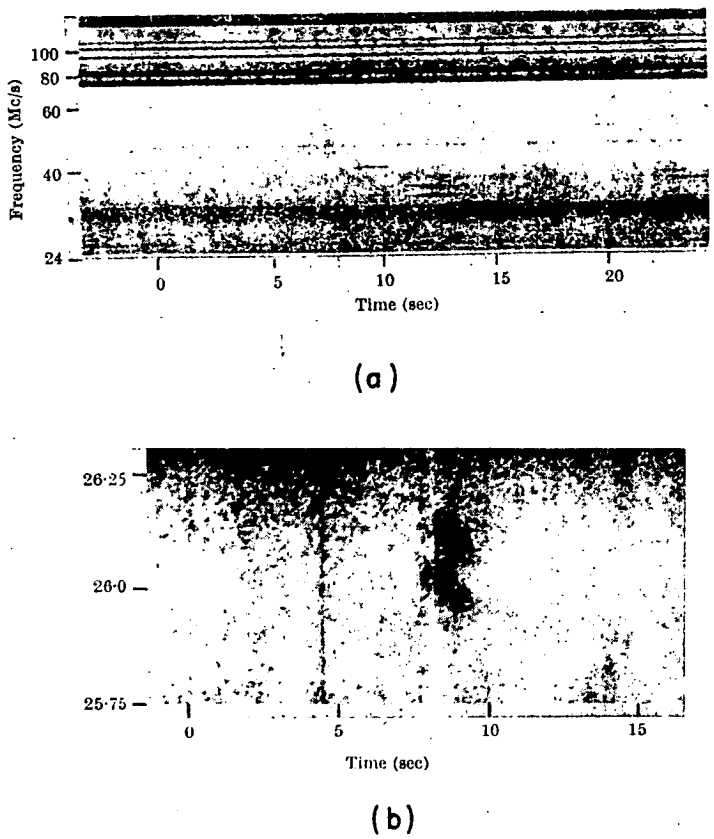


Figure 11.1 (a) Wide range record showing a split pair group. (b) Narrow range record of a single split pair showing the frequency-time slope.

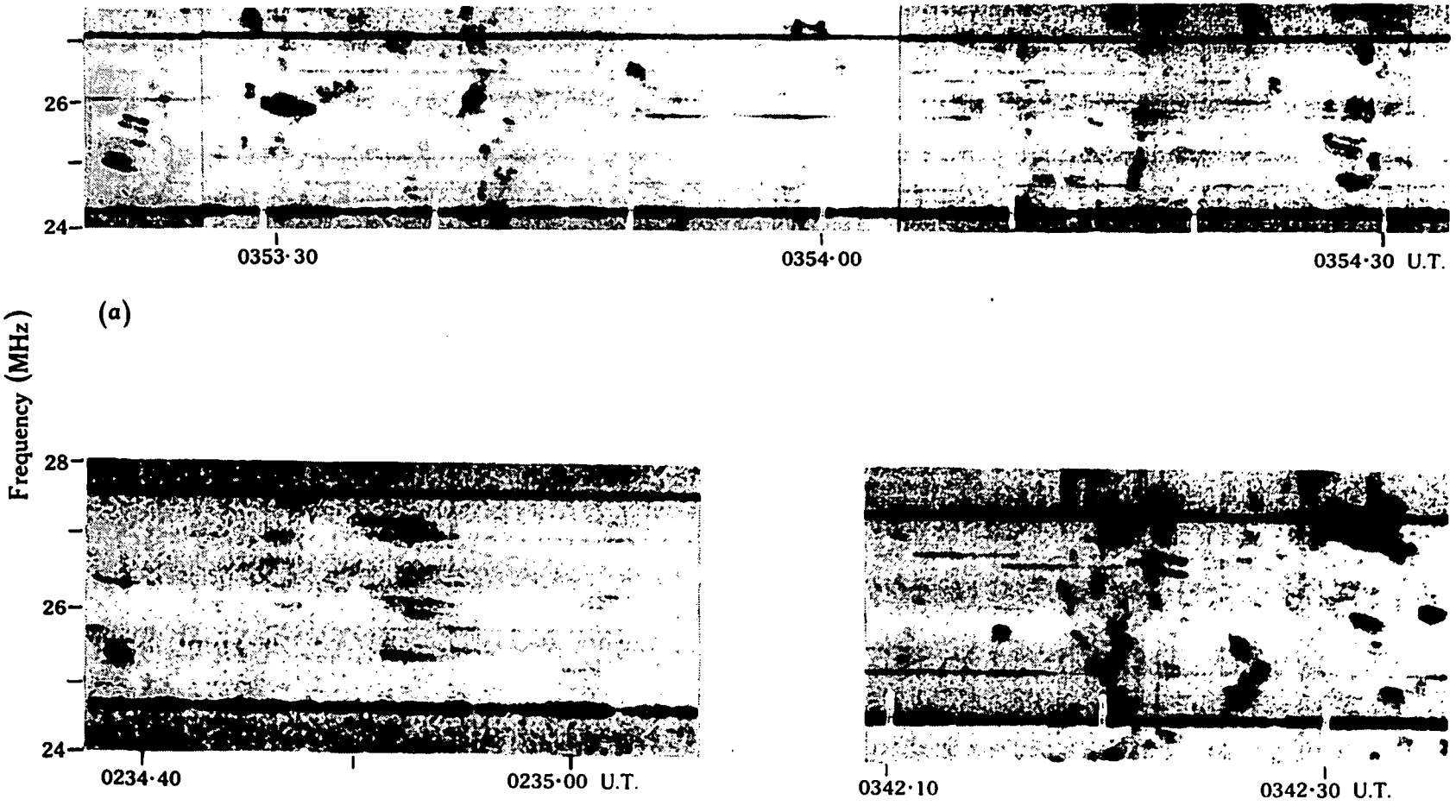


Figure 11.2 Records of bursts observed on March 17, 1966, (a) showing frequency splitting; triple splitting is shown at 0354.28 U.T. (b) and (c) show typical chains of bursts.

The properties of the bursts discussed below are based mainly on the 24-28 MHz observations made during the March, 1966, event. Typical sections of the records obtained in this period are shown in Figure (11.2).

## 11.3 Properties of the Bursts.

### (a) Occurrence.

The bursts were recorded during most periods of solar activity between March, 1966, and March, 1967, however by far the greatest number were recorded during the major storms in March of 1966 and 1967. During these storms the occurrence rate rose as high as 200 per hour for a period of a few days. The 1966 event was associated with a single spot group near the limb of the Sun. The daily occurrence of bursts during this storm is shown in Figure (11.4) from Ellis and McCulloch (1967), together with the occurrence rates of type III bursts and drift pairs and the location of the spot group on the Sun.

At other times some bursts were observed in association with weak solar activity. The bursts usually occurred in groups of 5-10 although on occasions isolated bursts were recorded. There is a tendency for the bursts to be distributed along a band in the frequency-time plane like a type III burst. These bands or chains were recognisable on the 24-28 MHz records but were more convincing on the wider range records. Figure (11.3) shows typical chains recorded in the frequency range 26-48 MHz (Ellis and McCulloch, 1967). Some of these chains are actually weak type III events with burst pairs superimposed.

The nuber of bursts observed increased with decreasing observing frequency as shown in the histogram of Figure (11.5). No

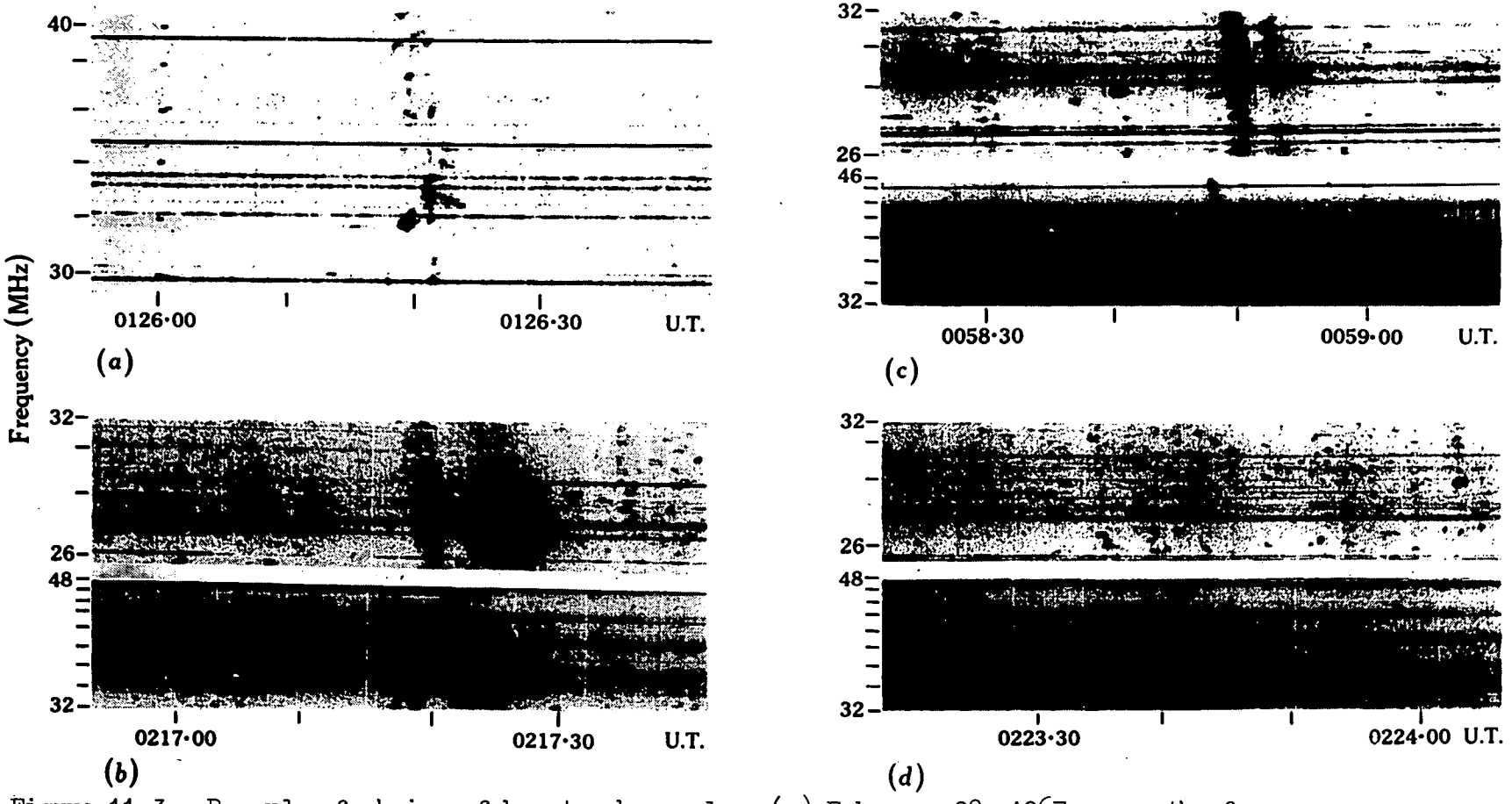


Figure 11.3 Records of chains of bursts observed on (a) February 28, 1967, over the frequency range 30-40 MHz. (b) and (c) March 10, 1967, showing chains with associated diffuse emission. (d) Typical occurrence of bursts during a noise storm. (Ellis and McCulloch, 1967)

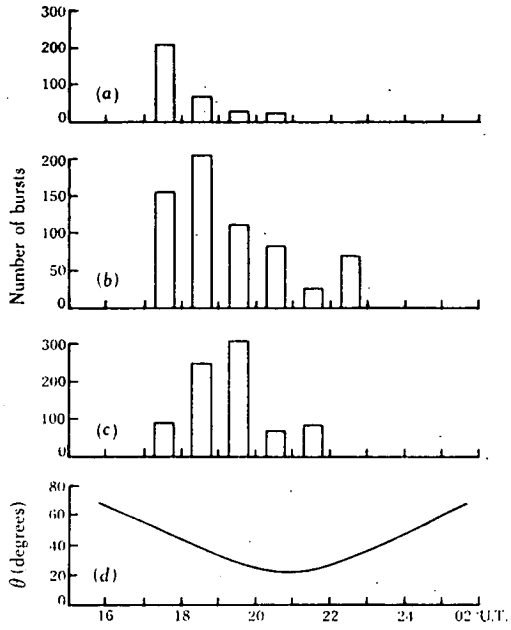


Figure 11.4 Daily occurrence of (a) double bursts for the solar event of March 17-24, 1966. Also shown are the occurrence of (b) type III bursts and (c) drift pairs. The angle between the radius through the associated spot group and the direction of the observer is shown in (d).

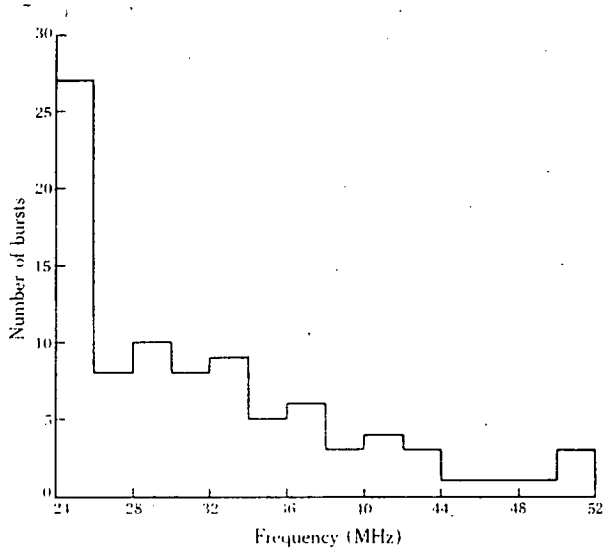


Figure 11.5 Occurrence of bursts on January 30-31, 1967, as a function of wave frequency for a single event. (Ellis and McCulloch, 1967)

bursts were ever observed above a frequency of 60 MHz.

(b) Frequency Separation of the Elements.

The average frequency separation between the components of the bursts increases with frequency between 24 and 28 MHz, Figure (11.6), although at any one frequency the separation varies widely from burst to burst. Figure (11.7) shows the distribution of frequency separation $\Delta f$ for bursts occurring in the range 24 to 26 MHz. The mean value of $\Delta f$ at 25 MHz is about 0.1 MHz. The frequency separation for bursts which occur in individual chains increases with the frequency of the bursts.

A significant proportion, about 10%, of all bursts recorded had three elements. An example of such a burst is shown in Figure (11.2). Microphotometer scans of normal bursts and one triple burst are shown in Figure (11.8). The double bursts fall into two categories, one in which the higher frequency element of the pair is considerably stronger than the lower element, and a smaller category in which both elements of the pair are of approximately equal intensity. The triple bursts resemble members of the first category combined with an additional element at a higher frequency of about the same intensity as the low frequency element of the pair.

(c) Bandwidth.

For bursts in the frequency range 24-28 MHz the bandwidth of the lower frequency element is usually around 50 kHz, while the bandwidth of the higher frequency element shows a wide variation from 40-300 kHz. The distribution of bandwidths of the lower frequency elements of bursts near 25 MHz is shown in Figure (11.9). The generally smaller bandwidth of the lower frequency element is shown in the

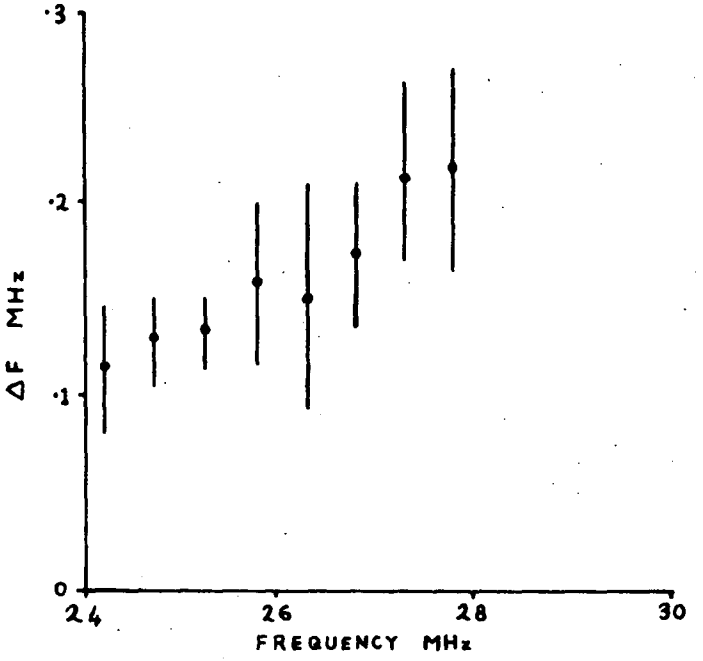


Figure 11.6 Mean variation of the frequency interval between the burst elements with wave frequency for the event of March 17, 1966. The length of the vertical bars corresponds to the standard deviations.

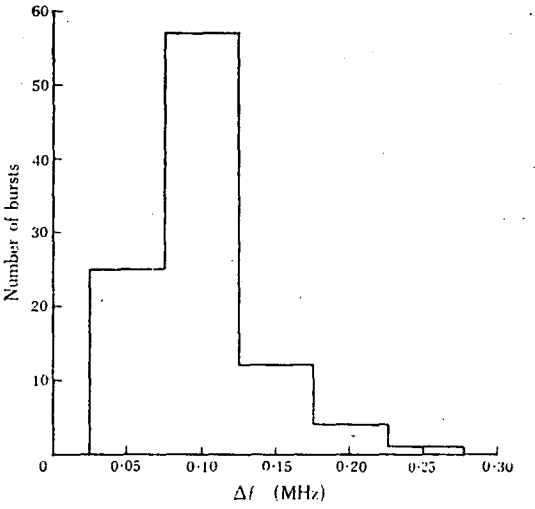


Figure 11.7 Distribution of the frequency interval between the bursts recorded on March 17, 1966, for frequencies between 24 and 26 MHz.

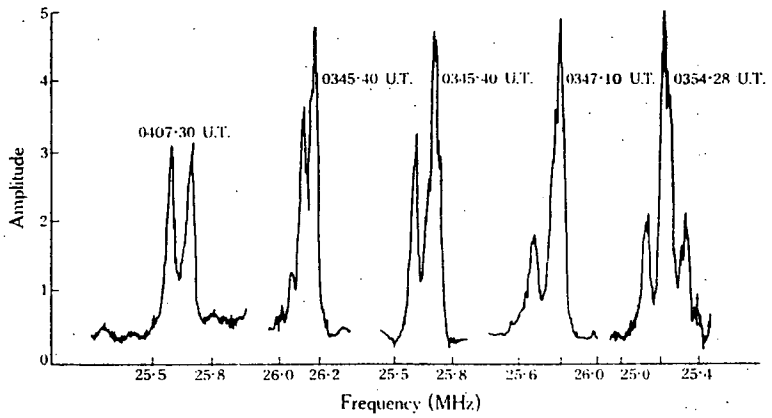


Figure 11.8 Microphotometer scans showing the variation of amplitude with wave frequency for individual bursts on March 17, 1966. The burst at 0354.28 U.T. shows an example of triple frequency splitting.

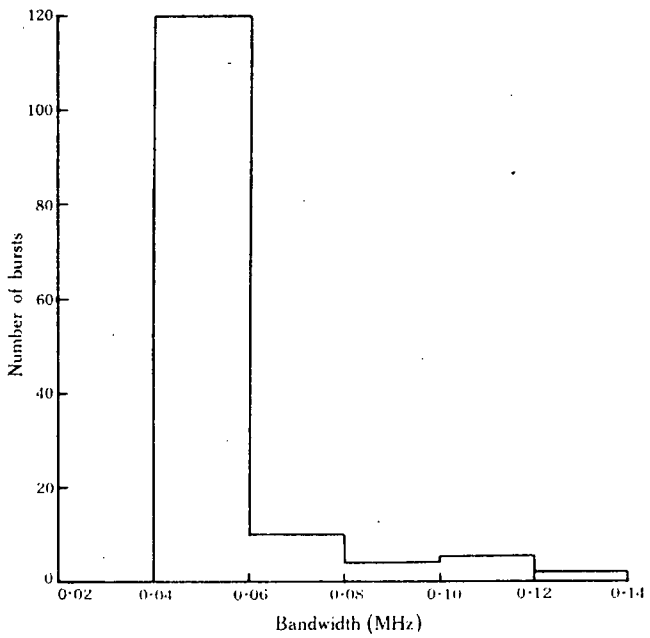


Figure 11.9 Bandwidth of the lower frequency elements of bursts near 25 MHz recorded on March 17, 1966.

microphotometer tracings of Figure (11.8).

(d) Duration of the Bursts.

The bursts recorded in the frequency range 24-28 MHz have a mean duration of 1.2 sec although individual durations varied fairly widely about this value as shown in Figure (11.10).

(e) Time Interval Between the Bursts.

The two components of the bursts do not in general begin at the same time. On the average the lower frequency element begins about 0.1 sec prior to the other although there is a wide scatter in the relative starting times as shown in Figure (11.11).

(f) The Frequency-Time Slopes of the Bursts.

The mid-frequency of each element of a burst is found to show either a zero or negative frequency drift with time. The mean frequency drift is -0.1 MHz/sec although there is considerable variation about this value, (Figure (11.12). No bursts with positive frequency time slopes were observed. The mean frequency drift rate is greater for bursts at higher frequencies (Figure 11.13) in much the same way as the frequency interval between the elements is greater at higher frequencies (Figure 11.6), suggesting a correlation between the frequency-time slope and $\Delta f$. However, the slope does not appear to be correlated with $\Delta f$ for bursts occurring in a narrow frequency interval between 26 and 27 MHz (Figure 11.14).

## 11.4 Emission Mechanisms.

(a) Correlation with Type III Bursts.

The occurrence of chains of burst pairs which resemble type III bursts and the superposition of some chains on weak type III bursts

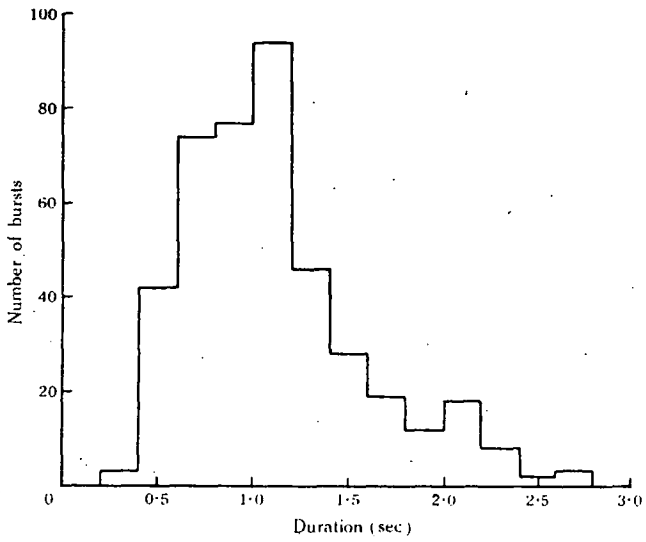


Figure 11.10 Distribution of the durations of elements of bursts in the frequency range 24-28 MHz recorded on March 17, 1966.

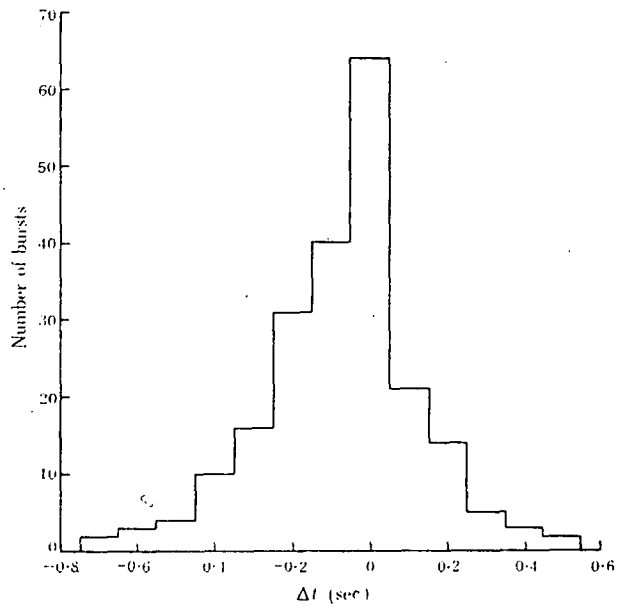


Figure 11.11 Time differences Δt from the beginning of the upper element to the beginning of the lower element for bursts in the frequency range 24-28 MHz recorded on March 17, 1966.

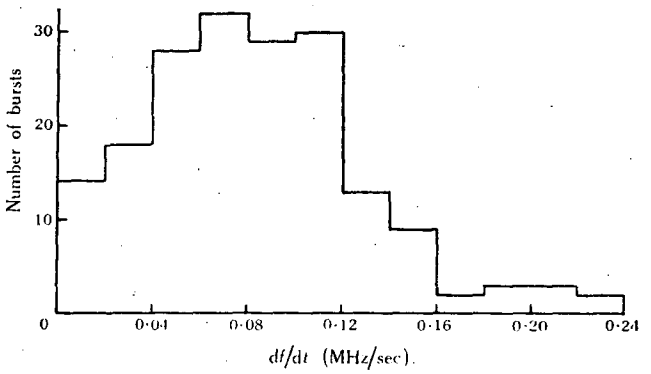


Figure 11.12 Distribution of frequency-time slopes for bursts in the frequency range 24-28 MHz recorded on March 17, 1966.

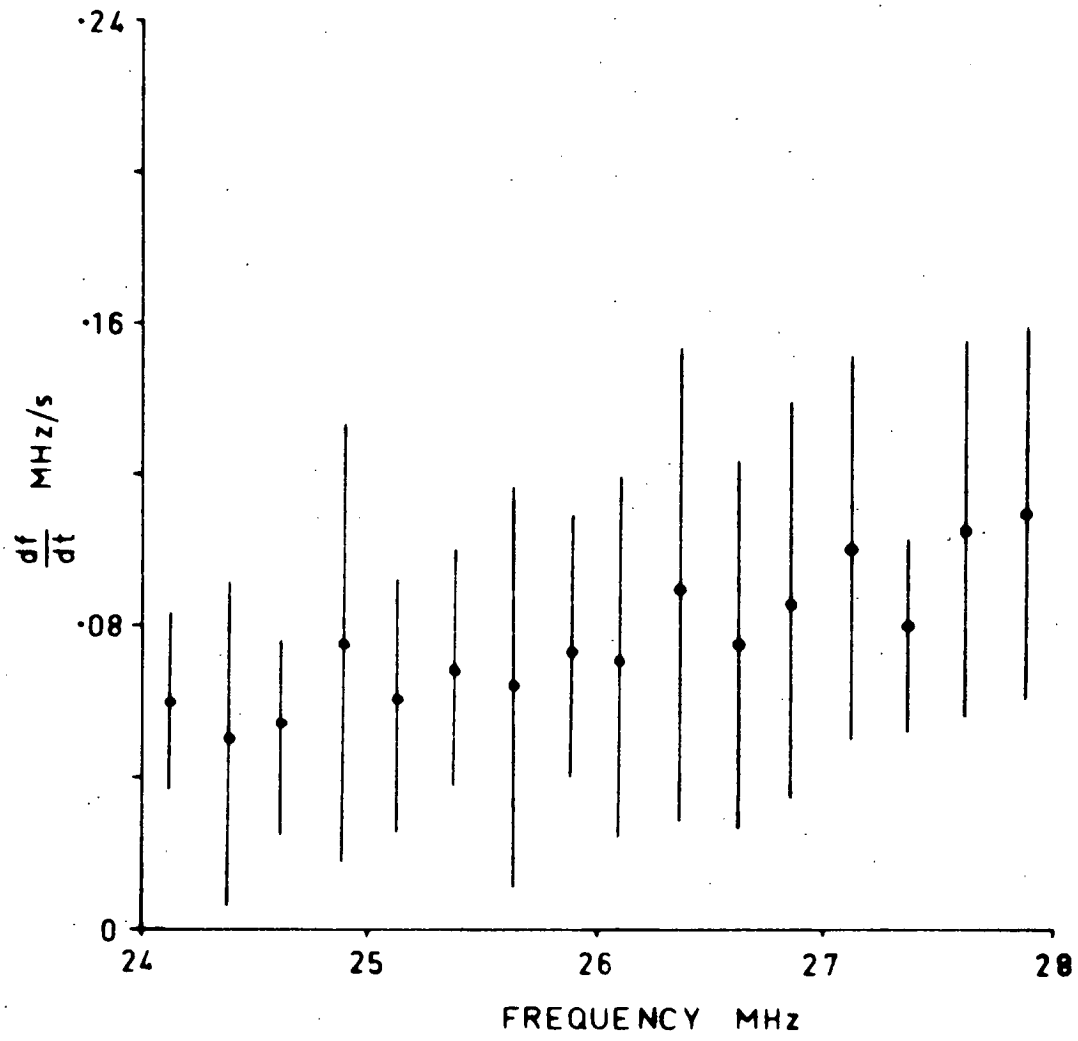


Figure 11.13 Variation of the mean frequency-time slope as a function of frequency for bursts recorded on March 17, 1966. The lengths of the vertical bars are standard deviations.

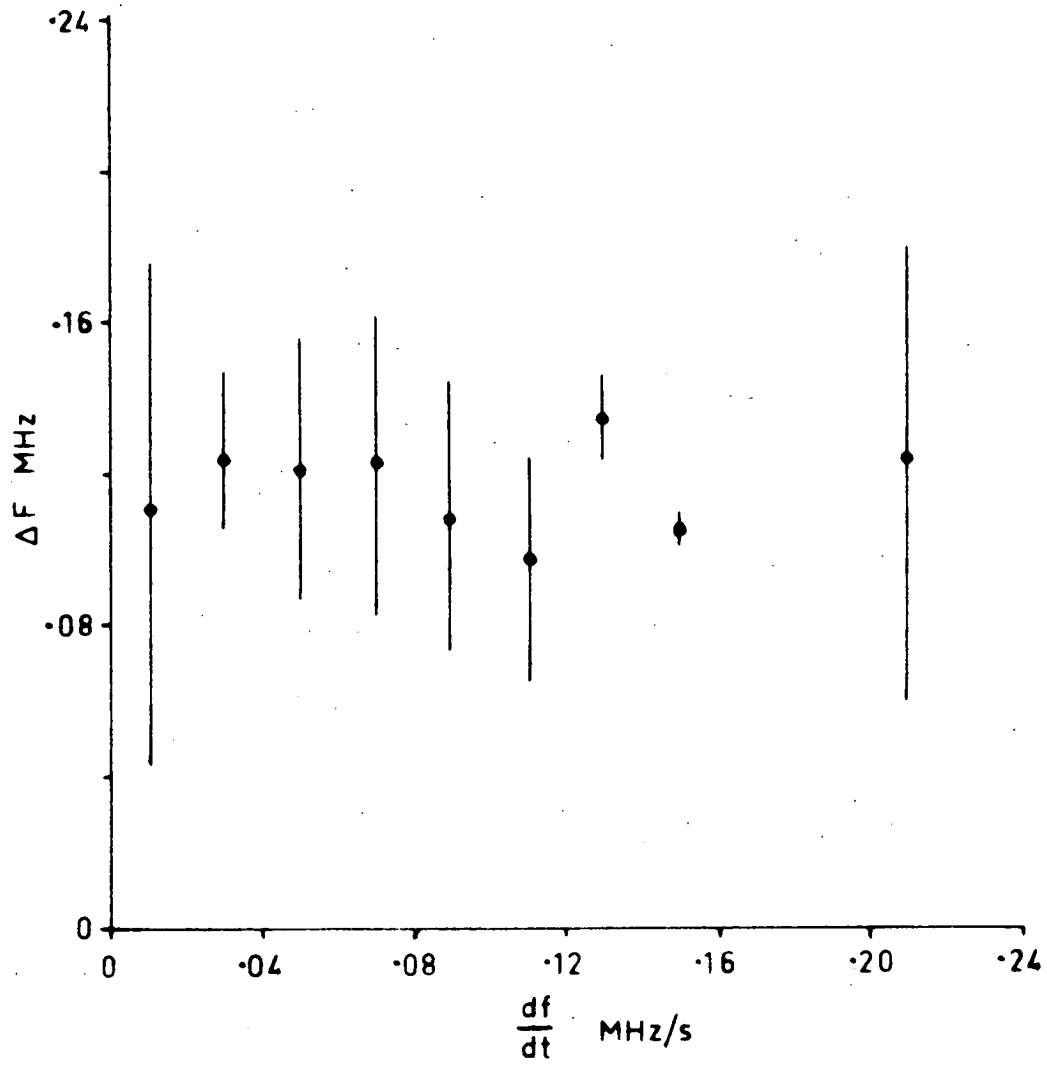


Figure 11.14 Variation of the mean frequency interval between bursts as a function of their frequency-time slope for bursts in the frequency range 26-27 MHz. The lengths of the vertical bars are standard deviations.

suggest a close correlation between the generation of the pairs and type III bursts. The type III emission is plasma radiation excited by energetic streams of electrons (v in the range 0.3 to 0.5c) moving outwards along the coronal streamers. The frequency-time slopes of the pairs on the other hand indicate longitudinal velocities of less than 0.05c. The possibility arises that the disturbances responsible for the type III bursts move out through the corona and excite radiation whenever they meet a low velocity bunch of electrons, giving rise to chains of burst pairs. If there are only isolated bunches of electrons along the path of the "invisible" type III, then isolated pairs will be generated.

(b) Electromagnetic Radiation.

The observation of triple bursts suggests the possibility that magnetoionic triple splitting is responsible. In this case the emitted frequencies would be at $\omega = \omega_o$ and $\omega \simeq \omega_o \pm \frac{1}{2}\omega_H$ and due to the stop zone just below $\omega_o$ only the two higher frequency components could escape. The polarisations of the two elements in this case would be opposite. The only way in which triple bursts could be obtained is for emission to occur at the second harmonic in which case we have $\omega = 2\omega_o$ and $\omega \simeq 2\omega_o \pm \omega_H$. However we might then associate a triple burst near some frequency $\omega$ with a double burst whose elements are oppositely polarised at a frequency near $\omega/2$. The experimental data does not appear to support this idea (Ellis and McCulloch, 1967).

An alternative method of obtaining double bursts is from Doppler shifted cyclotron radiation. Fung (1966) has shown that a helical electron stream moving in the solar corona can emit cyclotron radiation which is most easily observed in the o-mode near the second

harmonic of the gyrofrequency. It may be possible for suitable orientations of the Sun, the electron stream and the observer, to see radiation which was initially emitted in two different directions. The radiation in the forward direction propagates directly to the observer, while radiation in the backward direction at the lower frequency could be reflected low down in the corona and then propagate to the observer. In this way a double burst would be obtained with the lower frequency element delayed with respect to the upper frequency element. This in fact is the direct opposite of the normal occurrence (Figure 11.11).

The Doppler effect also predicts that the frequency separation between the elements should depend upon the velocity of the stream which in turn should be related to the frequency-time slope of the burst. Both the frequency separation and frequency time slope of the bursts increase with the frequency of the burst, Figures (11.6) and (11.13), but the slope does not appear to be correlated with $\Delta f$ for bursts occurring in a narrow frequency interval, Figure (11.14).

(c) Plasma Radiation.

Plasma waves may be excited in a magneto-active plasma at frequencies where the group velocity tends to zero. This occurs at the plasma frequency $\omega_o$ and at the hybrid resonance frequencies $(\omega_o^2 + \omega_H^2)^{\frac{1}{2}}$ and $\omega_o\, \omega_H\, (\omega_o^2 + \omega_H^2)^{-\frac{1}{2}}\, M^{-\frac{1}{2}}$ where M is the ratio of ion to electron mass. In order for these disturbances to escape from the solar corona they must be converted to electromagnetic waves by either Rayleigh scattering on irregularities or combination scattering between plasma waves. Only radiation above the plasma frequency $\omega_o$ may escape. Some of the possible frequencies are $\omega_o$, $(\omega_o^2 + \omega_H^2)^{\frac{1}{2}}$, $2\omega_o$

$2\,(\omega_o^2 + \omega_H^2)^{\frac{1}{2}}$ and $(\omega_o^2 + \omega_H^2) + \omega_o\,\omega_H\,(\omega_o^2 + \omega_H^2)^{-\frac{1}{2}}\,M^{-\frac{1}{2}}$. See Tidman, Birmingham and Stainer (1966) for a full discussion of the possible combination frequencies.

Solar emissions of type II and type III are both identified with plasma radiation and both show harmonic properties. In fact the presence of harmonics in the emission is usually taken as strong evidence for plasma radiation. In order to consider plasma radiation as the source of the pairs it is important to look for radiation at the first and second harmonics. There is some circumstantial evidence for the existence of harmonics for these bursts, Ellis and McCulloch (1967), and this supports the plasma hypothesis.

The frequencies of the pairs observed in the frequency range 24 to 28 MHz would normally be identified with the plasma frequency $\omega_o$ and the upper hybrid resonance frequency $(\omega_o^2 + \omega_H^2)^{\frac{1}{2}}$ The third element of the triple bursts may be identified with the combination frequency $\omega_o\,\omega_H\,(\omega_o^2 + \omega_H^2)^{-\frac{1}{2}}\,M^{-\frac{1}{2}} + (\omega_o^2 + \omega_H^2)^{\frac{1}{2}}$. In the solar corona the condition $\omega_o \gg \omega_H$ is often satisfied and the three frequencies become

$$\omega_1 = \omega_o$$

$$\omega_2 \simeq \omega_o + \tfrac{1}{2}\,\omega_H^2/\omega_o$$

$$\omega_3 \simeq \omega_o + \tfrac{1}{2}\,\omega_H^2/\omega_o + \omega_H\,M^{-\frac{1}{2}}$$

As only frequencies above $\omega_o$ can escape from the corona we would expect the intensity and bandwidth of the lower frequency element to be reduced. Provided we can estimate the part of the lower frequency element to associate with $\omega_o$, the frequency intervals $\omega_2 - \omega_1$ and $\omega_3 - \omega_2$ give measures of the gyrofrequency and hence the magnetic field strength at a given plasma level in the corona. This may provide a much more frequent estimate of coronal magnetic fields than

those presently obtained from the relatively rare type II events. The field strengths required to account for the splitting at the 25 MHz plasma level are of the order of 2 gauss.

## 11.5 Conclusions.

The observed properties of the burst pairs may be summarised as follows:-

(1) They occur fairly regularly at frequencies below 60 MHz.

(2) Duration is in the range 1-2 sec.

(3) Frequency interval between their elements is a few hundred kHz.

(4) Wave frequency generally decreases with time at about 0.1 MHz/sec.

(5) Bursts may occur either in isolation, in chains associated with type III bursts, or in large numbers during noise storms.

(6) Triple splitting is observed in about 10% of bursts.

The properties of the bursts that would be expected from transverse and longitudinal radiation in a plasma have been examined. The observed properties appear to be inconsistent with those expected from transverse electromagnetic radiation. The resonance frequencies expected for plasma waves at $\omega_o$ and $(\omega_o^2 + \omega_H^2)^{\frac{1}{2}}$ are the most promising of those considered. The predicted variations of magnetic field strength and electron density with solar radius determined from these bursts have been examined by Ellis (1967). He finds that the variations are consistent with accepted models of the solar corona. If the frequencies of the bursts can in fact be identified with the resonance frequencies $\omega_o$ and $(\omega_o^2 + \omega_H^2)^{\frac{1}{2}}$ then we have a method of determining magnetic field strengths high up in the solar corona.

## 11.6 References.

ELLIS, G.R.A. (1967) Nature 213, 790

ELLIS, G.R.A. and P.M. McCULLOCH (1966) Nature 211, 1070

ELLIS, G.R.A. and P.M. McCULLOCH (1967) Aust. J. Phys. 20, 583

FUNG, P.C.W. (1966) Aust. J. Phys. 19, 489

TIDMAN, D.A., T.J. BIRMINGHAM and H.M. STAINER (1966) Astrophys. J. 146, 207

# APPENDIX A.

## RAY TRACING IN JUPITER'S MAGNETOSPHERE

The problem of tracing the path of a radio wave through an ionised medium can be subdivided into three parts. The first is to derive a set of differential equations which describe the path of the ray. The second is to arrange these equations into a suitable form so that the differential co-efficients may be evaluated easily. The third and final part is the integration of the equations. This usually involves an iterative procedure on a digital computer.

### (a) The Derivation of the Differential Equations.

Jupiter is surrounded by an ionised plasma whose density is determined by the dipole magnetic field and the rapid rotation rate of Jupiter. To a good approximation the density distribution and magnetic field intensity will be symmetrical about Jupiter's magnetic axis, hence it is convenient to set up a system of spherical polar co-ordinates $(r, \theta, \varphi)$ centered on the planet with axis coincident with Jupiter's magnetic axis.

The refractive index at a point in Jupiter's magnetosphere depends on the co-ordinates $(r, \theta, \varphi)$ of that point through the ionised particle density and magnetic field strength. It also depends on the wave normal angle $\chi$ at that point, i.e. the angle between the wave normal direction and the magnetic field direction.

At each point in the magnetosphere, we set up another set of co-ordinates whose axes $(P_r, P_\theta, P_\varphi)$ are parallel to the $(r, \theta, \varphi)$ axis respectively. We consider a ray at the point $(r, \theta, \varphi)$ and draw a line

parallel to the wave normal direction and of length equal to the refractive index $\mu$. Let $(P_r, P_\theta, P_\varphi)$ be the co-ordinates of its end point. Then $(P_r^2 + P_\theta^2 + P_\varphi^2)^{\frac{1}{2}} = \mu$, and the direction cosines of the wave normal are $\frac{P_r}{\mu}, \frac{P_\theta}{\mu}, \frac{P_\varphi}{\mu}$. The co-ordinates $(P_r, P_\theta, P_\varphi)$ are called the wave normal components at the point $(r,\theta,\varphi)$. Let the wave normal successively take all possible directions. The locus of the points $(P_r, P_\theta, P_\varphi)$ form a surface called the refractive index surface. Since the refractive index depends only on the wave normal angle $\chi$ the refractive index surface will be a solid of revolution about the magnetic field direction. The refractive index can then be expressed as a function of the position and wave normal direction.

$$\mu = \mu(r, \theta, \varphi, P_r, P_\theta, P_\varphi)$$

The equation of the refractive index surface may be written

$$G(r, \theta, \varphi, P_r, P_\theta, P_\varphi) \equiv \frac{(P_r^2 + P_\theta^2 + P_\varphi^2)^{\frac{1}{2}}}{\mu(r, \theta, \varphi, P_r, P_\theta, P_\varphi)} = 1$$

Two important points arise from the concept of the refractive index surface.

(1) The normal to the refractive index surface at a point $(P_r, P_\theta, P_\varphi)$ is in the direction of the ray having those wave normal components.

(2) If $\underline{P}$ is the vector defined by the point $(P_r, P_\theta, P_\varphi)$ and if the medium is sufficiently slowly varying then

$$\text{curl } \underline{P} = 0$$

The requirement that the medium be slowly varying is just the condition that geometrical optics may be applied.

The first condition leads to the equations for the propagation of the ray

$$\dot{r} = c\frac{\partial G}{\partial P_r} \tag{1}$$

$$\dot{\theta} = \frac{c}{r}\frac{\partial G}{\partial P_\theta} \tag{2}$$

$$\dot{\varphi} = \frac{c}{r\sin\theta}\frac{\partial G}{\partial P_\varphi} \tag{3}$$

The condition that curl $\underline{P}$ = 0 gives rise to three equations which describe the way in which the wave normal changes.

$$\frac{1}{c}\frac{dP_r}{dt} = \frac{1}{\mu}\frac{\partial \mu}{\partial r} + \frac{P_\theta}{r}\frac{\partial G}{\partial P_\theta} + \frac{P_\varphi}{r}\frac{\partial G}{\partial P_\varphi} \tag{4}$$

$$\frac{1}{c}\frac{dP_\theta}{dt} = \frac{1}{\mu r}\frac{\partial \mu}{\partial \theta} - \frac{P_\theta}{r}\frac{\partial G}{\partial P_r} + \frac{P_\varphi \cot\theta}{r}\frac{\partial G}{\partial P_\varphi} \tag{5}$$

$$\frac{1}{c}\frac{dP_\varphi}{dt} = \frac{1}{\mu r\sin\theta}\frac{\partial \mu}{\partial \varphi} - \frac{P_\varphi}{r}\frac{\partial G}{\partial P_r} - \frac{P_\varphi \cot\theta}{r}\frac{\partial G}{\partial P_\theta} \tag{6}$$

where c is the velocity of light.

This set of six equations are known as the Haselgrove equations, and need to be solved simultaneously if the path of the ray is to be determined. The equations as they stand are not in a convenient form to integrate. However, we can use the explicit form of G to evaluate its derivatives

$$\text{for example } \frac{\partial G}{\partial P_r} = \frac{\partial}{\partial P_r}\left\{\frac{(P_r^2 + P_\theta^2 + P_\varphi^2)^{\frac{1}{2}}}{\mu(r, \theta, \varphi, P_r, P_\theta, P_\varphi)}\right\}$$

$$= \frac{1}{\mu^2}\left\{P_r - \tfrac{1}{2}\frac{\partial \mu^2}{\partial P_r}\right\}$$

In order to evaluate $\frac{\partial \mu^2}{\partial P_r}$ it is necessary to consider the functional form of $\mu$. Clearly $\mu$ depends on the magnetoionic variables X, Y, Z.

$$\therefore \frac{\partial \mu^2}{\partial P_r} = \frac{\partial \mu^2}{\partial X}\frac{\partial X}{\partial P_r} + \frac{\partial \mu^2}{\partial Y}\frac{\partial Y}{\partial P_r} + \frac{\partial \mu^2}{\partial Z}\frac{\partial Z}{\partial P_r}$$

Now X and Y depend only on r, $\theta$, $\varphi$ not on $P_r$, $P_\theta$ and $P_\varphi$

so $$\frac{\partial X}{\partial P_r} = \frac{\partial Y}{\partial P_r} = 0$$

$$\therefore \quad \frac{\partial \mu^2}{\partial P_r} = \frac{\partial \mu^2}{\partial \chi}\frac{\partial \chi}{\partial P_r}$$

also $$\frac{\partial \mu^2}{\partial P_\theta} = \frac{\partial \mu^2}{\partial \chi}\frac{\partial \chi}{\partial P_\theta}$$

and $$\frac{\partial \mu^2}{\partial P_\varphi} = \frac{\partial \mu^2}{\partial \chi}\frac{\partial \chi}{\partial P_\varphi}$$

In order to calculate the dependence of the wave normal angle $\chi$ on $P_r$, $P_\theta$, $P_\varphi$ it is necessary to introduce the direction of the magnetic field. Let the direction of the field make angles $\beta_r$, $\beta_\theta$, $\beta_\varphi$ with unit vectors $\underline{r}$, $\underline{\theta}$, $\underline{\varphi}$, so that the direction cosines of the field with respect to the co-ordinate axes are $\cos\beta_r$, $\cos\beta_\theta$, $\cos\beta_\varphi$ The direction cosines of the wave normal with respect to the same set of co-ordinate axes are $\frac{P_r}{\mu}$, $\frac{P_\theta}{\mu}$, $\frac{P_\varphi}{\mu}$

The angle between them, the wave normal angle $\chi$, is given by

$$\cos\chi = \frac{1}{\mu}(P_r\cos\beta_r + P_\theta\cos\beta_\theta + P_\varphi\cos\beta_\varphi) \qquad (7)$$

If we take the partial derivative with respect to $P_r$ we get

$$\cos\chi\frac{\partial \mu}{\partial P_r} - \mu\sin\chi\frac{\partial \chi}{\partial P_r} = \cos\beta_r$$

$$\therefore \frac{\partial \chi}{\partial P_r} = \frac{1}{\mu\sin\chi}\left(\cos\chi\frac{\partial \mu}{\partial P_r} - \cos\beta_r\right)$$

but $$\mu^2 = P_r^2 + P_\theta^2 + P_\varphi^2$$

and $$2\mu\frac{\partial \mu}{\partial P_r} = 2P_r$$

$$\therefore \quad \frac{\partial \chi}{\partial P_r} = \frac{P_r \cos\chi - \mu \cos\beta_r}{\mu^2 \sin\chi} \tag{8}$$

Similar relations can be obtained for $\frac{\partial \chi}{\partial P_\theta}$ and $\frac{\partial \chi}{\partial P_\varphi}$. If we now change the independent variable in the Haselgrove equations to p, by putting $p = ct$, we can write the equations in a convenient form for integration

$$\frac{dr}{dp} = \frac{1}{\mu^2}\left\{ P_r + \frac{\mu \cos\beta_r - P_r \cos\chi}{2\mu^2 \sin\chi} \frac{\partial \mu^2}{\partial \chi} \right\} \tag{9}$$

$$\frac{d\theta}{dp} = \frac{1}{r\mu^2}\left\{ P_\theta + \frac{\mu \cos\beta_\theta - P_\theta \cos\chi}{2\mu^2 \sin\chi} \frac{\partial \mu^2}{\partial \chi} \right\} \tag{10}$$

$$\frac{d\varphi}{dp} = \frac{1}{r\mu^2 \sin\theta}\left\{ P_\varphi + \frac{\mu \cos\beta_\varphi - P_\varphi \cos\chi}{2\mu^2 \sin\chi} \frac{\partial \mu^2}{\partial \chi} \right\} \tag{11}$$

$$\frac{dP_r}{dp} = \frac{1}{2\mu^2} \frac{\partial \mu^2}{\partial r} + P_\theta \frac{d\theta}{dp} + P_\varphi \sin\theta \frac{d\varphi}{dp} \tag{12}$$

$$\frac{dP_\theta}{dp} = \frac{1}{2r\mu^2} \frac{\partial \mu^2}{\partial \theta} - \frac{P_\theta}{r} \frac{dr}{dp} + P_\varphi \cos\theta \frac{d\varphi}{dp} \tag{13}$$

$$\frac{dP_\varphi}{dp} = \frac{1}{2r\mu^2 \sin\theta} \frac{\partial \mu^2}{\partial \varphi} - \frac{P_\varphi}{r} \frac{dr}{dp} - P_\varphi \cot\theta \frac{d\theta}{dp} \tag{14}$$

(b) Evaluation of the Differential Coefficients.

We now introduce a specific model of the Jovian magnetosphere in order to facilitate the evaluation of the differential coefficients.

The magnetic field of Jupiter is assumed to be a pure dipole with a strength at the ground on the Equator of $H_{og}$. Then the field strength at a point $(r,\theta,\varphi)$ is

$$H = H_{og} \frac{(1 + 3\cos^2\theta)^{\frac{1}{2}}}{r^3}$$

The direction cosines of the field are

$$\begin{bmatrix} \cos\beta_r \\ \cos\beta_\theta \\ \cos\beta_\varphi \end{bmatrix} = \frac{1}{(1 + 3\cos^2\theta)^{\frac{1}{2}}} \begin{bmatrix} -2\cos\theta \\ -\sin\theta \\ 0 \end{bmatrix} \qquad (15)$$

The wave normal angle $\chi$ can be calculated using equation (7), but since we do not know the value of $\mu$ we use the fact that

$$\mu^2 = P_r^2 + P_\theta^2 + P_\varphi^2$$

then
$$\cos\chi = \frac{P_r \cos\beta_r + P_\theta \cos\beta_\theta + P_\varphi \cos\beta_\varphi}{(P_r^2 + P_\theta^2 + P_\varphi^2)^{\frac{1}{2}}} \qquad (16)$$

The value of the magnetoionic variable Y can be obtained directly from the magnetic field strength

$$Y = 2.8_{10}6 \, H_{og} \frac{(1 + 3\cos^2\theta)^{\frac{1}{2}}}{f\, r^3}$$

Provided we restrict ourselves to regions of the magnetosphere where the wave frequency is greater than the ion plasma frequency we can use the Appleton-Hartree equation as a sufficiently good approximation to the refractive index.

$$\mu^2 = 1 - \frac{X(1 - X)}{1 - X - \frac{1}{2}Y^2\sin^2\chi \pm (\frac{1}{4}Y^4\sin^4\chi + \{1 - X\}^2 Y^2\cos^2\chi)^{\frac{1}{2}}}$$

The use of this equation directly leads to complicated expressions for the derivatives. We will use an alternative method given by Capon.

We define
$$a = 1 + X\,Y^2\cos^2\chi - (X + Y^2)$$
$$b = 1 - X - \tfrac{1}{2}Y^2\sin^2\chi$$
$$c = 1 - X$$

Then it may be shown that

$$\mu^2 = 1 + q X$$

where q is a root of the equation

$$a q^2 + 2 b q + c = 0$$

then $q_o = \frac{- b + (b^2 - ac)^{\frac{1}{2}}}{a}$ gives $\mu^2$ for the ordinary ray

and $q_E = \frac{- b - (b^2 - ac)^{\frac{1}{2}}}{a}$ gives $\mu^2$ for the extraordinary ray.

Hence $$\frac{\partial q}{\partial X} = \frac{1}{2 (a q + b)} (1 + q^2 + 2 q - q^2 Y^2 \cos^2\chi) \quad (18)$$

$$\frac{\partial q}{\partial Y^2} = \frac{1}{2 (a q + b)} (q^2 + q \sin^2\chi - X q^2 \cos^2\chi) \quad (19)$$

$$\frac{\partial q}{\partial \chi} = \frac{1}{(a q + b)} (X q^2 + q) Y^2 \sin\chi \cos\chi \quad (20)$$

Then $$\frac{\partial \mu^2}{\partial X} = q + X \frac{\partial q}{\partial X} \quad (21)$$

$$\frac{\partial \mu^2}{\partial Y^2} = X \frac{\partial q}{\partial Y^2} \quad (22)$$

$$\frac{\partial \mu^2}{\partial \chi} = X \frac{\partial q}{\partial \chi} \quad (23)$$

Now $$\frac{\partial \mu^2}{\partial r} = \frac{\partial \mu^2}{\partial X} \frac{\partial X}{\partial r} + \frac{\partial \mu^2}{\partial Y^2} \frac{\partial Y^2}{\partial r} + \frac{\partial \mu^2}{\partial \chi} \frac{\partial \chi}{\partial r}$$

Because the dipole field is scale invariant the direction of the magnetic field is independent of r. Hence

$$\frac{\partial \chi}{\partial r} = 0$$

$\frac{\partial Y^2}{\partial r}$ may be obtained by differentiating equation (17).

The evaluation of the third differential $\frac{\partial X}{\partial r}$ shows the need for an analytic expression for X as a function of r.

We are using the model magnetosphere proposed by Melrose (1967).

We define $r_b = \left\{ \frac{7.76\, r}{\sin^2 \theta} \right\}^{\frac{1}{4}}$

then if $r \leqslant r_b$

$$X = \frac{8.061_{10}7\, N_o}{f^2} \exp\left\{ -\tfrac{1}{2} A \left\{ 1 - \frac{1}{r} - 0.043 \sin^2\theta \left( r^2 - \frac{1}{r} \right) \right\} \right\}$$

and if $r > r_b$

$$X = X_{(r=r_b)} \left\{ \frac{r_b}{r} \right\}^4$$

This model contains two parameters $N_o$ and A, the maximum density in the ionosphere and the scale height respectively.

We can now evaluate $\frac{\partial X}{\partial r}$ and hence $\frac{\partial \mu^2}{\partial r}$

Similarly we can evaluate $\frac{\partial \mu^2}{\partial \theta}$

$$\frac{\partial \mu^2}{\partial \theta} = \frac{\partial \mu^2}{\partial X} \frac{\partial X}{\partial \theta} + \frac{\partial \mu^2}{\partial Y^2} \frac{\partial Y^2}{\partial \theta} + \frac{\partial \mu^2}{\partial \chi} \frac{\partial \chi}{\partial \theta}$$

We also have $\frac{\partial \mu^2}{\partial \varphi} = 0$ since the magnetosphere is symmetrical with respect to $\varphi$.

This gives us all the differential coefficients needed to evaluate the Haselgrove equations at any point in the magnetosphere. The remaining problem is to set up the initial conditions and integrate the differential equations to obtain the ray path.

(c) Integration of the Differential Equations.

The Haselgrove equations are too complicated to solve explicitly so an iterative technique employing a digital computer is used.

The starting point of the ray was input by means of the

following parameters, the system III longitude of Io, the wave normal angle and its azimuth, and the velocity of the electrons accelerated by Io. The ratio of the magnetoionic variables X and $Y^2$ was then evaluated at Io, and was used in combination with the wave normal angle and the electron velocity to obtain a simultaneous solution of the Doppler equation and the Appleton-Hartree equation. This solution provided the wave frequency, refractive index and refractive index components.

The path of the ray is then computed by simultaneously integrating the six Haselgrove equations using a fourth order Runge-Kutta procedure. The end point of the ray is reached when the electron gyrofrequency exceeds 35 MHz. The coordinates of this point and the propagation time were printed.

The process was carried out on an Elliott 503 computer and some 5000 rays were traced. The average computer time per ray was about 12 secs.

A print up of the ray tracing program is given below in Elliott Algol which differs from the standard Algol 60 in a few minor points, the most important of which are outlined below.

Basic Symbols

| 503 Representation | Algol 60 |
|---|---|
| and | $\wedge$ |
| or | $\vee$ |
| £ | ' |
| ? | ' |
| div | $\div$ |
| * | $\times$ |

Output format setting

| | |
|---|---|
| print £ string ? | results in string being printed on the output device |
| print ££ character ?? | has the following results for the specified characters |

| Character | Interpretation |
|---|---|
| l | new line |
| s | space |
| r | blank (i.e. runout) |
| t | tabulate |
| h | stop |

The following standard procedures are used to control the output format of numbers.

| | |
|---|---|
| sameline | all characters printed on sameline unless a new line is called |
| prefix (££ character ??) | all numbers are prefixed by the character specified, see list above |
| digits (n) | an integer is printed with n digits, lead zeros are suppressed |
| freepoint (n) | a real number is printed with n significant digits |
| aligned (m,n) | a real number is printed with m digits preceding the decimal point and n digits following |
| scaled (n) | the number is printed in the form $a_{10}{}^{b}$ where a is of form aligned (1, n-1) and b is in the range -76 to +76. |

```
IO TO JUPITER RAY TRACE;
begin real r,thetam,phim,Pr,Ptheta,Pphi,No,Hog,a,stheta,ctheta,
      S2theta,C2theta,z,rootz,cbetat,nsquare,n,cxi,c2xi,s2xi,
      sxi,rb,rsquare,rcube,temp1,X,dXdr,dXdtheta,f,temp2,temp3,
      Ysquare,dY2dr,dY2dtheta,dxidtheta,alpha,beta,gamma,q,
      dn2dxi,dn2dY2,dn2dX,dn2dr,dn2dtheta,P,thetag,phig,S,B,h,
      cbetar,theta,phi,ff1,ff2,ff3,ff4,ff5,ff6,y1,lambda,start1,
      start2,start3,time,ngroup,omega,atten,aphi,hh,deltar,
      deltat,deltap,caphi,saphi,satheta,catheta,oneonb,eps,epson2;
      integer i,loops,lcount; real array y,ff[1:6];
      switch sss:=end,again;
      comment This program traces the path of rays generated by a
      Doppler cyclotron process near Io to a point near the surface
      of Jupiter where the electron gyrofrequency exceeds 35 MHz.
      The variables r, thetam, and phim are spherical polar coords
      with respect to Jupiters north magnetic pole. The components
      of the wave normal in each direction are Pr, Ptheta and Pphi.
      The intensity of Jupiters magnetic field at the equator is
      Hog and the maximum electron density in Jupiters ionosphere
      is No;
      procedure geomag(thetag,phig)to:(thetam,phim);
      value thetag,phig; real thetag,phig,thetam,phim;
      comment This procedure converts from geographic to
      geomagnetic coordinates based on the assumption that the
      magnetic pole is at a longitude of 183° and the magnetic
      axis is tilted 10° to the rotation axis;
```

```
        begin real sthota,cthota,cthm,x,y;
              cthota:=cos(thotag); sthota:=sin(thotag);
              cthm:=0.9848*cthota+0.1736*sthota*cos(3.194-phig);
              y:=-sthota*sin(3.194-phig);
              x:=(0.9848*cthm-cthota)/0.1736;
              phim:=arctan(y,x); thotam:=arccos(cthm);
        end;
procedure BOUNDARY(thota,phi); value thota,phi; real thota,phi;
comment Procedure BOUNDARY solves the Doppler equation
for radiation by particles with a velocity of C divided by
oneonb at awavenormal angle thota and azimuth phi. The
condition is solved at apoint on Ios orbit at longitude
phig. The refractive index, wave normal components and
frequency of emission are obtained;
        begin real XX,YY,temp,rsquare,sthota,cthota,limit,fhonfo,
              cphi,sphi;
              sxi:=sin(thota*B); cxi:=cos(thota*B); s2xi:=sxi*sxi;
              c2xi:=cxi*cxi;  cphi:=cos(phi*B);  sphi:=sin(phi*B);
              cthota:=cos(thotam);  sthota:=sin(thotam);
              z:=1.0+3.0*cthota*cthota;  rootz:=sqrt(z);
              cbotar:=-2.0*cthota/rootz;  cbotat:=-sthota/rootz;
              rsquare:=r*r;  temp:=1.0/r;  sthota:=sthota*sthota;
              cthota:=cthota*cthota;  rb:=(7.76*r/sthota)↑(0.25);
              temp2:=1.0/rb;  temp3:=rb*rb;
              XX:=8.061_10↑7*No*sqrt(sqrt(sthota))*exp(-0.5*a*
                 (1.0-temp2-0.043*sthota*(temp3-temp2)))*
                 temp3*temp3/(rsquare*rsquare);
```

```
            YY:=7.8361_10 12*Hog*Hog*z/(rsquare*rsquare*rsquare);
            fhonfo:=YY/XX;
            Ysquare:=(1.0+fhonfo+sqrt(1.0+2.0*fhonfo*
               (1.0-2.0*c2xi)+fhonfo*fhonfo))/(2.0*c2xi);
            aphi:=YY/Ysquare;  f:=sqrt(aphi);
            n:=abs(onoonb*(sqrt(Ysquare)-1.0)/cxi);
            Pr:=n*(sxi*cphi*cbotat+cxi*cbotar);
            Pthota:=n*(cxi*cbotat-sxi*cphi*cbotar);
            Pphi:=-sxi*sphi*n;
      ond;
procoduro function(y,ff);  array y,ff;
commont We set up the differential coefficients of the
Hasolgrovo equations in a form in which they can be
integrated using a fourth order Runge Kutta procedure.
The group refractive index ngroup, and the angle omega
between the wave normal and ray directions are calculated;
      begin r:=y[1];  thetam:=y[2];  phim:=y[3];
            Pr:=y[4];  Pthota:=y[5];  Pphi:=y[6];
            sthota:=sin(thetam);  cthota:=cos(thetam);
            S2thota:=sthota*sthota;  C2thota:=cthota*cthota;
            z:=1.0+3.0*C2thota;  rootz:=sqrt(z);
            cbotar:=-2.0*cthota/rootz;  cbotat:=-sthota/rootz;
            nsquare:=Pr*Pr+Pthota*Pthota+Pphi*Pphi;
            n:=sqrt(nsquare);
            cxi:=(Pr*cbotar+Pthota*cbotat)/n;  c2xi:=cxi*cxi;
            s2xi:=1.0-c2xi;  sxi:=sqrt(s2xi);
```

```
rb:=(7.76*r/S2theta)↑(0.25);  rsquare:=r*r;
rcube:=rsquare*r;  temp1:=-0.5*a;
if r<rb then
  begin temp2:=1.0/r;
        X:=3.061₁₀7*No/aphi*sqrt(stheta)*exp(temp1*
          (1.0-temp2-0.043*S2theta*(rsquare-temp2)));
        dXdr:=X*(temp2*temp2-0.043*S2theta*
              (2.0*r+temp2*temp2))*temp1;
        dXdtheta:=X*0.043*a*stheta*ctheta*
          (rsquare-temp2)+0.5*X*ctheta/stheta;
  end
else  begin temp2:=1.0/rb;  temp3:=rb*rb;
        X:=3.061₁₀7*No/aphi*sqrt(stheta)*exp(
          temp1*(1.0-temp2-0.043*S2theta*(temp3-
          temp2)))*temp3*temp3/(rsquare*rsquare);
        dXdr:=-4.0*X/r;
        dXdtheta:=X*0.043*a*stheta*ctheta*
          (temp3-temp2)+0.5*X*ctheta/stheta;
  end;
Ysquare:=7.3361₁₀12*Hog*Hog*z/(rcube*rcube*aphi);
dY2dr:=-6.0*Ysquare/r;
dY2dtheta:=-6.0*Ysquare*stheta*ctheta/z;
dxidthota:=-2.0*(Pr*sthota-2.0*Pthota*cthota)/
              (n*z*rootz);
gamma:=1.0-X;  beta:=gamma-Ysquare*s2xi*0.5;
alpha:=1.0+X*Ysquare*c2xi-X-Ysquare;
q:=(nsquare-1.0)/X;
```

```
            temp2:=0.5*X/sqrt(beta*beta-alpha*gamma);
            temp3:=q*q;
            dn2dxi:=2.0*temp2*(X*temp3+q)*Ysquare*cxi;
            dn2dY2:=temp2*(temp3+q*s2xi-X*temp3*c2xi);
            dn2dX:=temp2*(1.0+temp3+2.0*q-temp3*Ysquare*c2xi)+q;
            dn2dr:=dn2dX*dXdr+dn2dY2*dY2dr;
            dn2dtheta:=dn2dY2*dY2dtheta+dn2dxi*dxidtheta+
                              dn2dX*dXdtheta;
            temp1:=0.5/(nsquare)*dn2dxi;
            ngroup:=n-(dn2dX*X+dn2dY2*Ysquare)/n;
            omega:=2.0*nsquare/dn2dxi;
            ff1:=(Pr+temp1*(n*cbetar-Pr*cxi))/nsquare;
            ff2:=(Ptheta+temp1*(n*cbetat-Ptheta*cxi))/(r*nsquare);
            ff3:=(Pphi-temp1*Pphi*cxi)/(r*nsquare*stheta);
            ff4:=0.5*dn2dr/nsquare+Ptheta*ff2+Pphi*stheta*ff3;
            ff5:=0.5*dn2dtheta/(r*nsquare)-Ptheta*ff1/r+
                              Pphi*ctheta*ff3;
            ff6:=-Pphi*(ff1/r+ctheta*ff2/stheta);
            ff[1]:=ff1;  ff[2]:=ff2;  ff[3]:=ff3;
            ff[4]:=ff4;  ff[5]:=ff5;  ff[6]:=ff6;
            y[1]:=r;  y[2]:=thetam;  y[3]:=phim;
            y[4]:=Pr;  y[5]:=Ptheta;  y[6]:=Pphi;
        end function;
    procedure RKFOUR(x,y,f,h);  value h;     real x,h;  array y,f;
    comment Integrates the six differential equations simultaneously
    over an interval h;
```

```
            begin real hby2,hby6;  integer i;  array ybar,p[1:6];
                  procedure step(a,b,k1,k2);  value k1,k2;  real k1,k2;
                  array a,b;
                  for i:=1 step 1 until 6 do
                    begin p[i]:=p[i]+k1*f[i];  a[i]:=y[i]+k2*b[i]
                    end step;
                  hby2:=h/2.0;  hby6:=h/6.0;
                  for i:=1 step 1 until 6 do p[i]:=0.0;
                  function(x,y,f); step(ybar,f,1.0,hby2); x:=x+hby2;
                  function(x,ybar,f);  step(ybar,f,2.0,hby2);
                  function(x,ybar,f); step(ybar,f,2.0,h); x:=x+hby2;
                  function(x,ybar,f);  step(y,p,1.0,hby6)
            end RKFOUR;
      loops:=1000;  samelino;
      read phig,oneonb,eps;
      lcount:=3;  S:=57.295779513;  B:=0.01745329252;  phig:=phig*B;
      No:=3.5₁₀6;  a:=22.0;  Hog:=15.0;
      print ££1?No = ?,scaled(3),No,£  Hog = ?,alignod(2,1),Hog,
      £  a = ?,a,£  eps = ?,scaled(3),eps,£  beta = ?,1.0/oneonb,
      £  phig = ?,alignod(3,2),phig*S;
      print ££12?theta        phi          frequency   thetam      ?,
      £phim       fo ion       beta        time?;
again: read theta,phi;  if theta=1000.0 then goto end;
      thetag:=1.5708;  h:=1.0₁₀-8;  r:=6.0;  time:=0.0;
      ngroup:=0.0;  omega:=0.0;  hh:=h;
      geomag(thetag,phig,thetam,phim);
      BOUNDARY(theta,phi);
```

```
comment This sets up the initial conditions;
y[1]:=r;  y[2]:=thetam;  y[3]:=phim;  y[4]:=Pr;  y[5]:=Ptheta;
y[6]:=Pphi;  epson2:=0.5*eps;
function(y,ff);
print ££1??,aligned(3,2),theta,prefix(££t??),phi,scaled(4),f,n;
for i:=1 step 1 until loops do
      begin start1:=r;  start2:=thetam;  start3:=phim;
            RKFOUR(P,y,ff,h);
            deltar:=start1-r;  deltat:=start2-thetam;
            deltap:=start3-phim;
            dist:=sqrt(deltar*deltar+r*r*(deltat*deltat+
                deltap*deltap*s2theta));
            time:=time+0.2378*dist*ngroup*omega;
            lambda:=abs(deltar);
            start1:=r;  start2:=thetam;  start3:=phim;
            if lambda<epson2 then h:=h*2.0 else if lambda>eps
            then h:=h/2.0;
            if Ysquare*aphi> 1.225_10 15 then
              begin i:=loops+1;  h:=hh;
              end;
      end;
comment The previous loop integrates over successive intervals
h, after each step the electron gyrofrequency and the distance
travelled in the last step are computed. If these lie outside
set limits appropriate adjustments are made. The propagation
time is calculated;
```

```
        print prefix(ff t??),aligned(3,2),y[2]*S,y[3]*S,scaled(=),
        f*sqrt(X*5.447₁₀-4),(sqrt(Ysquare)-1.0)/(n*exi),time;
        lcount:=lcount+1;  if lcount=58 then begin top of form;
        lcount:=1;  end;
        goto again;
ond:    print ff r20hr50??;
end of program;
```

## PUBLICATIONS

A considerable portion of this thesis has been published in the following articles.

ELLIS, G.R.A. and P.M. McCULLOCH Decametric Radio Emissions of Jupiter. Nature 198, 275 : 1963

ELLIS, G.R.A. and P.M. McCULLOCH The Decametric Radio Emissions of Jupiter. Aust. J. Phys. 16, 380-97 : 1963

McCULLOCH, P.M. and G.R.A. ELLIS Observations of Jupiter's Decametric Radio Emissions. Planet. Space Sci. 14, 347-59 : 1966

KOMESAROFF, M.M. and P.M. McCULLOCH The Radio Rotation Period of Jupiter. Astrophysical Letters 1, 39-41 : 1967

McCULLOCH, P.M. The Effect of Io on Jupiter's Decametric Emissions. Proc. Ast. Soc. Aust. 1, 81-82 : 1968

McCULLOCH, P.M. Interpretation of the Radio Rotation Period of Jupiter in Terms of the Cyclotron Theory. Aust. J. Phys. 21, 409-13 : 1968

ELLIS, G.R.A. and P.M. McCULLOCH Frequency Splitting of Solar Radio Bursts. Nature 211, 1070-71 : 1966

ELLIS, G.R.A. and P.M. McCULLOCH Frequency Splitting of Solar Radio Bursts. Aust. J. Phys. 20, 583-94 : 1967

As well as these papers directly concerned with the thesis I have been associated in research in other fields resulting in the following publications.

HAYNES, R.F., P.A. HAMILTON and P.M. McCULLOCH Observations of 11 Radio Sources near 55MHz. Aust. J. Phys. 21, 539-42 : 1968

SLEE, O.B., M.M. KOMESAROFF and P.M. McCULLOCH Spaced Receiver Observations of Pulsed Radio Sources. Nature 219, 342-43 : 1968

KOMESAROFF, M.M., P.M. McCULLOCH, P.A. HAMILTON and D.J. COOKE Spectral Fine Structure in Pulsar Radiation. Nature 220, 358-60 : 1968

Reprints of most of these articles are included in the back of the thesis.